Advanced Dispersion Strategies of Carbon Nanofillers and their use to enhance Mechanical and Electrical Properties of Polyacrylonitrile Fibers

A Dissertation

Presented to

The Academic Faculty

by

Pedro J. Arias-Monje

In Partial Fulfillment

Of the Requirements for the Degree

Doctor of Philosophy in the

School of Materials Science and Engineering

Georgia Institute of Technology

December 2020

Advanced Dispersion Strategies of Carbon Nanofillers and their use to enhance Mechanical and Electrical Properties of Polyacrylonitrile Fibers

Approved by:

Dr. Satish Kumar, *Advisor*
School of Materials Science and Engineering
Georgia Institute of Technology

Dr. Karl Jacob
School of Materials Science and Engineering
Georgia Institute of Technology

Dr. Hendrik Heinz
Department of Chemical and Biological Engineering
University of Colorado Boulder

Dr. Kyriaki Kalaitzidou
School of Mechanical Engineering
Georgia Institute of Technology

Dr. Suresh Sitaraman
School of Mechanical Engineering
Georgia Institute of Technology

Dr. Naresh Thadhani
School of Materials Science and Engineering
Georgia Institute of Technology

Date Approved: Dec. 12, 2020

Space is neither cold nor dark. It is full of light and our eyes only require an object for that light to shine upon. That light is also energy, energy that once is part of you, or any other object, you can either accumulate or dissipate.

Pedro J. Arias-Monje, 2020

ACKNOWLEDGEMENTS

This document was completed thanks to the incredible support of many people, some of which have been part of my life for as many years as I am, while many others I am continuously finding in the path. Each of you have played a role in my formation as human being and I want to give you my deepest thanks.

My first mention goes to my family, who have loved me unconditionally and have been cheering me and helping me to see the bright-side every time I close my eyes. To my birth-family, my mom, dad, brothers, cousins, god-son, aunt, uncle and grandma, and to my chosen-family, Francisco. Thanks would not suffice.

To my undergrad and grad school-acquired family, thanks as well. Laura, Aleja, Juan, Yami, Tats and Diego, Jo, Ming, Hamza, Narayan, Hongfang, Neha, Camila, Eric, David, Natalia, Amanda, Abigail, Michelle and many many many others. I am happy to have shared with you so much and can't wait to create many more memories with y'all during the life ahead.

To my academic mentors, Claudia, Jonathan, Sarath, Hugo and Satish, thanks. Each of you have undoubtedly inspired my approach to science and my life.

Dr. Kumar, Satish, I am happy to have joined your research group and to be part of such an amazing research team and family. Kishor, Prabhakar, Huibin, and again, Jo, Ming, Hamza and Narayan, it has been a pleasure working with you. I will miss meeting y'all in the lab and office, our discussions and the coffee breaks. Clive, Sourangsu, Jeff, Po-Hsiang, Eddi, Shruti, Jiawei, Adam, Casey, it was great meeting you, however short was our time together at the research group.

I also want to acknowledge research collaborators that, outside Kumar's research group, directly contributed to the research here presented. Prof. Hendrik Heinz, Dr.

Amanda Garley, Samuel Hoff, Jordan Winetrout at University of Colorado Boulder; Dr. Jin Gyu Park, Dr. Zhiyong (Richard) Liang at Florida State University; Prof. Chao Wang, Dr. Canhui Wang, Han Zong at Johns Hopkins University. Thank you.

Finally, special thanks to Colciencias, Fulbright, Fulbright Colombia, Universidad Nacional de Colombia and Georgia Tech for supporting me, my education and research.

Thank you for reading this and all (or some of) the following lines.

Feel free to contact me to discuss any questions or ideas.

e-mail: pja@gatech.edu

TABLE OF CONTENTS

LIST OF TABLES

LIST OF FIGURES

Appendix E

Appendix F

SUMMARY

This study focuses on making next generation of polyacrylonitrile fibers containing carbon nanofillers, namely carbon nanotubes (CNTs) and carbon black (CB). Mechanically strong and electrically conducting poly(acrylonitrile) (PAN) fibers were obtained by incorporating up to (a) 15 wt% single wall carbon nanotubes (SWNTs) and (b) 15 wt% carbon black (CB) and 2 wt% multiwall carbon nanotubes (MWNTs). These fibers with tensile modulus of up to 32.1 GPa and electrical conductivity of 2.2 S/m rival some intrinsically electrically conducting polymer fibers without doping. Nanocomposite carbon fibers with up to (a) 25 wt% SWNTs and (b) 24 wt% carbon black and 3 wt% MWNTs were also produced, and it is shown that CNT inclusion improves tensile modulus, while the inclusion of CB can be used to lower the carbon fiber cost, while lowering the mechanical properties. Stretchable PAN fibers with up to 60 wt% CB were also produced by increasing the diameter of the CB particles.

Fibers with high SWNT loading of 15 wt% were possible by wrapping the SWNTs with poly(methyl methacrylate) (PMMA). The mechanism of PMMA wrapping of SWNTs was studied experimentally and theoretically (using molecular dynamic simulation). It is shown that PMMA wrapping can be used to increase filler-matrix interaction in the polymer fiber. It is further shown that PMMA wrapping is not detrimental to the filler-matrix interaction in the resulting carbon fiber. This is despite the fact that PMMA does not have carbon yield.

Effect of the carbon nanotubes and carbon black fillers on PAN solution/dispersion rheology has been studied. The effect of these fillers on fiber processability and fiber structure is also comprehensively studied. Research also includes stabilization and carbonization of the conductive CB/PAN nanocomposite fibers via Joule Heating to obtain low-cost carbon fibers.

CHAPTER 1: INTRODUCTION

1.1 Multifunctional and high-performance fibers

Development of synthetic and specialty polymer, ceramic, metallic and composite fibers has been, through recent history, at the center of many scientific developments, from the light bulb fiber[1] to optic fiber[2] and eventually high-speed internet. For tomorrow's more demanding applications, ranging from aerospace industry and electric vehicles to professional level sports goods, multifunctional and high-performance fibers are critical. Presently, planes are made of polymer composites reinforced with carbon fibers which provide mechanical integrity at lower weight than a metal framework.[3] Next generation carbon fibers[4–7] will not only have improved specific tensile strength and modulus, but will also allow for energy storage and/or integration of electric and electronic wiring and components, and for in-situ monitoring of fiber wearing and failure. Next generation of ubiquitous polymer fibers[8–12] will have improved thermal stability, sense fiber damage, serve as biosensors, provide electromagnetic shielding, and will generate heat, on demand, by applying electric current.

Carbon nanotubes could be at the center of many of these next generation fibers. Carbon nanotubes are exceptionally strong, with tensile strength and modulus of 100 GPa and 1 TPa, respectively. Furthermore, depending on the type of carbon nanotube, their optical, thermal and electrical properties can be tuned.[13] Thus, depending on the type of CNT used, it is possible to obtained various multifunctional fibers, e.g. fibers that are both strong and electrically conductive, or semiconducting and responsive to light and electromagnetic stimuli.[14]

Since carbon nanotubes have diameters of a few nanometers, they need to be arranged into macroscopic fibers or yarns to increase safety[15] and to be used in most macroscopic applications. This is done either by a) producing all-CNT yarns[16] or CNT-yarn-based composite fibers,[17,18] or by b) introducing CNTs into polymer fibers.[19,20] The work presented here focuses on the second approach, that allows the use of relatively short CNTs. Furthermore, introduction of CNTs into polymer fibers introduces other controllable variables beyond CNT type, namely, CNT content, matrix properties and filler-matrix interactions. In this work, poly(acrylonitrile) (PAN) was selected as the matrix for spinning of nanocomposite fibers with single and multiwall carbon nanotubes and with carbon black. Carbon black is another carbonaceous nanomaterial, of low-cost and commonly used in polymer industry, which, as discussed later, can also alter the properties of the nanocomposite fiber. PAN is of interest as it is used in textile industry and it is the predominant precursor to obtain high performance carbon fibers.[3,21]

1.2 Carbon Nanotubes (CNTs) yarns

CNT yarns are typically produced from a forest of CNTs[22] (a batch process) or by continuous fiber production by inline densification of CNTs synthesized by chemical vapor deposition.[23,24] Nonetheless, due to defects, impurities, reduced orientation and discontinuous length,[25] the mechanical properties of the macro-fiber (tensile strength of 3.7 N/tex and modulus of ~210 N/tex)[26] are low. Another approach to producing CNT yarns is the spinning of CNT solutions at liquid crystal conditions.[16] Behabtu et al. produced yarns from CNT-chlorosulfonic acid at CNT concentrations in the range of 2 to 6 wt. %.[27] In their contribution, the highest tensile strength and modulus of the CNT yarn was 1.3 and 120 GPa, respectively. More recently, Taylor et al. reported continuous carbon nanotube yarn with tensile strength and modulus of 4.2 GPa and 260 GPa, respectively, and an electrical conductivity of 10.9×10^6 S/m.[16]

Since carbon nanotubes are typically a few micrometers long, the macroscopic yarn typically fails by slippage of the nanotubes due to relatively weak van der Waals forces between them (relative to covalent bonding). To overcome this, post-treatment is performed: torsion of the fiber, densification of the CNTs, chemical functionalization, cross-linking of carbon nanotubes and/or polymer impregnation.[22,25] To the best of our knowledge, the strongest CNTs bundle/yarn yet, has been produced by bundling two ultralong (centimeter to decimeter length) horizontally aligned few-wall CNTs. Tensile strength of this assembled structure was over 80 GPa when measured over a gauge length of 1.5 mm.[28] However, producing this CNT yarn would be cost-prohibiting, and by increasing the bundling size, the yarn diameter (number of nanotubes), and its length, the slippage problems would remain. In fact, when 15 of the same ultralong few-wall nanotubes were bundled, the tensile strength of the resulting yarn was reduced to 57 GPa.[28]

1.3 Polymer-based nanocomposites with CNTs

Composites of polymer matrices with high-performance fillers have been reported to have high mechanical properties. Currently, polymer-carbon fiber composites are commercially used in the structure of aircraft and sporting goods and advanced composites[29] Considering that CNTs have higher specific tensile strength and modulus than carbon fiber, polymer-CNT nanocomposites are of particular interest. However, only a few polymer based nanocomposite systems with high loadings of CNT have been reported to achieve high mechanical properties.[30,31] Furthermore, in most of these reports, the mechanical properties of the CNT-composites are still lower than those predicted by the rule of mixtures.

Unidirectional tensile modulus of composites with fiber-like fillers are typically a volume-averaged value of the two component's tensile modulus: matrix and filler (see

Equation 1-1).[32] For equation 1, V_f and V_m are the volume fractions in the composite of the filler (carbon nanotubes in this case) and the matrix, respectively, and E_f and E_m are the tensile modulus of the filler and the matrix. However, as shown later, tensile modulus of the composite also depends on how the strain is transferred from the matrix to the filler and the effective tensile modulus of the filler which varies with its orientation. A similar rule of mixture can be used to estimate the unidirectional tensile strength of the composite when using a continuous fiber-like filler (see Equation 1-2).[32] Notice however that in Equation 1-2 the matrix tensile strength at the fiber failure strain is used (σ'_{m}), rather than the ultimate tensile strength of the matrix (σ_{m}). Still, as shown later, carbon nanotubes are typically discontinuous fillers, in which case the filler-matrix interactions are more relevant and will modify Equation 1-2.

$$E = E_f V_f + E_m V_m \qquad \text{Equation 1-1}$$

$$\sigma = \sigma_f V_f + \sigma'_m V_m \qquad \text{Equation 1-2}$$

In general, we can define three main parameters that determine how effective the tensile reinforcement of a matrix with a rod-like filler (like CNTs). These parameters are: i) CNT individualization and ii) CNT orientation, and iii) nature of the interface between the filler and the matrix. These parameters are further discussed in the following subsections, and can be summarized as depicted in Figure 1-1.

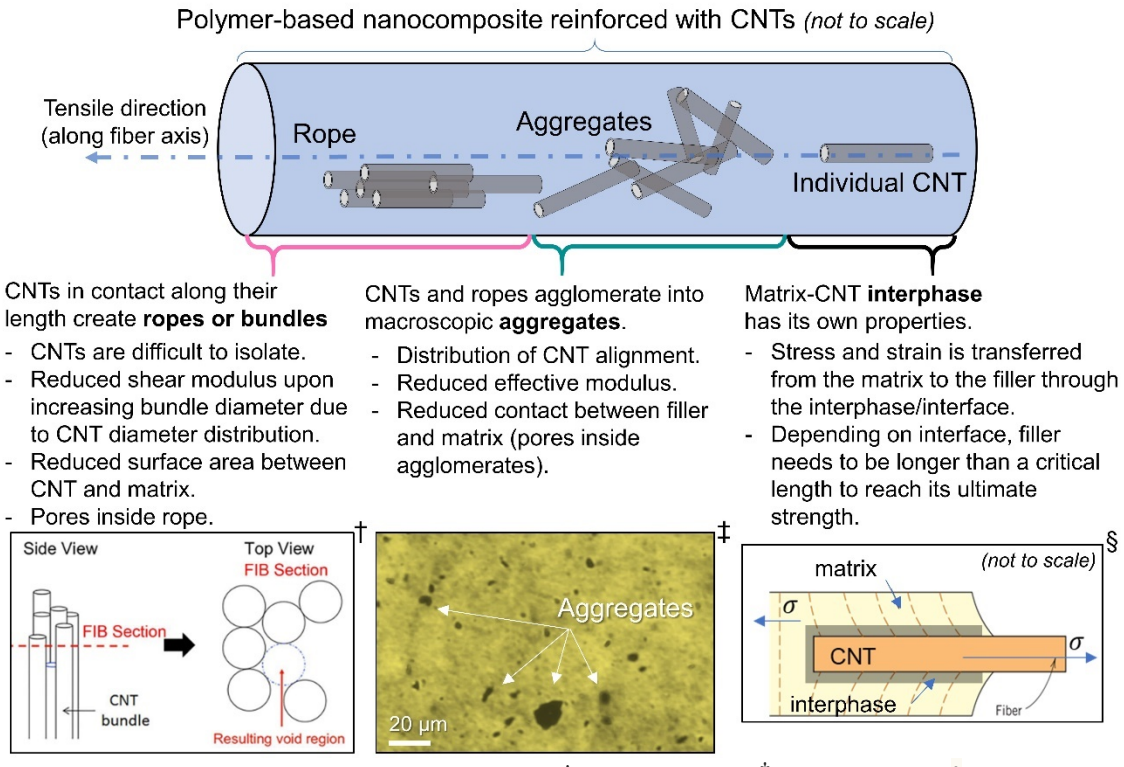

Notes: † *adapted from* [33]; ‡ *adapted from* [34]; § *adapted from* [35].

Figure 1-1. Illustration of a polymer based composite fiber reinforced with carbon nanotubes (CNTs) and the main parameters affecting tensile properties of the composite.

1.3.1 Effect of filler individualization and orientation

CNTs are 1D materials, with a typical aspect ratio from a few hundred to several thousand. Due to these characteristics and their carbon nature (sp^2 bonding), van der Waals forces attract nanotubes to each other, and they agglomerate into ropes and aggregates that are difficult to break (see Figure 1-1). A 'rope' is a crystal-like bundle of CNTs parallel to each other and hold together by van der Waals interactions.[36] Presence of these ropes difficult CNT individualization as it reduces interactions with the solvent or polymer during exfoliation. 'Aggregates' are bigger bundles of individual CNTs or ropes arranged in random orientations. Aggregates can also be described as local entanglements of CNTs and cause a distribution of CNT alignment.[37]

The effect of CNT orientation and individualization on reinforcing of polymer has been documented[30,38] and theoretical models can accurately predict it.[39] If the CNTs are

not perfectly aligned along the tensile deformation direction, the tensile modulus of the filler is reduced. Effective tensile modulus is estimated using Equation 1-3 and depends on the degree of misalignment ($\langle cos^2\,\theta\rangle$ and $\langle cos^4\,\theta\rangle$ are orientation parameters), the longitudinal (E_1) and traverse (E_2) modulus of the CNTs, its in-plane shear modulus (G_{12}) and its poisons ratio (υ_{12}).[39]

$$\frac{1}{E_f}=\frac{1}{E_2}+\left(\frac{1}{G_{12}}-\frac{2\upsilon_{12}}{E_1}-\frac{2}{E_2}\right)\langle cos^2\,\theta\rangle+\left(\frac{1}{E_1}+\frac{1}{E_2}-\frac{1}{G_{12}}+\frac{2\upsilon_{12}}{E_1}\right)\langle cos^4\,\theta\rangle \qquad \text{Equation 1-3}$$

For illustration, consider an individual SWNT misaligned by 5° with respect to the deformation axis, and assuming $E_1 = 750$ GPa, $E_2 = 15$ GPa, $G_{12} = 19.5$ GPa, $\upsilon_{12} = 0.17$ as summarized elsewhere,[39] the tensile modulus is reduced from 750 GPa to ~600 GPa. Even more, if instead of an individual SWNT, it was a 5° misaligned rope of 4.5 nm in diameter (less than 5 SWNTs together), the effective tensile modulus of the filler is further reduced to ~400 GPa due to reduction in the shear modulus to 6 GPa.[40] Finally, as mentioned before, agglomeration also affects tensile strength of the composite, due to slippage between nanotubes and the reduced interfacial area between the matrix and the filler.

Multiple strategies have been studied to improve the individualization and orientation of CNTs in the composite. Higher orientation and individualization can be achieved by post-processing of the composite (solid state processing), typically by drawing.[20] Yet, the effectiveness of this method is limited by the initial individualization of the nanotubes and by interaction forces between the matrix and filler. Higher individualization is also sought by creating better dispersions of the CNTs inside the matrix while still in the flow-state (either in solution or in melt) for fiber processing. Better dispersion and individualization of the nanotubes can be achieved by both mechanical and physico-chemical methods.

Mechanical strategies for CNT individualization customarily consist of ultrasonication, high shear mixing or milling with polymer solution or melt.[37,41,42] However, these mechanical processes also affect CNT integrity, reducing their length and integrity and need to be performed in dilute concentrations of CNTs in order to reach high individualization.[41] Also, once the sonication is stopped the CNTs tend to aggregate again, unless they are kept apart by some chemical or physical barrier. Physical barriers typically consist of polymer coating along the nanotube (or the rope) or surfactants that surround the external wall of the CNTs.[43,44] Surfactants can diffuse into the matrix as undesirable impurities, and polymer coating, if it is a polymer different than the matrix, can in some cases reduce stress transfer from the matrix to the filler, depending on the matrix-coating interactions.

Different strategies of polymer wrapping or coating of CNT have been reported to increase the solubility and dispersibility of CNTs in given matrices or solvents.[44] In fact, non-specific, non-covalent CH-π and polar-π interactions are considered by some authors as a general phenomenon between polymers and CNTs at low concentrations in organic solvents.[45] Modelling supports polymer adsorption on CNTs by the above mentioned forces along with van der Waals interactions.[46] Particularly interesting is the case reported with poly(methyl methacrylate) (PMMA) in DMF, because the polymer chain wraps helicoidally the individual SWNT,[47] while avoiding with it the coating of CNT ropes and aggregates (see Figure 1-2a). PMMA-wrapped-SWNTs, compared to non-wrapped SWNTs, have also been shown to be more stable while in dimethylformamide[47] (Figure 1-2b,c) and to improve filler dispersion in PMMA[48] and polyacrylonitrile matrix.[34] Furthermore, the experimentally observed ordered wrapping of PMMA onto SWNTs contradicts earlier simulation work that concluded non-conjugated, flexible polymers adsorb onto CNTs without order or a with partial order.[49,50] In chapter 2 of the present

document, the adsorption of PMMA and poly(methyl acrylate) (PMA) onto CNTs is studied, along with the effect of the polymer coating on the stability of CNT in organic solvents.

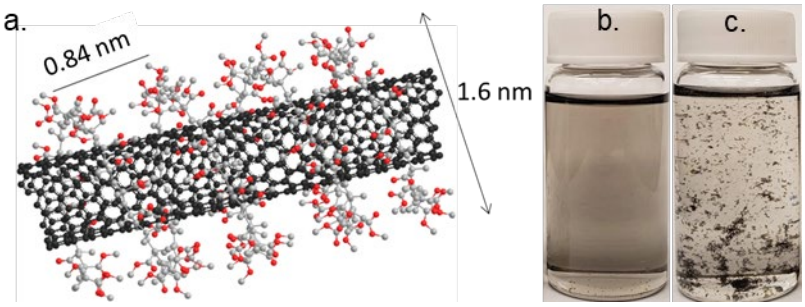

Figure 1-2. Poly(methyl methacrylate) (PMMA) wrapping of single wall carbon nanotube (SWNTs).
Ordered helical wrapping happens around individual SWNTs (a). Dispersion in DMF of the sonicated PMMA-wrapped-SWNTs is stable after one year (b), while sonicated SWNTs without PMMA precipitates a few minutes after sonication stops (c).

Finally, another strategy to perform nanotube individualization is by grafting of polymers[51] and/or chemical functionalization.[37,52,53] These covalent methods generate repulsion between the CNTs, thus resulting in high individualization. Additionally, if chosen properly, the attached groups can also increase interaction between CNT and polymer, increasing the interfacial shear strength (IFSS) between the two. However, formation of any covalent bonding with the CNT wall disrupts its sp^2 structure (to create sp^3 bonds), which ultimately changes the intrinsic properties of the nanotubes.[54] For reference, consider that the energy of sp^3 bond is lower than that of sp^2: 88 and 172 kcal/mol, respectively. For this reason, if surface modification of the CNT is to be performed, multiwall carbon nanotubes (MWCNTs) are preferred, thus only the external wall is affected while the internal ones remain pristine. However, as the number of walls in the CNTs increase, so does its density,[55] which ultimately reduces the specific mechanical properties of the composite.

1.3.2 Nature of the interface/interphase between the filler and the matrix

The final parameter that affects the efficiency of the composite reinforcement is the nature of the interface between the filler and the matrix. It is through this interface that the strain/stresses are transferred from the matrix to the filler.[56] If the interfacial shear strength between the polymer matrix and the filler is low, the composite will fail by filler slippage, and the filler will not reach its ultimate strength. Thus resulting in reduced mechanical properties of the composite.[32]

To ensure that the filler reaches its ultimate strength, the length of the CNT should be a few times longer than the matrix-filler critical length (l_c).[32] Critical length can be calculated by Equation 1-4, and depends on the filler diameter (d), its ultimate tensile strength (σ_f) and the interfacial strength between the filler and the matrix (τ_i). As a rule of thumb, the longer the filler and the higher the interfacial strength, the better the reinforcement. Exceptions to this rule are due to fracture or failure mechanisms, for example, composites with weaker interfacial strength are more probably to present crack arrest and blunting and dissipate energy via post-debond friction and fiber pull-out.[57] Equation 1-5 is the modified rule of mixture (Equation 1-3) to calculate the tensile strength of a composite with a filler length shorter than its critical length (discontinuous fiber reinforcement).

$$l_c = \frac{\sigma_f d}{2\tau_i} \qquad \text{Equation 1-4}$$

$$\sigma_c = \sigma_f V_f \left(1 - \frac{l_c}{2L}\right) + \sigma_m (1 - V_f) \qquad \text{Equation 1-5}$$

For comparison, consider the reinforcement of a PAN fiber (1 GPa tensile strength of neat fiber) with 10 wt. % SWNT (diameter 1 nm and 37.5 GPa tensile strength[58]) of 2 μm or 500 nm in length, and interfacial strength of 47 MPa.[34] The calculated tensile strength of this composite would be 5.2 or 3.7 GPa with CNTs of 2 μm or 500 nm,

respectively. For the example above, the critical length (l_c) is 400 nm. The goal is then to increase the interfacial strength between the matrix and the filler, while using nanotubes that are reasonably long (a few times longer than the critical length).

The interfacial strength or interfacial adhesion between the filler and the matrix is dictated by three different mechanism: i) physical interactions, ii) mechanical interlocking and iii) chemical bonding.[57] i) The physical interactions or the surface energy at the interface is a measure of how compatible one surface is to the other and if intermolecular forces are present. Surface energy is predicted by wettability parameters or solubility parameters and common models include Lifshit-van der Waals approximation[59] and the Hansen Solubility Parameters (HSP) model.[60] ii) Mechanical interlocking is generated due to entanglement or knot effect between the filler and polymer chains. Therefore, increasing the molecular weight of the polymer (radius of gyration and entanglements) increases the chances of mechanical interlocking.[61] Finally, if between the matrix and the filler new bonds are created (ionic, covalent or metallic), the adhesion mechanism is iii) chemical bonding.

All techniques to improve interfacial strength and reinforcement efficiency in composites can be described by these three mechanisms, including those for CNT-polymeric fiber composites. With pristine carbon nanotubes, the intermolecular interactions between the filler and the matrix are of low energy (dispersion forces), and the interfacial strength is supported mostly by physical interactions (no chemical bonding). Therefore, to increase the interfacial adhesion between pristine CNTs and the matrix, the most common alternative is to increase surface area (by improving dispersion of the nanotubes). On the other hand, higher energy interactions can be created by coating and/or functionalization of the CNT surface.[62] In general, many of the strategies used to improve IFSS also lead to a higher individualization of the CNTs, and, with it, to a higher

filler alignment within the composite. That is the case of the non-covalent functionalization of SWNTs with PMMA, that has been shown to increase filler dispersion and filler-matrix interactions while in PMMA[48] and PAN matrix.[34] In fact, up to 1% PMMA wrapped SWNT – PAN fibers have been reported by our research group prior to this thesis study.[34,63] The interfacial shear strength (IFSS) between CNT and polymer matrix increased 44 % (to 47 ± 3 MPa) when CNTs were dispersed following PMMA wrapping strategy, as compared to those CNTs that were dispersed without PMMA.[34] Chapter 3 of the present document focuses on the effect of the non-covalent functionalization of SWNTs with PMMA on the filler dispersion and the filler-matrix interactions when in poly(acrylonitrile) nanocomposite fiber, which significantly modified the nanocomposite tensile mechanical properties.

1.3.3 PAN nanocomposite fibers with CNTs

Several CNT-polymer nanocomposite fibers have been studied, and of special interest are those in which just the polymer matrix (at least in the fiber form) has high tensile mechanical properties (as ultra-high molecular weight polyethylene, UHMWPE) or can be converted by further treatment to materials with high mechanical properties e.g. polyacrylonitrile (PAN) precursor for carbon fibers. In this work, we focus on the use of PAN as matrix. As mentioned earlier, PAN fiber is of interest as it is used in the textile industry and it is the predominant precursor of high performance carbon fibers.[3,21]

Literature reports of PAN fibers with CNTs are summarized in Table 1-1. Inclusion of CNTs in PAN fibers is of further interest as CNT presence increases polymer fiber mechanical properties, electrical conductivity, chemical stability and polymer crystallinity. Furthermore, CNT generates graphitic templating during PAN fiber stabilization and carbonization, which should ultimately improve the mechanical properties of the nanocomposite carbon fiber.[33] Effect of CNT on the cyclization and carbonization of PAN has also been reported while in nanocomposite films.[64]

Table 1-1. Mechanical and electrical properties of various PAN/CNT fibers

CNT content	Type of CNT†	Spinning technique	Tensile modulus (GPa)	Tensile strength (GPa)	Electrical conductivity (S/m)	Ref.
15 wt%	SWNTs	Dry-jet wet-spinning	32.1 ± 0.5	0.83 ± 0.20	2.2 ± 0.5	This work
1 wt%	SWNTs		28.7 ± 2.7	1.07 ± 0.14		[65]
1 wt%	Amino-MWNT in-situ PAN polymerization	wet-spinning	28.4 ± 1.7	0.83 ± 0.05		[66]
1 wt%	FWNTs	Dry-jet wet-spinning	24.5 ± 0.8	1.06 ± 0.11		[67]
1 wt%	FWNTs		22.1 ±3.2%*	1.06 ±10.4%*		[68]
5 wt%	MWNTs		10.8 ± 04	0.41 ± 0.2		[69]
5 wt%	VGCNFs		10.6 ± 0.2	0.33 ± 0.13		[69]
5 wt%	MWNTs		10.8 (13.0)**	0.41 (0.34)**		[70]
10 wt%	SWNTs		16.2 ± 0.8	0.33 ± 0.02		[71]
15 wt%	MWNTs		(7.9)**	(0.20)**	1.2 ± 1.0 4.8***	[70]
0.8 wt%	COOH-MWNTs	Plasticized spinning	10.9	0.47		[72]
0.8 wt%‡	MWNT	wet-spinning	1.3 (1.07)**	0.04 (0.034)**	2.6×10^{-6}	[73]
1.9 wt%	MWNTs in-situ PAN polymerization		9.3		1×10^{-4}	[74]
0.5 wt%	F-Ph-MWNTs		2.5 ± 0.3	0.08 ± 0.006		[75]
3 wt%	MWNTs			0.33 ± 0.02		[76]
0.1 wt%	Oxidized-MWNTs	Electro-spinning§	0.4	0.12		[77]
0.8 wt%	SWNTs		3.8	0.12	2.5	[78]
20 wt%	COOH-MWNTs		4.4	0.04		[79]
20 wt%	Oxidized-MWNTs		14.5	0.28	0.5 – 1.0	[80]

† Single wall carbon nanotubes (SWNTs), Few wall carbon nanotubes (FWNTs), Multiwall carbon nanotubes (MWNTs), vapor-growth carbon nanofiber (VGCNFs), fluoro phenyl functionalization (F-Ph-). ‡ Reported porosity of 85 %. § Measured for the produced fiber mat. * Error reported as coefficient of variation. ** Reported values in N/tex are shown. *** After annealing at 180 °C

However, spinning of PAN fibers reinforced with CNTs is challenging especially at relatively high CNT loading. High performance PAN fibers are obtained by dry-jet wet-spinning.[81] In this spinning technique, the polymer fiber is generated in air from a polymer solution of relatively low solid content and then passes to a coagulation bath in which the gel-fiber is obtained.[81] CNT presence changes the viscoelastic properties of the PAN solution,[82,83] which restricts the operational window to obtain fibers.[84] For that reason, prior to this work, inclusion of single wall carbon nanotubes (SWNTs) in PAN fibers spun by dry-jet wet-spinning had been limited to a maximum of 10 wt%.[71] Furthermore, fiber spinning conditions used in said work[71] limited the PAN and PAN nanocomposite fiber mechanical properties. Chapter 4 of the present work shows that by doing non-covalent functionalization of SWNTs with poly(methyl methacrylate) it is possible to obtained PAN fibers at higher filler loading than that previously reported and with good tensile modulus. This new 15 wt% SWNT PAN nanocomposite fiber and its tensile and electrical properties are included in Table 1-1 for comparison. Chapter 5 focuses on the effect the high SWNT content had on the resulting carbon fibers via conventional furnace stabilization and carbonization.

1.4 PAN nanocomposite fibers with other fillers

Given the industrial importance of PAN and the derived carbon fibers, several other fillers have been included in PAN solution, in order to alter the nanocomposite fiber properties (see Table 1-2). Efforts have been centered in improving mechanical properties, electrical conductivity, flame retardancy, and thermal stability of the polymer fiber, as well as for increasing the mechanical properties and surface area of the resulting carbon fiber. Another common objective of introducing fillers (other than CNTs) in PAN fibers is to reduce cost and to use, in part, renewable materials.

Table 1-2. PAN nanocomposite fibers produced with various fillers, excluding CNTs

Filler † (max. filler content)	Spinning method	Property expected to be affected by filler presence.	Ref.
CB + MWNT (15 wt% + 2 wt%)	Dry-jet wet-spinning	Mechanical reinforcement and electrically conductive polymer. Low cost carbon fiber.	This work
CB (60 – 70 wt%)		Conductive polymer fiber.	
Fe_3O_4 (10 wt%)		Mechanical reinforced and paramagnetic polymer fiber.	85
Cellulose (10 wt%), CNC (40 wt%)		Carbon fiber partially obtained from renewable, low cost source.	86,87
CNC (40 wt%)		Polymer fiber partially obtained from renewable, low cost source.	88
Lignin (30 wt%)		Polymer fiber partially obtained from renewable, low cost source. Porous carbon fiber.	89
BNNT (5 wt%)		Mechanical reinforcement and thermal stability of polymer and carbon fiber.	90
GONR (1 wt%)		Mechanical reinforced and porous polymer and carbon fiber.	91
Fe_3O_4 (9 wt%)	Electrospinning	Magnetic polymer fiber.	92
Fe@Feo (10 wt%)		Magnetic carbon fiber.	93
Fe, Ni, Cr (15.5 wt%)		Carbon fibers for hydrogen storage.	94
Graphene (< 0.1 wt%)	Wet-spinning	Tensile strength and modulus of carbon fiber.	95
GO (1 wt%)		Tensile strength and modulus of polymer fiber – precursor to carbon fiber.	96
Benzoxazine-CB (12 wt%) Ag-CB (20 wt%)		Electrical conductivity.	97
Bioglass (3 wt%)		Biocompatible porous carbon fiber.	98
CoBi-MoS_2 ‡ (2 wt%)		Flame-retardant, mechanically reinforced, porous polymer fiber.	99

†Fillers: carbon black (CB), multiwall carbon nanotubes (MWNT) cellulose nanocrystals (CNC), boron nitride nanotubes (BNNT), graphene oxide nanoribbon (GONR), graphene oxide (GO), Cobalt borate-covered molybdenum disulfide (CoBi-MoS_2).

Carbon black is of special interest as it is a low-cost commodity, electrically conductive, that can induce flame retardancy in polymer matrix.[100,101] Furthermore, given its deep penetration in industry,[102] recent research is focusing in finding environmentally-friendly production pathways.[103,104] Chapter 6 focuses on processing, structure and properties of PAN fiber reinforced with carbon black and multiwall carbon nanotubes and on how this novel fiber can be used to stabilize and carbonize PAN precursor to carbon fiber via Joule heating.

1.5 Thesis objectives and the document layout

The objectives of this project are to study the dispersion of carbon nanotubes (CNTs) in organic solvent and polyacrylonitrile matrix and the effect of carbon nanotubes and carbon black (CB) particles on the processing, structure and properties of polyacrylonitrile (PAN) fibers with high filler loading of up to 15 wt% carbon nanotubes and up to 70 wt% carbon black.

In Chapter 1, relevant literature including previous efforts in dispersing CNTs and CB in PAN is presented.

In Chapter 2, dispersion of carbon nanotubes via non-covalent polymer wrapping is studied. Effect of CNT diameter, solvent used and polymer tacticity is revealed. Results indicate that ordered wrapping of polymer around CNTs is sustained by non-specific CH-π and van deer Waals interactions.

In Chapter 3, single wall carbon nanotubes (SWNTs) helically wrapped with poly(methyl acrylate) (PMMA) are used to produce nanocomposite PAN fibers with up to 5 wt% SWNT. It is demonstrated that PMMA becomes part of the filler-matrix interphase and affects filler-matrix interactions.

In Chapter 4, PMMA-wrapped-SWNTs are used to produce PAN fibers with up to 15 wt% SWNTs. Mechanically strong and electrically conductive nanocomposite fibers are obtained with high filler loading of 15 wt% SWNTs, while significantly reducing the processing time required to obtain the spinning dispersion. Effect of high SWNT loading on the fiber processing and structure is also discussed.

In Chapter 5, carbon fibers with up to 25 wt% SWNTs are produced via convection furnace from the precursor fibers produced in Chapter 4. The PMMA wrapping in the precursor fibers is not detrimental to the filler-matrix interaction in the resulting carbon fiber. This is despite the fact that PMMA does not have carbon yield.

In Chapter 6, PAN fibers with up to 70 wt% CB, as well as fibers containing 15 wt% CB and 2 wt% multiwall carbon nanotubes (MWNTs) are obtained. Effect of carbon black on the fiber processing, structure and properties is studied and discussed. Joule Heating of conductive PAN nanocomposite fibers to stabilize PAN structure and to obtain low-cost and low energy consuming carbon fibers is also explored.

In Chapter 7, the thesis conclusions are presented. Recommendations for future work are discussed in Chapter 8.

Finally, Appendixes A to E contains supplementary information for Chapters 2 to 6, respectively. Appendix F it is shown that SWNTs can be dispersed in co-solvent systems.

CHAPTER 2: NON-COVALENT ORDERED WRAPPING OF CARBON NANOTUBES BY FLEXIBLE, NON-CONJUGATED POLYMERS: CASE STUDY OF TWO ACRYLATE POLYMERS

Preamble

In this chapter, we aim to understand the mechanism behind the non-covalent ordered wrapping of poly(methyl methacrylate) (PMMA) onto single wall carbon nanotubes (SWNTs), using molecular dynamics simulation (MDS) and laboratory experiments.

The MDS results shown here were obtained through an on-going collaboration with Prof. Hendrik Heinz of the University of Colorado Boulder and his team, which included Dr. Amanda Garley, Samuel E. Hoff and Marcus Sharp. Transmission electron microscope images shown in this chapter were provided by Drs Chao Wang and Canhui Wang of Johns Hopkins University.

Some of the experiments in this chapter were published in the manuscript entitled: "*Interaction of Poly(methyl acrylate) with Carbon Nanotubes as a Function of CNT Diameter, Chirality, and Temperature*".[105] This research paper is co-first authored by Dr. Amanda Garley and this thesis author (Pedro J. Arias-Monje), in collaboration with Samuel E. Hoff, Marcus Sharp, Dr. Satish Kumar and Dr. Hendrik Heinz.

2.1 Abstract

The non-covalent ordered wrapping of poly(methyl methacrylate) (PMMA) onto single wall carbon nanotubes (SWNTs) demonstrates that non-conjugated, amorphous, flexible polymer chains can create diameter-specific ordered structures around carbon nanotubes (CNTs). In order to propose a mechanism by which this wrapping happens, we studied the PMMA and poly(methyl acrylate) (PMA) adsorption onto different CNTs (single, few and multi-wall) by sonication in nine different solvents. Effect of PMMA tacticity was also studied. Polymer adsorption and order were determined by thermogravimetric analysis and x-ray characterization, respectively, of buckypapers produced by vacuum filtration. We propose that flexible polymers can create ordered wraps around CNTs when, defined by the polymer conformation, the polymer forms loops and folds around the CNT that are stabilized by π-CH and van der Waals interactions and the CNT curvature. The presence and effect of solvent is pivotal for the orderly wrapping as it can change backbone rotation statistics and polymer conformation. Our proposed mechanism, based on experimental results and molecular dynamic simulations, is not specific to PMMA or acrylate polymers and suggests that the diameter-specific, ordered wrapping of CNT could happen with other flexible, non-conjugated polymers.

2.2 Introduction

Non-covalent adsorption of polymer onto carbon nanotubes (CNTs) has been extensively studied since the discovery of CNTs. Polymer-adsorbed CNTs can be more easily dispersed in solvents and improve filler dispersion in polymer nanocomposites.[44] Furthermore, polymer wrapping has also been used to separate CNTs based on diameter and/or chirality[106,107] and for creating devices in which polymer adsorbed-CNTs are an active or passive component.[108] This adsorption is enabled by various interactions that depend on the polymer structure,[45,109] including π-π, cation-π, NH-π and non-specific π-

CH interactions. The main advantage of using non-covalent adsorption instead of polymer grafting is that the CNT wall structure is left pristine with the former. Also, the adsorption process is relatively simpler than the in-situ polymerization one.

Polymers adsorbed at the surface of CNTs have been shown to have three possible conformations: i) ordered wrapping (typically a helical coil or extended conformation), ii) wrapped with no specific form (but with local order or lamellar-like structure) or iii) adsorbed random coil. Of these, the ordered wrapping is particularly relevant because it allows a stable coating that remains after unbound polymer and solvent are removed.[44] Furthermore, it is expected that the orderly wrapped-CNTs have stronger filler-matrix interactions in the nanocomposites, than when the adsorbed polymer has other conformations instead.[56,110]

Until recently, modeling had shown that the ordered wrapping was exclusively of rigid, conjugated polymer chains,[111] while flexible chains adsorbed with local order or in random coil conformations.[49,50] Because of this, most of the studied systems to do diameter-specific and ordered wrapping of CNTs have used copolymers of fluorene[106,112] and pyridine.[107,113] Uniform coating of SWNTs with polystyrene sulfonate and several polyvinyl pyrrolidone copolymers has also been reported, while in water and aided by surfactant.[113] Similarly, current models explaining CNT diameter-specific polymer binding have only been validated for conjugated, rigid polymers.[114]

However, recent experiments have shown that poly(methyl methacrylate) (PMMA), a non-conjugated, flexible polymer, can create an ordered helical wrap around single wall carbon nanotubes (SWNTs).[47] These recent results of the helical wrapping of PMMA onto SWNTs contradict earlier simulations; probably because said previous simulations used nanotubes of smaller diameter and were done in absence of solvent.[111] Another possible explanation of the divergence of the molecular dynamic simulations with experimental

results is that the former underestimated the effect of π electrons in CNTs.[46] SWNTs with helically wrapped PMMA (PMMA-SWNTs) have already been used to increase filler dispersion and to engineer the matrix-filler interphase in PMMA and PAN composites.[34,48] Furthermore, more recent molecular dynamic simulation has shown that another acrylate polymer, namely poly(methyl acrylate) (PMA), can create folded structures of local order around CNT, depending on the CNT type and diameter and the temperature of the system.[105]

The ordered helical wrapping of PMMA onto SWNTs and the partially ordered adsorption of PMA onto CNTs demonstrates that flexible chains can be adsorbed in an orderly form and in the absence of π-π, cation-π and NH-π interactions between the polymer and CNT. However, there is no understanding yet of what promotes the PMMA helical wrapping of SWNTs while in dimethylformamide (DMF), dimethyl sulfoxide (DMSO) or nitromethane, the only solvents in which the PMMA wrapping have been experimentally studied and shown to occur.[47,63] Understanding of the PMMA wrapping and the PMA partially-ordered adsorption is of high interest because it can give light to, if and how other flexible non-conjugated polymers can show a similar orderly wrapping.

In this contribution, we studied the effect of CNT diameter and solvent in the adsorption of PMMA and PMA, as well as the effect of PMMA tacticity. The observed trends on polymer adsorption and ordered wrapping are compared to the reported experimental and simulated behavior of rigid polymers. Finally, based on the observed trends, a general mechanism for ordered wrapping of CNTs is proposed.

2.3 Experimental

2.3.1 Materials

The various carbon nanotubes (CNTs) used for this study are presented in Table 2-1, along with corresponding average external diameters and catalyst content. The

following solvents were provided by Sigma-Aldrich: dimethylformamide (DMF, ACS grade, 99.8%), toluene (≥99.5%), tetrahydrofuran (THF, anhydrous, ≥99.9%), methyl ethyl ketone (MEK or 2-butanone, ≥99%), 1-methyl 2-pyrrolidinone (NMP, ≥99.5%) and decalin (cis & trans, ≥98%). Ethylene glycol (EG, ≥98%) and 1,4-dioxane, acetonitrile (≥98%), and ethyl acetate (≥99.5%) were provided by Fisher Scientific, EMD and VWR, respectively. The used atactic poly(methyl methacrylate) (a-PMMA, Sigma-Aldrich) had a weight average molecular weight (Mw) of 350,000 g/mol, the isotactic PMMA (iso-PMMA, Scientific Polymer Products) a Mw of 300,000 g/mol and the poly(methyl acrylate) (PMA, Sigma-Aldrich) a Mw of 40,000g/mol. All the used polymers were in solid form and used as received, except the PMA, which was provided as 40 wt.% toluene solution and for which solvent exchange was done with DMF prior to its use in the solutions/dispersions with CNTs and PMA in DMF. Solvent exchange was performed by adding DMF to the PMA/toluene solution without CNTs, followed by vigorous hand shaking and then mild evaporation of the solvent with higher vapor pressure i.e. toluene; the resulting PMA solution in DMF was 5.9 wt.%.

Table 2-1. Various carbon nanotubes used for Chapter 2 experiments.

CNT label	Average external diameter (nm)	Catalyst content (wt.%)	Material reference and provider
SWNT	0.9	< 3	P0271 HiPco type
DWNT	2	< 4	P0-40330
FWNT-1	2.7	< 6	X0-231U
FWNT-2	3	< 2	X0-122U
MWNT-1	8	< 30	Nanocomp
MWNT-2	25	< 5	Cheaptubes

2.3.2 CNT buckypapers production

A typical procedure for the production of CNT buckypapers is described next, this procedure was used in the preparation of all samples, while varying CNT type, solvent

and polymer. Firstly, 14 mg of the polymer were dissolved in 100 ml of the solvent at 50 °C, while 14 mg of the CNTs were added to a separate 100 ml of the solvent and sonicated for 2 h at room temperature. Then, the polymer/solvent and CNT/solvent solutions/dispersions were combined and further sonicated for 24 h. Some selected dispersions were left still after sonication for up to 48 h to qualitatively evaluate dispersion stability. Finally, buckypapers were produced by vacuum filtration of the polymer-CNT dispersions using a PTFE filter with pore size of 1 μm. After the excess solvent was removed, the vacuum filtration continued by adding 20 ml of fresh solvent as a means to wash out excess polymer not adsorbed onto the CNTs. This washing step was repeated twice. Then, the buckypapers were removed from the PTFE filter and left to dry in a vacuum oven for 24 h at 50 °C. Following a similar protocol, CNT buckypapers without polymer were produced for control purposes.

The produced buckypapers will be labeled in the format *polymer/CNT/solvent*, indicating the polymer, CNT type and solvent used, although no solvent remains after sample production. Thus, the a-PMMA/SWNT/DMF sample is the buckypaper produced after filtration of the a-PMMA and SWNT dispersion in DMF.

2.3.3 Characterization

Buckypapers were characterized by thermogravimetric analysis (TGA) and wide-angle x-ray diffraction (WADX). Polymer content of the produced buckypapers was measured by TGA (TA Instruments Q-500) by heating in nitrogen atmosphere at 350 °C until constant weight. Then, atmosphere was changed to air and the temperature was raised to 900 °C to verify the catalyst content of the CNTs. WADX was performed on a Rigaku Micromax-003 with an R-axis IV++ detector at operating voltage and current of 50 kV and 0.6 mA, respectively (Cu $K\alpha$ $\lambda=0.1542$ nm). X-ray data were analyzed with AreaMax and Jade software.

2.4 Results and Discussion

2.4.1 Effect of CNT diameter

PMA content was lower in the buckypapers produced with SWNT and MWNT-2, as compared to all other samples (see Table 2-2), indicating comparably more PMA adsorption onto CNTs of intermediate diameter i.e. between 2.7 and 8 nm than when smaller (1 nm) or larger (25 nm) diameter CNTs were used. XRD characterization showed that the buckypapers with CNTs in the 2.7 to 8 nm range had an increased amorphous signal centered at ~21° 2θ, which corresponded to the PMA amorphous peak (see Figure 2-1). Buckypapers with SWNT and MWNT-2 did not show this amorphous signal as the PMA content was low (see PMA/MWNT-2 in Figure 2-1 and Table 2-2). These experimental results qualitatively agree with those found from molecular dynamic simulations of PMA with SWNTs and DWNT with diameters in the 0.81 to 2.03 nm range.[105]. It has been reported that, in the studied range, PMA adsorption onto CNTs increases with tube external diameter, and that PMA forms a partially ordered structure.[105] These simulations[105] show that, depending on the CNT diameter and chirality, PMA's backbone conformation and side group orientation changes and with it the free energy of binding between polymer and CNT.

Table 2-2. PMA content of the produced PMA/CNT/DMF buckypapers while varying CNTs.

PMA/CNT/DMF buckypaper with indicated CNT	PMA content (wt.%)
SWNT	< 1 %
DWNT	10 %
FWNT-1	13 %
FWNT-2	12 %
MWNT-1	9 %
MWNT-2	< 5 %

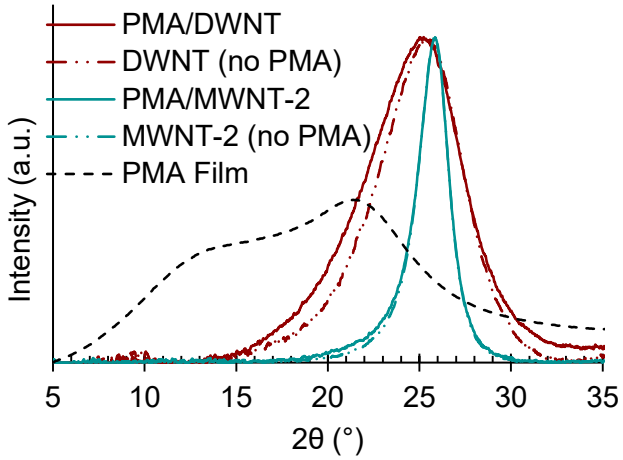

Figure 2-1. WAXD of buckypapers produced with DWNT and MWNT-2 with and without PMA in DMF, and of a PMA film without CNTs.

Dependence of the adsorption of PMMA with CNT diameter has also been observed experimentally. Davijani and Kumar[47] studied the adsorption of PMMA in DMF onto single, few and multiwall carbon nanotubes (SWNT, FWNT-1 and MWNT-2 in Table 2-1). They found that the polymer content was 37, 9 and 7 wt.% in the buckypapers produced with SWNT, FWNT-1 and MWNT-2, respectively,[47] thus suggesting a comparably preferred PMMA-CNT interaction with nanotubes of lower diameter than with those of larger diameter. Furthermore, the x-ray determined ordered helical wrapping of PMMA was observed only with SWNTs and not when FWNTs or MWNTs were used.[47]

Following Davijani and Kumar[47], PMMA wrapped SWNT dispersions were observed in a high resolution transmission electron microscope (HR-TEM). Images were collected on samples obtained by submerging the TEM grid for a few seconds in the SWNT dispersion after the sonication stopped, followed by vacuum evaporation of the solvent. Figure 2-2a,b show the ordered helical wrapping of a the PMMA molecule onto an individual SWNT. Although the sample also contained large diameter SWNT ropes with PMMA attached in random conformation (Figure 2-2c). The helical wrapping observed via HR-TEM had a pitch varying between 1.5 and 3.0 nm, which is about twice that predicted

via molecular simulations (0.83 nm)[47] and measured via x-ray diffraction (0.80 - 0.91 nm see Figure 2-3).

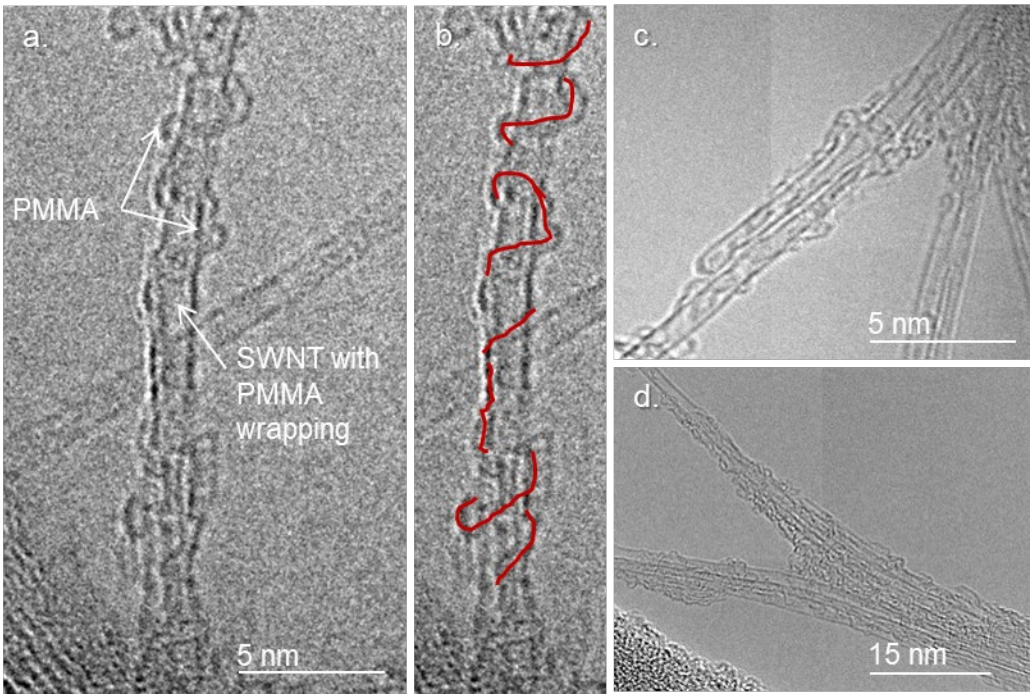

Figure 2-2. HR-TEM images of SWNTs sonicated in DMF and PMMA after solvent removal via evaporation. Polymer wrapping in (a) is highlighted in (b). (c) and (d) show SWNT ropes wrapped with PMMA in random conformation.

2.4.2 Effect of solvent

Experimental results show that the adsorption and ordered wrapping of non-conjugated, flexible PMA and PMMA onto CNTs strongly depends on the solvent used during dispersion. Table 2-3 summarizes the TGA-measured polymer content of each buckypapers produced with PMMA and SWNTs when the changing solvent, while the XRD of selected buckypapers is shown in Figure 2-3. Similar results are presented in Table 2-4 and Figure 2-4 for experiments done with PMA and FWNT-2 when changing the solvent.

The lowest PMMA adsorption was observed when sonication was performed in NMP (14 wt.%), and the largest when DMF and acetonitrile were used instead (~34 wt.%).

The buckypapers produced from dispersion in DMF and NMP showed the crystalline-like peak at 2θ 10.6°, which corresponds to the pitch of the ordered helical wrapping of the PMMA. This ordered wrapping of PMMA has been observed only in two other solvents, dimethyl sulfoxide (DMSO) and nitromethane.[63]

Table 2-3. PMMA/SWNT buckypapers produced in various solvents.
PMMA content of the produced PMMA/SWNT buckypapers while varying solvent. Hansen Solubility Parameter (HSP) interaction distance between solvents and PMMA or CNT, solvent's dipole moment and polarizability, calculated surface tension between SWNT and selected solvent.

Solvent used	PMMA content (wt %)	Solvent *Ra* with *		Solvent properties		SWNT-solvent surface tension (mN/m)*
		PMMA ($MPa^{0.5}$)	SWNT ($MPa^{0.5}$)	Dipole moment (D)	Polarizability ($Å^3$)	
NMP	14 %	2.2	7	12.3	10.7	0.8
Decalin	20 %	11.7	8.4	0	17.4	2.5
Acetone	29 %	6.3	9.2	2.9	6.5	6.0
MEK	30 %	6.0	7.4	2.7	8.2	5.3
DMF	33 %	7.4	10.8	3.9	7.9	1.5
Acetonitrile	34 %	10.0	14.3	3.9	4.4	3.9
DMSO**	NR	7.8	11.6	4.4	8	0.4
Nitro-methane**	NR	10.0	14.4	3.4	4.9	1.5

* Ra is the interaction distance between two molecules, in this case, solvent and PMA or CNT. Individual HSP and surface energy values and their source are found in Table A 1 and Table A 2 in Appendix A, along with the equations used to calculate the corresponding pair parameters. Listed solvent properties were taken from[115,116].
**PMMA ordered wrapping was previously reported[63] without data on polymer content (no reported (NR)).

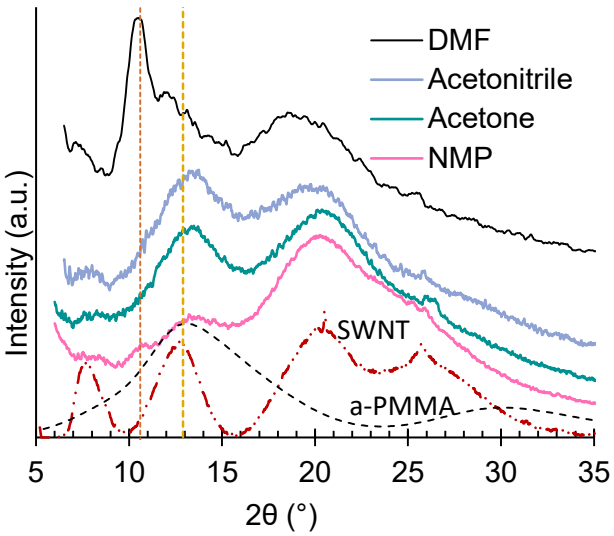

Figure 2-3. Integrated WAXD spectrum of PMMA/SWNT buckypapers produced from dispersions in various solvents.
Vertical lines are centered at 2θ 10.6 and 12.9°, that correspond to the helical pitch of ordered PMMA and the amorphous PMMA signal, respectively.

No direct correlation of PMMA content or presence of the ordered helical wrap can be observed with the Hansen Solubility Parameter (HSP) interaction distances between the solvents and the SWNTs or the PMMA, nor with selected solvent properties like dipole moment and polarizability. However, among the studied solvents, the ordered helical wrap structure was observed only in those buckypapers produced from solvents with which the SWNT-solvent surface tension is lowest, i.e. NMP, DMF, DMSO and nitromethane. However, PMMA content did not correlate with the SWNT-solvent surface tension. The high PMMA content in the buckypapers produced from the dispersions in MEK and acetone (~30 wt.%) in which helical wrapping was not observed, compared to the low PMMA content of the NMP sample (14 wt.%) that had the ordered structure, indicates that the tendency towards helix formation is not necessarily related to the amount of PMMA that is adsorbed at the CNT surface. Thus, it is possible to have high SWNT-polymer interaction but not ordered wrapping, depending on the solvent used.

Table 2-4. PMA/FWNT-2 buckypapers produced in various solvents.
PMA content of the produced PMA/FWNT-2 buckypapers while varying solvent. Hansen Solubility Parameter (HSP) based interaction distance between solvents and PMA or CNT, solvent's dipole moment and polarizability and appearance of the dispersion 48 h after sonication ended.

Solvent used	PMA content (wt %)	Solvent *Ra* with *		Solvent properties		SWNT-solvent surface tension (mN/m) *
		PMA ($MPa^{0.5}$)	CNT ($MPa^{0.5}$)	Dipole moment (D)	Polarizability ($Å^3$)	
THF	< 5 %	1.3	6.1	1.7	7.8	3.4
Toluene	< 5 %	6.8	7.4	0.4	12.4	3.03
DMF	12 %	9.2	9.6	3.9	7.9	1.0
1,4-dioxane	13%	4.0	7.7	0.5	8.6	1.8
MEK	22 %	5.0	7.0	2.7	8.2	4.5
Ethyl Acetate	24 %	3.1	7.7	1.8	8.9	4.7

* Ra is the interaction distance between two molecules, in this case, solvent and PMA or CNT. Individual HSP and surface energy values and their source are found in Table A 1 and Table A 2 in Appendix A, along with the equations used to calculate the corresponding pair parameters. Listed solvent properties were taken from[115,116].

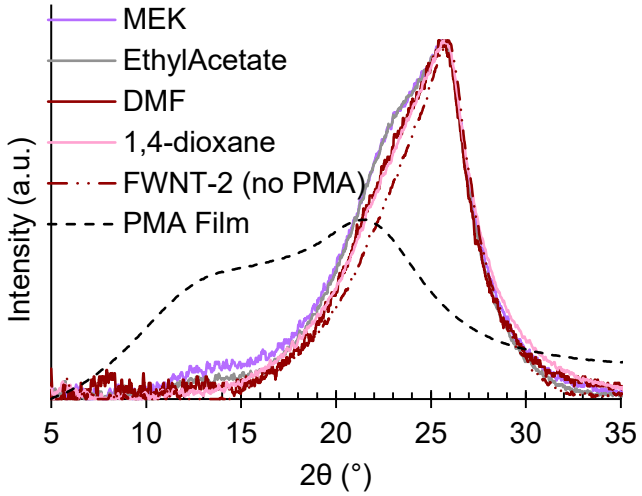

Figure 2-4. Integrated WAXD of PMA/FWNT-2 buckypapers produced in MEK, Ethyl Acetate, DMF and 1,4-dioxane, of a FWNT-2 buckypaper without PMA, and of a PMA film without CNTs.

Changing the solvent used during PMA/FWNT-2 dispersion from DMF to MEK and ethyl acetate increased the PMA content up to 24 wt.% (see Table 2-4). Still, when

comparing the XRD of the FWNT-2 film without PMA and that of the PMA//FWNT-2 buckypapers, only the amorphous ~21° 2θ signal is observed, corresponding to amorphous PMA (see Figure 2-4). Interestingly, PMA/FWNT-2 dispersion in ethyl acetate was not stable and strong precipitation was observed. This happened despite the high solubility of PMA in ethyl acetate (HSP interaction distance of 3.1 $MPa^{0.5}$) and that the PMA/FWNT-2/ethyl acetate buckypaper had the largest PMA content within the studied samples. This suggests that although strong PMA/FWNT-2 interactions were present while in ethyl acetate, the adsorbed polymer molecules did not stabilize FWNT-2, probably due to changes in the polymer conformation, as discussed below. This result also differs from that obtained with PMMA and SWNT in DMF, in which the high polymer adsorption (~33 wt.%) resulted in a stable dispersion over the course of several months (more than 6 months) and after 2 h of centrifugation at 1000g force.[34] High stability of the PMMA-wrapped-SWNTs in DMF was also observed despite the relatively large HSP interaction distance between PMMA and DMF (9.6 $MPa^{0.5}$).

PMA content did not relate to polymer or CNT solubility in the given solvent, nor the listed solvent properties. Furthermore, no ordered wrapping was observed in any solvent, even though CNT surface tension with DMF and 1,4-dioxane were as low as those of the solvents in which PMMA orderly wrapped SWNTs. This demonstrates that ordered helical wrapping is not solely controlled by the CNT-solvent surface tension, although it still is dependent of the solvent used (see Table 2-3 and previous discussion).

2.4.3 Effect of PMMA tacticity in the adsorption of polymer onto SWNT

The WAXD of the SWNT buckypapers produced while changing PMMA tacticity is presented in Figure 2-5. The 2θ 10.6° peak of the ordered helical wrapping of atactic PMMA (a-PMMA) was not observed when isotactic PMMA (iso-PMMA) was used instead. The iso-PMMA/SWNT/DMF buckypaper showed a symmetric broad peak at 2θ 12.9°,

coinciding with the asymmetric amorphous peak of iso-PMMA without SWNTs. The change in breadth and symmetry of this peak reveals that iso-PMMA adsorbed onto SWNTs with partial order, but not in the highly ordered helical conformation that is associated with a-PMMA. Finally, the TGA-measured polymer content decreased from 33 wt% to 25 wt% upon using isotactic PMMA instead of atactic, thus indicating preferred SWNT-polymer interactions upon using the atactic stereoisomer.

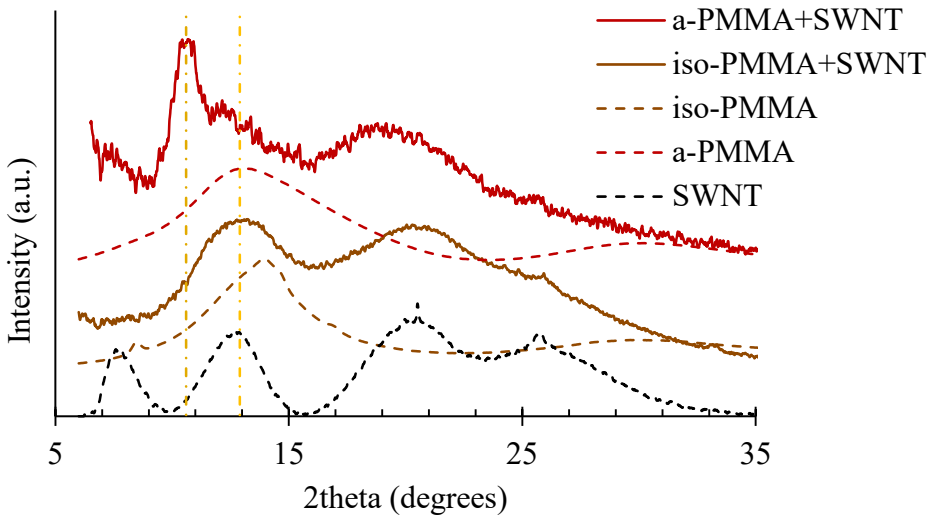

Figure 2-5. WAXD of buckypapers produced from DMF dispersions of SWNT with either atactic PMMA (a-PMMA) or isotactic PMMA (iso-PMMA).
WAXD of each polymer film without SWNT and the SWNTs powder (without polymer) are also included. Vertical lines are centered at 2θ ~10.6 and ~12.9°, that correspond to the helical pitch of ordered PMMA and the amorphous PMMA signal, respectively.

2.4.4 Effect of polymer wrapping on the solubility of the CNT

We argue that the polymer wrapping of CNTs does not necessarily improve CNT solubility in polymer matrices and solvents in which the unbound polymer is miscible. Supporting this is the already described precipitation of the PMA-wrapped FWNT-2 after sonication in ethyl acetate. Similarly, PMMA-wrapped-SWNTs, have been reported to precipitate when DMF solvent is exchanged for ethyl acetate[117] despite the high solubility of PMMA in this solvent. The precipitated SWNTs in ethyl acetate show the ordered helical conformation of the PMMA,[117] indicating that precipitation happens despite the presence

of the polymer wrapping and not because said polymer coating is lost during the solvent exchange.

Solubility of the polymer-wrapped CNTs is probably controlled by the orientation of the side groups and backbone of the polymer adsorbed onto the CNT surface, which could significantly affect solvent-polymer interactions. Effect of the side group orientation on the surface energy of PMA and PMMA films has been previously determined by sum frequency generation vibrational spectra and water contact angles.[118] In their publication, Zhang et al. produced films of PMA and PMMA with varied surface structure i.e. orientation of the methyl ester side group and the polymer backbone. Depending on surface structure, water contact angle changed up to 15°, which signifies the surface energy of the polymers strongly depended on the polymer side group and backbone orientation. Molecular dynamic simulations of PMA onto CNT in vacuum has shown that the polymer chain prefers to adsorb while orienting its methyl ester group outwards the CNT surface.[105] This explains then why the PMA-wrapped-CNTs precipitated in ethyl acetate despite the high solubility of PMA in this solvent. Similarly, for PMMA, the modelled helical conformation shows the preferred orientation of side groups outwards the SWNT surface.[47]

2.4.5 Diameter-dependent CNT wrapping with non-conjugated, flexible polymers

CNT diameter-dependent polymer adsorption and wrapping has been experimentally observed by several other authors,[47,119–122] predominantly with conjugated, semi-rigid polymers of the polyfluorene and poly(p-phenylene vinylene) types. CNT diameter has been previously found to affect CNT interactions with both solvents and polymers. With respect to the CNT-solvent interaction, surface energy[123] and solvent-solubility[124] increase upon increasing tube external diameter. Similarly, polyfluorenes[114] and polyethylene[50] binding to CNT has been estimated to increase with tube external diameter.

The ordered polymer wrapping of CNT of specific diameters has been justified by the effect of CNT diameter and chirality in the polymer-CNT contact and by the effect of diameter in the re-bundling of CNTs. On the one hand, it has been proposed that polyfluorenes selectively wrap CNT with diameters that allow low energy configurations based on the chain torsion angle,[112] and that CNT of certain chiral angles promote polymer adsorption by the alignment of the polymer chain's conjugated groups (π-π interactions).[125] Based on these assumptions, polyfluorenes copolymers with bulky alkyl side groups have been studied to control the CNT diameter at which preferred wrapping happens.[106,126] On the other hand, since CNT-CNT binding energy also increases with CNT diameter,[114,127] it has been argued that the polymer wrapping of preferred CNTs diameter is caused by the competitive process of polymer adsorption and CNT re-bundling.[114]

Experimental studies with polyfluorenes have shown that the selective adsorption on CNTs of certain diameters can be hindered by the solvent system used, arguably due to changes in polymer conformations and CNT solubility in the solvent.[128] This study also suggested that more flexible polymers are less selective of the CNT diameter.[128] Our results show however that the ordered PMMA wrapping of SWNTs (~ 1 nm diameter) can happen in a broad range of solvents that are poor or good with both PMMA and SWNTs (see Table 2-3 and Figure 2-3).

For the wrapping of SWNTs with polyvinyl pyrrolidone (PVP) in aqueous solution and in the presence of sodium dodecyl sulfate (SDS), PVP binding is loss upon addition of tetrahydrofuran,[113] supposedly due to the reduction of the SWNT-water surface tension. This later explanation assumes that the entropic cost of producing an ordered polymer wrap must be offset by reducing the contact area between SWNT and a solvent with which surface energy is high. However, the ordered helical wrap of SWNTs with PMMA was only

observed in solvents with which the SWNTs had low surface energy (see Table 2-3). Similarly, simulations of PMA have shown that, depending on the CNT diameter and not the solvent (or absence of it) the polymer acquires conformations more or less adsorbed to the CNT surface.[105]

Ordered helical wrapping of PMMA onto SWNTs was only observed in solvents with which the CNT had low surface energy (see Table 2-3) because of improved CNT-solvent contact (i.e. wetting). Firstly, reduced surface energy facilitates wetting of the CNTs, upon which sonication can more effectively exfoliate the CNT bundles. Secondly, improved wetting can also reduce the tendency towards CNT reaggregation during sonication, with which time-average CNT-CNT distance increases while in continued sonication. It has been previously estimated that beyond a separation of 10 Å CNT-CNT interactions are zero.[129] It should be noted however that improved wetting does not translate to higher solubility, since the later one also relates to CNT reaggregation after sonication has stopped. Finally, improved wetting and CNT-CNT distance also facilitate the infiltration by polymer molecules between CNTs, while still allowing proximity of the polymer to the CNT during the changes of chain conformations required to create the ordered structure. Still, CNT-solvent surface energy alone does not guarantee the creation of ordered wrapping, as observed for PMA and FWNT-2 in 1,4-dioxane and DMF (Table 2-4).

The question is then, how does the solvent, CNT diameter and polymer tacticity define the adsorption and ordered wrapping of PMMA and PMA in which π-π interactions are not possible? We hypothesize that the ordered wrapping is created when, during the random coiling of the polymer, backbone loops and folds are created and can be stabilized by the CNT curvature through non-specific CH-π and van der Waals interactions and alignment of the polymer backbone with the chiral structure of the CNTs. Solvent plays an

important role here because the it influences the rotational statistics of polymer[130] and the chain persistence length,[131] thus the possible coil conformations. Polymer adsorption and wrapping by this mechanism does not exclusively depend on solvent or polymer properties or specific CNT-polymer interactions. Similarly, ordered wrapping is not more or less likely to happen with less or more flexible polymers; it rather depends on how likely partially ordered conformations of the polymer chain, in a given solvent, can be stabilized by a given CNT diameter.

The result with isotactic PMMA further supports our hypothesis of the ordered wrapping being controlled by chain conformation. Tacticity of the methyl ester and ester groups has been previously shown to modify the solubility parameter and chain conformation of PMMA,[132] polymer rigidity and glass transition behavior[133] along with other properties of the bulk polymer.[134] Chang and Woo[133] studied the glass transition behavior of the miscible blends of iso-, a- and syndiotactic- (s-) PMMA, and observed that the blend glass transition did not correlate linearly with composition. They concluded that this was caused by tacticity-dependent molecular interactions, generated by the polar nature of the side group. Furthermore, the glass transition of pure iso-, a- and s-PMMA are, respectively, ~52, ~107 and ~124°C,[133] showing the strong dependence of the polymer conformation and free space with its tacticity.

Molecular dynamic simulations indicated that partially ordered structures can be created when syndiotactic PMA is adsorbed onto CNTs and stabilized by CH-π interactions, while the polymer backbone twists and folds to follow the CNT curvature and its chiral structure. Figure 2-6 shows snapshots of PMA adsorption onto zig-zag SWNTs with diameters 0.83 and 1.49 nm. Adsorbed PMA has a partially ordered conformation (folded structure) in the SWNT of larger diameter (Figure 2-6b). Figure 2-6c shows that the backbone of the polymer is closest to the SWNT surface (distance < 4 Å) and hence

that the PMA-CNT interactions are of the CH-π and/or van der Waals type. Considering that for the simulated 100-monomer PMA and 1.49 nm SWNT the calculated free energy of binding was about -2 kcal per mol monomer, these interactions generated binding strength equal to several covalent bonds (i.e. 200 kcal/mol).[105]

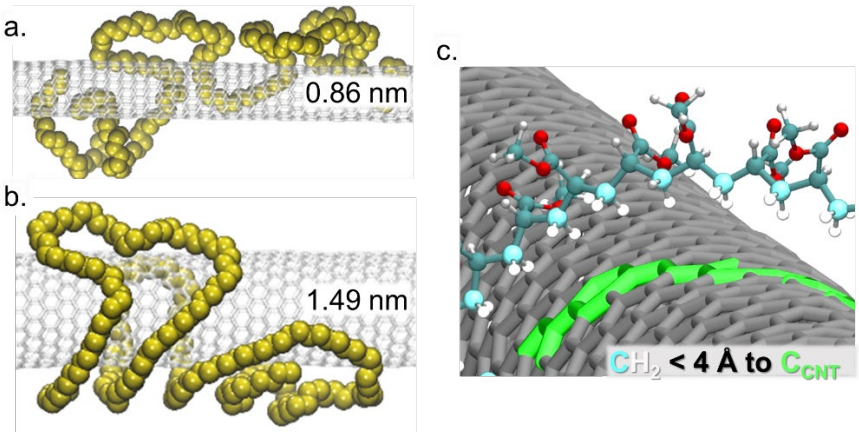

Figure 2-6. Snapshots of polymer backbone adsorbed onto zigzag nanotubes. Adsorption onto SWNTs (a) 0.86 and (b) 1.49 nm diameter after ~ 10 ns in vacuum and at 75 °C. (c) Close up of the adsorbed PMA backbone to the 1.49 nm SWNT. The orientation of the CH_2 towards the surface supports CH-π interactions as a driving force for polymer-CNT binding.

2.5 Conclusions

Similar to what has been previously reported for conjugated and semi-rigid polymers, poly(methyl methacrylate) (PMMA), a non-conjugated, flexible polymer, adsorbs onto CNTs of specific diameter creating an ordered helical wrapping. We report here that this ordered wrapping and the amount of PMMA adsorbed depends not only on the CNT diameter but also on the solvent and polymer tacticity. However, ordered wrapping and amount of PMMA adsorbed are not directly related to polymer or CNT solubility in the solvent, or solvent properties, neither to CNT surface energy with the given solvent. Absorption of poly(methyl acrylate) con CNTs was also shown to depend on the CNT diameter and solvent used. PMA has been shown by molecular dynamic simulations (MDS) to adsorb onto CNTs in vacuum while creating partially ordered structures.

Furthermore, MDS results confirm that adsorption of PMA is sustained by CH-π and van der Waals interactions that are non-specific to acrylate polymers.

Based on the experimental and simulation results detailed here, we propose that non-conjugated, flexible polymers can adsorb onto CNTs, creating partially and fully ordered structures. This occurs when certain conformations of the polymer can be stabilized by the CNT curvature and its interaction with the polymer backbone.

3 CHAPTER 3: EFFECT OF PMMA MOLECULAR WEIGHT IN SWNT DISPERSION AND COMPOSITES' PROPERTIES AT LOW SWNT LOADING (5 wt%)

Preamble

In this chapter, we demonstrate that the interphase between SWNTs and the PAN matrix in PAN nanocomposite fibers can be engineered by wrapping PMMA around the SWNTs and by changing the PMMA molecular weight. PAN fibers in this Chapter 3 have 5 wt% SWNTs.

Chapter 3 and Appendix B are already published as "*Engineering the Interphase of Single Wall Carbon Nanotubes/Polyacrylonitrile Nanocomposite Fibers with Poly (methyl methacrylate) and Its Effect on Filler Dispersion, Filler−Matrix Interactions, and Tensile Properties*"[34] manuscript first-authored by the author of this thesis (Pedro J. Arias-Monje) and in collaboration with Dr. Amir A. Bakhtiary Davijani, Mingxuan Lu, Jyostna Ramachandran, Mohammad Hamza Kirmani and Dr. Satish Kumar. PAN fibers with 1 wt% SWNT were produced and characterized by Dr. A. A. B. D. during his Ph.D. thesis.

3.1 Abstract

Mechanical reinforcement of polymer nanocomposites with pristine Single Wall Carbon Nanotubes (SWNTs) beyond 1 wt. % loading is challenging because SWNT-SWNT contacts generate filler aggregation and reduce polymer-filler interaction. Furthermore, SWNT cannot be covalently functionalized without affecting their inherent properties. In this study, filler individualization and filler-matrix interactions were tuned by helically wrapping the SWNTs with poly(methyl methacrylate) (PMMA) -a non-covalent method- and by changing the PMMA molecular weight. Polyacrylonitrile nanocomposite fibers were produced by dry-jet wet spinning using 5 wt. % PMMA-wrapped-SWNTs. It is demonstrated that PMMA-wrapping becomes part of the filler-matrix interphase. Increasing the molecular weight of the PMMA wrapping improves SWNT individualization but appears to reduce filler-matrix interaction. Relatively high fiber mechanical properties were obtained when SWNTs wrapped with relatively low molecular weight (15000 g/mol) PMMA were used. Potential applications of these fibers have been discussed.

3.2 Introduction

Sonication of dispersions of single wall carbon nanotubes (SWNTs) with poly(methyl methacrylate) (PMMA) in dimethylformamide (DMF) has been shown to produce an ordered wrapping of PMMA around the SWNTs[47] (Figure 1-2a in Chapter 1). Figure 3-1a shows the normalized (normalized to the ~1590 cm^{-1} signal) Raman spectra of fibers produced with 1 wt.% SWNTs when the SWNTs were PMMA wrapped (PAN/PMMA-SWNT) or pristine (PAN-p-SWNT). Typical radial breathing mode (RBM), D, G and G' Raman peaks of the SWNTs are observed. Intensity ratio of D/G peaks was the same in the PAN fibers reinforced with pristine (p-SWNT) and PMMA-wrapped (PMMA-SWNT) fillers, indicating that no change in the SWNT's sp^2 structure during the wrapping process. In other words, PMMA modification is non-covalent. The RBM normalized to the

233 cm^{-1} band is presented in Figure 3-1b, as a function of filler type and fiber draw ratio. The RBM peak that most strongly changed upon PMMA wrapping of the SWNT was that at ~ 268 cm^{-1}, which is referred to as RBM2. A list of observed RBM peaks is given in Figure B 2. The peak at 268 cm^{-1} is a function of SWNT-SWNT interactions caused by agglomeration,[135,136] and can therefore be used as a qualitative indicator of SWNT individualization when compared to the total RBM area. RBM2 relative intensity was significantly lower in samples produced with PMMA-SWNT than in those with p-SWNT, indicating then a higher degree of filler individualization in the former case.

Upon drawing of the nanocomposite fibers, RBM2 intensity strongly decreased in the PAN fibers with p-SWNT and showed a small increase in those with PMMA-SWNT. It was previously reported that drawing of CNT/polymer nanocomposite fibers promotes exfoliation of the nanofiller,[65] which is consistent with the described behavior of the PAN/p-SWNT fiber. The increase of the RBM2 intensity upon drawing of the fiber with PMMA-SWNT suggests that SWNT-SWNT contacts and/or SWNT bundles are created, probably due to polymer crystal growing in the bulk of the matrix. Another explanation to the observed phenomena is the increase in SWNT-polymer packing density after drawing and its possible effect on the SWNT RBM spectra. It has been reported that not only substrate or bundling affect the resonance window profile of the SWNT, but also the presence of surfactants or other species adsorbed onto the SWNTs.[137,138]

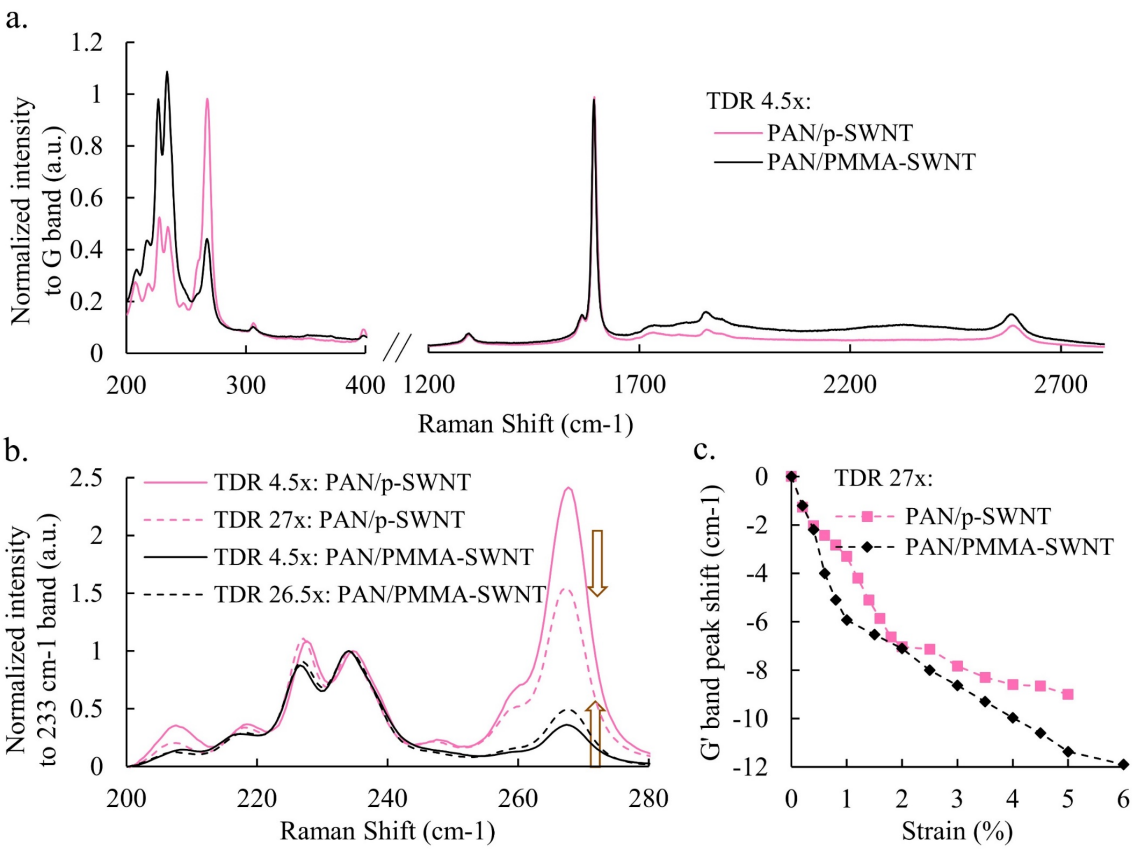

Figure 3-1. Raman characterization of PAN nanocomposite fibers with pristine-SWNTs (PAN/p-SWNT) and PMMA-wrapped-SWNTs (PAN/PMMA-SWNT).
(a) Raman spectra using un-polarized laser of PAN/p-SWNT, and PAN/PMMA-SWNT fibers of draw ratio 4.5x. (b) RBM profiles of various fibers at listed total draw ratios (TDR). (c) Shift of the SWNT G' band upon straining of the fully drawn nanocomposite fibers as listed in Table 2.

Figure 3-1c presents the observed shift of the G' peak upon straining the macroscopic fiber, which was used to estimate the straining of the SWNT and the interfacial shear force (IFSS) between the filler and the matrix. Please refer to the Appendix B.1 and ref[67] for detailed explanation of the SWNT straining and the IFSS calculations. Maximum G' shift was -9.0 ± 0.7 and -12.5 ± 0.9 cm^{-1} for the PAN fiber with p-SWNT and PMMA-SWNT, respectively. The maximum strain experienced by the SWNT upon fiber straining was 0.24 and 0.34 %, for PAN/p-SWNT and PAN/PMMA-SWNT fibers, respectively. Overall, the IFSS increased from 32.9 ± 2.7 to 47.5 ± 3.2 MPa upon using PMMA-wrapped SWNTs instead of p-SWNTs. An increase in the IFSS is expected

when increasing the filler-matrix surface area (improving filler dispersion) and/or increasing the interactions between the filler and matrix, and this generally translates to improve mechanical properties of the composite.[56,139] PAN nanocomposites fibers with 1 wt.% Few Wall Carbon Nanotubes (aspect ratio ~2800) have been previously reported to have an IFSS of 30.9 MPa, and up to 44.3 MPa when lower filler loading of 0.1 wt.% was used. The experimental and theoretical IFSS values for several other CNT/polymer systems can be found in recent reviews.[62,139] However, it should be noted that comparison of absolute IFSS values of different systems reported based on different measurement protocols is difficult, due to the plethora of factors that affect these values. Still, the increase in IFSS upon PMMA-wrapping translated to a modest increase in the mechanical properties of the nanocomposite fiber.[34] Improvement in IFSS and mechanical properties of the composite has also been reported when the PMMA-wrapped-SWNTs are incorporated in PMMA films.[48]

It is of interest to understand and to deconvolute the two mechanisms by which the use of PMMA-wrapped-SWNTs increases IFSS: i.e. (i) by direct modification of the filler-matrix interactions, and (ii) by changing the filler dispersion and hence the available polymer-SWNT surface area.

In this chapter, the effect of the PMMA molecular weight on SWNT dispersion and on the structure and mechanical properties of PAN nanocomposite fiber is studied. It is shown that the PMMA wrapping remains after spinning and consequently becomes part of the filler-matrix interphase.

3.3 Experimental

3.3.1 Materials

SWNT HiPco™ (grade sp300, lot # PO 271) with an average diameter of 0.9 nm were obtained from Carbon Nanotechnologies Inc. SWNTs had a 2 wt.% catalyst content

as measured by Thermo Gravimetric Analysis (TGA). A list of the observed chiralities by Raman from 785 nm laser is included in the Appendix B (Figure B 2). Poly(methyl methacrylate) (PMMA) of weight-average molecular weight (Mw) of 15,000, 350,000 and 996,000 g/mol and dimethylformamide (DMF, ACS grade, 99.8% purity) were obtained from Sigma-Aldrich. PMMA with Mw of 97,000 g/mol was acquired from Supelco (Sigma-Aldrich). Poly(acrylonitrile-co-methacrylic acid) (PAN, 4 wt. % copolymer) with viscosity average molecular weights of 247,000 and 500,000 g/mol were obtained from Japan Exlan Co. (Osaka, Japan).

3.3.2 SWNTs helically wrapped with PMMA

SWNTs were dispersed in DMF in the presence of PMMA in a sonication bath for 24 hours at room temperature. SWNT:PMMA mass ratio was 1:1, and SWNT content during dispersion was 5 mg SWNT/dL in DMF. This protocol has been previously reported[47] and allows for the production of SWNTs helically wrapped by PMMA. This PMMA-wrapped-SWNT will be referred hereinafter as PMMA-SWNT.

DMF/SWNT dispersions with and without PMMA were characterized by Raman, UV-Vis spectroscopy, and dynamic light scattering (DLS). UV-Vis spectra were collected on a Perkin Elmer Lambda 35 from 300 nm to 1000 nm. Raman spectra were collected using a HORIBA XploRA ONE (785 nm laser) spectrometer with 50x or 100x objective and 1800 grating. DLS was conducted using a BI-200SM system (Brookhaven Instruments co.), by collecting the scattered signal from a linearly polarized 532 nm laser at 90°, collection time was 2 min while solutions were kept at 25 °C. For DLS and UV/Vis measurements the dispersed 5 mg SWNT/dL in DMF were further diluted to 1:20 ratio by mass in DMF.

3.3.3 PAN/DMF solutions with PMMA-wrapped-SWNTs

DMF/PAN/PMMA-SWNT dispersions for fiber spinning were prepared by first dispersing the desired amount of PAN in 100 ml of DMF by continuous mixing (at 150 rpm) for 1 h at 0 °C. Then the temperature was gradually raised to 70 °C to dissolve the polymer, and the polymer solution was further mixed for 1 h at 70 °C. Subsequently, PMMA-SWNT in DMF were added to the polymer solution and the excess solvent was distilled under vacuum (< 40 mbar) at ~70 °C, until reaching the desired amount of SWNT in the PAN solution. Solid content of the spinning solutions was measured by TGA (Q500, TA Instruments) by heating to 130 °C in air atmosphere until constant weight was achieved. Rheology of spinning dispersions was measured using an ARES rheometer in frequency sweep mode between 0.5 and 500 rad/s, strain of 1% and at room temperature. Parallel plates of 25 mm and 1 mm gap were used.

3.3.4 Nanocomposite fibers

For spinning, a system by Hills Inc. was used, with a single filament set-up with 200 μm diameter spinneret. Polymer dispersions were extruded at a flow rate of 1 cc/min. For this study, two different sets of fibers were produced. Barrel, spinneret and coagulation bath temperatures can be found in Appendix B (Table B 3). The air gap between the spinneret and the coagulation bath was 3 to 5 cm in all cases. Fibers were collected at a stretch ratio of 3x and stored overnight in methanol bath at -40 °C prior to a two-stage drawing. Cold drawing (1st stage drawing) was done while keeping the as-spun fiber submerged in methanol chilled at -40 °C and hot drawing (2nd stage drawing) by passing the fiber through a glycerol bath at 165-175 °C. Two-step drawing has been previously demonstrated to significantly increase the tensile properties of high-performance polymer films[140] and fibers.[141] Total draw ratio is calculated as the product of the spinning stretch ratio, the cold draw ratio and the hot draw ratio. All as-spun fibers have a total draw ratio

of 3x (no further drawing after fiber spinning), while fully drawn fibers refer to fibers that were stretched at about 80% of the draw ratio at break during the two-stage drawing. The 80% of the breaking draw ratio was selected to achieve high modulus, while ensuring continuously drawn fiber without significant breaks.

A summary of the fibers produced is presented in Table 3-1. Two different PMMA molecular weights were used for the wrapping of the SWNTs: 15,000 and 350,000 g/mol. Thus, two PAN composite fibers were produced, one with 5 wt.% SWNT wrapped with PMMA of 15,000 g/mol (referred as: PAN/15k.PMMA-SWNT) and a second one with 5 wt.% SWNT wrapped with PMMA of 350,000 g/mol (referred as: PAN/350k.PMMA-SWNT). Both nanocomposite fibers had 5 wt.% SWNTs, but considering the PMMA:SWNT ratio used, PAN content was 90 wt.%. The control fiber without SWNTs for this sample set is referred as PAN-b.

Table 3-1. Various fibers produced in chapter 3.

Fiber ID	PAN molecular weight (g/mol)	SWNT content* (wt.%)	PMMA molecular weight (g/mol)
PAN-b	500,000 g/mol	0	-
PAN/15k.PMMA-SWNT		5	15,000
PAN/350k.PMMA-SWNT		5	350,000

*Note: SWNT content refers to the amount of SWNT without considering the PMMA wrapped around the SWNTs or free in the nanocomposite fiber.

Fibers were characterized by wide angle x-ray diffraction (WAXD) (bundles of 64 filaments) and Raman spectroscopy (single filament). WAXD was conducted on a Rigaku MicroMax-003 beam generator (Cu $K\alpha$ $\lambda = 0.1542\ nm$, operating at 50 kV and 0.60 mA) equipped with an R-axis IV++ detector. Raman characterization included SWNT's orientation factor determination using a polarized incident laser, by measuring the change of the G band intensity as a function of fiber orientation (VV configuration), as reported elsewhere.[142] SWNT straining during deformation of the macroscopic fiber was evaluated

by measuring the displacement of the G' band upon strain of a 1-inch filament, as reported elsewhere[67] and detailed in Appendix B.1. All the reported Raman-based data, including orientation and SWNT strain are an average of measurement on at least three different samples. Scanning Electron Microscopy (SEM) images were collected from the uncoated samples at an accelerating voltage of 3 kV and at a working distance < 4 mm on a Hitachi SU8230. The reported diameter of the observed fibril-like structures is based on more than 35 measurements in at least 3 different samples per fiber type. Single filament tensile testing was performed on a FAVIMAT+ (Measured Solutions, Inc.) using a gauge length of 1 inch, and a strain rate of 1%/s. Linear density was determined by inline vibroscope.

3.4 Results and discussion

Prior to nanocomposite fiber spinning, DMF/PMMA/SWNT dispersions and PMMA-SWNT buckypapers were prepared while changing the molecular weight of the PMMA. This was done to evaluate the effect of PMMA molecular weight on SWNT dispersion. The measured hydrodynamic radius and the UV/Vis absorbance spectra of the dispersions are presented in Figure 3-2. Figure 3-2b also shows the UV/Vis spectrum of SWNT sonicated in DMF without PMMA. Normalized RBM band and XRD of the buckypapers produced by vacuum filtration of the dispersions are included in Figure 3-2c and d.

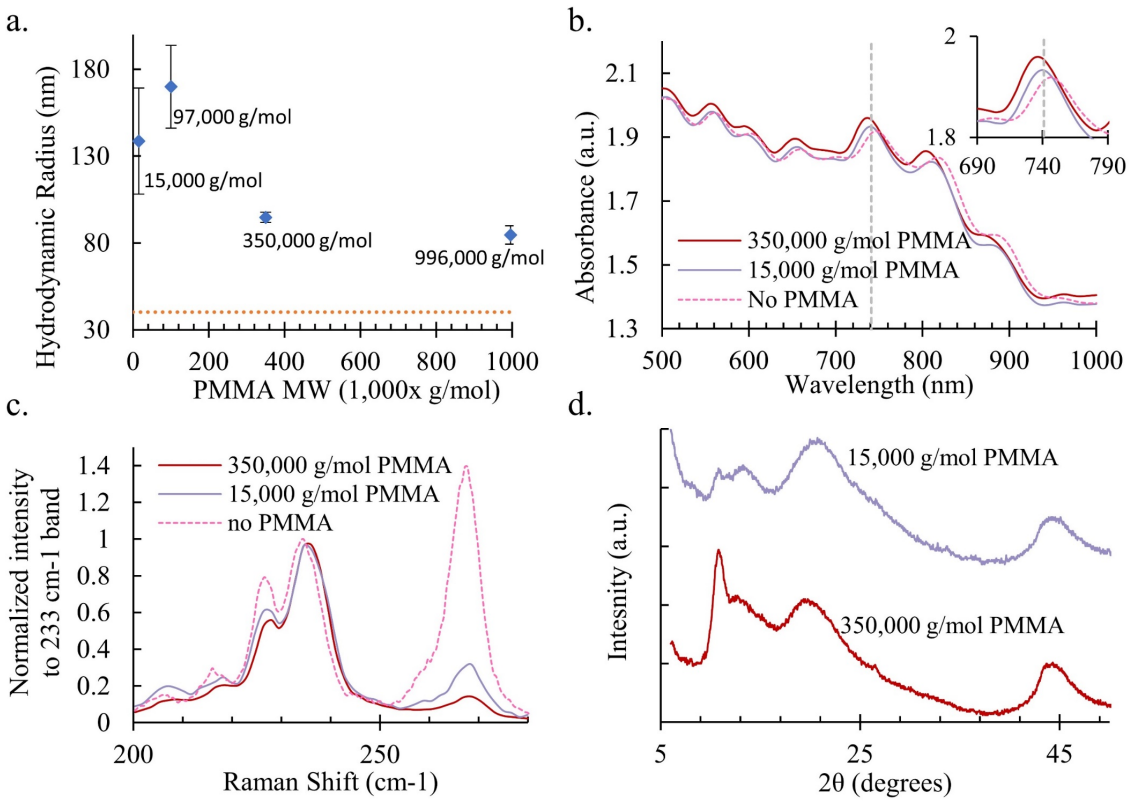

Figure 3-2. Measured (a) hydrodynamic radius and (b) van Hove transitions of PMMA/SWNT dispersions in DMF, and the (c) RBM band Raman spectra and (d) X-ray diffraction of produced buckypapers using various PMMA molecular weights (as listed in respective figures) for SWNT wrapping.
Dotted line in (a) shows the estimated hydrodynamic radius for an individual SWNT of 1 nm diameter and 500 nm length.

A higher PMMA molecular weight was associated with a smaller hydrodynamic radius, and larger shift of the van Hove transitions towards shorter wavelength in SWNT dispersion in DMF, as well as a lower relative intensity of the RBM2 peak in the buckypapers. These results indicate that increased PMMA molecular weight resulted in reduced SWNT bundle size and decreased SWNT-SWNT contacts, thus increased SWNT individualization. On the other hand, the DMF/SWNT dispersion without PMMA showed larger hydrodynamic radius, higher RBM2 intensity and red-shift of the van Hove transitions, as compared to than the dispersions that contained PMMA (see Figure 3-2b and c). Measured hydrodynamic radius was larger than 300 nm for pristine-SWNT sonicated in DMF, and macroscopic agglomerates were observed as soon as sonication

stopped. PMMA-SWNT dispersions in DMF remained stable for many-many months (more than 6 months) after stopping the sonication. They were also stable after 2 hours of centrifugation at 1000 g-force, and did not result in sedimentation. Unstable dispersions of pristine-SWNT in DMF has been previously documented.[64,124] Finally, longer PMMA molecules created stronger 10.8° 2θ X-ray diffraction peak (Figure 3-2d), which has been associated with the ordered helical wrapping of PMMA around the SWNT.[47]

The reason for the improved SWNT individualization with increased PMMA molecular weight can be analyzed by comparing the data presented in Figure 3-2 and the amount of PMMA fixed to the SWNTs after sonication with PMMA of various molecular weight. The amount of PMMA adsorbed onto the SWNTs has been previously estimated[47] by thermal gravimetrical analysis (TGA) of the buckypapers produced by filtration of sonicated DMF/PMMA/SWNT dispersions. It is assumed that during filtration and extensive washing, polymer molecules not strongly attached to the SWNTs are removed; and that for the PMMA-SWNT system most of the PMMA in the buckypaper is helically wrapped around the SWNTs. It has been reported that regardless of the PMMA molecular weight (range of 8,000 to 996,000 g/mol), the buckypapers contained ~37% PMMA,[47] signifying that the amount of PMMA wrapped to the SWNTs does not depend on the polymer molecular weight. However, an increase in the 2θ ~10.8° peak intensity was observed upon increasing PMMA molecular weight (Figure 3-2d). These results indicate that for the conditions studied here, the increase of the SWNT individualization with increase in the PMMA molecular weight (Figure 3-2a-c) must be due to the increase of the PMMA helix order (Figure 3-2d), and not to the amount of PMMA wrapped. Upon wrapping with longer polymer molecules, the number of chain ends is reduced, which translates in fewer chances of helix disruption and fewer chances of the exposed surface of the SWNTs and, consequently, less SWNT-SWNT contacts. This can be further illustrated by

estimating the number of PMMA molecules required to wrap any given SWNT length. For example, a SWNT length of ~140 nm is helically covered by one PMMA molecule of molecular weight of 350,000 g/mol. To cover the same SWNT length with PMMA of molecular weight of 15,000 g/mol, 23 PMMA molecules are needed. Assumptions used for these calculations are given in Appendix B.2.

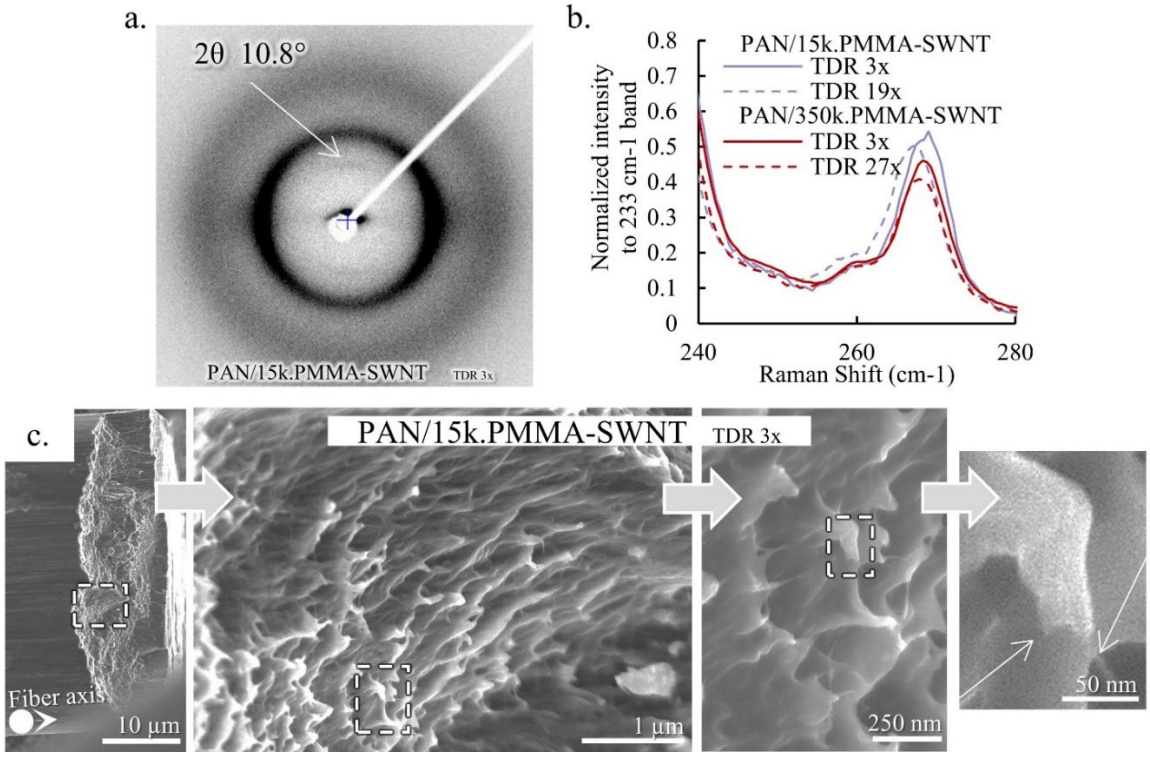

Figure 3-3. XRD, Raman and SEM characterization of PAN nanocomposite fibers with PMMA-wrapped-SWNTs with different PMMA molecular weight: 15,000 g/mol (PAN/15k.PMMA-SWNT) or 350,000 g/mol (PAN/350k.PMMA-SWNT).
(a) WAXD pattern of the as-spun PAN fiber with 5 wt.% SWNTs wrapped with PMMA of 15,000 g/mol (PAN/15k.PMMA-SWNT). The 2θ peak intensity at 10.8° at the meridional position is indicated by an arrow for clarity. (b) RBM2 peak for fibers produced with PMMA-wrapped-SWNTs of two different molecular weights before and after drawing. Molecular weight of PMMA are 15,000 and 350,000 g/mol, in fibers PAN/15k.PMMA-SWNT and PAN/350k.PMMA-SWNT, respectively. (c) SEM images at different magnifications of the fibrillar-structures present at the cross-section of as-spun fiber PAN/15k.PMMA-SWNT. White arrows in right-most image indicate one carbon nanotube and one site of plastic deformation (probably caused by a second carbon nanotube) in the same fibril.

Effect of polymer molecular weight during non-covalent wrapping of carbon nanotubes in the filler-filler contacts and dispersion has been previously documented. Polyvinylpyrrolidone (PVP) and poly(4-vynilpyridine) have been used to wrapped Multiwall Carbon Nanotubes (MWNT),[143] significantly increasing MWNT dispersion upon increase of polymer molecular weight.

The effect of PMMA molecular weight used for SWNT wrapping was also investigated in PAN nanocomposite fibers with SWNT content of 5 wt.% (see Table 3-1). SWNTs wrapped with PMMA of 15,000 and 350,000 g/mol were used and since the PMMA:SWNT ratio was 1:1, the PAN content of these fibers was 90 wt.%. Rheological data and optical images of the polymer dispersions used for fiber spinning are presented in Figure B 3 at Appendix B. Polymer solutions containing higher PMMA molecular weight used for SWNT wrapping resulted in better filler dispersion and a lower complex viscosity at 1 rad/s, as compared to the solutions using lower molecular with PMMA (see Figure B 3).

Both as-spun (total draw ratio of 3x) nanocomposite fibers with 5 wt.% SWNT wrapped with PMMA showed a 2θ peak at 10.8° (see Figure 3-3a, only 2D image of fiber with PMMA wrapping of 15,000 g/mol is shown). This peak was not evident in the fibers with 1 wt.% SWNT (PAN/PMMA-SWNT), which can be attributed to the low filler content. Furthermore, the 10.8° peak signal was present only in the meridional component of the WAXD, indicating that the PMMA ordered structure was along the fiber axis and, therefore, along the SWNT axis. This shows that SWNTs were still helically wrapped by the PMMA after solution processing and gel spinning, and should therefore be considered part of the SWNT-PAN interphase in the fiber. The 10.8° peak almost disappeared after fiber drawing of the fibers, see Figure B 4 in Appendix B. Absence of this peak indicates that the highly

ordered helical structure gets disturbed/smeared by the shear forces present during fiber drawing.

Figure 3-3b shows the normalized RBM2 peak of the nanocomposite fibers with 5 wt. % SWNT wrapped with PMMA of two different molecular weights before and after drawing. RBM2 intensity was slightly lower in the fibers with nanotubes wrapped with PMMA of higher molecular weight (PAN/350k.PMMA-SWNT), as compared to the lower molecular weight PMMA. RBM2 intensity decreased upon fiber drawing, in fibers with both PMMA molecular weight. The reduction in the relative intensity of the RBM2 band upon drawing of the 5 wt.% SWNT fibers with PMMA-wrapped filler differs from the behavior observed for fibers with 1 wt.%.[34]

Figure 3-3c presents several images at different magnifications of the fracture surface of the as-spun fiber produced with SWNTs wrapped with PMMA of 15,000 g/mol (PAN/15k.PMMA-SWNT (TDR 3x), showing fibrillar-structure formed by SWNTs and the associated polymer. Within one fibril, there may be one SWNT or more than one SWNT, individualized or bundled. These fibrillar structures are a result of plastic deformation. Diameter of the observed structures were 57 ± 6 and 32 ± 3 nm for the as-spun fibers PAN/15k.PMMA-SWNT and PAN/350k.PMMA-SWNT, respectively. Comparative additional SEM images are available in Figures S5 and S6. Diameter of these fibrillar structures should be expected to be a function of SWNT bundle size and filler-matrix interaction. Larger bundles can be formed due to increased SWNT-SWNT contacts, which were more prominent upon using PMMA of lower molecular weight for the wrapping, as indicated by the RBM differences in the polymer dispersion and fiber. Assuming that each fibrillar structure contains one SWNT bundle, it can be estimated that the bundle diameter was ~10 nm (~95 nanotubes) in PAN/15k.PMMA-SWNT fiber and ~5 nm (~29 nanotubes) in PAN/350k.PMMA-SWNT.

Tensile properties and structural parameters of the as-spun (3x) and drawn fibers are listed in Table 3-2. As-spun PAN/15k.PMMA-SWNT fiber had approximately 100 %, 40 % and 170 % higher tensile strength, modulus and elongation at break, respectively, than the as-spun PAN/350k.PMMA-SWNT fiber. No significant difference was measured in PAN crystal size and a slight increase in orientation factor of PAN crystal and SWNT was found in the as-spun fiber with SWNT wrapped with 15,000 g/mol PMMA as compared to the 350,000 g/mol PMMA.

Table 3-2. Mechanical properties and structural parameters of PAN fiber without filler and with 5 wt. % SWNT wrapped with 15,000 and 350,000 g/mol PMMA at different total draw ratios.

	PAN-b	PAN/15k.PMMA-SWNT		PAN/350k.PMMA-SWNT		
Total draw ratio (TDR)	24x	3x	19x	3x	18x	27x
Fiber diameter (μm)	11.5 ± 0.2	30.2 ± 0.4	12.3 ± 0.2	28.0 ± 0.7	12.5 ± 0.5	10.4 ± 0.1
X_c (%)	53	36	57	38	48	62
L_{PAN} (nm)	9	3.6	12.7	3.5	10.6	11
Ratio $d_{\sim 17^\circ}/d_{\sim 30^\circ}$	1.72	1.66	1.72	1.64	1.73	1.73
f_{PAN}	0.89	0.30	0.82	0.24	0.83	0.90
f_{SWNT}[a]	NA	0.87	0.89	0.84	0.90	0.94
RBM2 peak (%)[b]	NA	15	16	12	11	12
Tensile Strength (MPa)	896 ± 28	208 ± 4	944 ± 38	108 ± 5	672 ± 13	837 ± 19
Tensile Modulus (GPa)	19.2 ± 0.4	11.9 ± 0.1	24.7 ± 0.3	8.5 ± 0.3	18.4 ± 0.2	21.8 ± 0.2
Elongation at break (%)	7.4 ± 0.2	35 ± 3	8.9 ± 0.3	13 ± 3	8.1 ± 0.2	7.8 ± 0.2

Notes: [a] 2nd order orientation factor of SWNTs calculated from Raman signal by following the G band intensity upon rotation of the fiber with respect to the incident polarized beam. [b] RBM2 peak area as a percentage of total area of RBM bands (150-350 cm^{-1}) of the Raman spectra using un-polarized laser. TDR of 3x corresponds to the as-spun fibers.

The improvement of the mechanical properties of the as-spun fiber upon using lower PMMA molecular weight demonstrates that the wrapping has a direct effect in the filler-matrix interactions, and not only in the filler dispersion. Filler dispersion was significantly better in PMMA-SWNT dispersions in DMF and buckypapers when higher molecular weight PMMA was used for wrapping, which translated to the observed

differences in the RBM spectra and fibril diameter of the as-spun fibers. However, nanocomposite fiber mechanical properties were higher in the PAN fiber with SWNT wrapped with 15,000 g/mol PMMA. This has been explained by considering an increase in the filler-matrix interactions, as discussed later in this document.

PAN/15k.PMMA-SWNT fiber had a maximum draw ratio of 19x, while PAN/350k.PMMA-SWNT fiber could be drawn up to 27x, however, a sample of the latter with a draw ratio of 18x was also studied for comparison. All the composite fibers had a PAN crystal size larger than that of the control fiber. This is consistent with the results observed for the fully drawn fibers containing 1 wt.% SWNT (see previous section). PAN/15k.PMMA-SWNT fiber at a draw ratio of 19x had larger PAN crystal than the PAN/350k.PMMA-SWNT fibers at comparable (18x), as well as at higher (27x) draw ratios. Typically, higher PAN fiber draw ratios correspond to higher crystal size,[67,141.] However, the PAN/15k.PMMA-SWNT fiber (19x) had larger PAN crystals than the PAN/350k.PMMA-SWNT fiber (27x). This could have originated by stronger filler-matrix interactions that promoted interfacial crystallization around the SWNT bundles. Another possible explanation is that the increased distance between fillers (caused by increased bundle size) in PAN/15k.PMMA-SWNT fiber provided a less restricted environment for polymer crystal in the matrix bulk. However, no differences were observed in the dependence of tan δ with temperature of the fully drawn fibers (see Figure B 7 in Appendix B).

Fully drawn PAN/15k.PMMA-SWNT fiber have ~30 % and ~20 % higher tensile modulus and elongation at break with respect to the control fiber, respectively, and 13 % and 14 % higher corresponding values with respect to the fiber with SWNT wrapped with 350,000 g/mol PMMA. Interestingly, when analyzing together the mechanical and structural data, it is observed that PAN/15k.PMMA-SWNT (19x) fiber had higher tensile

modulus than PAN/350k.PMMA-SWNT (27x) fiber despite the former one having filler with lower orientation and lower degree of SWNT individualization (Table 3-2), and therefore a filler with lower effective tensile modulus.[39] To further understand these results, the SWNT straining behavior upon the axial deformation of the nanocomposite fiber was studied by Raman spectroscopy, and is discussed next.

Figure 3-4 presents the SWNT G' shift upon straining of the fully drawn fibers with 5 wt.% filler. The maximum G' shift (S_m) upon fiber straining was ~8.4 ± 0.4 and ~7.8 ± 0.3 cm^{-1} for the PAN/15k.PMMA-SWNT and PAN/350k.PMMA-SWNT fibers, respectively, while the G' shift rate (S_r) of the two corresponding fibers up to 0.4 % fiber strain was -17 and -8 cm^{-1}/%. G' shift rate was estimated as the linear slope of the G' shift between 0 and 0.4 % fiber strain. The measured G' maximum shift indicates that SWNTs were subjected to the same total strain (and hence same stress) upon fiber deformation, for the two PMMA molecular weights used. More so, for both fibers, a plateau was reached in the G' shift, which denotes interphase or matrix failure. Because of this, the method described for estimation of the IFSS in 1 wt.% SWNT fibers cannot be used for the 5 wt.% SWNT fibers. In contrast, the difference in the G' shift rate indicates that before interphase failure, the strain in the macroscopic fiber was more effectively transferred to the filler in the fibers using 15,000 g/mol PMMA than the one with 350,000 g/mol PMMA. The composite fiber modulus has been previously found to be proportional to the Raman shift rate[57] and in elastomer composites, proportional to the filler-polymer interactions.[144] However, several other factors have been reported to affect the G' shift rate, like filler dispersion, orientation and length.[67,145–147]

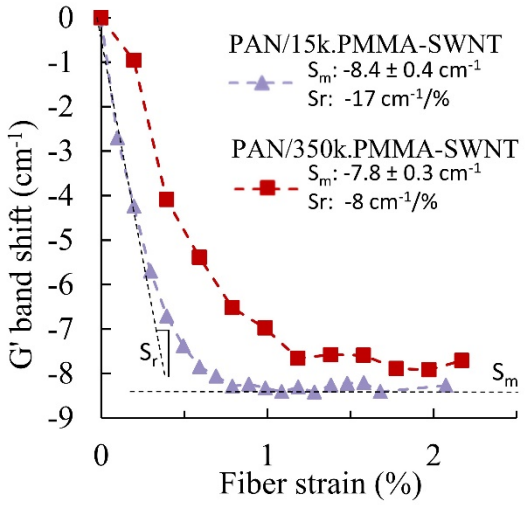

Figure 3-4. Shift of the G' band as a function of strain for fully drawn fibers with 5 wt.% SWNT PAN/15k.PMMA-SWNT (TDR 19x) and PAN/350k.PMMA-SWNT (TDR 27x). Maximum G' shift (S_m) and G' shift rate (S_r) are indicated for each fiber.

Our experimental results show that increasing the molecular weight of the PMMA wrapping increased the order of the helical wrap (Figure 3-2d), while the amount of wrapped PMMA remained about the same for the two molecular weights. A more ordered PMMA helix allowed for better individualization of the SWNT by decreasing SWNT-SWNT contacts and bundle size (Figure 3-2a-c and Figure 3-3b). However, the same phenomenon reduced matrix-SWNT interactions in the composite, as evident from the G' shift rate measured upon deformation of the two fully drawn fibers (Figure 3-4). Higher PMMA molecular weight used for SWNT wrapping is useful for SWNT individualization, while the lower PMMA molecular weight results in increased filler-matrix interaction and increased tensile properties. To the best of our knowledge, this is the first study on the nanocomposite mechanical properties, by changing the molecular weight of the polymer used for non-covalently wrapping of SWNTs, and where the polymer used for wrapping is different than the matrix polymer. Further comparison of the results in this study, with those obtained when changing the molecular weight of the polymer used in grafting the carbon nanotubes is included in Appendix B.3, along with the discussion of the pair interactions of the ternary system PAN-PMMA-SWNT (Appendix B.4)

An important question is, what are the potential applications of polymer/carbon nanotube nanocomposite fibers in general, and of PAN/SWNT fibers of the type presented in this paper. The quest for making polymer/CNT composite fibers started with the aim of making high strength, high modulus fibers at very high CNT loading (greater than 60 wt.%) that exhibit high strength and high modulus that far exceeds today's state-of-the-art carbon fibers. However, after over 20 years of research, this goal has not yet been achieved. PAN is THE precursor for current high strength and intermediate modulus carbon fibers. Addition of CNTs, at relatively low loading, as reported in this manuscript, would allow for the development of a new class of carbon fibers, which exhibit high strength, high modulus, as well as increased electrical and thermal conductivity, as compared to the PAN based carbon fibers without CNT. In addition, PAN/SWNT fibers themselves can find applications based on the SWNT properties. These applications may be based on the PAN/SWNT fiber mechanical, electrical, thermal, and optical properties, response to electromagnetic radiation, or due to a combination of two or more of these.

3.5 Conclusions

Poly(methyl methacrylate) (PMMA) was used to create ordered non-covalent wrapping around Single Wall Carbon Nanotubes (SWNTs). PMMA wrapping remains after fiber spinning and, therefore, becomes part of the nanocomposite's interphase. We also demonstrated that increasing PMMA molecular weight increases SWNT individualization (as measured by Raman radial breathing mode) by increasing the order of PMMA helical wraps around SWNT. Engineering of the filler-matrix interphase and the nanocomposite fiber mechanical properties can be done by wrapping the SWNT with PMMA and changing the PMMA molecular weight. Wrapping of the SWNTs with PMMA of 15,000 g/mol molecular weight resulted in higher tensile property fibers than using 350,000 g/mol PMMA.

4 CHAPTER 4: PROCESSING, STRUCTURE AND PROPERTIES OF NANOCOMPOSITE PAN FIBER WITH HIGH LOADING OF SWNTs (15 wt%)

Preamble

In this chapter, we study mechanically strong and electrically conductive PAN nanocomposite fibers with up to 15 wt% SWNTs. Results from Chapter 2 are used to improve the spinning dispersion protocol and to reduce processing time. Results from Chapter 3 are used to engineer the nanocomposite's filler-matrix interphase.

Chapter 4 and Appendix C are already published as "*Processing, structure and properties of polyacrylonitrile fibers with 15 weight percent single wall carbon nanotubes,*"[117] manuscript first authored by the author of this thesis (Pedro J. Arias-Monje) and in collaboration with Mingxuan Lu, Jyostna Ramachandran, Mohammad Hamza Kirmani and Dr. Satish Kumar.

4.1 Abstract

For the first time, a polyacrylonitrile (PAN) fiber with up to 15 wt% single-wall carbon nanotubes (SWNTs) was produced by dry-jet spinning while maintaining good SWNT individualization. These fibers exhibited a tensile modulus of 32.1 GPa, tensile strength of 0.8 GPa, and axial electrical conductivity of 2.2 S/m. This was possible by using SWNTs that were non-covalently wrapped with poly(methyl methacrylate) (PMMA-SWNTs). Furthermore, this non-covalent PMMA functionalization significantly reduced the amount of solvent and time needed for the processing of the spinning solution, as compared to the methods used in prior studies. Rheology of the spinning solutions and mechanical properties and structural parameters of the produced fibers were related to the filler individualization, filler content and presence of filler-matrix interaction. Potential applications of this PAN fiber with high SWNT loading are briefly discussed.

4.2 Introduction

Polymeric fibers containing carbon nanotubes (CNT) are of interest due to their potential of achieving good mechanical properties, electrical and thermal conductivity.[20] Polyacrylonitrile (PAN)/CNT fibers are of further interest as they can be converted to carbon/CNT composite fiber.[33,75] While many polymer/CNT fibers can be spun from melt,[148,149] PAN/CNT fibers are spun from solution.[71,73,79,150,151] Spinning from solution is used industrially to obtain continuous PAN fibers in roll-to-roll processing. PAN solution, and PAN/CNT dispersions can also be spun by other techniques to produce nonwoven mats. These techniques include electrospinning and centrifugal spinning.[152,153] To date, there are number of limitations in the development of PAN/CNT fibers. These limitations include the following: (1) Low filler content. In the fiber spinning studies to-date, the CNT content, particularly single wall carbon nanotubes (SWNTs) and small diameter carbon nanotubes, has been limited to about 10 wt%, while the PAN content is 90 wt%.[71] Filler

content has been limited by the effect of filler in the spinning solution rheology and its spinnability. To take full advantage of the CNT properties, the CNT to polymer ratio needs to be increased, to as high a value as possible, and the polymer-CNT interface needs to be engineered to provide an effective load transfer from polymer to CNT.[56,57,75] (2) Low mechanical reinforcement of the nanocomposite. With few exceptions,[65–67] CNT mechanical properties have not yet translated into high fiber mechanical properties.[20,68,72,73,154] Prior to this report, the highest tensile modulus achieved for a PAN nanocomposite fiber was 28.7 GPa, with a SWNT content of 1 wt%,[65] and 28.4 GPa with 1 wt% amino-functionalized-multi wall carbon nanotubes.[66] (3) Extensive processing. During solution processing of PAN/CNT fibers, CNTs have been dispersed at a very dilute concentrations, typically less than 100 mg per dl of solvent,[65,68,71,155] and as low as 0.7 mg/dl.[67,73] Dilute CNT dispersions are used to improve filler dispersion in the nanocomposite. CNT agglomeration and poor mechanical properties of the nanocomposite have been achieved when the concentration of the CNT dispersion is high (330 mg/dl). However, reducing dispersion concentration significantly increases time and energy usage as excess solvent is typically removed by distillation.

Here, we report progress in all these areas. This is the first study, reporting successful spinning of PAN/CNT fibers with 15 wt% SWNT, exhibiting a tensile modulus of 32 GPa. The amount of solvent used during processing of SWNT with PAN was reduced by increasing SWNT dispersion concentration from 7 mg/dl to ~200 mg/dl by introducing a step of co-solvent induced phase separation. The PAN-SWNT interface was modified using poly(methyl methacrylate) (PMMA) in non-covalent wrapping onto SWNTs.[34,47]

4.3 Experimental

4.3.1 Materials

Poly(acrylonitrile-co-methacrylic acid) (PAN, 4 wt% copolymer) with viscosity average molecular weight of 500,000 g/mol was obtained from Japan Exlan Co. (Osaka, Japan). Atactic poly(methyl acrylate) (PMMA) with a weight average molecular weight of 350,000 and 15,000 g/mol was obtained from Sigma-Aldrich. Single wall carbon nanotubes (SWNTs) HiPco™ (lot. # PO 271) were obtained from Carbon Nanotechnologies Inc. Average tube diameter was 0.9 nm and catalyst content 2 wt%. Dimethylformamide (DMF, ACS grade, 99.8%) was obtained from Sigma-Aldrich, and ethyl acetate (≥99.5%) was provided by VWR. Prior to use, ground-PAN powder and SWNT were dried, separately, for 24 h at 60 °C in vacuum. DMF and ethyl acetate were used as received, but recovered solvents were also used. Recovered DMF and ethyl acetate were obtained by double simple distillation of the by-products of the steps required to obtain the spinnable SWNT/PAN dispersion, and these steps are described below. Details of the solvent recovery can be found in the Appendix C.2.

4.3.2 PMMA-wrapped-SWNTs

SWNTs were non-covalently wrapped with PMMA following a similar protocol to that developed by Davijani and Kumar[47]. Briefly, dried SWNTs were sonicated in DMF for 2 h and then mixed with a PMMA solution in DMF. Final SWNT and PMMA content in the DMF was kept ensuring a mass ratio of 1:1. SWNT content of the final DMF dispersion was either 5 - 7 mg/dl or 110 mg/dl, as detailed in Table 4-1. These dispersions were further sonicated for 24 h and then immediately used in the two-following processes, as the case may be: (i) removal of free PMMA, (ii) preparation of spinning PAN/DMF solutions with PMMA-wrapped-SWNTs. PMMA-wrapped-SWNTs are herein referred as PMMA-SWNTs. Table 4-1 also shows how the PMMA molecular weight and SWNT content were

varied. Effect of the PMMA molecular weight in the filler dispersion and filler-matrix interaction has been previously studied.[34]

Table 4-1. Composition of the spinning solutions prepared for this chapter 4 and used for PAN and PAN nanocomposite fiber spinning, along with conditions used for PMMA-wrapping of the SWNTs.

Spinning solution label	PAN	1wt%	5wt%-A	5wt%-B	15wt%
PMMA-wrapping of SWNTs					
SWNT content (mg/dl)	NA	110*	110*	5*	7* (~200)**
PMMA Mw (g/mol)	NA	350,000	350,000	15,000	15,000
Composition of the spinning solution					
Total solid content (g/dl DMF)	10.5	9.4	9.3	9.1	6.6
SWNT content † (wt%)	NA	1	5	5	15
PAN content † (wt%)	100	98	90	90	79
Total PMMA content † (wt%)	NA	1	5	5	6‡
Adsorbed PMMA § (wt%)		0.4	1.8	1.8	6‡
Free PMMA content § (wt%)		0.6	3.2	3.2	0
Processing time (days)	1	1	2	15	3

* solvent used during sonication was DMF.
** after solvent exchange the SWNT content in ethyl acetate was ~200 mg/dl.
† respect to solids of the spinning solution i.e. PAN, PMMA and SWNT. Calculated from the amount of SWNT and polymers used during SWNT wrapping and distillation.
‡ free PMMA was removed from the PMMA/SWNT/DMF dispersions by solvent exchange with ethyl acetate followed by water-induced phase separation.
§ calculated assuming ~37% of the PMMA added is adsorbed onto SWNTs, creating PMMA-wrapped-SWNTs, and ~63% remains as free PMMA.

4.3.3 Removal of free PMMA from PMMA/SWNT dispersions in DMF

Sonication of the PMMA/SWNT dispersions causes about 58 wt% of the PMMA present to helically wrap the SWNTs, while the remaining ~42% remains in free solution. This has been determined by comparing the polymer content of buckypapers produced from the PMMA/SWNT dispersions by removal of the DMF by either vacuum filtration (~37 wt% PMMA) or evaporation (~50 wt%).[47]

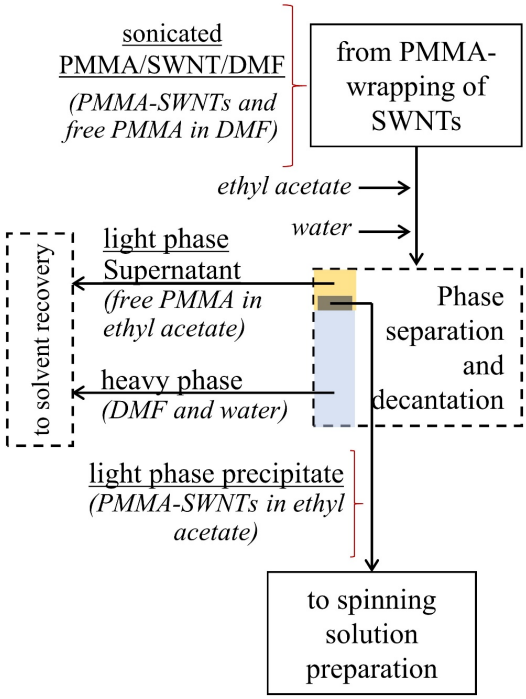

Figure 4-1. Flow diagram summarizing the phase separation and decantation process done after PMMA-wrapping of the SWNTs and prior to the preparation of spinning solution with 15 wt% SWNTs.
With this additional step DMF is exchanged for ethyl acetate (lower boiling point solvent), free PMMA is removed, and PMMA-wrapped-SWNT dispersion (7 mg SWNT per dl) is concentrated to a slurry of ~200 mg/dl.

Excess PMMA was removed by solvent exchange with ethyl acetate followed by induced phase separation. The process is summarized in Figure 4-1. Ethyl acetate was added to the sonicated PMMA/SWNT dispersion in a ratio 0.75 to 1 vol/vol ethyl acetate to DMF and the container was shaken by hand. Immediately after, distilled water was added in a ratio of 1.75 to 1 vol/vol water to DMF. The container was vigorously hand shaken one last time and the mixture transferred to a separation funnel. The separation funnel was left still for about 2 h, upon which the system underwent phase separation due to ethyl acetate/water immiscibility and density differences. The heavy phase was transparent and composed of water, DMF and a small amount of ethyl acetate. The light phase was comprised of supernatant and precipitate. The light phase supernatant was composed of ethyl acetate and the free PMMA, while the precipitate was a slurry of the

PMMA-SWNTs in ethyl acetate (~200 mg/dl). Composition of these phases was determined by fraction evaporation of the heavy phase and the light phase supernatant. Distribution of the free PMMA and PMMA-SWNT was determined by producing films of the whole light phase (supernatant and precipitate) and the light phase precipitate, followed by thermo gravimetric and wide-angle x-ray diffraction characterization of said films. Further details of these experiments and its results are available in the Appendix C.1.

4.3.4 PMMA/SWNT/PAN spinning solutions

Preparation of the spinning solution started in all cases by mixing dried PAN with DMF chilled at ~0 °C. Dispersion was stirred for 1 h before rising the temperature to 70 °C, after which stirring continued for another hour. The desired amount of PMMA-wrapped-SWNTs in either DMF (with free PMMA) or ethyl acetate (without free PMMA) was added to the PAN solution and the excess solvent was removed by vacuum distillation (~70 °C, < 40 mbar). Solid content of the DMF spinning solutions varied with the amount of SWNTs, as shown in Table 4-1. Table 4-1 also shows the composition of solids of the spinning solutions, which is expected to be the same composition of the solid fibers. Spinning solution with 15 wt% SWNTs was prepared using the PMMA-SWNT slurry in ethyl acetate, thus without free PMMA. For the spinning solutions with 1 and 5 wt% SWNTs, the sonicated PMMA/SWNT/DMF dispersions were used directly in the preparation of the spinning solution.

Solid content was measured by thermal gravimetric analysis (TGA) by heating the spinning solutions to 130 °C in air atmosphere until constant weight was reached, using a Q500 machine (TA Instruments). An ARES rheometer was used to measure the rheological properties of the spinning solutions while in using parallel plates of 25 mm diameter and 1 mm gap. Linear viscoelastic region was verified for all solutions by doing

strain sweeps from 0.1 to 10% at 0.5, 50 and 250 rad/s. Viscosity was determined doing a frequency sweep from 0.5 to 500 rad/s at 1% strain. Optical images of the spinning solutions were taken by transmission mode in a Leica DM2500 P. Wide angle x-ray diffraction (WAXD) was performed on films produced by drying spinning solution over a glass slide under vacuum at ~ 50 °C. Vacuum-dried films of the spinning solutions were self-standing after being removed from the glass slide and used without further modification. WAXD was performed on a Rigaku MicroMax-003 (transmission mode), operating at 50 kV and 0.60 mA (Cu $K\alpha$) and with a R-axis IV++ detector. Collected images were processed with AreaMax software, and the diffraction patterns with Jade.

4.3.5 PAN fibers with PMMA-wrapped-SWNTs

Spinning solutions listed in Table 4-1 were spun to obtain PAN fibers without SWNT and with PMMA-wrapped-SWNTs by dry-jet wet-spinning. Thus, nanocomposite fibers with 1, 5 and 15 wt% SWNT were produced. Two fibers with 5 wt% SWNT were produced, labeled 5wt%-A and 5wt%-B, to show the effect of the concentration of the SWNT/DMF dispersion on the fiber mechanical properties. Spinning was performed on a single filament system (Hills Inc.) using a 200 μm spinneret. Barrel and spinneret temperatures were ~65 and ~55 °C, respectively. Dry-jet wet spinning was done by extruding the spinning solutions at 1 cc/min (> 4 g/h of fiber depending on the solid content of the spinning solution), with an air gap (3-5 cm) between spinneret and the methanol coagulation bath chilled at -40°C. Stretch ratio during spinning was 1.3× for the PAN fiber with 15 wt% SWNT and 3× for all the other fibers. Collected samples were stored submerged in methanol maintained at -40°C prior to two-stage drawing. First step drawing consisted of a mild stretching (at a draw ratio between 1.1 and 1.5×) while keeping the feeder roller in chilled methanol and the collector roller in room temperature methanol. Second step drawing was done by passing the fiber through a glycerol bath (kept at 165-

170 °C) during stretching (draw ratio between 5 and 7×), while both feeder and collection spools were submerged in methanol. All collected fibers were vacuum dried at 40 °C for two days prior to further testing.

Single filament tensile testing (at least 25 filaments) was done on a FAVIMAT+ (Measured Solution, Inc.), with inline vibroscope for linear density measurement. Gauge length was 1 inch and applied strain rate was 1%/s. Dynamic mechanical analysis (DMA) was performed while in air in an RSA III, on bundles with equivalent diameter 800-1000 μm, by increasing the temperature from 30 to 180 °C at a heating rate of 1 °C/min and applying cyclic strain of 0.1% at 0.1, 1 and 10 Hz. WAXD was performed on bundles of 64 filaments, on the same machine already described. Small angle x-ray scattering (SAXS) was measured by transmission signal from fiber bundles on a Panalytical Empyrean, operating at 40 kV and 0.40 mA. SAXS data were collected at a step size of 0.01°, 22 s per step and while rotating the fiber bundle at 12 rpm. Raman characterization was done on a HORIBA XploRA ONE with a 785 nm laser. A motorized translation stage (Thorlabs) was used to deform the nanocomposite fiber while estimating the SWNT strain by shift of the Raman measured G' band, following the protocol previously described in elsewhere.[67] Reference[67] also describes the methods used for estimation of the SWNT orientation in the PAN fibers by polarized Raman spectroscopy, following the intensity dependence of G band with the angle between fiber in linear polarizer. Scanning electron microscopy (SEM) was done on uncoated samples on a Hitachi SU8230. Accelerating voltage was 3 kV and working distance 4 mm or less. Cross-sections of the fibers were obtained by either cutting the sample at room temperature or while submerged in liquid nitrogen, which generated cross sections with plastic deformation or brittle fracture, respectively. At least 10 filaments were observed by SEM and representative images were selected. Electrical conductivity of selected nanocomposite fibers was measured by 2-probe method in a

Keithley 2400 source-meter, by measuring the resistance of small bundles of fibers; distance between probes was varied between 5 and 15 mm and current applied between 0.025 and 0.1 mA). Current range was selected to ensure that measurements were within Ohm's law region. No thermal aging was done on the fibers.

Fibrils were obtained by submerging fully drawn fibers in DMF at 120 °C for 6 h during magnetic stirring. These dissolved fibers in DMF are herein named fibril solution. Imaging of the fibrils was done by submerging copper grids (300 mesh with carbon coating) in the fibril solution. UV-Vis spectra of the fibril solutions were obtained in the range 300 to 1000 nm on a PerkinElmer Lambda 35.

Two quantitative indirect methods were used to estimate the SWNT dispersion reached in the nanocomposite fibers. The first one is based on Raman spectroscopy and consists of following the predominance of the ~268 cm^{-1} (RBM2) peak with respect to the total area of the radial breathing mode (RBM), an indirect but quantitative approach explained elsewhere.[34,135] The second one consists of using the measured tensile modulus of the nanocomposite fiber, to estimate the SWNT bundle diameter of each fiber. Detailed explanation of this method is available in Appendix C.3. Briefly, given the experimentally measured relationship between SWNT-bundle shear modulus and its diameter[40] and its effect on the effective tensile modulus of the filler,[20] we estimated the bundle diameter in each fiber at which the tensile modulus contribution of the filler matched the measured tensile modulus of the fiber. This approach is similar to the one presented elsewhere.[67,71]

4.4 Results and discussion

4.4.1 Effect of SWNT dispersion and SWNT content on the spinning solutions and fiber spinning

As detailed in the experimental section, a total of five spinning solutions were prepared (see Table 4-1), one without filler (PAN) and the other four with PMMA-SWNT at SWNT contents 1, 5, 5 and 15 wt% respect to the total solids. One of the 5 wt% SWNT spinning solutions (5wt%-A) was prepared by evaporation of 110 mg/dl PMMA/SWNT dispersions in DMF, while the second one (5wt%-B) by evaporating similar dispersions at a concentration of 5 mg/dl. Differences between spinning solutions 5wt%-A and 5wt%-B allowed to study the effect of SWNT dispersion quality, at a given SWNT concentration.

Figure C 2a in Appendix C shows the integrated WAXD patterns in the 10 – 20° range of films produced from the spinning solutions by vacuum drying, while a deconvolution of the observed peaks for the sample with 15 wt% SWNT is presented in Figure 4-2a and Figure C 2b. The 10 to 20° range is particularly interesting because it shows the PMMA ordered helical around SWNTs and the PAN crystalline structures. The peak at 2θ ~10.8° has been previously shown to be due to the ordered helical PMMA wrap around SWNTs.[47] Its presence in the films demonstrated that such wrapping remained after solvent evaporation and continuous stirring and, for 15wt% spinning solution, after solvent exchange, evaporation and continuous stirring. The non-covalent nature and structure of this PMMA wrapping has been described in previous works.[34,47] The 2θ ~17° signal corresponds to that of the PAN crystal and depending on the chain packing can be a single or double peak, depending if the PAN molecule packing is hexagonal or orthorhombic, respectively.[156] For the films produced here, see deconvolution in Figure 4-2a, two distinct peaks (~16.8 and ~17.2°, (200) and (110) planes, respectively) were observed. The fact that we observed two peaks in the films, is particularly interesting, as

such deconvolution is not always possible for vacuum-dried PAN films without stretching,[157,158] most likely due to low crystal perfection. This orthorhombic structure is typically only observed when PAN films or fibers are produced by coagulation in non-solvents.[140,156,159]

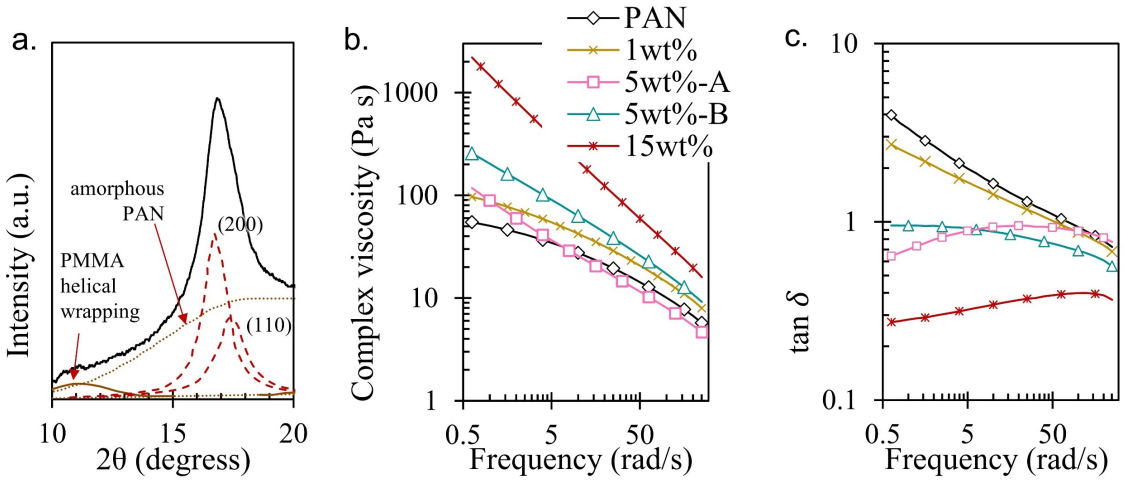

Figure 4-2. Deconvoluted XRD peaks of dried film produced from spinning solution with 15 wt% SWNTs and rheological properties of spinning solutions listed in Table 4-1. (a) Deconvoluted peaks in the 10 to 20° WAXD range for the film produced by vacuum-drying from the spinning solution with 15 wt% SWNT, showing the PMMA helical structure (2θ ~10.8°), two crystalline PAN peaks centered at 2θ 16.8 and 17.2° and the amorphous PAN signal. (b) Complex viscosity, and (c) tan δ dependence on frequency, of the spinning solutions at various SWNT concentrations (1 to 15 wt.%) and filler dispersion conditions (5wt%-A and -B). Legend is the same for figures b and c.

Zhang et al.[160] observed the double ~17° peak in vacuum-dried PAN/SWNT films. In their case, they sonicated dilute PAN/DMF solutions (molecular weight ~520 000 g/mol, 25 mg polymer per dl of solvent) along with SWNTs (filler content 50 wt%), followed by solution shearing and then vacuum-drying. They found that the orthorhombic (200) (110) reflections were distinguishable in films when a continuous tubular PAN coating was created around the SWNTs.[160] Zhang et al.[160] hypothesized that such uniform coating was induced by polymer epitaxial interactions with the SWNTs graphitic surface upon shearing of the PAN molecules with well-individualized SWNTs, however no evidence of such interactions was provided. Several other authors have used vacuum-drying to produced

PAN films with single, double and multiwall carbon nanotube and vapor-growth carbon nanofibers (filler content from 5 to 20 wt%)[158,161] and with cellulose nanocrystals (filler content from 5 to 40 wt%).[157] However, in all these cases, the planes (200) and (110) cannot be distinguished and instead a broad 17° peak is observed, indicating the presence of low-order small orthorhombic crystals. Main differences between these works[157,158,161] and that of Zhang et al.[160] is that in the former the fillers were sonicated prior mixing with the PAN solution, and semi-dilute PAN solutions were vacuum dried, instead of dilute solutions. Films produced from the spinning solutions in Table 4-1 had the double peak at ~17°, similar to that observed by Zhang et al,[160] but experimental conditions were closer to those previously used by other authors.[157,158,161] We hypothesized that the orthorhombic crystal structure was present in the vacuum-dried PAN films produced here because our SWNTs were helically wrapped by PMMA and said PMMA-SWNTs had good interaction with the PAN molecules, which facilitated the formation of uniform PAN coating along the filler. Interaction between PMMA-SWNT and PAN was possible due to improved dispersion and SWNT-matrix contact. Considering the amount of PMMA fixed to the SWNTs after sonication, it is estimated that only about 17% of the SWNT length is covered by the PMMA,[34] which signifies that the majority of the SWNT length can directly interact with the PAN. Effect of PMMA wrapping in the filler-matrix interactions has been previously described in PAN nanocomposite fibers.[34]

Rheological properties of the spinning solutions are summarized in Figure 4-2b,c, and Figure C 2c and Table C 1 in Appendix C, while optical images of the spinning solutions can be found in Figure C 3 of the same Appendix. Rheology of the polymer solutions is strongly affected by the quality of dispersion of the SWNTs, as observed by comparing the spinning solutions 5wt%-A and 5wt%-B that have the same filler content but dispersed by sonication under different conditions (see Table 4-1). Figure C 3 shows

that both solutions presented agglomerates of various size, however, spinning solution 5 wt%-A had more and larger agglomerates than 5wt%-B, indicating that the later had better dispersed SWNTs. Similarly, spinning solution 5wt%-B had larger viscosity and storage modulus than 5wt%-A (Figure 4-2), which can be explained by improved filler dispersion in spinning solution 5wt%-B. Solution homogeneity, estimated by how close to 2 is the slope of the log G' vs log G'' (see Table C 1), was also higher in spinning solution 5wt%-B (slope of 1.02) than in solution 5wt%-A (slope of 0.71).

However, improving the dispersion of the PMMA-wrapped-SWNTs in the 5wt%-B required the use of more dilute PMMA/SWNT dispersions in DMF: 110 vs 5 mg of SWNT per dl for 5wt%-A and 5wt%-B spinning solutions, respectively. Diluting the filler dispersion also increased the energy cost, processing time and labor. Reaching the desired SWNT concentration in the spinning solution 5wt%-A demanded evaporating 500 ml of DMF from the polymer solution, which required ~2 days. On the other hand, for the spinning solution 5wt%-B, 10.5 liters of DMF had to be evaporated, which increased the processing time to ~15 days. These long solution preparation times were caused by having to evaporate the excess solvent under mild conditions (<70 °C and vacuum), despite the high-boiling point of DMF (~153 °C) and its reduced vapor pressure upon increasing solid content. These evaporation conditions were selected to ensure gentle boiling, thus avoiding loss of polymer at the walls of the glass reactor, and thermal degradation and/or change in conformation of the PAN molecule. The change in conformation at temperatures larger than 70 °C has been documented in the literature.[162]

To overcome these drawbacks while increasing the SWNT content further to 15 wt%, the spinning solution preparation protocol was modified to include a step that exchanged the PMMA-wrapped-SWNTs from DMF to ethyl acetate (boiling point of DMF and ethyl acetate is, respectively, 153 and 77.1 °C) and increased the concentration of

the filler dispersion added to the PAN solution to about 200 mg/dl. Following this protocol, instead of evaporating 22.5 liters of DMF over a period of one month (estimated if following a similar protocol to that of solution 5wt%-B), 15wt% spinning solution was prepared by evaporating 1 liter of ethyl acetate over 3 days. Figure C 3c,f shows the optical images of the 15wt% spinning solution. In this figure, agglomerates were comparable to those observed for the spinning solutions with 5 wt% SWNT, even though SWNTs were added to the PAN solution while precipitated in ethyl acetate (slurry of 200 mg/dl).

Increasing the SWNT content increased the viscosity and elastic component of the polymer dispersions. Among the prepared solutions, that with 15 wt% SWNTs had the largest viscosity and G' and the lowest tan δ over the entire evaluated frequency range (see Figure 4-2b,c and Figure C 2c), even though it had the lowest total solid content (see Table 4-1) amongst various solutions. Furthermore, G' dependence at low frequencies (< 2.5 rad/s) (ω) also decreased with SWNT content (see Table C 1), from G'~ $\omega^{1.11}$ and $\omega^{0.95}$ for PAN and 1wt% spinning solutions, respectively, to $\omega^{0.14}$ for the spinning solution with 15 wt% SWNTs. A linear viscoelastic response of a monodisperse polymer is expected to have a G'~ ω^2, while for a nearly perfect polymer network a G'~ ω^0 is expected. Observed change upon introduction of SWNTs and at reduced solid content indicates the creation of a network, probably due to filler-polymer association, rather than polymer entanglements alone. This rheological behavior has been previously described upon inclusion of carbon nanotubes,[41,83,163] and is the reason why we decided to reduce the solid content of the spinning solution to ensure spinnability. Highly elastic polymer solutions cannot be spun by dry-jet wet-spinning because of excessive die-swelling and jet-discontinuity.[84]

The low damping factor (high elastic component) of the polymer solution with 15 wt% SWNT, also affected the maximum stretch ratio during spinning. Fibers produced

from 15wt% had to be collected at a stretch ratio of 1.3×, while all the other fibers were collected at 3×. A 15wt% polymer solution with even lower solid content (5.1 g/dl) was also produced to further reduce the solution viscosity and elastic component (see Figure C 4 in Appendix C), however, such solution was not spinnable by dry-jet wet-spinning. Stretch ratio during spinning is affected by the elastic component of the polymer solution because, at low enough damping factors, not all the stored energy is released upon leaving the spinneret and some continue after gel formation at ca. -40 °C. This was observed every time polymer solutions with 5 and 15 wt% SWNT were spun without stretching: when the spun stretch ratio was lower than 1×, the spun fibers heavily recoiled in the coagulation bath. Such recoiling was not observed in those fibers produced from the polymer solution without SWNT.

4.4.2 Effect of SWNT dispersion and SWNT content on the fiber structure and properties

As summarized in Figure 4-3 and Table 4-2, tensile properties of the fully drawn nanocomposite fibers increased with SWNT content for all fibers except for the fiber 5wt%-A. The 5wt%-A fully drawn fiber (total draw ratio, TDR 16.2×) had a similar tensile modulus and a lower tensile strength than the PAN fiber without SWNTs (TDR 24×). On the other hand, fiber 5wt%-B (TDR 19.4×), with the same SWNT content as fiber 5wt%-A, had a tensile modulus ~30% higher than that of the control PAN fiber, and with no change in the tensile strength.

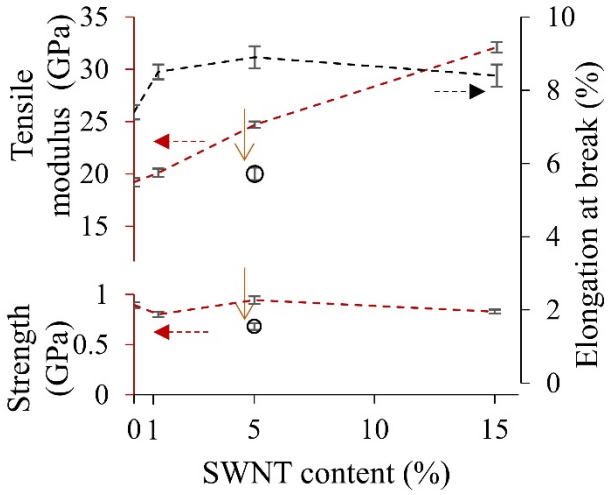

Figure 4-3. Tensile mechanical properties of various fully drawn fibers PAN fibers with PMMA-SWNT when changing SWNT content and SWNT dispersion protocol.
Vertical arrows indicate the decrease in tensile properties upon decreasing SWNT dispersion, while horizontal arrows indicate respective axis. Data points are connected by dashed lines to guide the eye.

Differences in the mechanical properties of fibers 5wt%-A and -B were caused by difference in filler individualization rather than total draw ratio. This can be better illustrated by comparing the mechanical properties of fiber 5wt%-A (TDR 16.2×) with a 5wt%-B fiber drawn at even lower draw ratio. Properties of such 5wt%-B fiber with a TDR of 14× are listed in Table C 2. Tensile properties of the 5wt%-B (TDR 14×) fiber are still higher than those of the 5wt%-A (TDR 16.2×) fiber, which is expected of fibers 5wt%-B with better individualized SWNTs. Differences in filler individualization result from the previously discussed differences in filler dispersion, which also affected the spinning solution rheology. Differences in filler dispersion of the nanocomposite fibers were verified by two indirect methods: a. analysis of the Raman radial breathing mode (RBM) and b. fitting of the measured fiber tensile modulus to the rule of mixture approximation. Detailed explanation of these methods and how they relate to SWNT individualization are available in the experimental section and Appendix C.2. Complete RBM spectra of fibers 5wt%-A and -B is presented in Figure C 5 and RBM2 predominance is listed in Table 4-2. The larger predominance of the RBM2 (method a) of fiber 5wt%-A as compared to that of fiber

5wt%-B (20 and 15%, respectively), indicate that the former had a poorer SWNT dispersion. Similarly, SWNT bundle diameters estimated by method b) of 5wt%-A and 5wt%-B fibers were 5.3 and 1.3 nm, respectively. Poorer filler individualization in fiber 5wt%-A is probably also the reason why this fiber had a lower maximum draw ratio than fiber 5wt%-B as relatively large SWNT bundles/agglomerates can act as defects in the nanocomposite fiber and cause it to fracture at low draw ratios.

Table 4-2. Structural parameter and mechanical properties of PAN fiber and PAN nanocomposite fibers with various amount of SWNTs prepared from spinning solutions listed in Table 4-1.

Fiber label	PAN	1wt%	5wt%-A	5wt%-B	15wt%
Stretch ratios*	3×1.5×5.3	3×1.5×5	3×1×5.4	3×1.3×5	1.3×1.1×7
Total draw ratio (TDR)*	24×	22.5×	16.2×	19.4×	9.8×
Fiber diameter (μm)	11.5 ± 0.2	12.9 ± 0.3	15.1 ± 0.6	12.3 ± 0.2	13.2 ± 0.2
X_c[a] (%)	53	54	45	57	38
L_{PAN}[b] (nm)	9	11.0	13.2	12.7	11.2
Ratio[c] $d_{\sim 17°}/d_{\sim 30°}$	1.72(4)	1.71(3)	1.71(2)	1.72(0)	1.73(1)
f_{PAN}[d]	0.89	0.79	0.80	0.82	0.85
f_{SWNT}[e]	NA	0.90	0.91	0.89	0.91
RBM2 peak (%)[f]	NA	19	20	15	16
Tensile Strength (MPa)	896 ± 28	802 ± 28	681 ± 35	944 ± 38	829 ± 20
Tensile Modulus (GPa)	19.2 ± 0.4	20.1 ± 0.4	20.0 ± 0.6	24.7 ± 0.3	32.1 ± 0.5
Elongation at break (%)	7.4 ± 0.2	8.5 ± 0.2	10.1 ± 0.3	8.9 ± 0.3	8.4 ± 0.3
Estimated SWNT bundle diameter (nm)[g]	NA	2.2	5.3	1.3	2.3

Notes: * TDR = SSR×CDR×HDR, with TDR: total draw ratio, SSR: as-spun stretch ratio, CDR: cold-drawn ratio (1st stage drawing), HDR: hot-drawn ratio (2nd stage drawing). [a] PAN crystallinity from integrated WAXD measurements. [b] Crystal size from 2θ ~17° peak according to Scherrer's equation with $k = 0.9$. [c] Ratio of d-spacing of diffraction peaks reflections at ~17° and ~30°. [d] 2nd order Hermann's orientation factor calculated from azimuthal scans of 17° peak. [e] 2nd order orientation factor of SWNTs calculated from polarized Raman spectroscopy. [f] RBM2 peak area as a percentage of the total area of RBM bands (150-350 cm^{-1}) of the Raman spectra using un-polarized laser. [g] calculated as

the SWNT bundle diameter required to obtain the measured tensile modulus from the modified rule of mixture (see discussion and Appendix C.3).

Differences in the mechanical properties and filler individualization of fibers 5wt%-A and 5wt%-B were caused by differences in the filler dispersion protocol used for these fibers (see Table 4-1) and further show why several authors preferred dispersing the carbon nanotubes in copious amount of excess solvent prior to its addition to the polymer solution[65,67,71] or mixing with PAN.[164] Addition of filler dispersion to PAN solution at concentration as low as 0.7 mg/dl have been reported,[67] while typical spinnable polymer solutions have solid content between 5 and 20 g/dl, depending on the PAN molecular weight (see for example [165] about the production of PAN-gel films).

SWNT individualization is more difficult to achieve upon increasing filler content, given the increased probability of filler-filler contacts. Notice for example that estimated SWNT bundle diameter in 1wt% fiber was less than half that in fiber 5wt%-A, even though the same filler dispersion protocol was used for both fibers. Still, good SWNT dispersion in the nanocomposite fiber was maintained upon increasing the SWNT content to 15 wt%. RBM2 predominance of fibers 15wt% and 5wt%-B was similar (16% and 15%, respectively). Estimated SWNT bundle diameter by the rule of mixture was 2.3 nm in fiber 15wt%, larger than that of fiber 5wt%-B, but significantly better than that of fiber 5wt%-A. Furthermore, SEM imaging of the fully drawn and as-spun 15wt% fibers showed well dispersed fillers at the cross-section (see Figure 4-4c-d, i-k and Figure C 6), while few agglomerates were observed on the outside of the fiber (Figure 4-4a-b, g-h). Presence of the agglomerates only near the surface of the fiber indicates that the agglomerates observed in the spinning solution (Figure C 3c,f) were exfoliated due to shearing during spinning and drawing.

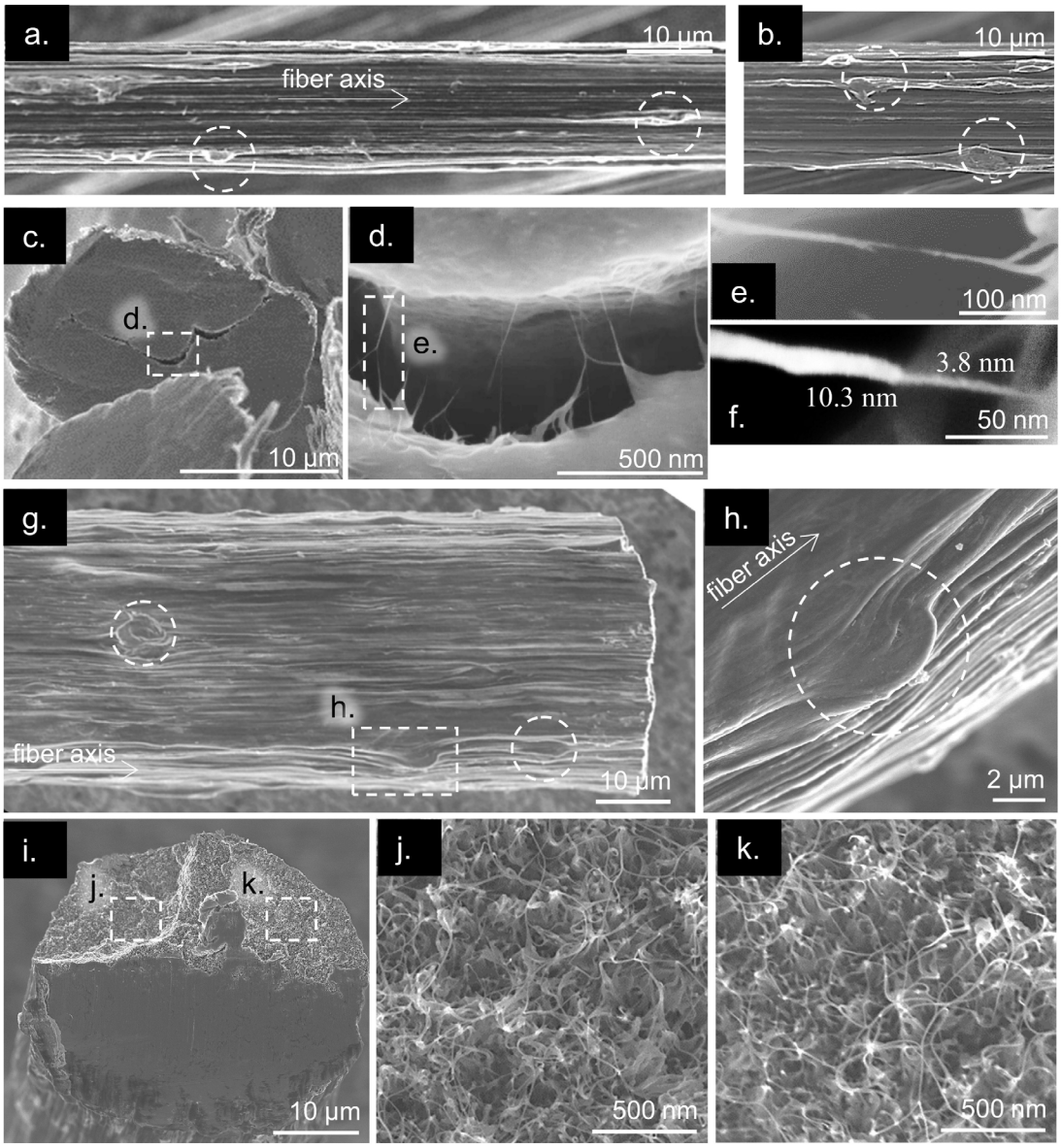

Figure 4-4. Scanning electron micrographs of (a-f) fully drawn (TDR 9.8×) and (g-k) as-spun (TDR 1.6×) 15wt% SWNT fibers.
Side-view (a-b, g-h) and cross-section (c-d, i) of the fibers were imaged. (e-f) are high magnification images of fibrils with the observed step change in diameter in (d). Images at higher magnification (j-k) of the highlighted areas in the as-spun fiber's cross-section (i) show uniform distribution of the SWNTs. Fiber cross-sections were obtained by cutting it, while submerged in liquid nitrogen. Infrequent agglomerates, indicated by dotted encirclements in (a-b, g-h), were visible only near the fiber surface. Additional micrographs are available in Figure C 6 in Appendix C.

WAXD characterization of the fully drawn fiber containing 15 wt% SWNTs showed that the carbon nanotubes were still helically wrapped by the PMMA, confirming that the

PMMA becomes part of the SWNT-PAN interphase. Our earlier report[34] on the effect of PMMA wrapping molecular weight on the structure and properties of fibers with 5 wt% SWNTs showed that the PMMA peak at 2θ ~10.8° remained after fiber spinning. However, the ~10.8° peak was not observed after fiber drawing. We show here (see Figure 4-5) that at higher SWNT content (15 wt%), the PMMA helical peak is visible in the fully drawn fibers.

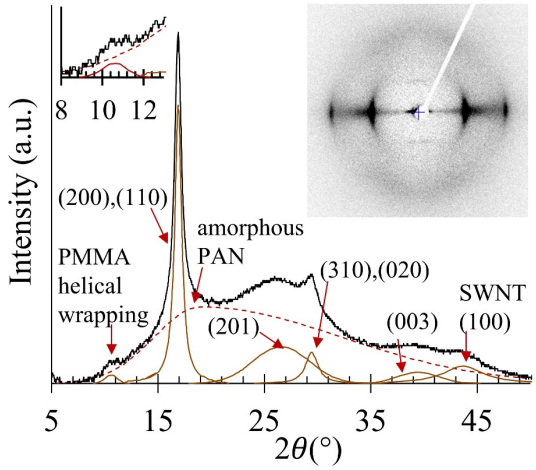

Figure 4-5. Integrated signal from the wide-angle x-ray diffraction (WAXD) of the fully drawn (TDR 9.8×) 15 wt% SWNT fiber, with insets showing the PMMA-helical-originated diffraction peak (2θ ~10.8°) and the 2D WAXD image.

Among the prepared nanocomposite fibers and despite its lower TDR, PAN crystals in 15wt% fiber had the $d_{\sim 17^\circ}/d_{\sim 30^\circ}$ ratio closest to that of the high-packing density hexagonal crystal ($d_{\sim 17^\circ}/d_{\sim 30^\circ} = \sqrt{3}$). This was probably caused by high-shearing of PAN molecules near the SWNT surface. Still, fiber 15wt% had smaller crystallinity and crystal size than the fibers with 5 wt% SWNTs. It could be argued that the difference is a result of the lower TDR, however, it should be noted that the crystallinity and crystal size is bound to be limited by the higher content of well-dispersed SWNTs: upon increasing filler content, less PAN molecules can fit in the space between fillers and their movement will be restricted. Increase at low filler content and decrease at high filler content of the PAN crystal size has been previously observed in PAN fibers with cellulose nanocrystals[88] and

PAN films with vapor grown carbon nanofiber.[166] Such dependence with SWNTs content had not been clearly observed before[71,161] due to the limitation in producing PAN samples with high-content (>10 wt%) well-dispersed SWNTs. Small angle x-ray scattering signal of 15wt% and PAN fibers is presented in Figure C 7. Both fibers showed a comparable monotonous decrease in intensity with increase in the scattering vector. An obvious SAXS signature due to the presence of mostly individual SWNTs was not observed.

SEM images of brittle rupture (Figure 4-4h-k) at the cross section of the 15wt% fiber (TDR 9.8×) showed fibrils with a step-wise change of diameter (Figure 4-4k) from ca. 10.3 ± 0.5 nm to 3.8 ± 0.5 nm. Fibrils of similar diameter were obtained after dissolving the fully drawn fibers in DMF at 120 °C for 6 h. Fibrils obtained from 15wt% fiber (see Figure 4-6b-d) were 10.4 ± 0.6 nm in diameter, but structures as thin as 3.3 nm were also observed. In fact, these fibrils showed a step-wise diameter distribution (Figure C 8). UV-Vis characterization of these fibrils while in DMF dispersion showed typical van Hove transitions of highly individualized SWNTs (Figure 4-6a). Fibrils obtained from the dissolution of fiber 5wt%-B had comparable diameters (ca. 9.0 ± 0.6 nm and 2.8 nm, Figure C 9) and comparable van Hove transitions to those obtained from the fiber with 15 wt% SWNTs.

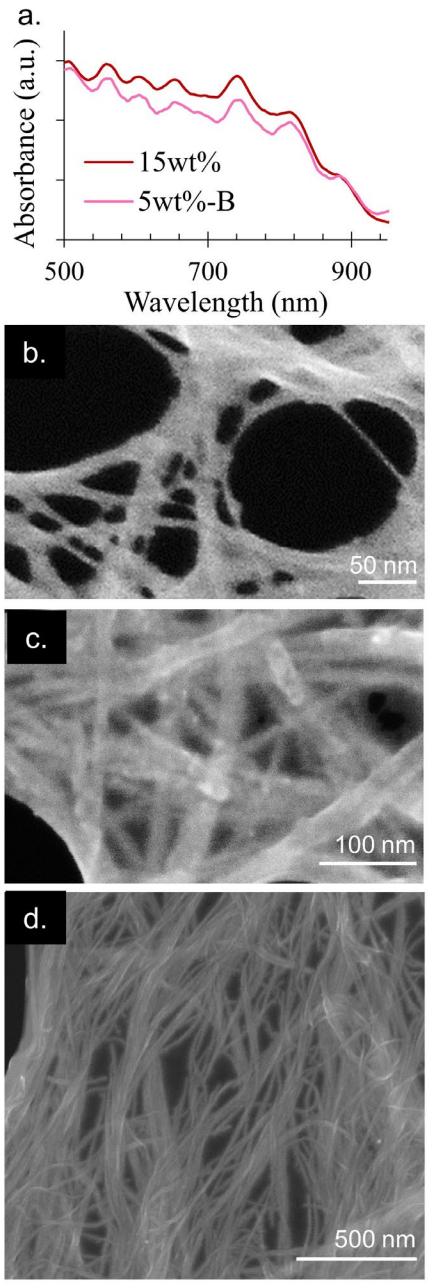

Figure 4-6. (a) UV-Vis spectra of DMF dispersion in which fully drawn fibers 15wt% (TDR 9.8×) and 5wt%-B (TDR 19.4×) were dissolved.
Fibers broke-down to fibrils, presumed to be SWNT bundles covered in PAN, as observed by scanning electron microscopy at different magnifications of dissolved 15wt% fiber (b-d). Images of fibrils obtained from 5wt%-B fiber are given in Figure C 9 in Appendix C.

Fibrils have been previously observed after dissolution of PAN fibers reinforced with 1 wt% pristine-SWNT and characterized by transmission electron microscopy (TEM) [65] and in other carbon nanotube/polymer systems.[167] Fibrils obtained from PAN/SWNT

fibers[65] were ca. 20 nm in diameter and formed by a PAN coating of ca. 8 nm thick around bundles of 2 SWNTs. We believe that the fibrils observed here (Figure 4-4k and Figure 4-6b-d) are formed by PMMA-wrapped-SWNT (Figure 4-5) bundles covered by PAN. This assumption further explains the two different fibril diameters measured: thin structures (3.3 nm) would correspond to the SWNT bundles with or without a thin PAN coating, while the fibrils of 10 nm are SWNT bundles covered by a thicker PAN coating.

Differences in the fibril diameter and PAN coating thickness between the previously reported PAN/SWNT fiber[65] and those produced here was caused by increasing the filler content in the fiber. Reported fiber with pristine-SWNTs had 1 wt% filler[65] and an estimated distance between fillers of 12 nm. On the other hand, for fibers with 5 and 15 wt% SWNT, the estimated filler-filler distance is 6 and 4 nm, respectively, explaining the thinner fibrils measured here. Calculation of distance between fillers assumes fully individualized nanotubes and was done considering an ideal filler hexagonal arrangement as described elsewhere.[141]

PAN/SWNT fibrils in nanocomposite fibers[65] and PAN coated SWNTs in films produced by vacuum-drying[160] are believed to be caused by interactions between pristine-SWNTs and PAN. PMMA-wrapping of SWNTs increased said interactions: firstly, our previous report compared the matrix filler interaction of pristine-SWNT and PMMA-SWNTs in PAN fibers with 1 wt% filler by indirectly measuring SWNT strain during tensile deformation in the nanocomposite fiber.[34] It was concluded that upon PMMA-wrapping, the SWNTs experienced larger strain rate and maximum strain than pristine-SWNTs, thus PMMA-wrapping improved strain transfer from the matrix to the filler.[34] Secondly, a similar approach was used to determine filler strain in the 15wt% fiber (TDR 9.8×) produced in the current work (see experimental section and Figure C 10). G` shift rate ($S_r$) and maximum G` shift (G_m) of the 15wt % fiber were -44 cm^{-1} per unit strain and -9.2 ± 0.4 cm^{-}

[1], respectively. The G′ shift is proportionally related to the SWNT strain, as reported elsewhere.[168] For comparison, S_r values reported for pristine-single and few wall carbon nanotube while in PAN,[67] epoxy[146] and poly(vinyl alcohol)[145] matrix were -28.4, -15 and -35 cm^{-1}/%, respectively. Interestingly, measured S_r for SWNTs in 15wt% fiber was also larger than previously reported for 5wt%-B (-21 cm^{-1}),[34] despite both fibers having PMMA-wrapped-SWNTs. Differences could be caused of the effect the SWNT loading has in the amount of PAN that is part of the interphase and that remains in the bulk of the polymer, or because free PMMA was removed in the 15 wt% SWNT fiber while it remained in the 5 wt% one (Table 4-1).

Tensile modulus and elongation at break of the 15 wt% SWNT fiber were ~70% and ~14% higher than that of the control fiber. These higher mechanical properties were obtained albeit 15 wt% SWNT fiber had the lowest maximum draw ratio and the lowest PAN crystallinity among all the prepared samples, thus demonstrating improved properties were caused by reinforcement provided by the filler. Contrary to fiber 5wt%-A, the lower total draw ratio of fiber 15wt% cannot be attributed to the presence of SWNT agglomerates acting as defect points and promoting fiber breakage during drawing. Rather, it is probable that the maximum draw ratio of fiber 15wt% was limited by the lower as-spun stretch ratio reached for this fiber. Similar phenomena has been previously reported for PAN fibers[140] and was illustrated here by producing a 5wt%-B fiber at an stretch ratio during spinning of 1× (see Table C 2). Fiber 5wt%-B spun at a stretch ratio of 1× had a strain at break during tensile testing of 2.3%, and during hot drawing the fiber could only be stretched to a total draw ratio of 13.6×. On the other hand, when the stretch ratio during spinning was increased to 3×, the strain at break increased to 38% and total draw ratio to 19.4×.

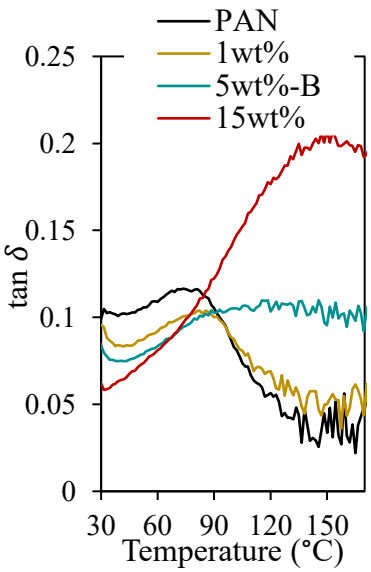

Figure 4-7. Tan δ (a) at 0.1 Hz as a function of temperature for PAN/SWNT nanocomposite fibers prepared with PMMA-wrapped-SWNTs at the indicated filler contents.

Interactions between the PMMA-wrapped-SWNTs and the PAN matrix were also evident during dynamic-mechanical analysis (DMA) of the fully drawn fibers, as the SWNT affected the mobility of the amorphous PAN molecules. DMA data is summarized in Figure 4-7 and Figure C 11 and fully discussed subsequently. As expected, at room temperature, tan δ of 1wt% fiber was lower than that of the control PAN fiber, caused by a decrease in the fiber loss modulus and increase in its storage modulus. tan δ at room temperature further decreased upon increasing the SWNT content, despite an increase in the fiber loss modulus (see Figure C 11a in Appendix C). This behavior was caused by the changes in PAN crystal size and the mobility of amorphous regions. At low filler content (1 wt% SWNT), domain size of amorphous regions and their viscous component decreased since the PAN crystal size changed from 9 to 11 nm. As filler content increased (5 and 15 wt% SWNT) and PAN crystal size remained large, mobility of the amorphous molecules was further reduced, thus increasing its modulus. Similar phenomena has been observed in as-spun and fully drawn PAN fibers with varying content of cellulose nanocrystals.[88]

The described thermal behavior is particularly interesting when compared to that previously observed from other PAN and PAN/filler fibers. Foremost, the absence of the α transition in the control PAN fiber has been previously documented for several other drawn PAN fibers,[69,71,88] indicating that most of the amorphous polymer is not within truly amorphous regions, but rather within paracrystalline regions.[159] Shifting of the β_c transition towards larger temperatures and overall decrease of the tan δ, is expected upon reduction of the free volume within the paracrystalline regions and has been observed upon inclusion of several rod-like fillers.[65,69,71,88] However, overall increase of the tan δ beyond the β_c transition seems to happen only in those systems with SWNT and DWNT, but not with fillers of larger diameter,[69] even when loads as high as 40 wt% are included.[88]

The observed increase of the tan δ beyond β_c in 5wt%-B and similar fibers[69] should not be attributed to a α transitions but rather to the effect of filler-matrix interactions. As summarized in Table 4-2, SWNT presence increased the PAN crystal size without change of the PAN crystallinity (compare PAN and 5wt%-A fibers), thus without change in the amorphous region, i.e. transition is not of the α type. It is also unlikely that it corresponds to a first order transitions (α_c), as such thermal change is typically shown as a sharp peak.[159] Free PMMA content of the 5wt%-B fiber was 3.2 wt% and could have contributed to changes of the thermal-mechanical behavior, however, other authors have reported a similar behavior to that of 5wt%-B fiber in pure PAN/SWNT fibers.[69] Instead, it is likely that the broad increase in tan δ beyond β_c is originated by the presence of PAN interactions with the PMMA-wrapped-SWNTs that restricts chain mobility[169] or altogether chain reptation.[170]

The increase of tan δ beyond β_c observed for 15wt% fiber (Figure 4-7) was probably caused by filler matrix-interactions (just discussed for fiber 5wt%-B) and increase of amorphous contribution. Since PAN crystallinity of the 15wt% fiber was lower than that

of all the other fibers, it is possible to assume that thermal transitions of the α type were also present. Furthermore, previous work on PAN gel films and fibers have shown that at low draw ratios (therefore low crystallinity) the tan δ magnitude of the α transition is larger than that of the β_c ones.[159]

The PAN nanocomposite fiber with 15 wt% SWNT can be used for other applications on its own: upon changing the SWNT type, it should be possible to produce PAN nanocomposite fibers with tunable thermal and electrical properties and, at high enough filler concentration much of the filler properties should transfer to the PAN nanocomposite fiber. Applications can be based on Joule heating [11] and piezoelectric response of CNTs[9], and as biosensors.[10] To illustrate one of these applications, we measured the electrical conductivity of our 15 wt% fiber. Even though we had a mix of semiconductor and metallic SWNTs (expected average conductivity 1 ×10^4 S/m), the 15 wt% nanocomposite fibers had an electrical conductivity (σ) of $14.3 \pm 1.2\, S/m$ before drawing (TDR 1.6× and tensile modulus 12.2 GPa) and of $2.2 \pm 0.5\, S/m$ after drawing (TDR 9.8× and tensile modulus 32.1 GPa). Compared to reported PAN fibers with 15 and 20 wt% multi-wall carbon nanotubes, our 15 wt% fiber has 5 orders of magnitude higher electrical conductivity before thermal annealing and 3 times larger tensile modulus and tensile strength.[11] Therefore, these fibers are also suitable for Joule-heating based applications. Mechanical and electrical properties of PAN/CNT fibers from literature have been compared to this study in Table 1-1.

4.5 Conclusions

The modified procedure for preparation of the spinning polymer solution with high SWNT loading allowed a significant reduction in the processing time, and should be more appropriate for industrial scale production than the traditional protocol that includes extended distillation. Despite adding a slurry of SWNTs (> 200 mg/dl) to the polymer

solution the 15 wt% SWNT nanocomposite fiber had well dispersed filler, with an estimated bundle diameter of 2.3 nm. This fiber had a tensile modulus of 32.1 GPa, demonstrating matrix reinforcement at high filler loading. We show here that PMMA-wrapping of the SWNTs remains after fiber spinning and drawing, and thus becomes part of the filler-matrix interphase. PMMA-wrapped-SWNTs interact with PAN matrix as demonstrated by: (a) nanocomposite fiber dissolved into fibrils resistant to extended DMF treatment (6 h at 120 °C), which have been previously documented to happen when pristine-SWNT bundles are covered by PAN. (b) Measured G' shift rate upon straining of the fiber with 15 wt% SWNTs was -44 cm^{-1}/%, one of the highest reported values for a SWNT/nanocomposite system. (c) Dynamic mechanical transition behavior of the composite fibers was modified by the presence of PMMA-wrapped-SWNTs. (d) Films produced by vacuum-drying of PAN solutions with PMMA-wrapped-SWNTs had similar crystalline structure than that previously obtained when SWNT bundles are uniformly coated by PAN. Overall, electrical conductivity and tensile properties of the 15 wt% SWNT PAN fibers produced here with PMMA-wrapped-SWNTs were significantly higher than that previously reported for other PAN fibers with high carbon nanotube concentrations.

5 CHAPTER 5: CARBON FIBERS PRODUCED FROM PAN FIBERS WITH PMMA-WRAPPED-SWNTs

Preamble

In this chapter, PAN nanocomposites fibers produced in Chapter 4 with 5 and 15 wt% SWNTs are carbonized and the effect of SWNT, PMMA wrapping, and free PMMA on the carbon fiber structure and properties is studied.

Transmission electron microscopy images in this chapter were obtained through a collaboration with Dr. Jin Gyu Park and Dr. Zhiyong (Richard) Liang at Florida State University.

5.1 Abstract

Carbon nanotube (CNT)/carbon (CNT/C) nanocomposite fibers were produced with up to 25 wt% single wall carbon nanotubes (SWNTs) via stabilization and carbonization of polyacrylonitrile (PAN) precursor fibers containing up to 15 wt% SWNTs. Effect of filler loading on the CNT/C fiber structure and properties is studied, and the filler effect on PAN stabilization is discussed. Filler-matrix interactions took place despite the fact that the precursor fiber had SWNTs wrapped with poly(methyl methacrylate) (PMMA), a polymer without carbon yield. Tensile modulus of CNT/C fiber with 25 wt% SWNTs was 324 ± 20 GPa, while that of the control PAN based carbon fiber was 288 ± 9 GPa. Strategies to further improve the tensile properties of this CNT/C fiber are briefly discussed.

5.2 Introduction

Inclusion of carbon nanotubes (CNTs) in polyacrylinitrile (PAN) fibers is interesting because said nanocomposite fibers can be used as a precursor for carbon nanotube/carbon (CNT/C) nanocomposite fiber. CNT/C nanocomposites are advanced materials that could outperform state of the art carbon fibers and carbon fiber-reinforced composites; thus CNT/C nanocomposites could be used for advanced applications like the structure of space vehicles.[171] While a typical approach to production of CNT/C composite is infiltration of self-standing CNT structures with carbon-precursor polymers,[172–174] direct inclusion of CNT in carbon precursor is interesting as it can maximize contact between filler and matrix and should allow the production of high performance nanocomposites at reduced CNT loading.

Many studies have focused on the inclusion of CNTs in PAN and its post-treatment to obtain CNT/C nanocomposite fibers.[72,75,76,79,153,175–177] Inclusion of CNTs in PAN precursor has been shown to promote graphitic templating of the PAN around CNTs[33,178]

and affect the PAN stabilization and carbon fiber's tensile properties.[179] However, PAN derived CNT-C nanocomposite carbon fibers still have relatively low mechanical properties, due to presence of CNT aggregates and bundles, which facilitate the presence of voids and reduce filler-matrix contact.[33] Thus, obtaining a high-performance CNT/C fiber from CNT/PAN precursor is still an open problem.

PAN fibers produced in Chapters 3 and 4 with 5 and 15 wt% single wall carbon nanotubes (SWNTs) were stabilized and carbonized to obtain CNT/C fibers. These precursor fibers were of interest because of the high filler individualization and good mechanical reinforcement achieved by SWNTs that were helically wrapped with poly(methyl methacrylate) (PMMA). Furthermore, these fibers also presented the opportunity to study how the CNT/C fiber is affected by the presence of a polymer without carbon yield (PMMA) at the SWNT-PAN interface. Prior studies have shown how different functional groups on the CNTs affect the PAN stabilization and carbon fiber tensile properties,[75,180] However, to the best of our knowledge, there are not prior studies of CNT/C fibers obtain from PAN fibers with CNTs helically wrapped with a polymer.

5.3 Experimental

5.3.1 PAN nanocomposite precursor fibers

Precursor fibers carbonized and reported in this chapter were those listed in Table 5-1 and produced in Chapter 4. Thermal shrinkage of these precursors fibers was studied using a TA Q400 thermomechanical analyzer. Filament bundles of at least 85 μm equivalent diameter were heated in air atmosphere from room temperature to 265 °C at a rate of 3 °C/min, followed by isothermal heating at 265 °C for 170 min. During this process, bundles were subjected to engineering stresses in the 15 – 30 MPa range and their length change was monitored.

Table 5-1. PAN nanocomposite fibers studied in this chapter.

Precursor Fiber ID	Precursor fiber composition†			
	SWNT content (wt%)	PAN content (wt%)	Total PMMA content (wt%)	Free PMMA content (wt%)‡
5wt%-B	5	90	5	3.2
15wt%	15	79	6§	0§

† calculated from the amount of SWNTs, PMMA and PAN used during SWNT wrapping and spinning solution preparation.
‡ free PMMA content was estimated assuming ~37% of the added PMMA is adsorbed onto the SWNTs.
§ free PMMA was removed following the protocol summarized in Figure 4-1 in Chapter 4.

5.3.2 Precursor fiber stabilization and carbonization

Filament bundles with equivalent diameter of at least 85 μm were batch stabilized and carbonized in an MHI H17HT2.5x24 tube furnace. Bundles were kept under tension during the stabilization and carbonization by connecting the bundle's end to graphite and stainless-steel weights. Fibers 5wt%-B were kept at an engineering stress of 25 MPa, while fibers 15wt% were kept at 30 MPa. The two-step stabilization was carried out while passing air through the tube furnace. 1st step of the stabilization consisted in heating from room temperature to 265 °C at a heating rate of 3 °C/min, followed by isothermal heating at 265 °C for 170 or 330 min. Then, during the 2nd step, the temperature was raised from 265 to 305 °C at a rate of 3 °C/min, followed by a 10 min isothermal treatment at 305 °C. Fibers were carbonized by heating in nitrogen atmosphere from room temperature to 1315 °C at a rate of 5 °C/min, followed by a 10 min isothermal hold at 1315 °C, then the furnace was turned off and allowed to cool down for 4 h before removing the carbon fiber samples.

Single-filament tensile testing was conducted on a Solids Analyzer III (TA Instruments) by mounting individual fibers on paper tabs with a gauge length of 12.5 mm and using a strain rate of 0.1 %/min. At least 15 filaments were measured per sample and no compliance correction was done on the measured tensile modulus. Scanning electron microscopy (SEM) was conducted on uncoated samples on a Hitachi SU8230. Wide-angle

X-ray diffraction (WAXD) of carbon fiber bundles was collected on a Rigaku MicroMax-003 operating at 50 kV and 0.60 mA and coupled to an R-axis IV++ detector. Electrical conductivity was estimated using a Keithley 2400 source-meter. Individual carbon fiber filaments were mounted on non-conductive glass and silver paste was used to create electric contact points along the fiber. Distance between electric contact points was between 5 to 20 mm and the resistance was measured while applying 0.1 mA current.

5.4 Results and Discussion

5.4.1 Effect of high SWNT loading on carbon fiber structure and properties

The structural parameters and the mechanical and electrical properties of the nanocomposite carbon fibers depended on the amount of SWNTs present in the precursor fiber, as summarized in Table 5-2. Estimated SWNT content in the carbon fibers was 9 and 25 wt% for those fibers produced from the PAN precursors with 5 and 15 wt% SWNTs, respectively. At comparable times for the 1st step of the stabilization, i.e. 170 or 330 min, carbon fibers obtained from the precursor with 15 wt% SWNTs had slightly higher tensile strength and significantly higher tensile modulus than carbon fibers obtained from the precursor with 5 wt% SWNTs. Furthermore, fiber with 25 wt% SWNTs obtained from the fiber stabilized at 265 °C for 300 min (25-CF2) had slightly higher tensile modulus than the control carbon fiber produced under similar conditions but without SWNTs (see Table 5-2). TEM imaging of fiber 25-CF2 shows that well dispersed SWNTs served as templates for the formation of concentric graphite planes (Figure 5-1a,b). This suggests the presence of SWNT-carbon matrix interactions, despite the fact that SWNTs were covered with a non-carbonizing polymer, the PMMA (see chapter 4).

Table 5-2. Mechanical and electrical properties of nanocomposite carbon fibers produced from PAN precursors with 5 and 15 wt% SWNT and while changing stabilization time.

Carbon Fiber ID	Control-CF [a]	9-CF1	9 -CF2	25-CF1	25-CF2
SWNT in Precursor (wt%)	0	5		15	
Estimated SWNT composition in the carbon fiber (wt%) [b]	0	9		25	
Engineering stress during stabilization (MPa) [c]	30	25		30	
Hold time at 265 °C (min)	170	170	330	170	330
Diameter (μm)	8.2 ± 0.2	7.8 ± 0.6	8.1 ± 0.2	7.8 ± 0.6	8.9 ± 0.6
Tensile strength (GPa)	2.08 ± 0.29	0.84 ± 0.12	0.49 ± 0.09	0.99 ± 0.13	1.25 ± 0.24
Tensile modulus (GPa) [d]	288 ± 9	198 ± 26	160 ± 53	229 ± 24	324 ± 20
Strain at break (%)	0.79 ± 0.10	0.38 ± 0.04	0.30 ± 0.06	0.35 ± 0.05	0.37 ± 0.05
$f_{(002)}$ [e]	0.81	0.82	0.83	0.88	0.86
$L_{(002)}$ (nm) [f]	1.8	1.4	1.5	1.5	1.5
$L_{(10)}$ (nm) [f]	2.0	2.6	2.9	2.8	2.7
Electrical conductivity (kS/m)	59.6	NM	30 ± 3	NM	67 ± 7

Notes: NM: not measured.

[a] as reported elsewhere[89] for a PAN precursor fiber produced by similar conditions to those listed in Chapter 4 but from PAN of 250,000 g/mol molecular weight.

[b] filler content in the carbon fiber was calculated assuming a PAN carbon yield of 56 wt%, total loss of PMMA and no SWNT mass loss.

[c] engineering stress value was kept during stabilization and carbonization.

[d] reported tensile modulus of fibers with 9 and 25 wt% SWNTs were not compliance corrected.

[e] 2nd order orientation factor calculated for the graphitic (002) peak.

[f] crystal size of (002) and (10) planes was from 2θ ~26° and 43°, respectively, assuming a shape factor of 0.9.

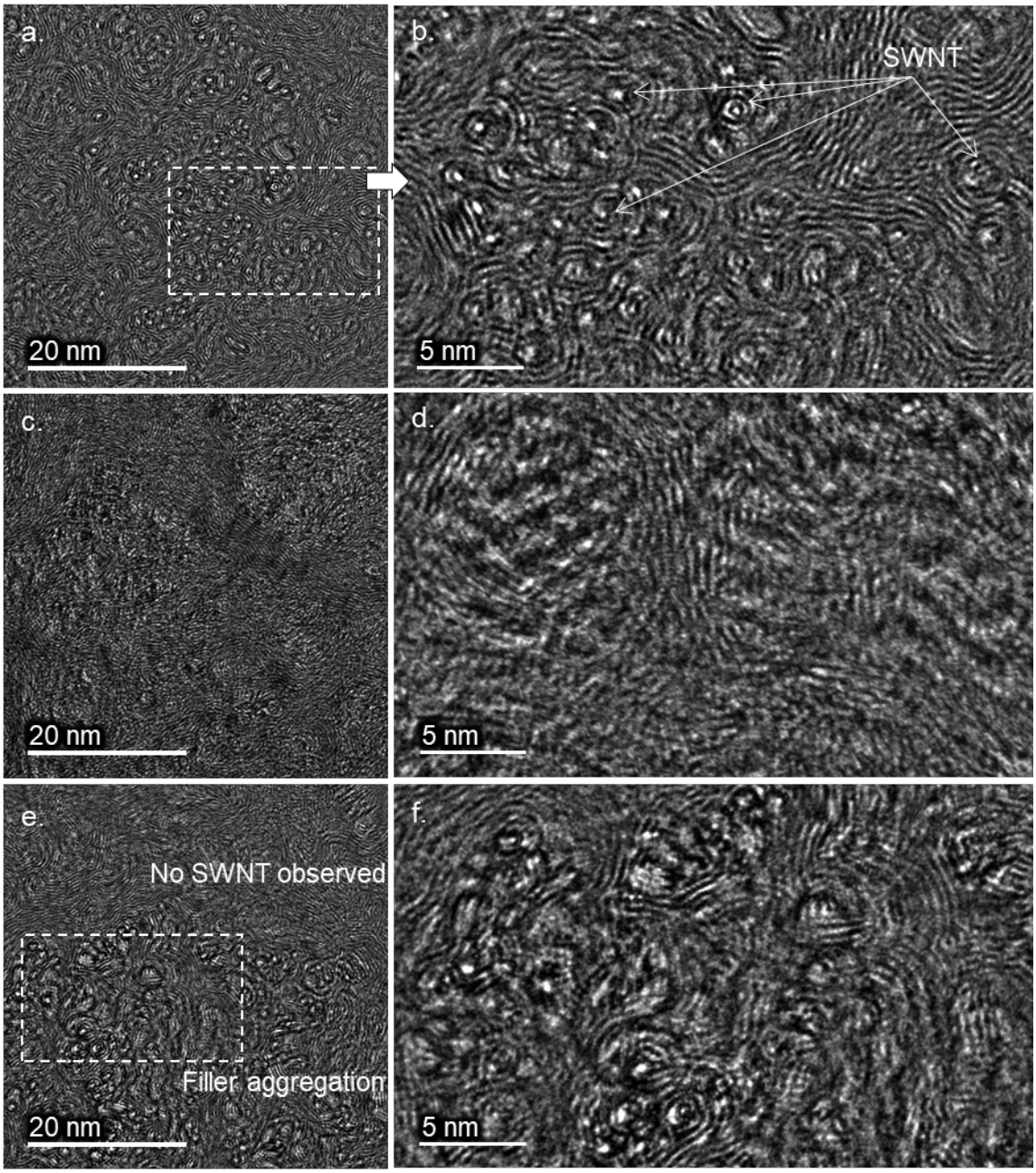

Figure 5-1. Transmission electron micrographs of 25-CF2 carbon fiber cross-section. TEM specimens were prepared by focused ion-beam (FIB) etching. Well-dispersed SWNTs and surrounding concentric graphite planes can be observed in the fiber cross-section (a,b). (c-d) are regions with few SWNTs and (e-f) are regions that appear to show SWNT aggregates.

SWNT presence modified the structure of the PAN-derived graphitic planes. Foremost, the axial orientation of the graphite (002) planes, quantified by the 2nd order Hermann's orientation factor, was significantly higher in carbon fibers with 25 wt% SWNTs

(0.88 and 0.86 in fibers 25-CF1 and 25-CF2, respectively) than in the control carbon fiber (0.79) and in the carbon fibers with 9 wt% SWNTs (0.82 and 0.83 in fibers 9-CF1 and 9-CF2, respectively). In previous work[33] carbon fibers produced with 1 and 0.5 wt% few wall carbon nanotubes have also shown an increase in the Hermann's orientation factor. Azimuthal data of these fibers with lower filler loading, as extracted from the original manuscript,[33] is also plotted in Figure 5-2a. Comparison of the (002) azimuthal data upon increasing CNT content shows how the filler content directly relates to the (002) orientation (see Figure 5-2a) and was highest in the carbon fiber with 25 wt% SWNT. As reported elsewhere,[33] the graphitic orientation increased as carbon nanotubes acted as templating agents for ordered graphite formation. As shown in Figure 5-1b, similar results are obtained here: concentric graphite planes were formed around the SWNTs and SWNT bundles. This is particularly interesting because SWNTs in the precursor fibers used here were wrapped with PMMA and PMMA and PAN are immiscible polymers.

Another major effect of the large loading of SWNTs in carbon fiber 25-CF2, was the change in the turbostratic structure of the matrix. In PAN-derived carbon fibers, the graphitic layers are not ordered in a hexagonal structure, instead these layers have several rotations, translations and curve onto each other, a distorted structure known as turbostratic carbon that forms an asymmetric 2θ ~25.3° diffraction peak.[181] WAXD results for the carbon fibers here prepared are presented in Figure 5-2b. The graphite (002) peak of 25-CF2 fiber was more skewed, had a larger full width at half maximum and larger d-spacing than that of the carbon fiber with fewer SWNTs (9-CF2). This is caused because upon increasing filler concentration, the graphite crystal size is decreased and the graphitic planes tend to be more turbostratic. Compare for example Figure 5-1 that shows two different areas of the same 25-CF2 fiber, in which local density of SWNTs and graphitic plane twisting were higher (images a and b) and lower (images c an d).

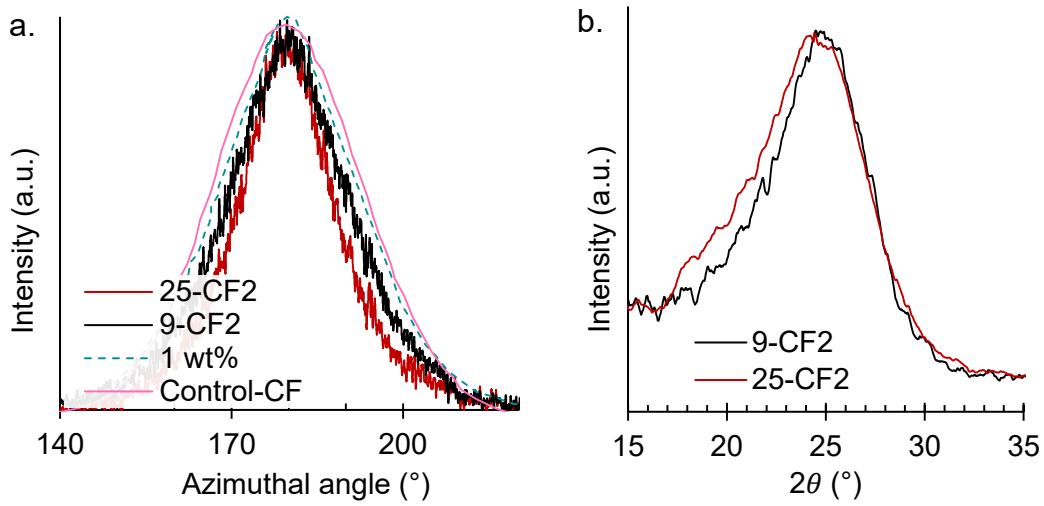

Figure 5-2. Wide-angle X-ray data of carbon fibers 9-CF2 and 25-CF2 produced from PAN precursors with 5 and 15 wt% SWNTs, respectively.
(a) Azimuthal scan of the (002) peak of nanocomposite carbon fibers prepared here (9-CF2 and 25-CF2) and two carbon fibers reported elsewhere[33] and produced from a PAN precursor with 1 wt% few-walls carbon nanotubes (1 wt %) and without filler (Control-CF). (b) Graphite (002) peak in equatorial scans of carbon fibers 9-CF2 and 25-CF2. Equatorial diffraction scans in the 5 – 55° 2θ range and azimuthal scans of the 2θ ~25.3° peak in the 90 to 270° Φ range are available in Figure D 1 in Appendix D.

Turbostratic structure in carbon fibers has been related to increased tensile strength due to hindering crack propagation,[182] and to increased tensile modulus due to larger shear modulus between graphitic planes and whiskers.[183] Furthermore, alignment of the graphite planes is directly related to the tensile modulus of the carbon fiber.[183] However, tensile modulus and strength of 25-CF2 were slightly higher and significantly lower, respectively, than those of the control carbon fiber. This was caused because despite the high filler individualization observed in Figure 5-1a,b for the carbon fiber 25-CF2, some larger diameter SWNT bundles were also observed in the fiber cross section (see Figure 5-1e,f). In fact, some SWNT aggregates of up to 1.5 μm diameter were observed (see Figure D 2 in Appendix D). Thus, although high SWNT exfoliation was reached by using SWNTs wrapped with PMMA and sonication, there were also SWNT aggregates. This indicates that the SWNT dispersion protocol described in Chapter 4 should be further optimized. SEM characterization of several filament cross-sections

showed that large SWNT aggregates, as well as voids were common. It is noted that void-free cross-sections were also observed (Figure 5-3a,d). Presence of voids explains why the tensile strength of the 5wt%-B and 15wt% derived carbon fibers was significantly lower than that of the control carbon fiber (2.1 GPa, see Table 5-2) and that of other carbon fibers produced from precursors with 1 wt% CNT content after batch stabilization and carbonization optimization[176] (4 GPa).

Ordered graphitic formation around SWNTs and SWNT bundles is expected to a consequence of filler-matrix interactions. Figure 5-3 shows the cross-section of carbon fibers 9-CF2 (a-c) and 25-CF2 (d-g), in which fibril-like structures were widely observed. Fibril diameter in fiber 9-CF2 was as large as 30 nm (Figure 5-3b), but in some regions the fibril diameter was as small as 7 nm (Figure 5-3c). On the other hand, fibril diameter in fiber 25-CF2 was always smaller than 10 nm (see Figure 5-3e-g). Similar nanofibrils with 20 – 50 nm diameter have been previously reported in the cross-section of PAN-derived carbon fiber when up to 1 wt% of the precursor was composed of few-wall carbon nanotubes.[33,175–177] Reduction of the fibril diameter in the carbon fibers with increasing filler content is probably associated with the amount of PAN present in between carbon nanotubes. As the CNT content increases, the CNT-CNT distance is reduced, as well as the amount of PAN that can be stabilized and carbonized around a given CNT. Nanofibrils in PAN/CNT derived carbon fibers have been previously shown via high-resolution TEM (HR-TEM) to be formed of highly ordered graphitic structure.[177]

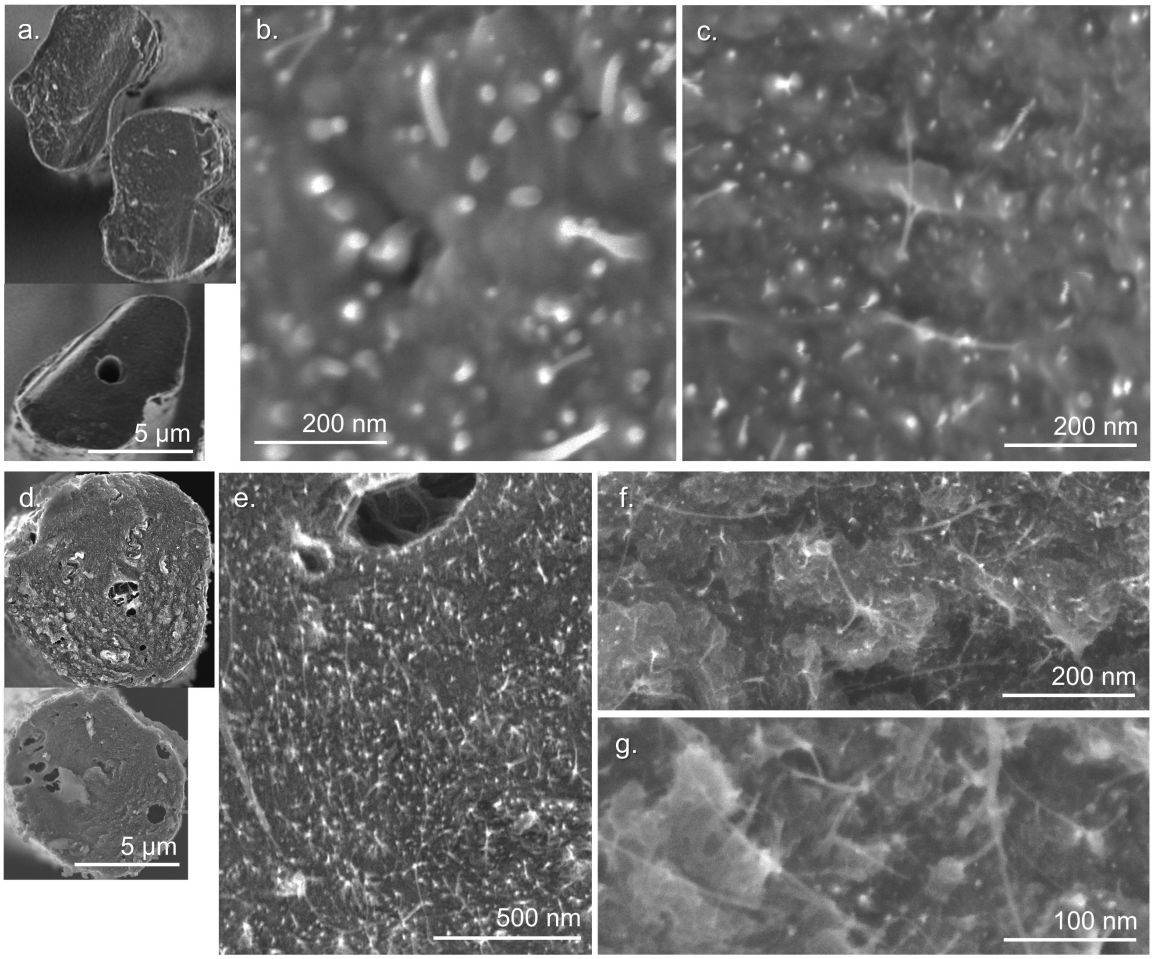

Figure 5-3. Scanning electron micrographs of cross-sections of carbon fibers 9-CF2 (a-c) and 25-CF2 (d-g) at different magnifications.

5.4.2 Effect of SWNT on PAN stabilization

Tensile properties of carbon fiber 25-CF2 were significantly higher than those of fiber 25-CF1. This suggests that longer times during the 1st step stabilization were beneficial, and that stabilization reaction was affected by the SWNT presence. SEM characterization showed that carbon fibers produced from fibers stabilized at 265 °C for 170 min (9-CF1 and 25-CF2, Figure 5-4) had more frequent relatively large voids near the fiber center, in addition to other irregular voids in no particular location. On the other hand, in carbon fibers from fibers stabilized at 265 °C with holding time of 330 min (9-CF2 and 25-CF2, Figure 5-3) the cross-section had no voids or only had a few irregular voids. While

the irregular voids probably correspond to large SWNT agglomerates (see Figure D 2), the voids near the cross-section center indicate radial heterogeneity during stabilization. Skin-core geometry in stabilized PAN fiber, produced because of radial heterogeneous stabilization, has been previously shown to lead to void formation at the carbon fiber core.[184–186] Heterogenous stabilization along the fiber radius is caused because PAN oxidation and cyclization are oxygen-diffusion limited and thermally controlled processes, respectively. On the one hand, during stabilization, PAN is homogenously cyclized across the fiber cross-section,[186] and upon cyclization the rate of oxygen diffusion in PAN is reduced.[187] On the other hand, oxidation of PAN depends on oxygen concentration profile through the fiber cross-section, which is highest near its surface and lowest at the fiber center.[188,189]

Oxygen diffusion is bound to be affected by the amount of SWNTs in the precursor fiber. Presence of a relatively low concentration of CNTs (1 wt%) in PAN fibers has been shown to reduce oxidation reaction rate during stabilization.[189] Such reduction in the oxidation reaction rate was observed despite the fact that activation energy of the oxidation reaction decreased upon CNT inclusion.[189] Therefore, the decreased in oxidation reaction rate is explained by reduced oxygen diffusion in the CNT-reinforced PAN matrix. Relatively high CNT content (10 wt%) in PAN fibers has been shown to increase oxidation reaction rate[190] due to the introduction of porosity at the surface of the precursor fiber. High CNT loading in polymer films has been previously shown to produce pores and increase oxygen diffusivity.[191] The SWNT reinforced PAN fibers carbonized here did have high filler content. However, filler alignment and individualization was high and no pores were observed in the PAN matrix (see Figure 4-4 and Table 4-2 in Chapter 4), except for the occasional SWNT aggregates distributed along the fiber (see Figure D 2). Hence, low oxygen diffusion in the radial direction is to be expected when stabilizing

fibers 5wt%-B and 15wt%, as compared to the control PAN fiber. This explains why tensile strength and modulus of the 15wt%-derived carbon fiber were higher upon longer stabilization times (see Table 5-2), and opens the possibility to further improve the tensile properties of fibers with 25 wt% SWNT. This will require optimization of stabilization conditions as has been done extensively for control PAN fibers.[175,176,184,186,192]

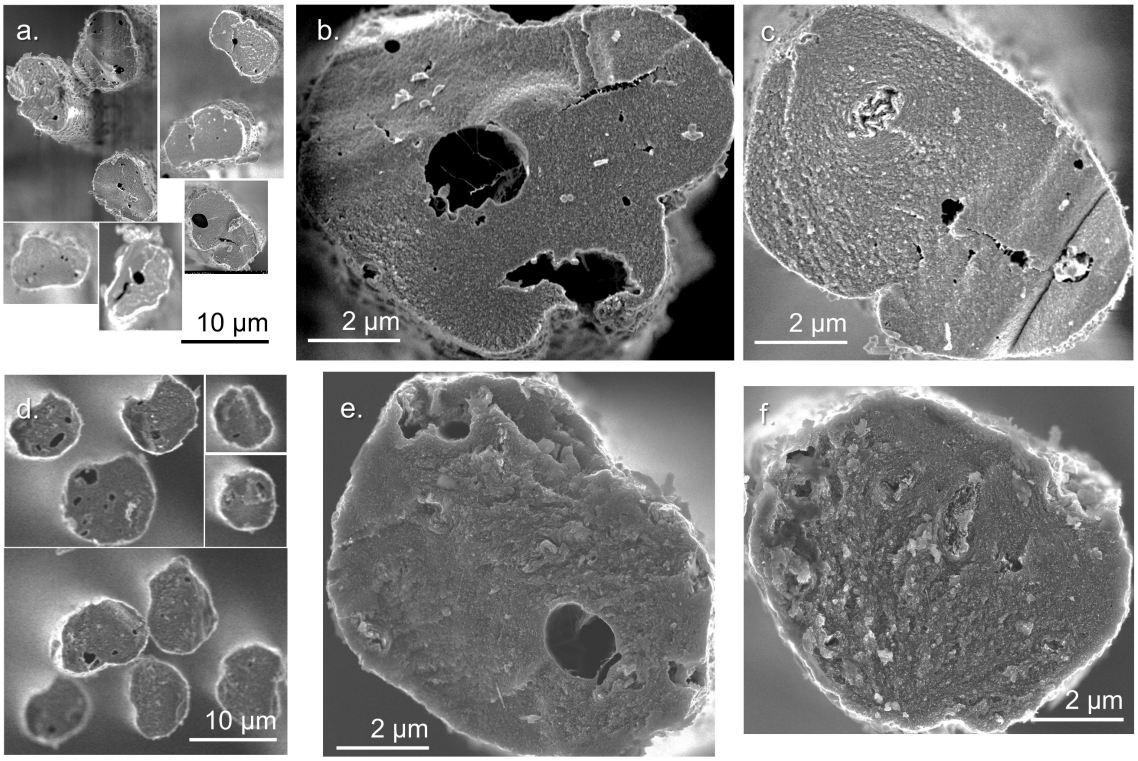

Figure 5-4. Scanning electron micrographs of cross-section of carbon fibers 9-CF1 (a-c) and 25-CF1 (d-g) at different magnifications.

5.4.3 Effect of PMMA used for filler dispersion on the carbon fiber structure and properties

Structural parameters and imaging characterization indicated that the presence of PMMA at the SWNT-PAN interphase was not detrimental to the filler-matrix interactions, even though PMMA does not have carbon yield. Specifically, graphite templating was observed via TEM imaging (Figure 5-1b) and fibrils were observed via SEM (Figure 5-3b,c

and e-g). Furthermore, graphitic (002) plane axial orientation was higher in fibers with higher amount of SWNTs (Figure 5-2b).

However, while fiber 25-CF2 had slightly higher tensile modulus than the control fiber, the carbon fibers with 9 wt% SWNTs had significantly lower tensile properties than the control fiber. Similarly, while increasing the stabilization time at 265 °C improved the mechanical properties of the fiber with 25 wt% SWNTs, the same increase in the stabilization time was detrimental to the mechanical properties of fibers with 9 wt% SWNTs (compare fibers 9-CF1 and 9-CF2 in Table 5-2).

These differences indicate that although helical wrapping of the SWNTs with PMMA does not reduce filler-matrix interaction, mechanical integrity of the carbon fiber is reduced when unbound PMMA is present in the nanocomposite precursor fiber. As listed in Table 5-1 and described in Chapter 4, carbon fibers with 9 wt% SWNTs were produced from precursor fiber 5wt%-B that also had 3.2 wt% PMMA that was not helically wrapping the SWNTs (and is referred to as free PMMA). However, carbon fibers with 25 wt% SWNTs were produced from precursor fiber 15wt% that did not have free PMMA, as in this case all the free PMMA was removed via solvent exchanged before preparation of the spinning solution. Two mechanisms are proposed to explain the effect of free PMMA on the carbon fiber properties. On the one hand, blending of PMMA and PAN has shown that PMMA presence induces porosity in the carbon fiber due to phase separation.[193–195] On the other hand, the low molecular weight (~15,000 g/mol) unbound PMMA in precursor fiber 5wt%-B may have increased the entropic relaxation of partially oriented amorphous PAN molecules during stabilization and ultimately reduce mechanical properties of the resulting carbon fiber.

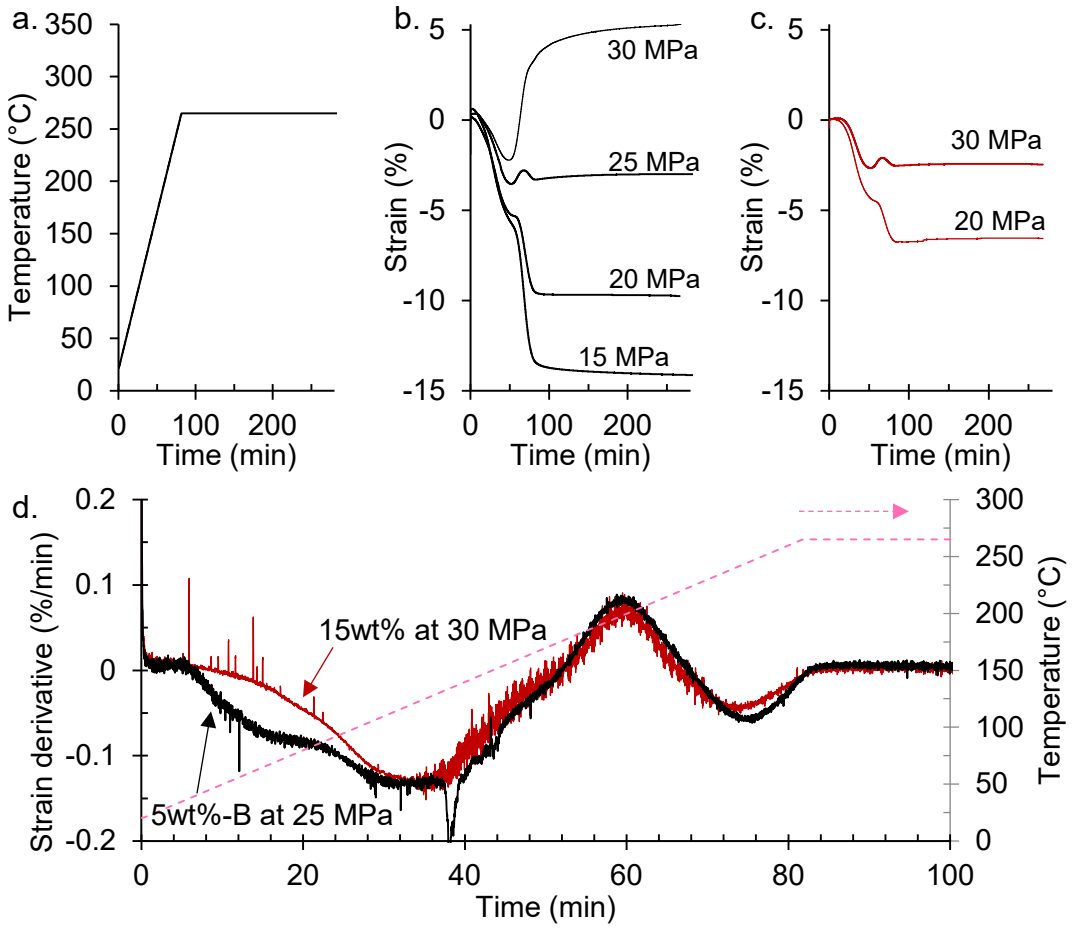

Figure 5-5. Thermo-mechanical analysis (TMA) of PAN nanocomposite fibers with (b) 5 and (c) 15 wt% SWNTs while changing the experimental conditions as listed in Table 5-1. Temperature profile is shown in (a). Bundles of 5wt%-B and 15wt% precursor fibers were kept at the indicated engineering stress. Negative strain values in (b) and (c) indicate fiber shrinkage caused by thermal relaxation of the PAN molecules. (d) is the strain derivative with time for precursor bundles of 5wt%-B and 15wt% at 25 and 30 MPa, respectively.

Effect of the free PMMA on the entropic relaxation of the PAN molecules was described via thermo-mechanical analysis (TMA) by measuring precursor fiber shrinkage during heating (see Figure 5-5). Precursor fibers 5wt%-B and 15wt% had comparable total shrinkage when the engineering stress was 25 and 30 MPa (see Figure 5-5b, c), which were the conditions used to produce the carbon fibers listed in Table 5-2. Still, fibers 5wt%-B showed two different physical shrinkage stages (entropic relaxation), with onset temperatures at 45 and 85 °C, see Figure 5-5d. Meanwhile, for the 15wt% fibers, only one

onset was observed at around 65 °C. Similar phenomena was observed when both fibers were subjected to lower engineering stress during stabilization (see Figure D 3).

The presence of free PMMA in the PAN amorphous and paracrystalline regions could affect fiber shrinkage due to an increase the molecular repulsive forces. Physical shrinkage has been observed to occur below PAN glass transition and cyclization temperatures because of repulsive forces between adjacent PAN dipoles in partially oriented amorphous and paracrystalline regions.[196] Furthermore, irregular intermolecular repulsion has been observed when acrylonitrile copolymers are used instead of PAN homopolymers,[196] indicating that small quantities of another polymer can also affect PAN shrinking behavior.

5.5 Conclusions

Carbon fibers with up to 25 wt% SWNTs (CNT/C composite fiber) were produced via stabilization and carbonization of PAN precursor fiber with PMMA-wrapped-SWNTs. Even though PMMA does not have carbon yield, the SWNT reinforced the carbon fiber matrix, as indicated by the following results: (a) carbon fiber produced from the precursor with 15 wt% SWNT had higher tensile modulus (324 ± 20 GPa) than the control fiber (288 ± 9 GPa); (b) nanofibrils were observed via SEM in the carbon fiber cross-section, which have been previously shown to have highly-ordered graphitic structure; (c) graphitic templating was observed via TEM surrounding well dispersed SWNTs; (d) orientation of the (002) plane increased with increasing SWNT content and was also higher than the orientation previously measured from carbon fibers produced under similar conditions from PAN precursor with and without 1 wt% carbon nanotubes. Furthermore, high SWNT loading increased the disorder of the graphite turbostratic structure and caused a reduction in the graphite crystal size. However, when unbound PMMA was present in the precursor fiber, carbon fiber tensile properties decreased with respect to those of the

control carbon fiber. CNT/C fibers contained large voids and macroscopic SWNTs agglomerates. This indicates that further optimization of the filler dispersion, stabilization and carbonization conditions should be pursued and may significantly improve the nanocomposite fiber tensile properties.

CHAPTER 6: PROCESSING, STRUCTURE AND PROPERTIES OF PAN AND PAN-DERIVED CARBON FIBERS WITH MODERATE AND HIGH LOADINGS OF CARBON BLACK

Preamble

The knowledge acquired in chapters 3 and 4 in producing PAN fibers with up to 15 wt% SWNTs and in chapter 5 in producing nanocomposite carbon fibers is used in this chapter to produce yet another nanocomposite PAN fiber with up to 60 wt% carbon black (CB), a low cost filler. Stabilization and carbonization of electrically conductive PAN fibers via Joule Heating is also explored. The Joule Heating approach can also be used with the SWNT/PAN fibers reported in chapter 4 and has the potential of significantly reducing the energy used in carbon fiber manufacturing.

Results presented in this chapter are obtained as part of an on-going project funded by the Advanced Research Projects Agency-Energy (ARPA-E). The objective of this project is to produce low-cost carbon fibers from carbon black. PI of the project is Prof. Chao Wang from Johns Hopkins University, and the co-PIs Prof. Liangbing Hu from University of Maryland, Prof. Satish Kumar from Georgia Institute of Technology and Prof. Ping Liu from University of California at San Diego.

6.1 Abstract

Poly(acrylonitrile) (PAN) nanocomposite fibers with 60 – 70 wt% (high loading) and 15 wt% (moderate loading) carbon black (CB) were produced via dry-jet wet-spinning in order to reduce PAN content and produce electrically conductive polymer fibers. CB particles caused pseudoplasticization of the spinning solution and CB rearrangement occurred during fiber drawing and PAN crystal growth. PAN fiber with 15 wt% CB (20 nm diameter) and 2 wt% multiwall carbon nanotubes (MWNTs) had tensile modulus and strength of 15.7 GPa and 686 MPa, respectively, and electrical conductivity of 3.6 S/m. Joule Heating was used to stabilize CB-PAN fiber bundles of up to 25 cm length and the operational window for carbonization via Joule Heating was defined. Carbon fibers containing about 24 wt% carbon black and about 3 wt% MWNTs were produced by heating in convection furnace, and its tensile strength and modulus values were 740 MPa and 58 GPa, respectively. This work presents a strategy to produce low cost carbon fibers, given the use of a low-cost filler, decreased polymer content and energy efficient stabilization and carbonization by Joule Heating.

6.2 Introduction

The market size of carbon fiber prepreg in 2019 was USD 4.7 billion and, pre-pandemic, it was estimated to grow by a factor of three by 2029.[197] Still, use of high-performance carbon fiber has been limited so far to a few industries and applications, such as aerospace, aircrafts, professional sport goods and luxury vehicles. The limited penetration of high-performance carbon fiber in industry is in part a consequence of its high cost, only affordable in specialty products that demand high mechanical, electrical and thermal properties and low density. Aeroespace grade carbon fiber is priced in the range of US $30 to 80/lb, while that used in sporting goods and wind turbines in the range

of US $8 to 20/lb.[197] Further cost reduction is required if carbon fiber is to be used on larger scale, and especially in the automotive industry.[198]

About 50 % of the cost of polyacrylonitrile (PAN)-derived carbon fiber is attributed to the cost of the polymer precursor, and it is also dependent on crude oil price.[198–200] Another 30 to 7 % of the carbon fiber cost is caused by the stabilization and carbonization treatments that the PAN fiber requires to obtain carbon fiber.[198–200] In order to reduce the precursor cost, research has focused on introducing cost effective and renewable fillers and on using textile grade PAN. To reduce the cost associated with stabilization and carbonization, novel treatments have been pursued, like electron ion beam treatment,[201] plasma treatment[202] and direct heating via Joule heating effect.[11,203]

Particularly interesting is the inclusion of carbon black (CB) in PAN fibers. Carbon black is a commodity extensively used in industry,[102] which is electrically conductive and can induce flame retardancy in a polymer matrix.[100,101] Furthermore, carbon black can be obtained via environmentally-friendly processes.[103,104] Recently, porous PAN fibers with diameters as low as 34 μm were produced via wet-spinning with 12 wt% of functionalized carbon black, achieving moderate tensile strength and electrical conductivity of 110 MPa and 9×10^{-2} S/m, respectively.[97] However, more research is needed to evaluate if PAN fibers with high tensile properties and conductivity can be achieved after carbon black incorporation, and if the resulting carbon fiber could be used in high-performance applications. A conductive CB-PAN fiber (> 1 S/m) is of interest because it could be heated via Joule Heating to induce PAN stabilization and carbonization, thus further reducing the cost for carbon fiber manufacturing.

In the present work, we use dry-jet wet-spinning technique to produce CB-PAN fibers. In order to achieve CB-PAN fibers with electrical conductivities greater than 1 S/m and to allow direct heating via Joule heating effect, two strategies were used: A) using

small quantities of carbon nanotubes (2 wt%, with respect to solids) along with moderate amounts of CB (15 wt%, with respect to solids), or B) using high quantities of carbon black (60 wt% and 70 wt%). The effect of filler loading on the processing, structure and properties of the PAN nanocomposite fibers was studied. Stabilization and carbonization via convection furnace and stabilization via Joule Heating of CB-PAN fibers with moderate amount of carbon black was studied.

6.3 Experimental

6.3.1 Materials

Three carbon black samples were obtained from Cabot Corp., with average particle size of < 20 nm (Monarch 700), > 70 nm (Monarch 120) and ~13 nm (Monarch 1300). Carbon black samples with average diameter of 240 and 280 nm were purchased from Asbury (5991R) and Cancarb (Thermax N991), respectively. Monarch 1300 ~13 nm) was functionalized by the manufacturer (proprietary functionalization), while all the other carbon black samples did not have any reported surface modification. All carbon black samples were used as received and their x-ray diffraction patterns are available in Figure E 1. Multiwall carbon nanotubes (SMW200, herein MWNTs) were purchased from SouthWest NanoTechnologies Inc. MWNT length was in the range of 3 to 6 μm and the average external diameter was of 12 ± 3 nm (containing 9 to 10 walls), as reported elsewhere.[204] Poly(acrylonitrile-co-methacrylic acid) (PAN, 4 wt% copolymer) with viscosity average molecular weight of 500,000 g/mol was obtained from Japan Exlan Co. (Osaka, Japan). Dimethylformamide (DMF, ACS grade, 99.8%) was obtained from Sigma-Aldrich and used as received.

6.3.2 Preparation of spinning dispersions

As summarized in Table 6-1, one fiber (Fiber A) was prepared with moderate CB content (15 wt%) and low MWNT content (2 wt%), and three different fibers with high CB

loading (60 wt%) while changing CB particle diameter (Fibers B to E). Two additional fibers with 70 wt% CB were prepared while simultaneously changing CB particle size and functionalization (Fibers F and G).

Table 6-1. Conditions used to prepare various fibers studied in this chapter.

Fiber ID	A-1 to A-3 [a]	B	C	D-1 to D-3 [a]	E-1 to E-3 [a]	F	G
Carbon black diameter (nm)	~ 20	~ 20	~ 70	~ 240	~ 280	~ 70	~ 13
CB content (wt%)	15	60	60	60	60	70	70
MWNT content (wt%)	2	NA	NA	NA	NA	NA	NA
Solid content of spinning dispersion (g/dL)	17.0	22.9	38.4	23.4	22.6	50.8	38.6
Spinneret diameter (μm)	200	500 [b]		350		500	
Coagulation bath [c]	Methanol	Methanol/DMAc (70/30 v/v)					
Stretching during spinning	2.9×	none	none	3.9×	3.9×	none	1.1×
Hot draw ratio (total draw ratio) [d]	5× (14.5×) 9.1× (26.4×)	2.5×	none (1×)	6.9× (27.1×) 10.3× (40.3×)	6.9× (27.1×) 14× (54.6×)	none (1×)	none (1.1×)

[a] Fibers A, D and E had high drawability and three different fibers (1 to 3) were prepared for study: Fibers A-1, D-1 and E-1 were as-spun fibers with as spun draw ratios of 2.9, 3.9 and 3.9×, respectively. Fibers A-2, D-2 and E-2 were fibers with moderate hot draw ratios, with total draw ratios of 14.5, 27.1 and 27.1×, respectively. Fibers A-3, D-3 and E-3 were fibers with maximum stable hot draw ratios, and with total draw ratios of 26.4, 40.3 and 54.6×, respectively.
[b] Spinning with 350 μm spinneret was attempted but jetting was not stable.
[c] Coagulation baths at 25 °C, DMAc stands for dimethyl acetamide.
[d] Total draw ratio is calculated as the product of as spun draw ratio and hot draw ratio.

For the PAN fiber with 15 wt% CB and 2 wt% MWNT (Fiber A), MWNTs were dispersed on DMF via 24 h sonication while at a concentration of 20 mg MWNTs per dL of DMF. After sonication, CB (< 20 nm) was added to the MWNT/DMF dispersion, and the solid concentration reached 160 mg (MWNT + CB) per dL of DMF. For making PAN fibers

with 60 and 70 wt% of CB (Fibers B to G, Table 6-1), CB/DMF at a concentration of 10 g/dL were sonicated for 24 h.

PAN solutions were prepared by mixing dried PAN with chilled (~ 0 °C) DMF for 1 h, followed by a temperature increase to 70 °C and further stirring for another 1 h. CB/DMF dispersions or MWNT+CB/DMF dispersions were incorporated to the PAN/DMF solution during stirring at 70 °C. Excess solvent was removed during continuous stirring via evaporation.

6.3.3 Fiber Spinning

Fibers were spun using a single filament spinning system designed and manufactured by Hills Inc. Spinneret diameter, coagulation conditions and other processing parameters are listed in Table 6-1. Barrel and spinneret temperatures were ~65 and ~60 °C, respectively, and air gap was 3 - 5 cm. Hot drawing was done while passing the fibers through a glycerol bath at ~ 165 °C.

6.3.4 Stabilization and carbonization via convection furnace

Filament bundles with equivalent diameter of at least 150 μm were batch stabilized and carbonized in an MHI H17HT2.5x24 tube furnace. Bundles were kept under tension at an engineering stress of 20 MPa during the whole stabilization and carbonization experiments by attaching them to stainless steel and graphite weights. Stabilization was done in air and heating at a heating rate of 3 °C/min to 265 °C, followed by a hold at 265 °C for 170 minutes. Then the temperature was increased to 305 °C at a rate of 3 °C/min, and held at 305 °C for 10 min. Carbonization on the convection furnace was done by heating in nitrogen from room temperature to 1315 °C at a rate of 5 °C/min, followed by a 10 min hold at 1315 °C.

6.3.5 Stabilization via Joule Heating

Stabilization of Fibers A-2 via Joule Heating was performed in air using a Keithley 2400 source-meter by varying applied power between 0.6 and 1 W, and the total time was up to 3.5 h. Power was applied by positioning the fiber bundle over graphite rods, which were 2.5 cm apart from each. Fiber bundle was kept under tension by hanging stainless steel and graphite weights at each end of the bundle. These graphite rods were connected to the power supply. Fibers were allowed to change length under an engineering stress of 30 MPa, and no conductive paint or adhesive was used to connect graphite rod and fiber bundle. Thus electric contact was directly provided by surface contact between the graphite rods and the fiber bundle that was kept in tension under the applied load. Stabilization of Fibers A-3 via Joule Heating was performed in a similar fashion to that described above, but by using a PS350 (Stanford Research Systems) power supply (in place of Keithly 2400) and in this case distance between graphite rods was maintained at 25 cm. Experimental setting used for Fiber A-3 Joule Heating stabilization is shown in Figure E 3.

Tensile properties were measured using a FAVIMAT+ (Measured solutions, Inc), or a Solids Analyzer III (TA Instruments). Strain rate was 1%/s for all precursor and stabilized fibers and 0.1%/s for carbon fibers. Scanning electron microscopy (SEM) was conducted on uncoated samples on a Hitachi SU8230. Wide-angle X-ray diffraction (WAXD) of fiber bundles was collected on a Rigaku MicroMax-003 operating at 50 kV and 0.60 mA and coupled to an R-axis IV++ detector. Electrical conductivity was measured using a Keithley 2400 source-meter by measuring the resistance of individual fibers between two probes while applying 0.1 mA current at known distances between probes.

6.4 Results and Discussion

6.4.1 Processing of CB-PAN fibers with high CB loading

Inclusion of carbon black in polyacrylonitrile solutions strongly affected the processing of fibers via dry-jet wet-spinning. As described in Chapter 4, pure PAN fibers can be produced from solutions with the same copolymer and molecular weight used here at a solid content of ~11 g/dL and complex viscosity of 50 – 150 Pa.s. However, as listed in Table 6-1, CB-PAN fibers were only spinnable when the solid content of the spinning dispersion was increased to 17 g/dL for fibers with 15 wt% CB and to > 22 g/dL for fibers with 60 wt% CB. Dispersions listed in Table 6-1 had larger solid content than that for control PAN, as the addition of carbon black results in decreased viscosity. Table E 1 presents the rheological properties of a control PAN (11 g/dl) and those of CB-PAN dispersions with 60 wt% CB of 20 and 70 nm particle diameter when solid content was 17 and 13.1 g/dL, respectively. Rheological properties of the dispersions for which spinning was possible (see Table 6-1) are presented in Table 6-2.

Table 6-2. Rheological properties of spinning dispersions listed in Table 6-1 and used to produce fibers A to G.

Spinning dispersion ID	A	B	C	D	E	F	G
Solid content (g/dL)	17.0	22.9	38.4	23.4	22.6	50.8	38.6
Complex viscosity (Pa.s)	352	1371	320	29	21	329	857
tan δ	0.87	0.22	1.25	3.66	4.98	1.92	0.55
log G’ vs log G’’ slope	1.04	0.57	1.05	1.43	1.50	1.19	0.68

Note: complex viscosity and damping factor at 1 rad/s. log G’ vs log G’’ slope is calculated in the 0.6 to 2.5 rad/s range.

Two different mechanism have been proposed to explain the reduction of polymer viscosity upon addition of carbon nanofillers. On the one hand, mixing of poly(butyl methacrylate) and polystyrene melts with carbon black has shown that viscosity is reduced when polystyrene is used due to supposedly low polymer-CB interactions, while viscosity

increases when poly(butyl methacrylate) is used due to preferable polymer-CB interactions.[205] On the other hand, addition of small quantities of carbon nanotubes to ultrahigh molecular weight polyethylene,[206] and uncured epoxy[207] and of functionalized silica nanoparticles to polypropylene[208] has been shown to decrease the polymer viscosity, as a consequence of selective polymer adsorption around the nanoparticles. This selective adsorption phenomenon has been studied by blending polymer nanoparticles with the respective linear polymer,[209] and it is believed that the presence of the nanoparticle changes the conformation of the linear polymer, including its free volume and therefore the polymer viscosity.[209]

Reduction of PAN viscosity upon CB addition is probably a consequence of the interactions between the three components of the dispersion: PAN, CB and DMF (solvent). PAN has a polar nitrile group which can interact with CB particles via dipole-π interactions with the graphitic layers and via dipole-dipole interactions with the functional groups at the CB surface. These PAN-CB interactions could cause a reduction in the polymer free volume. Furthermore, dipole-dipole interaction between PAN's nitrile group and DMF has been previously reported,[162,210] and has been associated to an increase in the hydrodynamic radius of PAN. Presence of CB in the spinning dispersion could also lead to a decrease in PAN-DMF interactions due to competitive processes, and therefore to a reduction in PAN hydrodynamic radius, polymer entanglements and dispersion's viscosity.

Table 6-3. Mechanical and electrical properties and structural parameters of various precursor fibers.

Fiber ID	A-3	B	C	D-3	E-3	F	G
Total draw ratio	26.4×	2.5×	1×	40.3×	54.6×	1×	1.1×
Diameter (μm)	21.3 ± 0.7	347 ± 20	377 ± 27	NM	38.5 ± 2.4	434 ± 90	338 ± 86
Tensile modulus (GPa)	15.7 ± 0.5	0.18 ± 0.06	0.44 ± 0.04	NM	7.1 ± 1.1	0.43 ± 0.09	0.90 ± 0.2
Tensile strength (MPa)	686 ± 39	1.9 ± 0.6	8.1 ± 0.6	NM	61 ± 3	7.4 ± 1.8	3.1 ± 0.3
Strain at break (%)	8.9 ± 0.4	3.4 ± 2.2	14.6 ± 2.1	NM	6.5 ± 0.5	1.8 ± 0.7	0.3 ± 0.1
X_{TOTAL_PAN} (%) [a]	54	NA					
$X_{\sim 17^\circ\ PAN}$ (%) [a]	NA	12.6	9.8	14.9	15.1	11.7	7.9
L_{PAN} (nm) [b]	9.3	2.9	5.2	6.5	5.7	8.4	7.7
d-$spacing_{PAN}$ (nm) [b]	0.526	0.519	0.523	0.531	0.532	0.525	0.524
f_{PAN} [c]	0.77	0.01	0.03	0.68	0.62	0	0
Electrical conductivity (S/m)	3.6 ± 1.6	0.6 ± 0.1	$< 1\times10^{-5}$	1.4×10^{-3}	$< 1\times10^{-5}$	4.4 ± 1.8	7×10^{-2}

Notes: not measured (NM). [a] PAN crystallinity of fibers A was calculated considering area of peaks at 2θ ~17, ~25, ~29 and ~40° as crystal content (see Figure E 2) respect to total XRD signal area. For fibers B to G, area fraction of the 2θ ~17° peak is shown instead, as the other PAN crystal peaks were dwarfed by the CB amorphous peak (see Figure E 4 and Figure E 5). [b] PAN crystal size and d-spacing calculated from equatorial scans. Scherrer's equation was used with k = 0.9. [c] PAN. [a] 2nd order Hermann's orientation factor calculated from azimuthal scans of the 2θ ~17° peak. Mechanical properties of fibers A, D and E were measured at a gauge length of 2.5 cm, while for fibers B, C, F and G, gauge length was 0.5 inch.

Continuous jetting formation during fiber spinning requires the presence of entanglements in the spinning dispersion. However, as discussed above, PAN entanglements were reduced upon CB addition. Therefore, CB-PAN dispersions were only spinnable at relatively high solid content. Interestingly, when CB diameter was larger than 200 nm, spinning was possible at relatively low dispersion viscosity and at relatively low solid content. This suggests that large CB particles acted as entanglement points and allowed continuous spinning. Furthermore, among the dispersions with 60 wt% CB, only

fibers D and E resulted in continuous jetting when the 350 μm spinneret. On the other hand, fibers B and C had to be produced with a spinneret of 500 μm diameter, as continuous jetting in these cases was not possible with 350 μm diameter spinneret. These differences could also be a consequence of the effect of CB size on dispersion homogeneity, which, as quantified by the log G' vs log G'' slope (Table 6-2), decreased with increase in CB diameter. This result indicates that CB of smaller diameter is also more difficult to mix homogenously in the spinning dispersion.

Another major effect of CB presence on the processing of CB-PAN fibers with high CB content was observed upon stretching the fibers during spinning and hot drawing. As listed in Table 6-1, despite the large spinneret diameter used for fibers B to G, only fibers D and E allowed significant drawing during spinning and hot drawing. Differences in the drawability were caused by differences in the PAN crystal structure obtained after spinning and gelation. In turn, the PAN crystal structure was affected by the CB size. As listed in Table E 2, as-spun fibers E-1 and D-1, had low predominance of the PAN crystal peak at 2θ ~17° (8.3 and 9.0 %, respectively) and small crystals (3.8 and 3.4 nm, respectively), while fibers B and C (see Table 6-3) had larger 2θ ~17° peak predominance (12.6 %) at comparable crystal size (2.9 nm) or comparable 2θ ~17° peak predominance (9.8 %) but larger crystal size (5.2 nm), respectively.

6.4.2 Structure of CB-PAN fibers with high CB loading

Differences in PAN crystal size and predominance of the 2θ ~17° peak, and the drawability of the as-spun fibers were caused by how the PAN crystal domains were formed around the CB particles. This is further illustrated by studying how the d-spacing of the PAN crystal 2θ ~17° peak changed depending on CB particle diameter. As-spun CB-PAN fibers with small diameter CB particles (20 and 70 nm, Fibers B and C in Table 6-3), had smaller d-spacing than fibers with larger diameter CB particles (240 and 280

nm, Fibers D-1 and E-1 in Table E 2). In control PAN fibers, d-spacing tends to decrease (packing density increase) upon drawing as the PAN orthorhombic crystal structure changes to hexagonal, caused in turn by a change of PAN conformation from helical to planar zig-zag.[65] Orthorhombic structure has also been related to the presence of solvent co-crystallized with the polymer.[156] Thus, small d-spacing in fibers B, C, F and G, right after spinning, indicates that the small diameter CB promoted PAN crystallization in hexagonal structure and inhibited solvent co-crystallization. On the other hand, large diameter CB in fibers D-1 and E-1 promoted the formation of orthogonal crystals with solvated polymer molecules. This polymer solvation and the high PAN amorphous content in fibers D-1 and E-1 allowed for increased drawability.

Interestingly, upon drawing of fibers D-1 and E-1, while predominance of the 2θ ~17° peak and crystal size increased (Figure E 5 and Table 6-3), the 2θ ~17° peak d-spacing did not change (Table 6-3 and Table E 2). This indicates that despite the high draw ratios (40.3 and 54.6× for fibers D-3 and E-3, respectively), PAN molecules did not acquire planar zig-zag conformation and crystal packing density remained the same as that of the as-spun fiber. This was probably a consequence of PAN coating the CB particles (see Figure E 6). This is further supported by comparing the orientation of the PAN crystals of fibers D and E to that in the control PAN fiber. A typical PAN fiber, produced through a spinneret diameter of 200 μm has PAN crystal orientation of ~0.10-0.2 after spinning, and as high as 0.9 after hot drawing. However, as-spun fibers D-1 and E-3 had orientation factor close to 0 (see Table E 2) and fully drawn fibers D-3 and E-3 had orientation factors of 0.68 and 0.62, respectively (see Table 6-3).

6.4.3 Properties of CB-PAN fibers with high CB loading

Tensile and electrical properties of fibers with 60 and 70 wt% CB are listed in Table 6-3 and Table E 2. As expected from the described processing and structure differences,

fiber E-3 had the highest tensile strength and modulus among the various fibers with high CB loading. However, typical fully drawn pure PAN fibers have crystal orientation exceeding 0.80, and tensile modulus and strength greater than 19 GPa and 900 MPa, respectively (see reported data of control PAN fiber elsewhere[117] and in Table 4-2 in Chapters 4 of this thesis). Furthermore, PAN crystal size of fibers with large CB diameter (D-3 and F-3) was about 6 nm, while in drawn control PAN fiber the crystal size can be as large as 9 nm. Comparing the structure of fibers D-3 and F-3, it is observed that larger and better oriented PAN crystals are obtained when CB size is decreased, owing probably to how easily the CB can be rearranged during crystal growth. Thus, we hypothesize that tensile strength and modulus of CB-PAN fibers with high CB loading could be further improved by changing the CB particle size distribution to better allow for high fiber drawability (large particles) and better PAN crystal growth and orientation (small particles).

Difference in CB's chemistry surface could also be behind the observed differences in the fiber tensile properties. Fibers F and G were produced with the same CB loading (70 wt%) while varying CB diameter and surface functionalization. As seen in Table 6-3, fiber G was slightly more brittle and had higher tensile modulus and lower tensile strength than fiber F.

Electrical conductivity of the various fibers also supports the hypothesis that CB particles are rearranged during drawing and crystal growth. Foremost, electrical percolation of spherical conductive particles in a nonconductive medium is reached when conductive particle concentration is larger than 16 %.[211] However, among the as-spun fibers with 60 wt% CB, i.e. fibers B, C, D-1 and E-1, only Fiber B had a measurable electrical conductivity of 0.6 S/m. This supports that non-conductive PAN coated the conductive CB particles, resulting in decreased electrical percolation. Then, upon drawing of fibers D-1 and E-1, CB particles were rearranged and electrical conductivity first

increased (fibers D-2 and E-2 in Table E 2) and then decreased (fibers D-3 and E-3 in Table 6-3).

An earlier report on CB-high density polyethylene composites have shown that percolation threshold depends on CB size and surface area, and that composite's conductivity changes with temperature.[212] This phenomena, named positive or negative temperature coefficient, has also been observed in CB-semicrystalline polymer blend composites near the melting temperature of any polymers, indicating its dependence on the mobility of the polymer as well as that of the carbon black.[213]

6.4.4 CB-PAN fibers with moderate CB loading

Fibers A with moderate 20 nm CB loading (15 wt%) and 2 wt% MWNTs had high spinnability and drawability. PAN crystal d-spacing of as-spun fiber A-1 was also lower than that of as-spun fibers D-1 and E-1, indicating larger packing density upon using CB of smaller diameter. This increased crystal packing density was also observed for Fiber B with 20 nm CB but significantly larger filler loading. Furthermore, PAN crystal size and orientation of fully drawn fiber A-3 was larger than that for fibers D-3 and E-3 (Table 6-3), which translated into significantly better mechanical properties for fiber A-3.

SEM imaging of Fiber A-3 shows that fiber had an irregular circumference, the MWNT were well distributed and PAN polymer was uniformly distributed around the filler particles (Figure 6-1). Due to this PAN coating and due to the relatively large as-spun diameter, PAN crystal orientation in Fiber A-3 was 0.77. This is significantly lower than that reported for control PAN fiber with an orientation of 0.89. However, the two fibers have comparable crystal sizes (see Table 6-3 and Table 4-2). Thus, fiber A-3 still had significantly lower tensile properties than control PAN fiber.

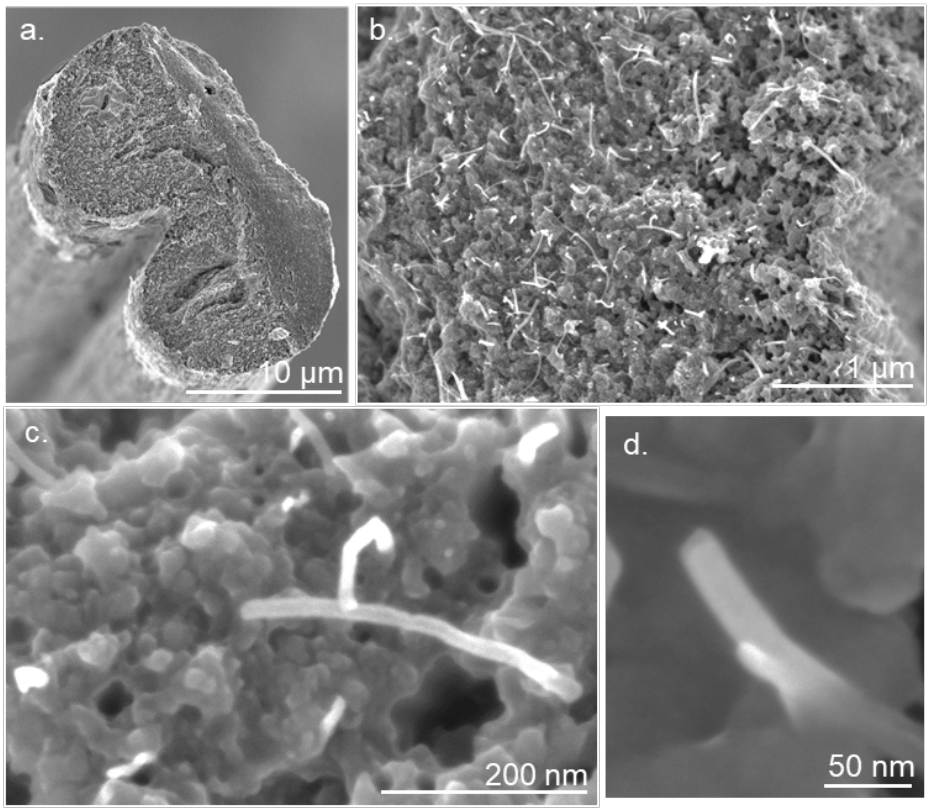

Figure 6-1. SEM images at different magnifications of Fiber A-3.

Similar to what was described for fibers D and E, electrical conductivity of fibers A also changed with draw ratio, indicating CB rearrangement during drawing and crystal growth. While as-spun fiber A-1 had electrical conductivity of 5×10^{-4} S/m, upon drawing the electrical conductivity increased to 13.6 S/m (fiber A-2) and then decreased to 3.6 S/m (fiber A-3). Electrical conductivity of drawn fibers A-2 and A-3 was significantly higher than that measured for drawn CB-PAN fibers with 60 wt% CB with larger CB diameter (see D-2, D-3, E-2 and E-3). This indicates that MWNT presence was critical to reaching the electrical percolation network along the fiber axis.

Electrical percolation network of fibers A-1, A-2 and A-3 was not solely made by MWNTs. Comparable electrical conductivity of single component nanocomposite MWNT-PAN fiber has only been reached when carbon nanotube content is greater than 15 wt%,[11] Comparable electrical conductivity has also been observed in bi-component PAN-

PAN/MWNT core-sheath fiber, when the sheath contained 10 wt% MWNTs in PAN.[214] Thus, CB was also part of the electrical percolation network for the fibers in the current study. We hypothesize that due to π-π interactions, CB particles associated at several points along the MWNT length, which facilitated electron pathways along the fiber radial direction, while MWNT, due to their large aspect ratio, created longitudinal electron pathways. Interaction between CB and MWNTs was observed in the CB+MWNT dispersion in DMF. Prior to mixing with PAN, MWNTs in a concentration of 20 mg/dL were sonicated for 24 h. After this, CB was added to the MWNT/DMF dispersion and the new CB+MWNT/DMF dispersion with a concentration of 160m mg/dL was sonicated for another 24 h. The resulting MWNT+CB dispersion was stable after several days, despite its high concentration. In contrast, MWNT dispersion in DMF at a concentration of 20 mg/dL and sonicated for 48 h were unstable and begun precipitating a few hours after sonication was stopped.

Overall, the CB-MWNT-PAN fiber produced here has good mechanical properties and relatively high electrical conductivity. This has been achieved by using a relatively low-cost filler, carbon black. A-3 and A-2 fibers have comparable electrical conductivity to that obtained for intrinsically conductive polymeric fibers such as polyaniline and polypyrrole prior to doping, and in some cases even after doping. An extensive review on several conductive polymer fibers is available elsewhere,[215] including state of the art polyaniline and polypyrrole fibers with electrical conductivity up to four order of magnitude larger than those of fiber A-2. However, fibers prepared here have tensile properties higher than those reported for polyaniline, polypyrrole with and without CNT inclusion.[215,216]

6.4.5 Stabilization of CB-PAN fibers with moderate CB loading via Joule Heating

PAN stabilization requires temperatures in the 250 to 380 °C and several reports are available concerning its chemistry and the changes caused in fiber's structure.[217] As

observed in Figure 6-2 by comparing the integrated WAXD signal of precursor fiber A-2 and that of the same fiber after convection furnace stabilization, PAN crystallinity is lost during stabilization and instead a broad peak at 2θ ~26° appears, which corresponds to the ladder structure of stabilized PAN.

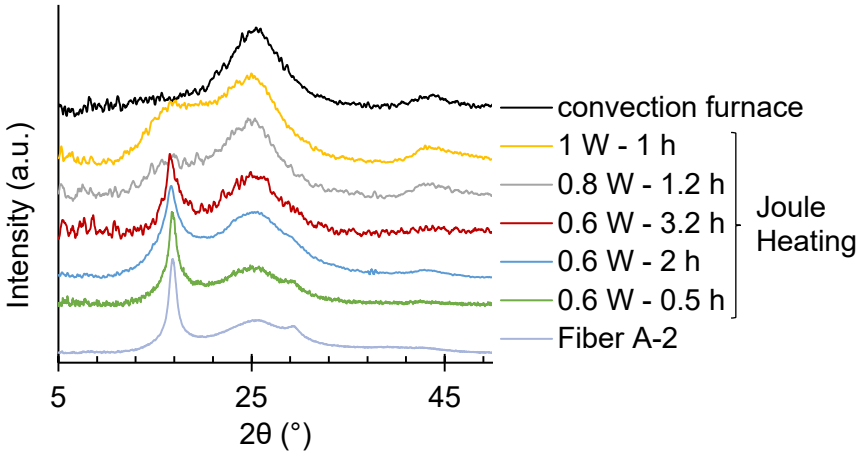

Figure 6-2. Integrated WAXD of precursor fiber A-2 and the same fiber after stabilization via convection furnace and via Joule Heating. Different Joule Heating conditions were studied, as listed. Power values should be normalized to the fiber bundle volume of 2.43 mm^3 to show power density.

Figure 6-2 also shows how the structure of the precursor fiber A-2 changed depending on the applied power density and holding time. The gradual loss of the PAN structure and formation of the ladder structure at higher electric power density and holding times indicates an increase in the extent of stabilization. This agrees with what is expected from Joule Heating, by which the power of heating is directly proportional to the electric power. Thus, at the given conditions, enough heat was generated via Joule Heating to reach stabilization reaction temperature.

PAN stabilization via Joule Heating has been previously reported for as-spun and low draw ratio PAN nanocomposite fibers with carbon nanotubes.[11] In this earlier report, temperature and PAN stabilization via Joule Heating were related to absolute current, fiber length and voltage, as controlling parameters. However, as established by the Joule-Lenz

power equation law: $P_{heat} = I^2R = V^2/R = IV = P_{electric}$, heating power ($P_{heat}$) is directly proportional to electric power ($P_{electric}$) and thus to any two of the three parameters in Ohm's law, voltage (V), current (A) and resistance (R), V = IR. Furthermore, due to heat dissipation and mass of the fiber, heat accumulated in the fiber is proportional to power density, not proportional to electric power. Therefore, the variable to control during Joule Heating is electric power density, which can be adjusted by controlling current, voltage and fiber resistance.

To illustrate this, fiber A-3 was also stabilized via Joule Heating (see Figure 6-3). In fiber A-2 Joule Heating stabilization, power was controlled via current, and in fiber A-3 it was controlled via voltage. Due to the low resistance of fiber A-2 (13.6 S/m fiber conductivity and bundle length of 2.5 cm), stabilization took place by applying no more than 10 mA current and voltage was no greater than 120 V. For this fiber, the absolute applied power was 1 W, and the electric power density was 0.41 W/mm^3. On the other hand, fiber A-3 had high resistance (3.6 S/m fiber conductivity and bundle length of 25 cm) and stabilization took place by applying voltage as high as 1700 V and current always lower than 5 mA. Thus, stabilization of fiber A-3 was done at absolute power of 5.5 W and power density of 0.37 W/mm^3. Fiber A-3 was not stabilized (Figure 6-3) when an absolute power of 1 W was applied, and the power density was only 0.06 W/mm^3. Please note that no absolute value of current and voltage is reported, because during stabilization the fiber resistance decreases, and therefore current and voltage values were adjusted to maintain constant power density. This reduction in fiber resistance upon PAN stabilization has also been observed in PAN nanocomposite fibers containing only carbon nanotubes.[11,203]

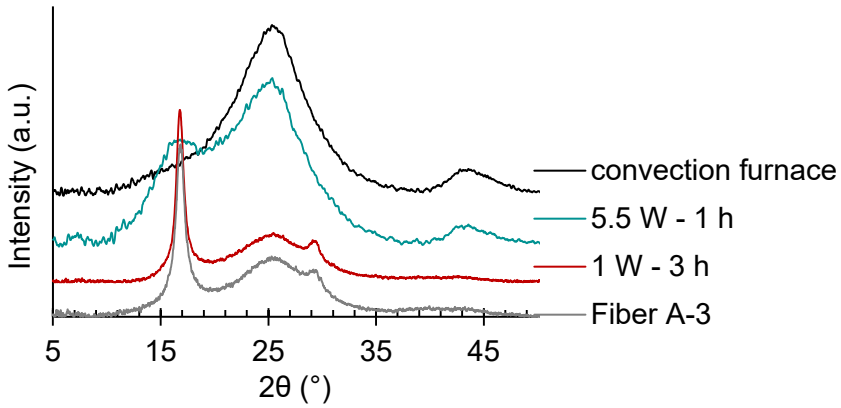

Figure 6-3. Integrated WAXD of precursor fiber A-3 and the same fiber after stabilization via convection furnace and via Joule Heating.
Different Joule Heating conditions were studied, as listed. Power values should be normalized to the fiber bundle volume of 15.1 mm^3 to show power density.

Mechanical properties of fibers A-2 and A-3 after convection furnace and Joule Heating stabilization are presented in Table 6-4. Tensile modulus, strength and elongation at break were virtually the same regardless of the method used for stabilization. However, fiber A-2 stabilized via Joule Heating had a slightly larger diameter than the one stabilized using convection furnace. This is despite the fact that applied engineering stress was higher during Joule Heating than during convection furnace stabilization. On the other hand, diameter of fiber A-3 did not change with stabilization method and despite PAN crystal orientation was higher for fiber A-3 than for the fiber A-2. Differences are attributed to the power increase rate which is proportional to the temperature increase rate. For fiber A-2, final power density was reached after 15 min (Figure E 7a), while for fiber A-3, power density was gradually increased over 100 min. Heating rate in convection furnace has been previously shown to affect ratio of intra to inter-chain cross-linking during stabilization, and fibers stabilized at higher heating rate have lower density.[187] This further shows how the applied power density is directly proportional to the accumulated heat and that Joule Heating can be used to stabilize PAN nanocomposite fibers instead of heating in convection furnace.

Table 6-4. Mechanical properties of stabilized fibers A-2 and A-3 via convection furnace and Joule Heating

Precursor fiber ID	A-2		A-3	
Diameter of precursor (μm)	27.7 ± 0.7		21.3 ± 0.7	
Stabilization method	Convection furnace	Joule Heating	Convection furnace	Joule Heating
Absolute power during Joule Heating (W)	NA	1	NA	5.5*
Electric power density during Joule Heating (W/mm^3)	NA	0.41	NA	0.37
Diameter of stabilized (μm)	29.0 ± 2.8	33.1 ± 1.7	27.4 ± 1.6	28.3 ± 2.2
Tensile modulus (GPa)	6.4 ± 1.1	6.5 ± 0.8	7.3 ± 0.6	7.7 ± 0.6
Tensile strength (MPa)	111 ± 21	118 ± 16	136 ± 8	188 ± 13
Strain at break (%)	2.8 ± 0.8	2.6 ± 0.9	4.4 ± 0.4	7.7 ± 0.6

Mechanical properties of stabilized fibers A-2 were measured at a gauge length of 5 mm, while for fiber A-3 the gauge length was 25 mm.
* Power density was gradually increased over 1 h.

Carbonization of these fibers via Joule Heating is also possible, but it was beyond our current capabilities. Reaching carbonization temperatures (> 1000 °C) via Joule Heating would require a significantly larger electric power density than that used for stabilization (0.4 W/mm^3 to reach 250 – 380 °C). However, in our experimental set-up, we were constrained to the power supply voltage and current limits, and to a reasonable sample size. Please note that although the Keithley 2400 and PS350 power supplies had absolute power limits of 20 and 25 W, respectively, these values can only be achieved within certain voltage and current limits. Furthermore, as discussed next, carbonization via Joule Heating will also require a multi-stage, preferably continuous, system. Our results indicate that stabilized CB-PAN fiber breaks at current area-densities higher than 5 mA/mm^2. Thus, in order to achieve higher power densities, higher voltages are required ($P_{electric} = IV$). However, voltage decreases and current increases at constant power due to the resistance decrease. Consequently, at constant power density, the current area-

density limit will be achieved unless the fiber bundle length is increased to counter the resistance's reduction.

6.4.6 Carbon fibers from CB-PAN precursor with moderate CB loading

Convection furnace-stabilized PAN nanocomposite fibers with 15 wt% CB and 2 wt% MWNTs were carbonized via convection furnace. Mechanical properties and structural parameters of carbon fibers obtained from precursor fibers A-2 and A-3 are listed in Table 6-5. This nanocomposite carbon fibers had significantly lower tensile modulus and strength than a typical control PAN-based carbon fiber produced under similar conditions.[89] The lower tensile strength can be explained by the large diameter of carbon fibers A-2 and A-3, which in turn suggest the presence of defects. Low tensile strength is also possible in nanocomposites when filler-matrix interactions are low and the unbound filler acts as a defect in the matrix.[32] SEM imaging of the fiber partially supports failure at the CB-carbon fiber interphase (see holes at the carbon fiber fraction in Figure 6-4). However, further characterization is required to distinguish if the observed structures are formed during fracture or correspond to high porosity in the carbon fiber itself. High porosity could be generated during carbonization if the stabilized PAN covering the CB particles were to decompose without carbon yield.

Interestingly, the carbon fiber obtained from A-2 had lower tensile modulus than the control carbon fiber even though the nanocomposite carbon fiber had graphite layers with fewer defects, as quantified by the Raman I_D/I_G ratio. The difference in the tensile modulus was caused by the effect of CB on the graphite ordering. Hermann's orientation factor values of carbon fibers derived from A-2 and A-3 were 0.57 and 0.60, while for the control carbon fiber a significantly higher orientation value of 0.81 was obtained.

To the best of our knowledge, this is the first study on the effect of moderate amount of carbon black in PAN-derived carbon fibers. Pitch-derived carbon fiber with 0.3

wt% CB in the precursor had been reported. [218] At this low CB loading, no effect on the axial orientation was observed, while the radial orientation of the graphitic pleats was found to be affected.[218]

Table 6-5. Mechanical properties and structural parameters of carbon fibers produced via convection heating from precursor CB-PAN fibers A-2 and A-3 and a control carbon fiber.

Precursor fiber ID	Control carbon fiber[89]	A-2	A-3
Draw ratio of precursor fiber	14.5×	14.5×	26.4×
Diameter (μm)	8.2 ± 0.2	22.1 ± 1.4	19.4 ± 1.1
Tensile modulus (GPa)	288 ± 9	58.5 ± 8.2	70.8 ± 8.2
Tensile strength (MPa)	2080 ± 290	740 ± 151	684 ± 100
Strain at break (%)	0.79 ± 0.10	1.1 ± 0.3	1.1 ± 0.1
$f_{(002)}$ [a]	0.81	0.57	0.60
$L_{(002)}$ (nm) [b]	1.8	1.6	1.6
$L_{(10)}$ (nm) [b]	2.0	2.8	2.8
I_D/I_G	2.5	1.1	NM

Notes: NM: not measured. [a] 2nd order Hermann's orientation factor calculated from azimuthal scans of the (002) graphite peak. [b] Crystal size of (002) and (10) planes from 2θ ~26° and ~43°, respectively, according to Scherrer's equation with $k = 0.9$.

The carbon fibers produced here are estimated to contain 24 wt% carbon black and 3 wt% MWNTs. This should translate into a significant reduction in the cost of the carbon fiber, as about 50 % of the carbon fiber cost is due to PAN polymer.[198–200] This carbon fiber can find applications based on it mechanical properties and cost factors. Furthermore, changing the carbon black size, functionalization, and fiber diameter, among other processing conditions, would allow for further improvements in mechanical properties.

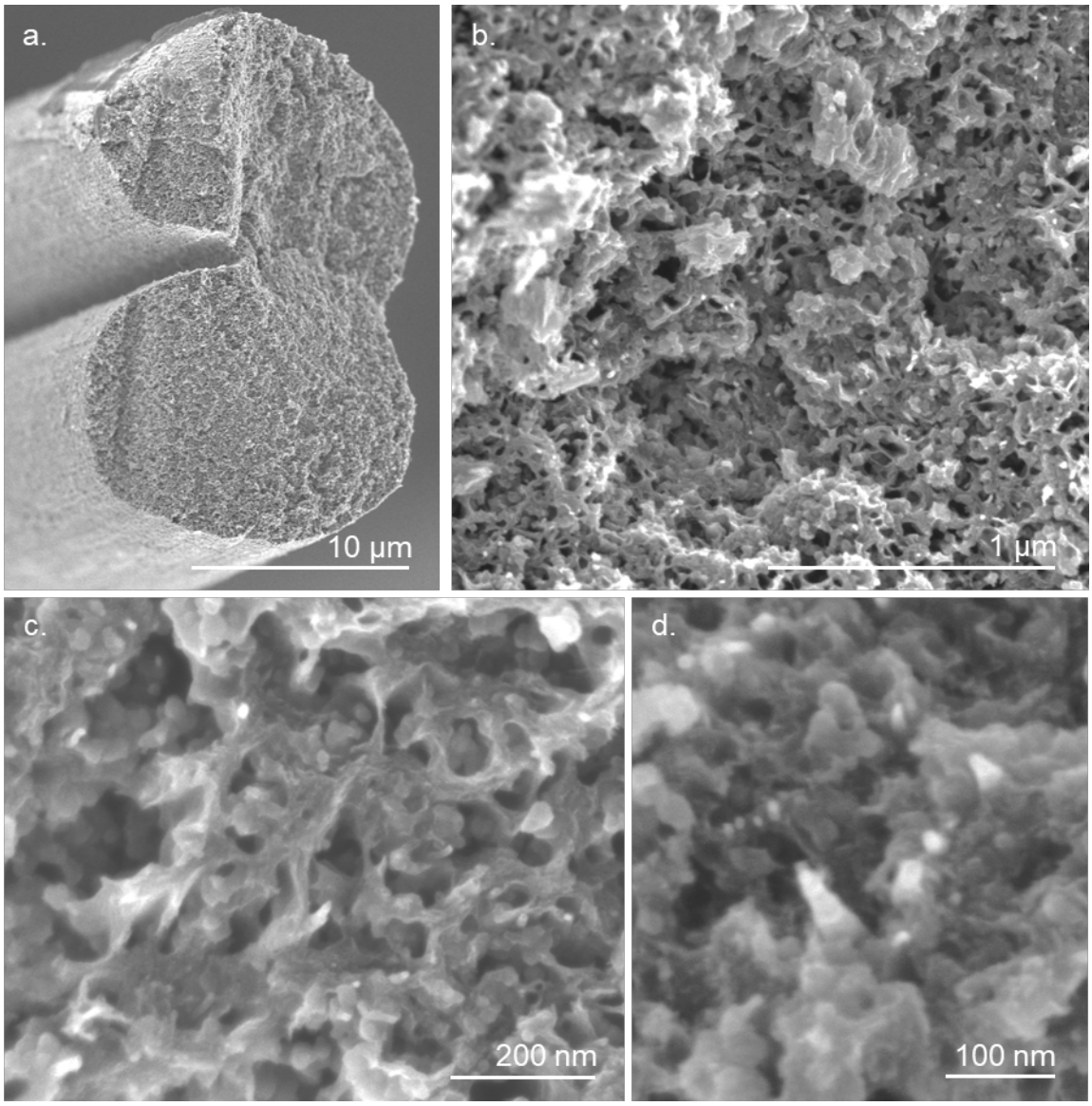

Figure 6-4. SEM images at different magnifications of carbon fiber produced via convection furnace from precursor fiber A-3. Stabilization of fiber A-3 was also done via convection furnace.

6.5 Conclusions

PAN nanocomposite fibers with 60 and 70 wt% carbon black (CB) were produced by dry-jet wet-spinning while using CB of different particle sizes, and also with 15 wt% CB and 2 wt% MWNTs. CB addition to PAN solution caused a reduction in the viscosity of the spinning dispersion Therefore solid content had to be increased in order to allow for fiber formation. Spinning solution homogeneity, spinnability and fiber drawability were observed

to be highest when larger CB particles (240 – 280 nm diameter) were used. These fibers exhibited good tensile properties. However, PAN crystal packing density and crystal size and fiber electrical conductivity were higher when small CB particles were used (20 – 70 nm diameter). These results were explained in terms of how the CB particles are rearranged during drawing and crystal growth.

PAN nanocomposite fibers with moderate CB loading (15 wt%) and 2 wt% MWNTs had tensile properties similar to those of the control PAN fiber and were electrically conductive. Electrical percolation network was achieved by the synergy of carbon black and carbon nanotubes. These PAN nanocomposite fibers were stabilized via Joule Heating, as well as by convection heating in a furnace. Joule Heating phenomena was accurately described, and it is concluded that a power density of > 0.41 W/mm^3 is required to achieve PAN stabilization. Discussion is presented for achieving carbonization via Joule Heating and its operational space. For the fibers here produced, the current area-density needs to be lower than 5 mA/mm^2 to avoid fiber breakage.

Nanocomposite carbon fibers with 24 wt% carbon black and 3 wt% MWNTs were produced via convection furnace stabilization and carbonization. These fibers had significantly lower mechanical properties than the state of the art PAN-derived carbon fibers produced under similar conditions.

CHAPTER 7: CONCLUSIONS

Flexible, non-conjugated polymers can adsorb onto CNTs of specific diameters and create partially and fully ordered structures sustained via non-specific CH-π and van der Waals interactions. We propose that this specific, ordered adsorption is a consequence of the random polymer conformations stabilized by the CNT surface, and that it depends on the rotational statistics of the polymer.

Non-covalent polymer wrapping of carbon nanotubes, and specifically of single wall carbon nanotubes (SWNTs) can be used to improve the nanoparticle dispersion and dispersion stability in different solvents. The polymer wrapping behavior is maintained after doing select solvent exchange, and these non-covalently functionalized carbon nanotubes can be used in polymer nanocomposites.

When poly(acrylonitrile) (PAN) nanocomposite fibers are produced via dry-jet wet-spinning with PMMA-wrapped-SWNTs, the PMMA wrapping remains after fiber processing, and thus becomes part of the filler-matrix interphase. Polymer wrapping affects filler-matrix interactions in the polymer nanocomposite. These filler-matrix interactions can be further tuned by changing the molecular weight of the polymer used for SWNT wrapping. PAN reinforced with polymer wrapped SWNTs can be produced with good mechanical properties and modest electrical conductivity.

PAN nanocomposite fibers with PMMA-wrapped-SWNTs can be used to obtained carbon nanotube/carbon (CNT/C) fiber composites. Even though PMMA does not have carbon yield, CNT/C fiber showed filler-matrix interaction and SWNT presence increases the axial orientation of the graphitic planes in the carbon fiber.

Carbon black, a cost-effective carbon nanofiller, can also be used to produce mechanically strong and electrically conductive PAN nanocomposite fibers, particularly when used in conjunction with relatively small quantities of carbon nanotubes. However, CB inclusion significantly reduces polymer orientation.

Electrically conductive PAN nanocomposite fibers can be stabilized by Joule Heating. PAN nanocomposite fibers stabilized via Joule heating have comparable mechanical properties to fibers stabilized via conventional convection heating. Boundary conditions required to stabilize electrically conductive PAN nanocomposite fibers by Joule heating have been determined.

The knowledge acquired in this study was used to obtain the following technological products:

- PAN nanocomposite fibers containing 15 wt% single wall carbon nanotubes (SWNTs) with a tensile modulus of 32.1 GPa, tensile strength of 830 MPa, and axial electrical conductivity of 2.2 S/m.
- PAN nanocomposite fibers with 15 wt% carbon black (CB) and 2 wt% multiwall carbon nanotubes (MWNTs), with a tensile modulus of 15.7 GPa, tensile strength of 686 MPa, and axial electrical conductivity of 3.6 S/m.
- Carbon nanotube/carbon (CNT/C) nanocomposite fibers with up to 25 wt% SWNTs, with a tensile modulus of 324 GPa, and a tensile strength of 1.25 GPa.
- Carbon/carbon (C/C) nanocomposite fibers with 24 wt% CB and 3 wt% MWNTs, with a tensile modulus of 70.8 GPa, and tensile strength of 0.68 GPa.

For comparison, control PAN fiber, obtained under somewhat similar conditions to the nanocomposite PAN fibers reported here , has a tensile modulus of 19.2 GPa, tensile strength of 896 MPa, and axial electrical conductivity of about 3×10^{-16} S/m. PAN-

derived carbon fiber, obtained under similar conditions to the nanocomposite carbon fibers, has a tensile modulus of 288 GPa and tensile strength of 2.08 GPa.

CHAPTER 8: RECOMMENDATIONS

Experimentally observed CNT diameter-dependent PMA and PMMA adsorption and PMMA ordered helical wrapping, and the molecular dynamics-predicted PMA folding studies, open a vast materials-design space that should be studied. In previous studies, conjugated, semi-rigid or rigid polymers chains have been almost exclusively evaluated for the wrapping and encapsulation of CNTs. Prior experimental observation of PMMA wrapping onto SWNTs by Davijani and Kumar, it was believed that flexible polymer chains will adsorb without specific order. Now we know that ordered wrapping of flexible polymers is possible, given the right solvent system, CNT diameter, and the polymer tacticity. Full understanding and exploitation of this phenomena should heavily rely on molecular dynamic simulations (MDS), to reduce experimental time and cost while surveying the experimental space. MDS studies will require careful selection of the force field and that of the interface force field parameters. This will allow the accurate representation of the electronic structure of the surveyed substances and their interactions.

Co-solvent assisted dispersion of carbon nanotubes, as explored in Appendix F, could improve filler dispersion and reinforcement efficiency in nanocomposite polymers without the need to do filler covalent functionalization or the non-covalent polymer wrapping. This strategy should be further investigated. Hansen Solubility Parameters (HSP) and surface energies could be used to predict and select other possible co-solvents. However, as new nanofillers are studied, with various surface functionalities (e.g. carbon black), measurement of appropriate HSP and surface energy parameters will be required.

Electrically conducting and mechanical strong PAN nanocomposite fibers produced here via continuous spinning are a new class of material to be added to the Ashby charts. However, during material selection, depending on the specific application, many other material characteristics and properties, not studied here, are also needed. Examples of these include, cost, performance during compression, bending, in humid vs dry conditions, and so on. Therefore, further characterization of the fibers reported here is required, so these fibers can be considered for relevant product design. Furthermore, the properties reported here (i.e. tensile strength, modulus, elongation at break and axial electrical conductivity) can be further improved by further process optimization.

There are large number of reports in the literature on processing, structure and properties of polyacrylonitrile nanocomposite fibers and PAN-derived carbon fibers. Experimental space is vast, and more laboratory experimentation and characterization are required. However, a simultaneous effort is needed for compiling the information that has already been generated. Data mining and data analytics should be used to consolidate the worldwide results reported over the years, and to create models that can support future material design. Specifically, for the carbon nano fillers for polymer composites, the following factors need to be evaluated: aspect ratio, the type of functionalization and its effect on filler dispersion and filler-matrix interaction, and different processing methods.

Carbonization of electrically conductive stabilized PAN nanocomposite fibers via Joule Heating is possible but has yet to be experimentally done. Although many carbon-systems have been used to reach high temperatures via electric power, carbonization by Joule heating for the axially oriented stabilized PAN nanocomposite fibers will require a sophisticated set-up, to achieve high mechanical properties. This is particularly true, given that the fiber resistance will continuously decrease with increasing temperature, and that

the effect of electron flow and the electric field on the PAN stabilization mechanism is yet to be analyzed. Further progress of this technology will require specific funding and a multi-disciplinary team.

Crosslinking of filler, before, during, and after fiber spinning should be studied. Consider for example the PAN-CB system, in which a CB network could provide additional elastic behavior and improve processability. PAN-derived carbon fiber with CB or CNTs, with filler-filler and filler-matrix bridging should have greatly enhanced tensile properties. Many CNT-CNT bridging techniques are already reported in the literature and can be evaluated for the nanocomposite systems described here.

Appendix A - Chapter 2

A.1 Additional tables for chapter 2

Table A 1.Dispersion, dipole-dipole and hydrogen bonding contributions of the Hansen Solubility Parameters (HSP) for the various CNTs, polymers and solvents used.

Component	δ_d	δ_p	δ_h
SWNT*	19.5	6.5	4.5
DWNT*	19.4	7.4	5.3
MWNT*	19.5	6.7	5.5
PMMA	18.6	10.5	5.1
PMA**	17.3	5.4	7.3
DMF	17.4	16.7	11.3
DMSO	18.4	16.4	10.2
Acetone	15.5	10.4	7
Nitromethane	15.8	18.8	5.1
NMP	18	12.3	7.2
Decalin	18	0	0
1,4-dioxane	17.5	1.8	9
MEK	16	9	5.1
Ethyl acetate	15.8	5.3	7.2
Toluene	18	1.4	2
THF	16.8	5.7	8

Unless otherwise noted, all data was taken from.[219] *HSP of CNTs were taken from.[124] **HSP of PMA were averaged from the reported values by[220,221]

Pair interaction distances (R_a) were calculated as per:

$$R_a^2 = 4\left(\delta_{d,1} - \delta_{d,2}\right)^2 + \left(\delta_{p,1} - \delta_{p,2}\right)^2 + \left(\delta_{h,1} - \delta_{h,2}\right)^2$$

Table A 2. Surface free energy (total, dispersive and polar contributions) of the various carbon nanotubes, polymers and solvents used.

Component	Surface free energy at 20 °C γ (mN/m)	γ^d at 20 °C (mN/m)	γ^p at 20°C (mN/m)
SWNT*	52.8[222]		
FWNT**	50		
MWNT	42.2[223]	35.2 ± 0.2	7.0 ± 0.3
PMMA	41.1	29.6	11.5
PMA	42.7[224]		
DMF	36.5[225]	25.2	11.3
DMSO	44[225]	36	8
Acetone	23.3[225]	16.5	6.8
Nitromethane	36.5[226]	22	14.5
NMP	40.8[225]	29.2	11.6
Decalin	32.2[227]	32.2	0
1,4-dioxane	33		
Ethyl Acetate	23.9	23.9	0
Toluene	28.4		
MEK	24.6		
THF	27.4		

* Reported surface free energy for SWNT was measured by AFM[222] and as such there is no report of the dispersive and polar contributions.
*Assumed to be 50 mN/m based on the expected changed of surface energy with fiber diameter[123] and the measured values for SWNTs (52.8 mN/m) and MWNTs (42.2 mN/m). Unless otherwise noted, solvent data was obtained from.[228]

Pair surface tension values were calculated by the Fowkes equation[229] that assumes a small contribution of the polar component, which should be the case of pristine CNTs: $\gamma_{12} = \gamma_1 + \gamma_2 - 2\sqrt{(\gamma_1\gamma_2)}$

A.2 Evaluation of the PMMA and PMA adsorption onto CNTs by analysis of the spreading coefficients

The tendency towards phase separation of any two phases by encapsulation of one of them by a third one can be estimated by comparing the values of spreading coefficients (λ).[230,231] The spreading coefficient is calculated according to, $\lambda_{ijk}=\gamma_{ik}-\gamma_{ij}+\gamma_{jk}$,

in which each pair $\gamma_{12}=\gamma_{21}$ is the surface tension between any two components, and $\lambda_{ijk}>0$ translates to spreading of phase j and separation of phase i from k, with phase j at the interphase. We performed such analysis for the polymer/CNT/solvent systems studied here and found that in most of the cases the differences in spreading coefficient supported encapsulation of the CNT by the polymer. This analysis is however does not fully represent the ternary system created upon ordered wrapping of the CNT by the polymer. A complete analysis of the surface tension between the three components is not possible because the polymer surface energy strongly depends on molecule conformation. On the other hand, the reported tension between solvent and CNT, is accurate because it refers to the initial thermodynamic state of solvent wettability of the SWNTs.

A.3 Is the PMMA ordered structure inside or outside the SWNTs?

Molecular dynamic simulations of perfluorooctanesulfonate (PFOS),[232] a small (500 g/mol) organic molecule, have shown that attractive interaction between PFOS and SWNTs increase with tube diameter when the organic molecule is adsorbed at the surface, similar to the results obtained for polymers adsorbed onto CNTs.[50,114] However, the authors showed that attractive interactions can be significantly stronger when the PFOS is placed inside the SWNT and that there is a CNT diameter at which the interactions are strongest.[232] This result supports CNT diameter-specific binding of organic molecules while inside the CNT. Dahal and Dormidontova[233] simulated poly(ethylene oxide) (PEO) with SWNTs while in water, and showed that the polymer spontaneously moves inside the SWNT, and that, stabilized by water molecules inside the CNT, can acquire ordered helix conformations in a narrow CNT diameter range.

These results[232,233] are strong evidence for CNT-specific ordered adsorption of the PMMA inside the SWNTs and stabilized by the solvent presence, rather than the CNT-curvature. However, several considerations contradict the inside-the-CNT mechanism.

Foremost, helical structure has been observed after solvent removal and vacuum drying of SWNT buckypapers. This indicates that although solvent presence is required to achieve the helical conformation, said conformation can remain after solvent removal. Secondly, it is reasonable to assume that diffusion of the polymer chain inside the CNT is energetically less favorable than adsorption at the CNT surface and would have a stronger dependence with the polymer molecular weight. Experimental results indicate that the amount of PMMA adsorb to the SWNTs does not depend on the molecular weight of the PMMA.[34,47] Finally, earlier reports of the wetting of carbon nanotubes with glycerol, polyethyleneglycol and water indicate that internal wetting is more probably with water than with the organic solvents studied.[234]

Appendix B – Chapter 3

B.1 Calculation of SWNT strain and SWNT-PAN Interfacial Shear Strength (IFSS)

Single filaments of the nanocomposite fibers were fixed in a straining stage while maintaining an initial gauge length of 1 inch. No pre-strain was applied to the fiber. Fibers fixed to the stage with some pre-strain were subjected to negative strain (gauge length was reduced) to ensure that the fiber was without straining before data collection. Raman data for the G' band (~ 2570 – 2590 cm^{-1}) were collected after subsequent step-wise 50 μm strain until reaching 5% strain. Upon straining of the fiber, G' band shifted to lower cm^{-1} values, as shown in Figure S 3, in which PAN/PMMA-SWNT fiber (1 wt.% SWNT and PMMA wrapping with 350,000 g/mol) was subjected to 3 % strain. Shift of the Raman peaks has been previously related to the strain of SWNTs strain[168] (ε_i) and, then with it, to the interfacial shear strength (IFSS).[67]

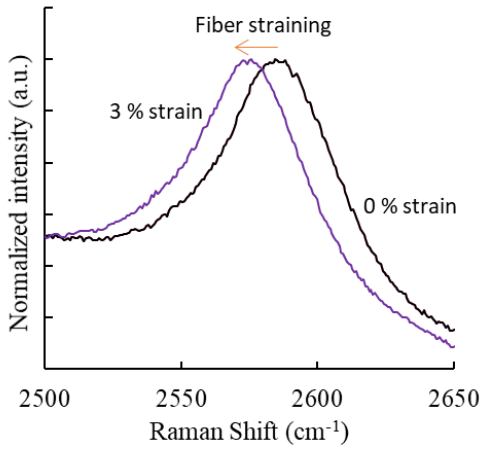

Figure B 1. G' peak of 1 wt.% SWNT wrapped with PMMA of 350,000 g/mol (PAN/PMMA-SWNT) before and after fiber straining.

SWNT strain (ε_i) was estimated assuming a G' shift rate of -37.3 $cm^{-1}/\%$.[168] IFSS was calculated assuming a modified shear-lag equation:[235]

$$IFSS = \frac{nE_{CNT}\varepsilon_i}{2}\tanh(ns), \qquad n^2 = \frac{2G}{\ln(R/r)E_{CNT}}$$

Where E_{CNT} is the SWNT modulus (760 GPa), G is the PAN shear modulus (assumed to be 1.5 GPa, from typical values measured for other high-modulus polymer fibers),[236] *s* is the ratio of SWNT length (500 nm) to SWNT radius (*r* = ~0.5 nm) and R is the distance between nanotubes assuming they are completely individualized and equidistant in a hexagonal arrangement (8 nm for 1 wt. % SWNT).

B.2 Calculation of number of PMMA molecules required to coat SWNTs

Davijani & Kumar[47] estimated that the ordered PMMA helix giving rise to the 2θ ~10.6° peak should have a pitch of about 0.83 nm, a diameter of 1.6 nm and be composed by ca. 21 PMMA repetitive units. This data can be used to estimate the number of monomers required to cover any given length of SWNTs, and given a polymer molecular weight, the number of molecules that will be attached to the SWNT surface.

This data can also be used to estimate the length of SWNTs that is covered after the wrapping procedure used here and initially reported in[47] and by assuming a SWNT density of 1.552 g/cm^3, diameter of 1 nm and length of 500 nm, PMMA density of 1.18 g/cm^3, and the helix geometry described before. After 24 h sonication of solutions of 5 mg SWNT + 5 mg PMMA in 100 ml DMF, the produced buckypapers by vacuum filtration are 37 wt.% PMMA. This polymer mass content corresponds to a helix cover of a single polymer molecule thick and about 85 nm long. Hence, product of this procedure 17% of the SWNT length is covered. The reason for this low surface cover, and its dependence or not to SWNT chirality and polymer tacticity should be further investigated. It is possible that only some of the nanotubes present in the SWNT sample are being wrapped. Diameter-selective polymer wrapping has been extensively documented and is believed to be caused by the competitive process of carbon nanotube re-bundling and polymer adsorption.[114]

B.3 Effect of polymer molecular weight in the mechanical properties of composites with polymer-grafted carbon nanotubes

Regarding the effect of the molecular weight of the polymer used for CNT wrapping on the mechanical properties of CNT/polymer nanocomposites, available literature is on covalent modification of the CNTs i.e. polymer-grafted carbon nanofillers.[237,238] It has been found that increasing molecular weight of the grafted polymer can decrease mechanical properties of the nanocomposite because of steric hindrance,[239] similar to what is observed in the mixing of branched polymer chains. The lower filler-matrix interaction described in this contribution upon increasing the molecular weight of the PMMA wrapping the SWNTs is not the same phenomenon. PMMA wrapping happens along the SWNT axis, and 'branches' or dangling PMMA groups are chain ends (discontinuities of the helix). Increasing the PMMA molecular weight increases the order of the helix, reduces the number of molecules required to wrap the SWNTs and the number of chain ends present i.e. chances of steric hindrance caused by dangling chain ends are reduced with larger molecular weight PMMA.

B.4 Analysis of pair interactions of the ternary system PAN-PMMA-SWNT

For the samples here prepared, it could be expected that the interface interactions will be dominated by the ternary system PAN-PMMA-SWNT, with SWNT-PMMA, SWNT-PAN interactions, as well as PAN-PMMA ones. Considering SWNT-polymer pairs, SWNT interactions with PAN and PMMA can be predicted by calculation of wetting parameters i.e. spreading coefficient, wetting tension and interfacial energy.[240] Wettability calculations are summarized in Table B 1 and suggest that SWNT-PMMA interactions are slightly more favorable than PAN-SWNT ones. This trend is also supported by molecular dynamic simulations of SWNTs in DMF with PAN and PMMA oligomers.[46] Interestingly, in that same report, it was predicted that polymer-SWNT interactions are lowest (within the studied cases) when PAN and PMMA were blended.

Regarding the PAN-PMMA interactions, PAN and PMMA are immiscible polymers, both with donor functionalities and their solubility depends on the molecular weight of the polymer chains, with increasing solubility (entropic interactions) upon reducing the mass of the molecules. Early reports indicate that the tensile modulus of immiscible polymer blends does not depend on their miscibility, but rather on the modulus of the components and their composition;[241] however, such conclusion was reached by blending different polymers and not as a function of molecular weight and molecular weight-induced immiscibility.

Finally, we must also stress that the described analysis of interface interactions do not fully convey the conditions of the here produced solid-state fibers, e.g. polymer crystallinity, packing and orientation, ordering of the helix structure and so on, which are expected to also affect the interphase properties.

Table B 1. Wettability parameters of polyacrylonitrile (PAN) and poly(methyl methacrylate) (PMMA) with carbon nanotubes (CNT).

Parameter	PMMA/CNT	PAN/CNT
γ_{sl} (mJ/m^2)	0.8	4.4
s (mJ/m^2)	-6.8	-19.6
ΔF (mJ/m^2)	36.0	32.4

γ_{sl} is interfacial energy, *s* is spreading parameter and ΔF is wetting tension. Calculated according to the Lifshitz-van der Waals approximation.[240] Equation and used parameters are as follows.

$$\gamma_{sl} = \gamma_s^{LW} + \gamma_l^{LW} + 2\left[(\gamma_s^+\gamma_s^-)^{0.5} + (\gamma_l^+\gamma_l^-)^{0.5} - \left(\gamma_s^{LW}\gamma_l^{LW}\right)^{0.5} - (\gamma_s^+\gamma_l^-)^{0.5} - (\gamma_s^-\gamma_l^+)^{0.5}\right];$$

$$s = \gamma_s - (\gamma_l + \gamma_{sl}); \qquad \Delta F = \gamma_s - \gamma_{sl}$$

Table B 2. Lifshitz-van der Waals parameters used for calculation of wettability parameters in Table B 1.

Parameter	CNT[242]	PMMA[243]	PAN[244]
γ (mJ/m^2)	36.8	42.8	52.0
γ^{LW} (mJ/m^2)	35.9	40.0	40.0
γ^+ (mJ/m^2)	0.2	0.4	1.2
γ^- (mJ/m^2)	1.4	6.8	18.0

B.5 Additional tables for chapter 3

Table B 3. Experimental conditions used during processing of fibers with 5 wt. % SWNT when varying molecular weight of the PMMA wrapping.

	PAN-b	PAN/15k.PMMA-SWNT	PAN/350k.PMMA-SWNT
PAN molecular weight [polyacrylonitrile-co-methacrylic acid]	500,000 g/mol		
Target SWNT content (wt.%) in the nanocomposite fiber	0	5	5
MW of PMMA used during wrapping	-	15,000 g/mol	350,000 g/mol
TGA measured concentration of polymer dispersion before spinning (g of solids per dl of solvent)	10.5	9.4	9.9
Spinneret temperature	70 °C	50-60 °C	
Coagulation bath temperature	- 40 °C	-30 °C to -10 °C	
Hot drawing bath temperature	165 °C	175 °C	
Drawing [TDR = SDR × CDR × HDR]	24 = 3 × 1.5 × 5.3	19.5 = 3 × 1.3 × 5	27 = 3 × 1.5 × 6 18 = 3 × 1.5 × 4

TDR: total draw ratio is calculated as a product of the spinning draw ratio (SDR), cold draw ratio (CDR) and hot draw ratio (HDR).
Produced fibers are control fiber (PAN-b), and 5 wt.% SWNT composite fibers with SWNT wrapped with 15,000 g/mol PMMA (PAN/15k.PMMA-SWNT) and 350,000 g/mol PMMA (PAN/350kPMMA-SWNT).

B.6 Additional figures for chapter 3

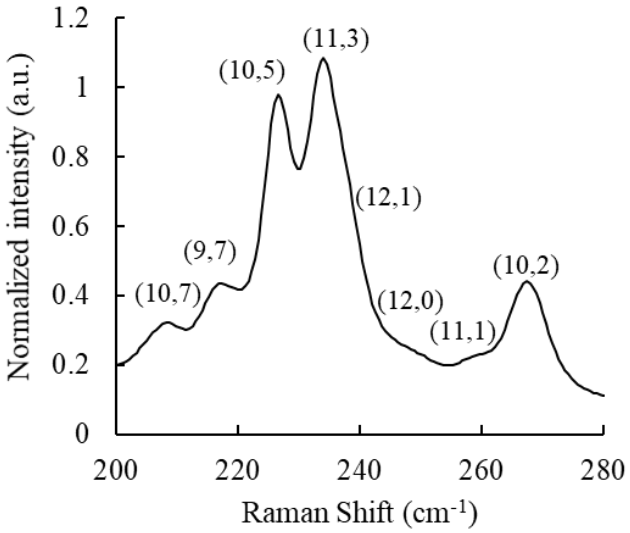

Raman shift (cm^{-1})	Chiral Index (n,m)	Diameter (nm)
204	(10,7) or (9,8)	1.15
215	(9,7)	1.08
225	(10,5)	1.04
233	(11,3)	1.00
236	(12,1)	0.98
245	(12,0)	0.94
255	(11,1)	0.90
266	(10,2)	0.87

Figure B 2. SWNT chiralities detected from fitting of the RBM Raman Shift observed under 785 nm excitation laser.
Side table presents the same information, along with the expected carbon nanotube diameter values.

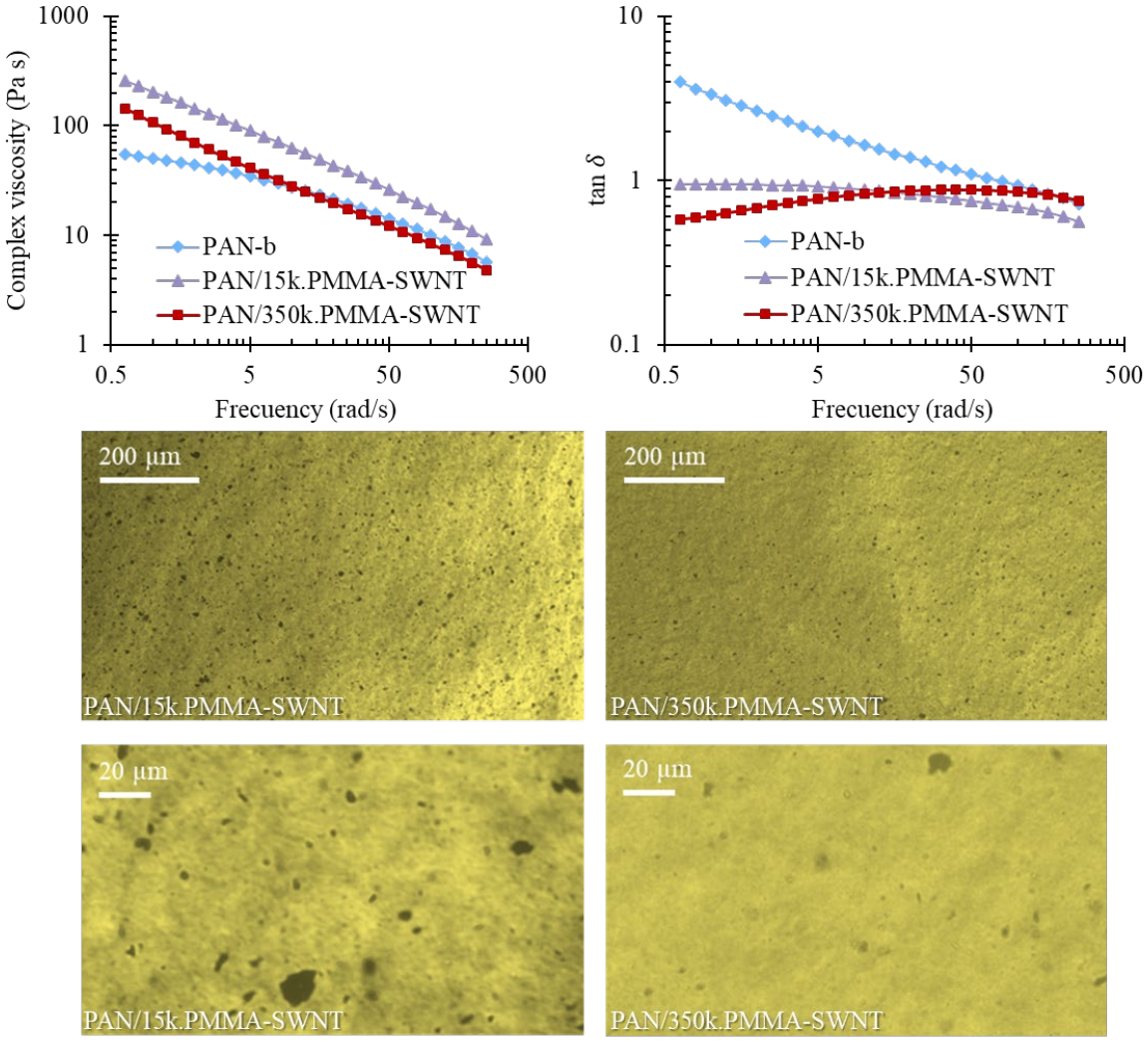

Figure B 3. Complex viscosity and tan δ at room temperature and optical images of the polymer solutions used to spin the fibers listed in Table 3-1.

.

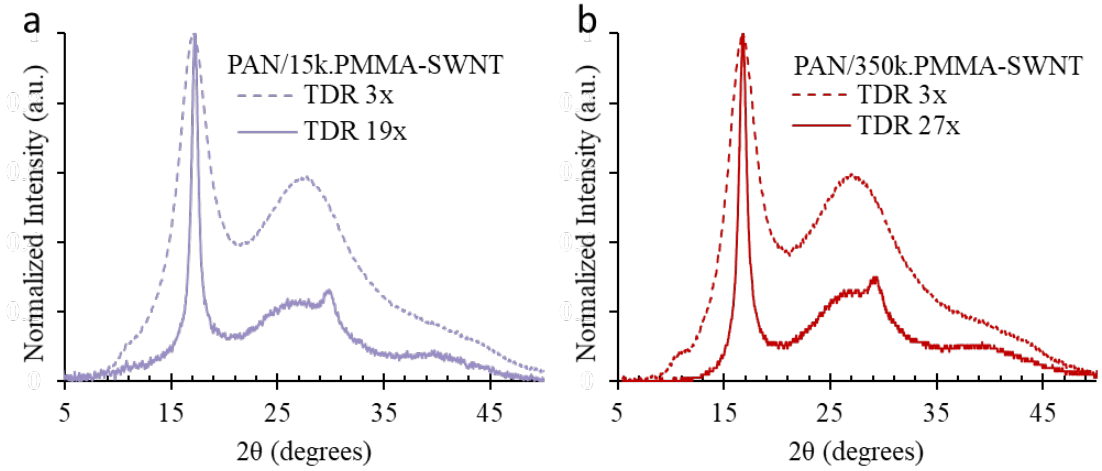

Figure B 4. Integrated WAXD of as-spun and drawn fibers with 5 wt. % SWNTs, (a) PAN/15k.PMMA-SWNT and (b) PAN/350k.PMMA-SWNT.

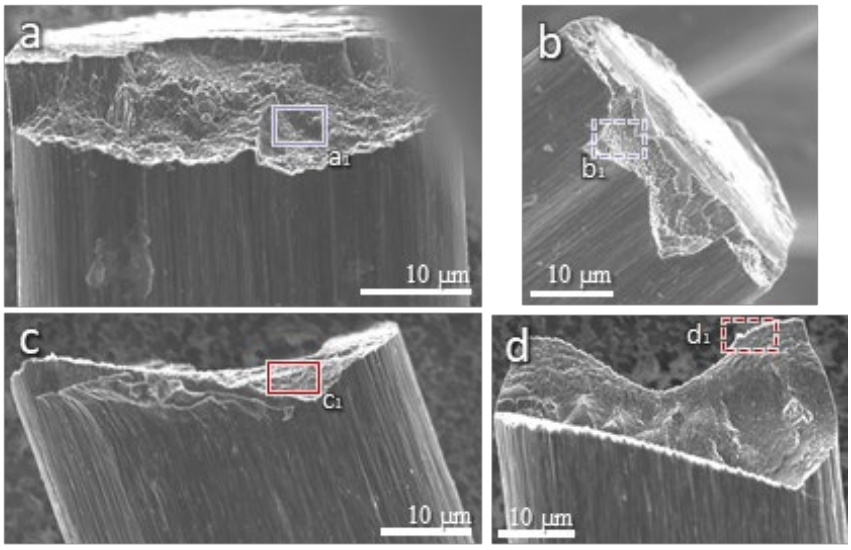

Figure B 5. SEM images of cross-sections of as-spun fibers PAN/15k.PMMA-SWNT (a and b) and PAN/350k.PMMA-SWNT (c and d).
Indicated areas (a1, b1, c1 and d1) are magnified in Figure S 6.

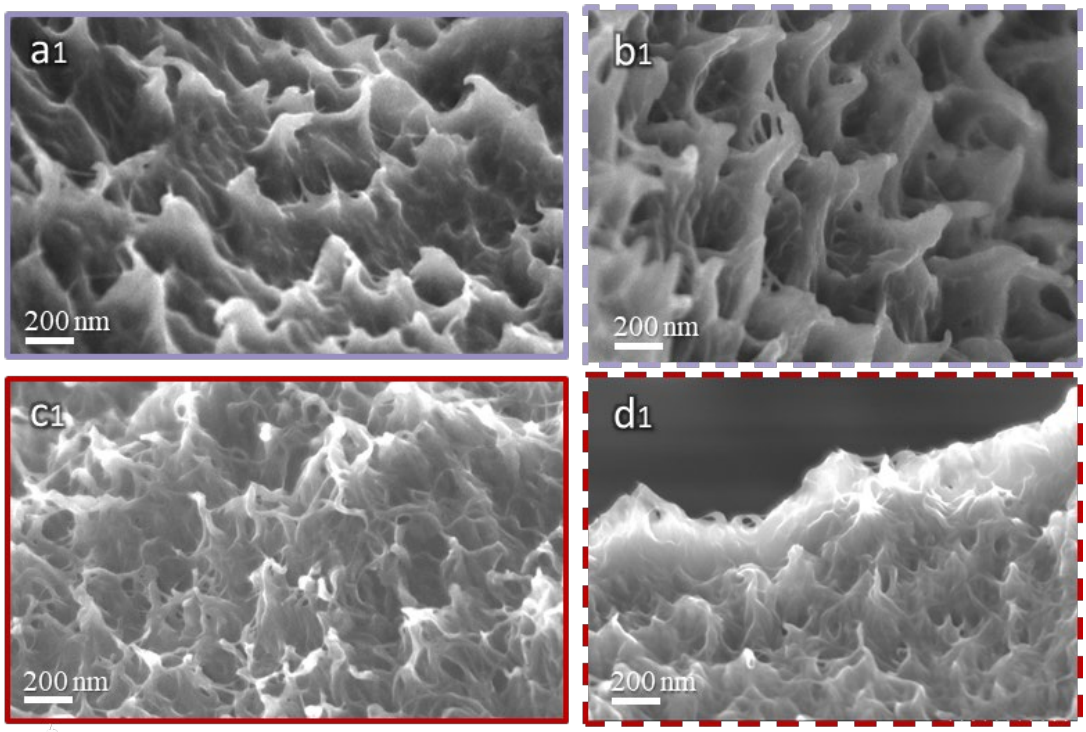

Figure B 6. Fibril-like structures observed at the cross-sections of the as-spun fibers with 5 wt.% SWNT when varying the PMMA molecular weight of the wrapping from 15,000 g/mol (a1 and b1) to 350,000 g/mol (c1 and d1).
Images a1, b1, c1 and d1 were obtained from the indicated areas in Figure S5.

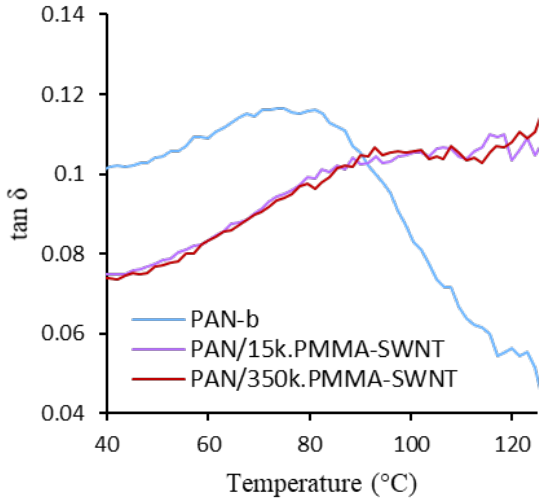

Figure B 7. tan δ as a function of temperature for PAN and 5 wt.% SWNT PAN nanocomposite fibers.
PMMA molecular weight wrapping the SWNTs is 15,000 g/mol and 350,000 g/mol in fibers PAN/15k.PMMA-SWNT and PAN/350k.PMMA-SWNT, respectively.

Appendix C – Chapter 4

C.1 Removal of free PMMA from PMMA/SWNT dispersions in DMF

Upon mixing the sonicated PMMA/SWNT/DMF dispersion with distilled water and ethyl acetate, the solution underwent phase separation: a heavy and a light phase. The heavy phase was clear, while the light phase further separated into a clear supernatant and a precipitate. The light phase precipitate contained the SWNTs at an estimated solid content of about 200 mg SWNT per dl of ethyl acetate. Determination of composition of each phase by fraction evaporation and the distribution of free PMMA and PMMA-wrapped-SWNTs by producing films from the supernatant by vacuum evaporation are described next.

At atmospheric pressure, the heavy phase showed three distinct boiling points, thus three different components. First boiling point was reached in the range 70 - 80 °C, corresponding to that of ethyl acetate. By keeping the temperature constant at the first boiling point 10% of the total volume was evaporated. The second boiling point was achieved by further increasing the temperature to about ~105 °C (boiling point of water). Boiling continued at this temperature until less than 30% of the initial total volume of the heavy phase remained. This remaining solvent had a boiling point close to 150 °C, which corresponds to that of DMF. No black residue was left after evaporating the totality of the heavy phase, demonstrating that SWNTs were exchanged to the light phase.

The light phase supernatant boiled completely at about 75 °C, demonstrating that it was mainly composed of ethyl acetate. Two SWNT films were prepared by mild vacuum evaporation at ~30°C. One film was produced by evaporating the whole light phase (supernatant and precipitate). The second film was produced by first removing the precipitate while still in the separation funnel, then mixing it with fresh ethyl acetate, and promoting phase separation by centrifugation until a new precipitate and supernatant were

formed. Washing process in ethyl acetate was repeated twice, after which the precipitate was left to evaporate/dry in vacuum at ~30 °C.

Composition and structure of the two SWNT films were studied by TGA and WAXD. The film produced from the totality of the light phase had an overall PMMA content of about 45 wt%, while the film produced from the light phase precipitate was ca. 25 wt% PMMA. Indicating thus that part of the PMMA remains in the supernatant, while other another part of it is still adsorbed onto the SWNTs.

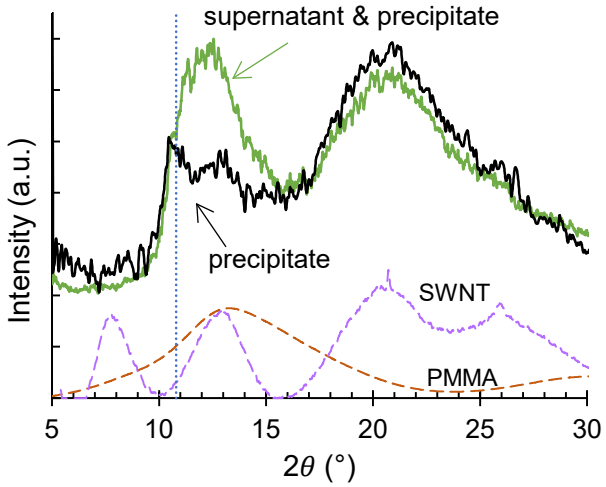

Figure C 1. Integrated WAXD of SWNT films produced by vacuum evaporation of the light phase precipitate and of the whole light phase (supernatant & precipitate).
Pure PMMA film and SWNT film are also included. Dotted line shows the ~10.8° 2θ position that corresponds to the helical wrapping of PMMA onto SWNTs.

Structure difference between the PMMA that remains in solution and the one that continued adsorbed to the SWNT was determined by WAXD. Figure C 1 shows that the film produce from the supernatant precipitate had a prominent peak at about 10.8° 2θ, which corresponds to the ordered PMMA helical wrap onto SWNTs.[47] On the other hand, in the film that also contains the supernatant, the 10.8° peak is dwarfed by that coming from the amorphous PMMA. Thus, it can be concluded that the described procedure allows for an increase in the solid content of PMMA-wrapped-SWNTs and the removal of unwrapped (excess) PMMA.

C.2 Solvent recovery

Ethyl acetate and DMF were recovered from the heavy phase and the light phase supernatant by simple distillation in vacuum, considering the boiling point difference of each solvent. Temperature was set to 50 °C and vacuum pressure was adjusted according to the solvent being and their respective boiling point at vacuum condition, i.e. 350, 110 and 15 mbar for ethyl acetate, water and DMF, respectively.[245] In order to reduce chances of co-evaporation and increase the purity of the distilled solvent after simple distillation, each distillation point was set to 100 mbar greater than that of the individual component. Solvents were distilled a second time, following the same protocol just described, to ensure solvent purity before further use.

C.3 Estimation of the SWNT bundle size from measured tensile modulus and modified rule of mixture

Measured tensile modulus of the composite (E_c) can be related to the tensile modulus of the filler (E_f) and the matrix (E_m) by considering the volume fraction of the filler (V_f) as in:

$$E_c = V_f E_f + \left(1 - V_f\right) E_m$$

In turn, the effective tensile modulus of the filler depends on the filler orientation $\langle\theta\rangle$, shear modulus (G_{12}), longitudinal modulus (E_1), transverse modulus (E_2) and the Poisson's ratio (v_{12}), as detailed by other authors[39]:

$$E_f = \frac{1}{E_2} + \left(\frac{1}{G_{12}} - \frac{2v_{12}}{E_1} - \frac{2}{E_2}\right)\langle\cos^2\theta\rangle + \left(\frac{1}{E_1} + \frac{1}{E_2} - \frac{1}{G_{12}} + \frac{2v_{12}}{E_1}\right)\langle\cos^4\theta\rangle$$

Here we assumed E_1 = 750 GPa, E_2 = 15 GPa (from elsewhere[246]), v_{12} = 0.17 (from[246]), $\langle\theta\rangle = \cos^{-1}(\sqrt{(2f_{SWNT}+1)/3}$ with f_{SWNT} the experimentally measured 2nd order Herman's orientation factor. Shear modulus (G_{12}) of SWNT bundles of various diameter

has been previously measured.[40] We used the reported data[40] to create the empirical relationship $G_{12} = 15.11\, D_B^{-0.80}$ by fitting a power-law equation within the limiting values for G_{12} of 19.5 GPa for individual SWNT and 0.7 GPa for a bundle of 20 nm.[40]

Thus, SWNT bundle size was estimated by simultaneous solution of the previous equations, determining the value of D_B at which the tensile modulus calculated by the rule of mixture equals that experimentally measured for the nanocomposite fibers.

C.4 Additional tables for Chapter 4

Table C 1. Complex viscosity, damping factor, G' and G'' scaling factors, and stretch ratio at spinning for the prepared spinning solutions.

spinning solutions (ss)	Complex viscosity (Pa s)	tan δ	value of x (G' ~ ω^x)	value of y (G'' ~ ω^y)	log G' vs log G'' slope	Stretch ratio at spinning
PAN	50	3.33	1.11	0.77	1.44	3×
1wt%	87	2.42	0.95	0.71	1.33	3×
5wt%-A	89	0.7	0.38	0.53	0.71	3×
5wt%-B	203	0.95	0.50	0.49	1.02	3×
15wt%	1471	0.28	0.14	0.21	0.66	1.3×

Note: complex viscosity and damping factor at 1 rad/s. Scaling factors (*x* and *y*) of G' and G'' with ω were obtained by fitting experimental data in the frequency range 0.6 to 2.5 rad/s to a power law equation. 0.6 to 2.5 rad/s range was also used for calculation of the log G' vs log G'' slope.

Table C 2. Structural parameter and mechanical properties of as-spun or mildly drawn PAN fiber and PAN nanocomposite fibers with various amount of SWNTs.

Fiber label	5wt%-B				15wt%
Stretch ratios*	1×	1×13.6	3×	3×1.3×3.6	1.6×
Total draw ratio (TDR)*	1×	13.6×	3×	14×	1.6×
Fiber diameter (μm)	49.4 ± 0.2	14.0 ± 0.2	30.2 ± 0.4	14.2 ± 0.2	33.7 ± 0.2
X_c[a] (%)	32	51	36	40	36
L_{PAN}[b] (nm)	3.5	11.2	3.6	12.2	3.6
Ratio[c] $d_{\sim 17^\circ}/d_{\sim 30^\circ}$	1.62	1.72	1.66	1.71	1.63
f_{PAN}[d]	0.1	0.85	0.3	0.80	0.18
f_{SWNT}[e]	NM	NM	0.87	0.89	0.67
Tensile Strength (MPa)	99 ± 11	890 ± 30	208 ± 4	717 ± 27	131 ± 1
Tensile Modulus (GPa)	8.9 ± 0.2	22.6 ± 0.8	11.9 ± 0.1	21.4 ± 0.3	12.2 ± 0.1
Elongation at break (%)	2.3 ± 0.4	9.1 ± 0.2	38 ± 3	10.0 ± 0.3	3.4 ± 0.2

NM: not measured.

C.5 Additional figures for Chapter 4

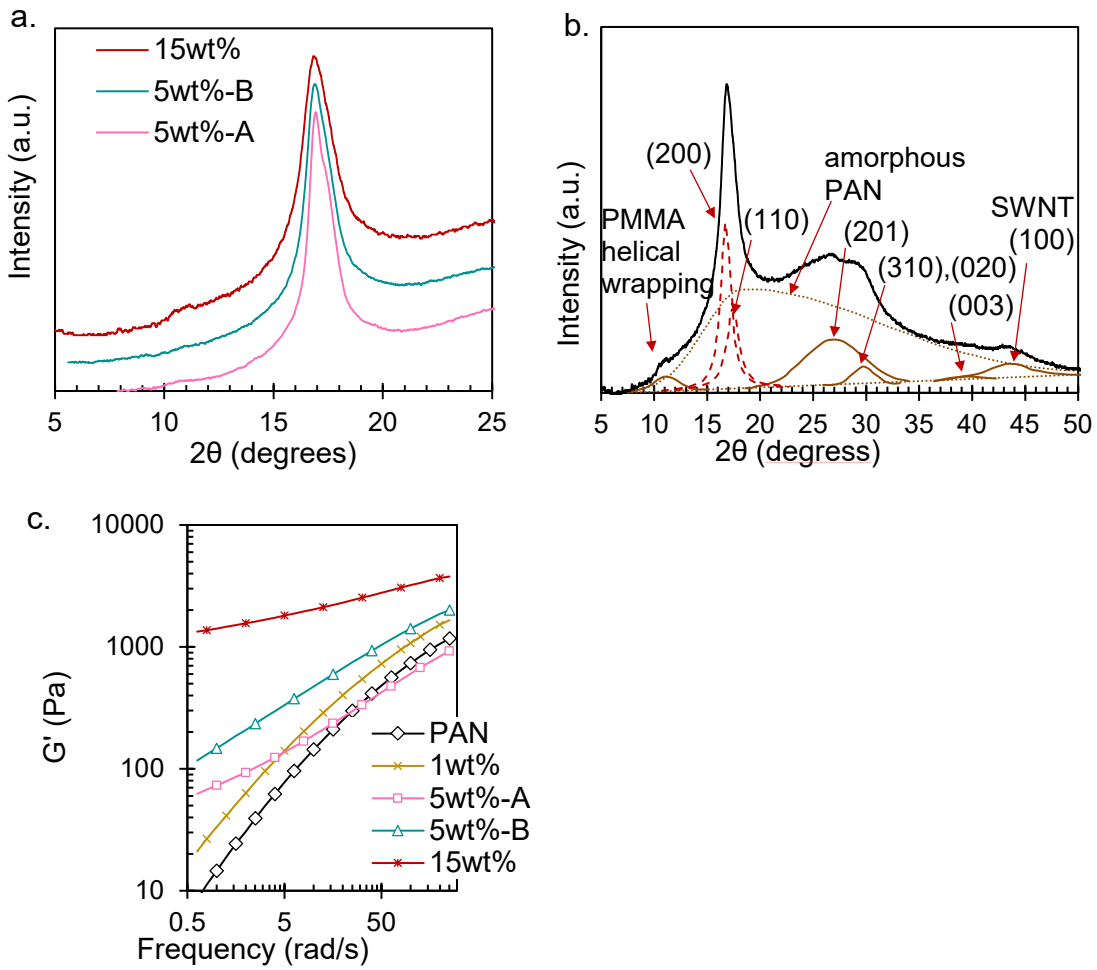

Figure C 2. XRD of several films and G' of spinning solutions produced for chapter 4. (a) WAXD of films produced by vacuum-drying of spinning solutions with 5 and 15 wt% SWNT. SWNTs in 5 wt% spinning solutions were dispersed following different protocols (-A and -B). Signals are shifted for clarity. (b) Deconvoluted peaks in the 5 to 50° region of the dried spinning solution 15 wt% SWNT. (c) G' dependence with frequency of the spinning solutions (ss) while changing SWNT content (1 to 15 wt.%) and the filler dispersion level (low to high dispersion for the 5 wt%-ss).

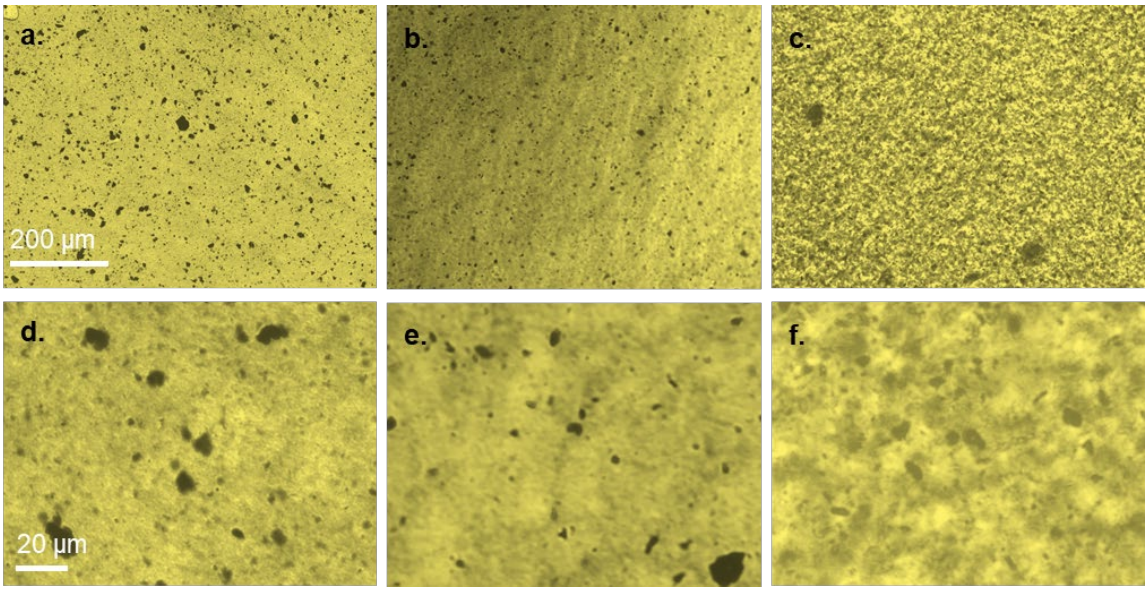

Figure C 3. Optical micrograph images of the 5wt%-A (a and d), 5wt%-B (b and e) and 15wt% (c and f) spinning solutions produced for chapter 4 at different magnifications. Scale bars are the same for images in each row. Note 1: SWNT agglomerates appear lighter in figure f, as compared to figures d and e, because the brightness and contrast were adjusted to overcome the lower transmittance of the sample. Note 2: presence of micro-sized aggregates typically reduces spinnability and fiber's final properties. That was not the case for the fibers produced here. We believe that the observed micro-size agglomerates, made of the PMMA-wrapped-SWNTs, were small and loose enough such that fiber spinning and drawing allowed for their exfoliation. Exfoliation of those micro-sized aggregates is supported by several data results: 1) SWNT individualization is high in fibers as measured by Raman RBM and estimated by rule of mixtures. 2) SWNT orientation, as determined by Raman spectroscopy, is also high, which should not be possible with randomly oriented agglomerates. 3) SEM characterization shows agglomerates only at fiber surface, not in the cross-sectional images (see figure 4 of the main document).

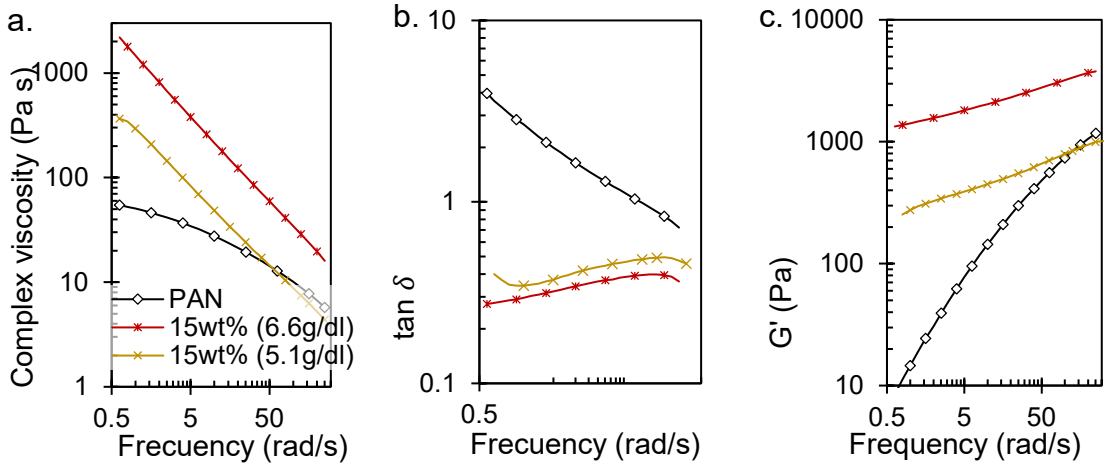

Figure C 4. Rheological properties of two spinning solutions with 15 wt% SWNTs (respect to solids) upon changing the content of solids with respect to solvent (i.e. 6.6 and 5.1 g/dl). The two 15 wt% SWNT spinning solutions were produced following the same protocol during SWNT wrapping, solvent exchange with ethyl acetate and mixing with PAN/DMF solution. A spinning solution of pure PAN (10.5 g solids per dl of solvent) is included for comparison. Spinning solution with lower solid content (5.1 g/dl) was not spinnable by dry-jet wet-spinning.

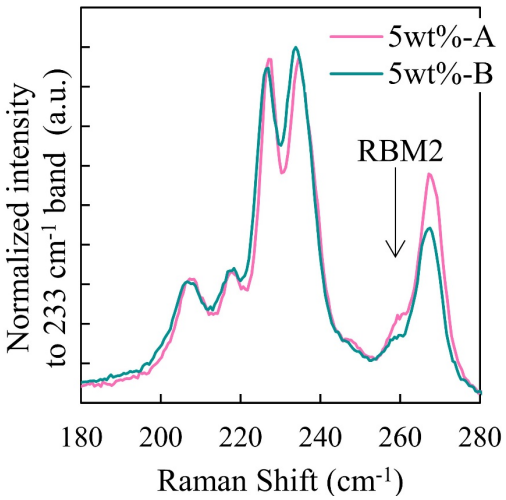

Figure C 5. Radial breathing mode (RBM) of fully drawn PAN fibers with 5 wt% SWNT. Both fibers have PMMA-wrapped-SWNTs but fillers were dispersed under different conditions (-A and -B) detailed in Table 4-1.

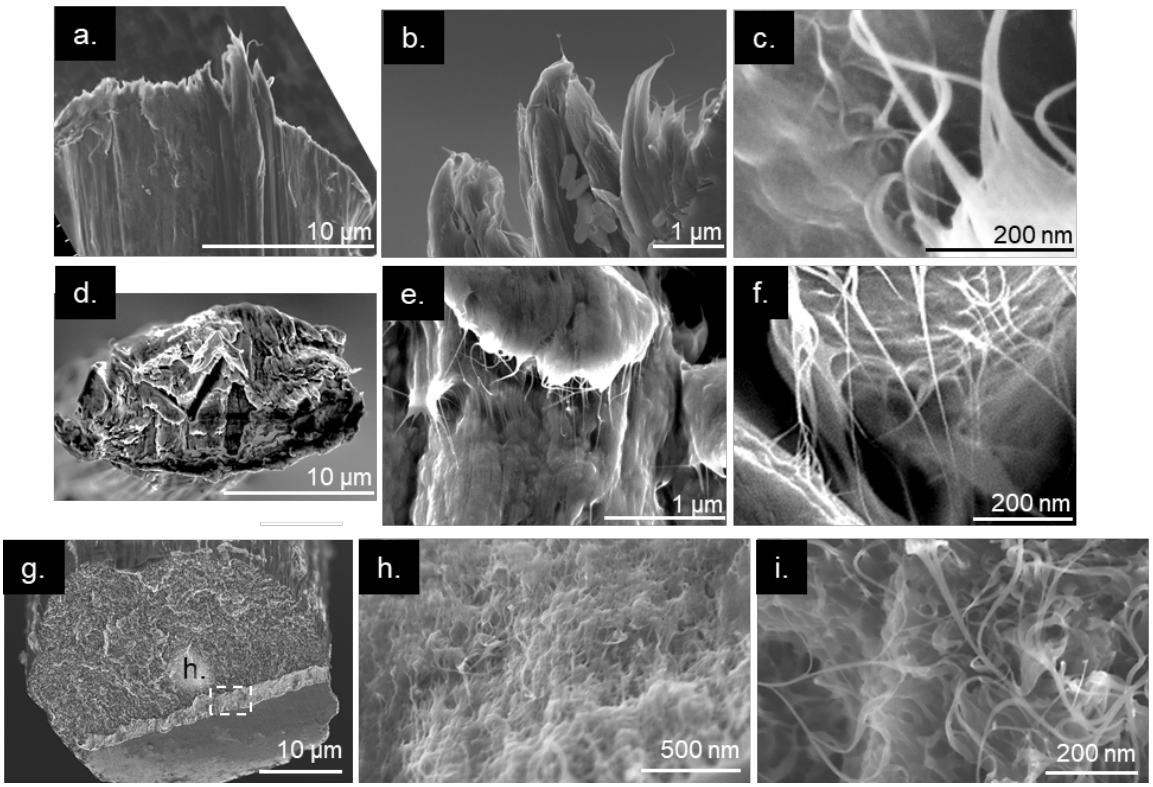

Figure C 6. Scanning electron micrographs of (a-f) fully drawn (TDR 9.8×) and (g-i) as-spun (TDR 1.6×) 15wt% fiber.

Cross section of the fully drawn fiber was produced by cutting the fiber at room temperature and showed plastic deformation.

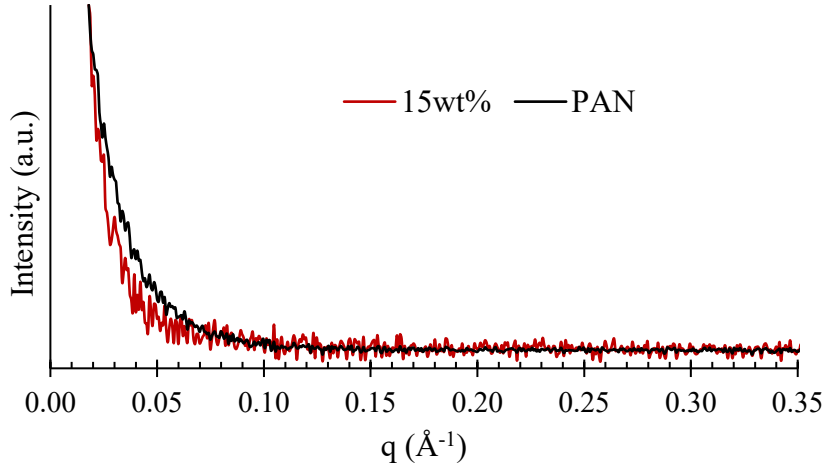

Figure C 7. Small angle x-ray scattering (SAXS) of fully drawn PAN (TDR 24×). and 15wt% (TDR 19.4×) fibers in the 0.02 to 0.35 Å^{-1} range (0.28 to 4.92° 2θ with $q = (4\pi \sin\theta)/\lambda$).

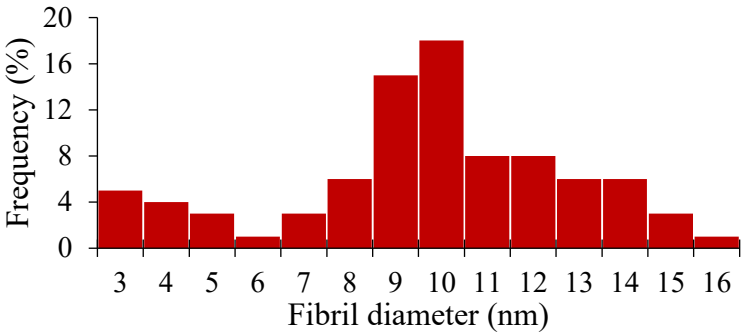

Figure C 8. Diameter distribution of fibrils obtained by dissolving fiber with 15 wt% SWNT in DMF at 120 °C for 6 h.

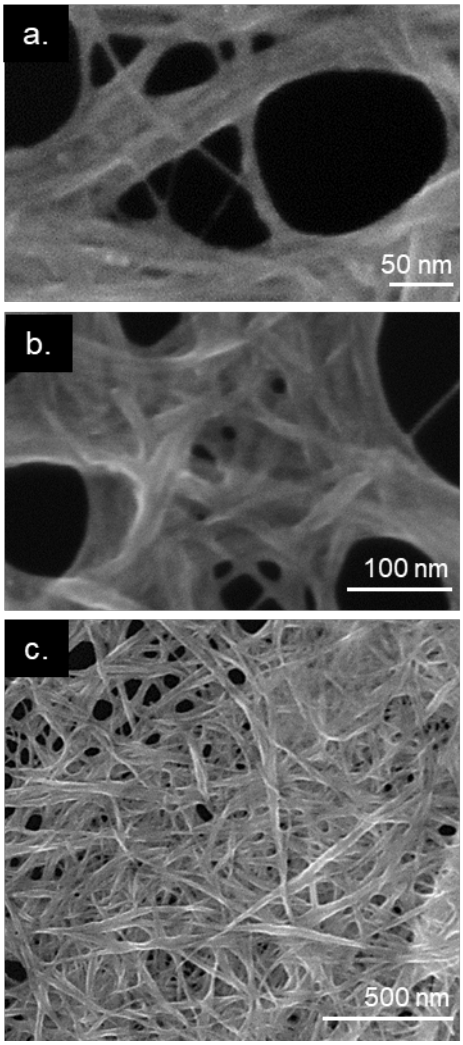

Figure C 9. Scanning electron micrographs at different magnifications (a-c) of the fibrils obtained after dissolving fully drawn (TDR 19.4×) 5 wt%-B fiber in DMF at 120 °C for 6 h.

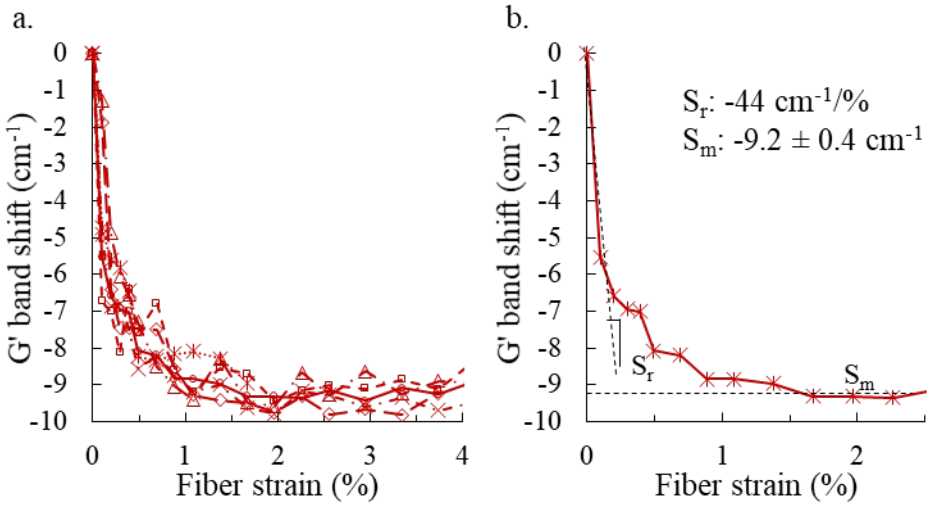

Figure C 10. Shift of the G′ band as a function of strain for fully drawn fibers with 15 wt % SWNT. Five different fibers were measured (a) and the average displacement is presented in (b).

Maximum G′ shift (Sm) and G′ shift rate (Sr) are indicated. Shifting of G′ is proportionally related to SWNT strain, as reported elsewhere.[168]

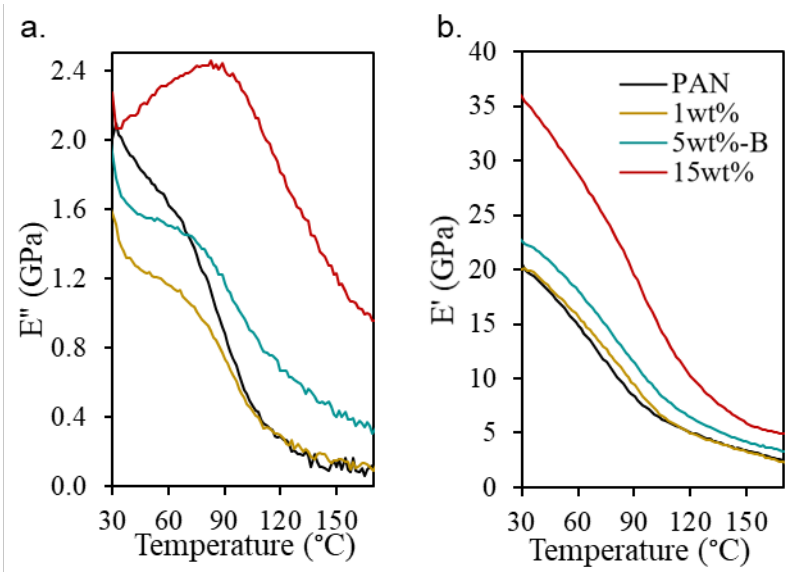

Figure C 11. Loss modulus E'' (a) and storage modulus E' (b) at 0.1 Hz as a function of temperature for PAN/SWNT nanocomposite fibers prepared with PMMA-wrapped-SWNTs at the indicated filler contents.

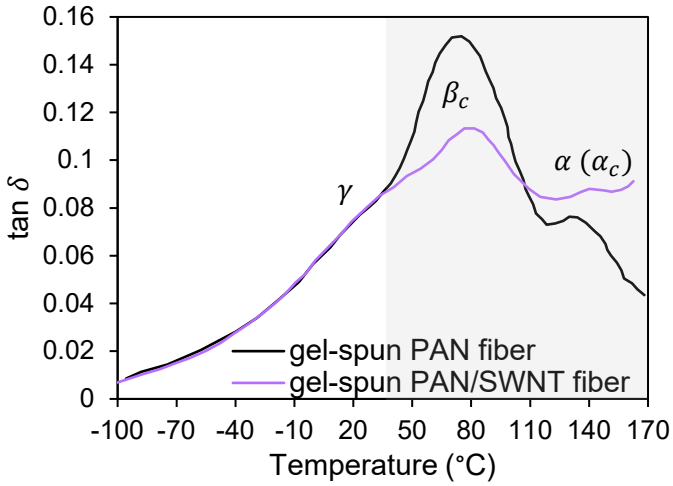

Figure C 12. Tan δ as a function of temperature for gel-spun PAN and 1 wt% SWNT PAN fibers (adapted from[65]).

Appendix D – Chapter 5

D.1 Additional figures for Chapter 5

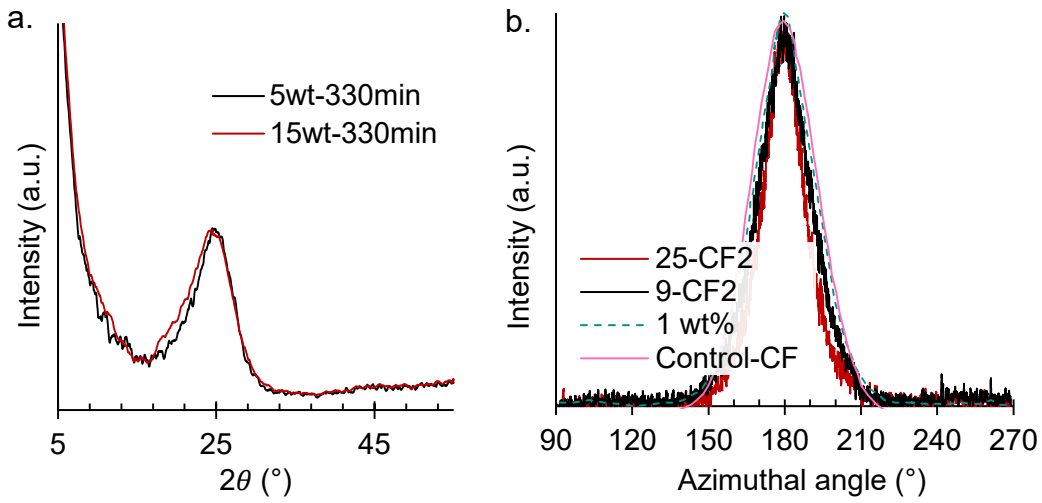

Figure D 1. Wide-angle X-ray data of carbon fibers produced from PAN precursors with 5 and 15 wt% SWNTs.
(a) Skewing of the (002) plane in equatorial scans of carbon fibers 5wt-330min and 15wt-330min. (b) Azimuthal scan of the (002) peak of nanocomposite carbon fibers prepared here (5wt-330min and 15wt-330min) and two carbon fibers reported elsewhere[33] (1wt and Control-CF) and produced from a PAN precursor with 1 wt% few-walls carbon nanotubes and without filler.

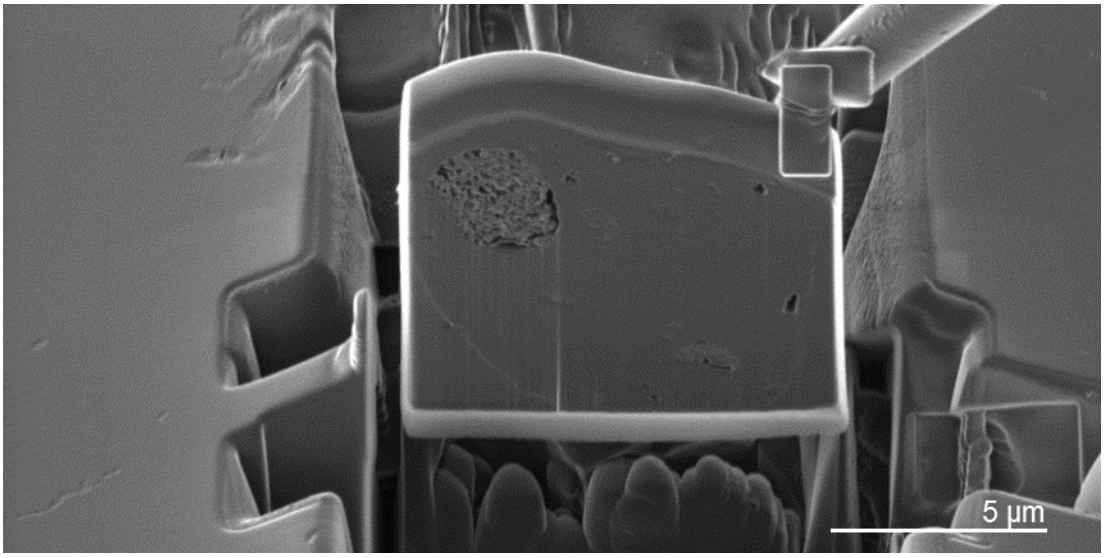

Figure D 2. Scanning electron micrograph of the sectioning of the carbon fiber via focused ion beam (FIB) milling.

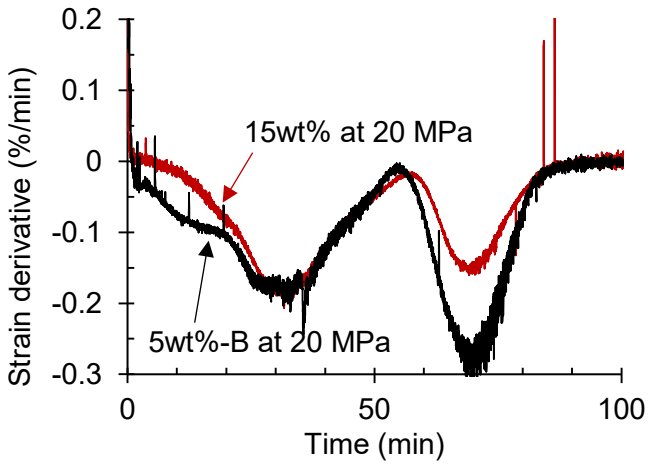

Figure D 3. strain derivative with time for precursor bundles of 5wt%-B and 15wt% at 20 MPa.

Appendix E – Chapter 6

E.1 Additional tables for Chapter 6

Table E 1. Rheological properties of a PAN solution used to obtain control PAN fiber and of CB-PAN dispersions with 60 wt% CB with two different particle sizes.

Dispersion ID	control PAN	CB-PAN with CB of 20 nm	CB-PAN with CB of 70 nm
Solid content (g/dL)	11	13.1	12.1
Complex viscosity (Pa.s)	50	30	8
tan δ	3.33	1.09	1.39
log G' vs log G'' slope	1.44	0.77	0.51

Note: complex viscosity and damping factor at 1 rad/s. log G' vs log G'' slope is calculated in the 0.6 to 2.5 rad/s range.

Table E 2. Mechanical and electrical properties and structural parameters of various precursor fibers.

Fiber ID	A-1	A-2	D-1	D-2	E-1	E-2
Total draw ratio	2.9×	14.5×	3.9×	27.1×	3.9×	27.1×
Diameter (μm)	53.8 ± 0.7	27.7 ± 0.7	NM	NM	NM	52.0 ± 3.2
Tensile modulus (GPa)	4.9 ± 0.3	13.3 ± 0.7	NM	NM	NM	2.7 ± 0.5
Tensile strength (MPa)	76 ± 3	494 ± 25	NM	NM	NM	32 ± 2
Strain at break (%)	20.4 ± 5.2	12.3 ± 0.6	NM	NM	NM	5.9 ± 0.6
X_{PAN} (%) [a]	45	50	NA			
$X_{\sim 17^\circ PAN}$ (%) [a]	NA		8.3	15.6	9.0	15.2
L_{PAN} (nm) [b]	3.7	9.1	3.8	6.5	3.4	6.8
d-$spacing_{PAN}$ (nm) [b]	0.524	0.526	0.532	0.527	0.532	0.530
f_{PAN} [c]	0.08	0.72	0.04	0.59	0.05	0.59
Electrical conductivity (S/m)	5×10^{-4}	13.6 ± 2.3	$<1\times10^{-5}$	2×10^{-3}	$<1\times10^{-5}$	9×10^{-4}

Notes: not measured (NM).). [a] PAN crystallinity of fibers A was calculated considering area of peaks at 2θ ~17, ~25, ~29 and ~40° as crystal content (see Figure E 2) respect to total XRD signal area. For fibers B to G, area fraction of the 2θ ~17° peak is shown instead, as the other PAN crystal peaks were dwarfed by the CB amorphous peak (see Figure E 4

and Figure E 5). [b] PAN crystal size and d-spacing calculated from equatorial scans. Scherrer's equation was used with k = 0.9. [c] PAN. [a] 2nd order Hermann's orientation factor calculated from azimuthal scans of the 2θ ~17° peak.

E.2 Additional figures for Chapter 6

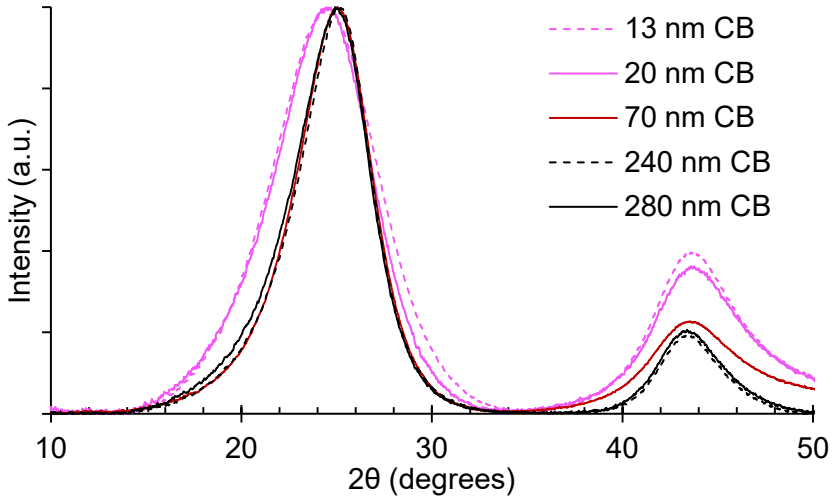

Figure E 1. X-ray diffraction of powder carbon black samples used in this study to prepare fibers A to G, as listed in Table 6-1.

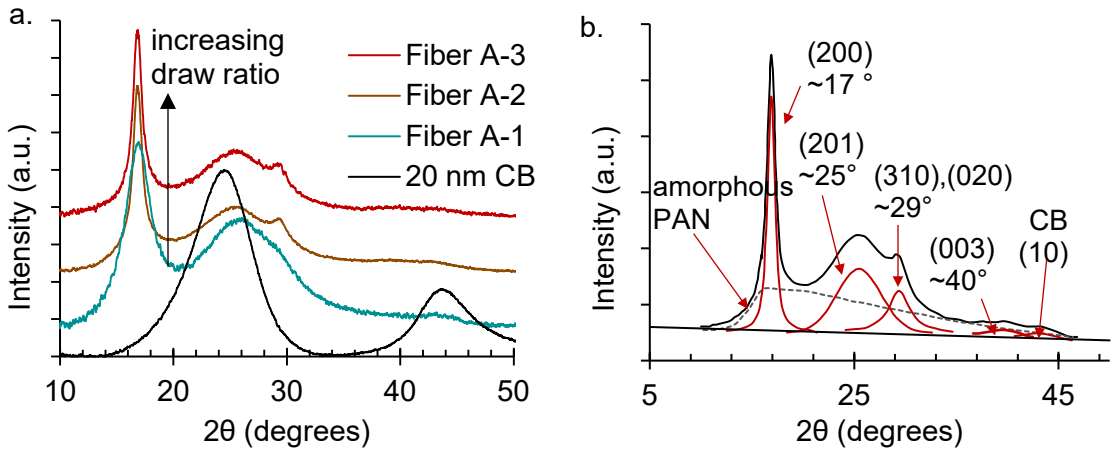

Figure E 2. (a) Integrated WAXD scans of Fibers A produced at different draw ratios, as listed in Table 6-1, and of carbon black of 20 nm used to produce these fibers with 15 wt% CB and 2 wt% MWNT. (b) Deconvoluted peaks of the integrated WAXD scan of Fiber A-3.

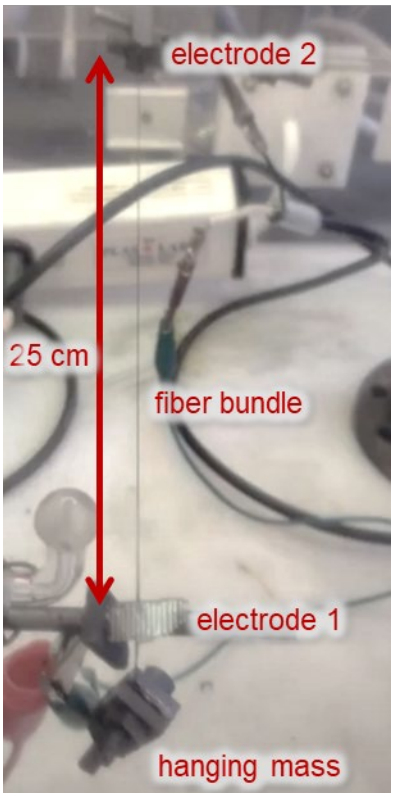

Figure E 3. Photograph showing setup used to stabilize bundle of fiber A-3 via Joule Heating at engineering stress of 30 MPa.

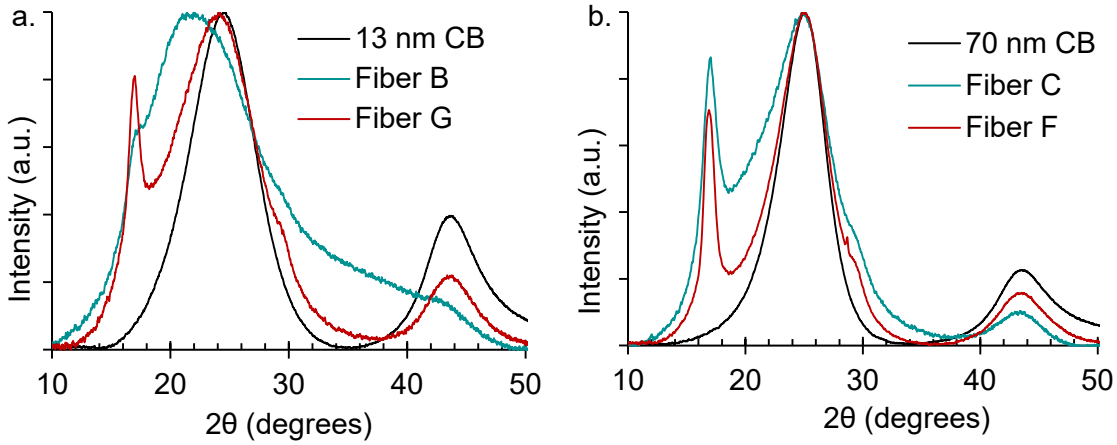

Figure E 4. Integrated WAXD scans of Fibers B, C, F and G and carbon black used in those fibers.

(a) Fiber B with 60 wt% carbon black of 20 nm diameter and Fiber G with 70 wt% of oxidized carbon black of 13 nm diameter. (b) Fiber C and F with 60 and 70 wt% CB, respectively, of carbon black of 70 nm diameter.

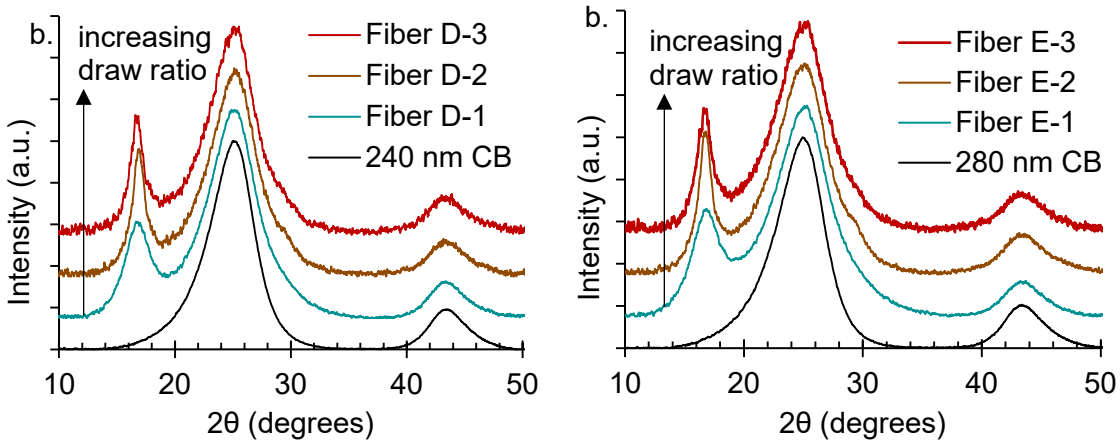

Figure E 5. Integrated WAXD scans of (a) fiber D and (b) fiber E produced at different draw ratios, as listed in Table 6-1. WAXD of corresponding carbon blacks of 240 nm and 280 nm diameter are also given,

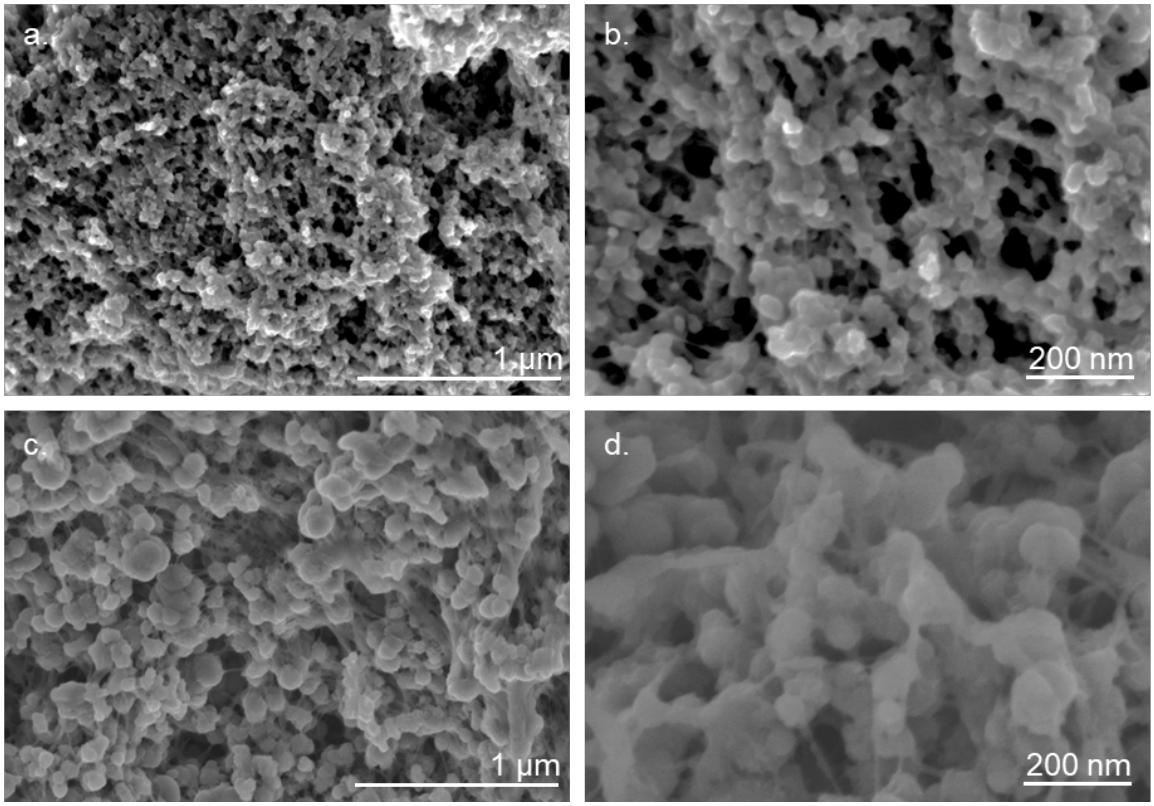

Figure E 6. SEM images at different magnifications of fiber B cross-section (a-b) with CB of 20 nm diameter, and of fiber C (c-d) with CB of 70 nm diameter.

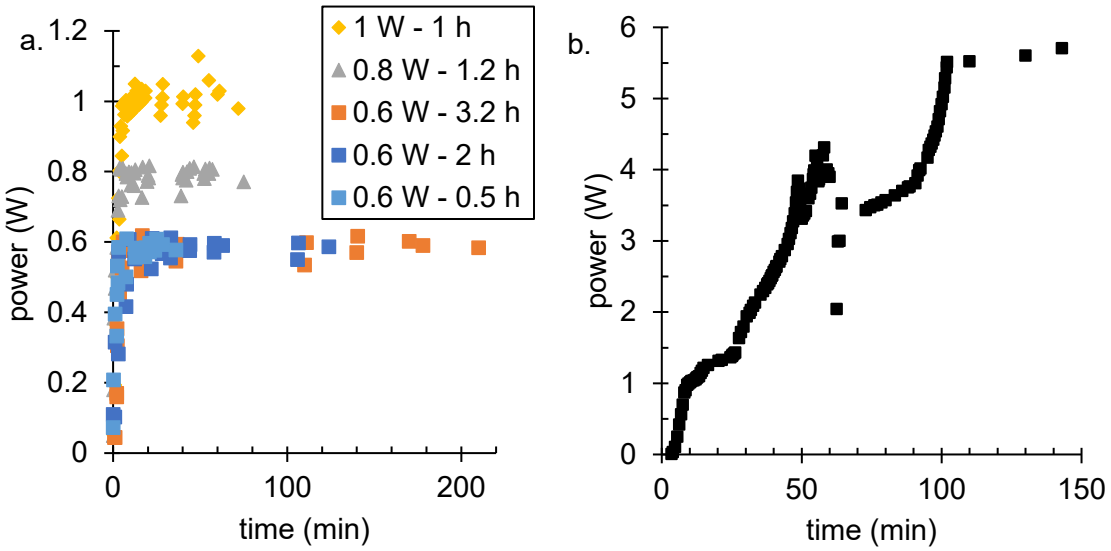

Figure E 7. Power profile used for stabilization via Joule Heating of fibers A-2 (a) and A-3 (b).

Appendix F – Improving CNT dispersion via co-solvent approach and its use in PAN nanocomposite fibers

F.1 Abstract

Dispersion of single wall carbon nanotubes (SWNTs) in dimethyl formamide (DMF) are more stable and a higher level of SWNT individualization is reached when co-solvents are used during SWNT sonication. Co-solvents studied have favorable π-π interactions with pristine SWNTs and polar interactions with DMF. Fibers were produced to evaluate if the filler reinforcement increased when using SWNTs sonicated in DMF with PMMA and the co-solvent rather than SWNTs sonicated in DMF and PMMA alone. Results were not conclusive given the large PMMA molecular weight used during dispersion in DMF and co-solvent.

F.2 Introduction

Individualization of CNTs in composite matrices is limited by the low solubility of pristine CNTs in most solvents and polymers. This in turn causes high CNT agglomeration at relatively low concentrations. Therefore, understanding of CNT solubility is of paramount importance to produce high performance composites from CNTs. Solubility of SWNT and CNTs has been the subject of debate over the years, and strong discrepancies can be found in the literature. For example, Cai et al. found in their work with HiPco-produced SWNTs that their solubility in DMF was 125 mg/L [247], while Yokoi et al. reported less than 7.5 mg/L in DMF with CVD SWNTs [248].

Such discrepancies were addressed by Detriche et al. [124] by estimating solubility after centrifugation. In their work, they evaluated a wide range of solvents and different CNT types and functionalities, including SWNT, DWNT and MWNTs. According to their findings, DMF is a *poor* solvent for pristine SWNT and can only effectively disperse MWNT and oxidized CNTs. Detriche et al. reported other solvents that are better for dispersing

SWNTs such as benzaldehyde, o-dichlorobenzene, α,α-dichlorotoluene, 1-choronaphthalene and hexachloroacetone. More impressively, their data support predictions by Hansen Solubility Parameters (HSP), in which solvents that have short interaction distances ($\sqrt{Ra^2}$) with SWNT are better at dispersing SWNTs.

In addition to the solvents listed above, other solvents have been reported to have high compatibility with pristine SWNTs. Davis et al. have proposed a phase diagram showing isotropic and liquid crystal behavior of SWNT in super-acids at concentrations smaller than 10 vol. %.[249] Such impressive behavior was possible because of non-covalent induced repulsion between the CNTs by protonation, and similar approaches have been used to produce CNT yarns.[27,249] Recently, Kim et al.[250] reported the mixing of 1:1 mol ratio of diphenylamine (DP) and benzophenone (BP) with SWNT at concentrations as high as 200 mg SWNT per 1 mL (< 20 wt.%). Such mixes were used to produce gels that retained the eutectic liquid solvent (mix of DP and BP) even at concentrations lower than 1 wt.%, and in turn, those gels were mixed with suitable polymers to fabricate composite films. Although not done originally by Kim et al, the high interaction between the SWNTs and the eutectic liquid can also be predicted by calculation of the interaction distance following the HSP approach.

On the other hand, other authors have found experimental results that contradict HSP predictions when evaluating multicomponent systems with polymers. When doing dispersions of SWNT in PMMA, Liu et al.[251] found that prior sonication of SWNTs in nitromethane and subsequent addition of PMMA and continued sonication, a good dispersion was achieved, even better than when DMF was used as a solvent in a similar dispersion protocol. Liu et al. attributed it to the high polar component of the nitromethane solvent (18.8 $\mathrm{MPa}^{0.5}$). However, according to the HSP prediction, DMF should be a better solvent than nitromethane for SWNT. This demonstrates that a better understanding of

the SWNT dispersibility in multicomponent systems is still needed and that such could offer new and initially unexpected alternatives to reach high CNT dispersion.

The use of multicomponent systems for dispersion of nanoparticles has been previously demonstrated, and a similar approach could be beneficial for SWNTs– polymer fiber nanocomposites. Chang et al.[252] reported that cellulose nanocrystals (CNC) are more effectively dispersed in DMF upon sonication if the CNC have a moisture content of 3.8 wt.%. In fact, in some cases (high solid content during dispersion), CNC dispersion was largest if a mix of water and DMF was used as solvent, rather than pure water or pure DMF. In this work, we study the dispersibility of SWNTs by using a co-solvent approach like that reported by Chang et al. Co-solvents were selected via HSP predictions and a selected system was used to produce polyacrylonitrile (PAN) nanocomposite fiber with 1 wt% SWNT.

F.3 Experimental

Unless otherwise noted, all solvents were purchased from Sigma Aldrich and used as received, as well as the poly(methyl methacrylate) (PMMA) of 996,000 g/mol. Single wall carbon nanotubes (SWNTs) HiPco™ (grade sp300, lot # PO 271) with an average diameter of 0.9 nm were obtained from Carbon Nanotechnologies Inc. Poly(acrylonitrile-co-methacrylic acid) (PAN, 4 wt. % copolymer) with viscosity average molecular weight of 500,000 g/mol was obtained from Japan Exlan Co. (Osaka, Japan).

By use of Hansen Solubility Parameters (HSPs) three solvents with short interaction distances ($\sqrt{Ra^2}$) with pristine SWNT were identified (see Table F 1). Such solvents are named here as Solvent 1 (mix of benzaldehyde and diphenylamine), Solvent 2 (benzaldehyde) and Solvent 3 (eutectic liquid from diphenylamine and benzophenone). Each of these solvents has calculated interaction distances with SWNT several times smaller than between SWNT and DMF (see Table F 1).

Table F 1. Interaction distance ($\sqrt{Ra^2}$) between different selected polymers, organic solvents and some solvent mixes.

	DMF	Methanol	DP	BP	80% BA + 20% DP	BA	40% DP + 60% BP (eutectic liquid)
					(Solvent 1)	(Solvent 2)	(Solvent 3)
SWNT	10.8	21.0	3.6	2.4	0.9	1.2	1.4
PAN	10.2	20.4	12.2	8.6	10.2	9.8	9.8
PMMA	7.4	19.0	7.8	2.8	3.5	9.3	4.7
DMF		12.3	12.8	8.8	10.2	9.6	10.2
Methanol			21.5	19.6	20.3	20.0	20.2

Note: Single Wall Carbon Nanotubes (SWNTs), polyacrylonitrile (PAN), poly(methyl methacrylate) (PMMA), dimethylformamide (DMF), diphenylamine (DP), benzophenone (BP) and benzaldehyde (BA).

F.3.1 SWNT dispersion

Dispersions were made by sonication of 7 mg of SWNT per dL of solvent during 24 h. All solvents were filtered by means of a 0.2 μm pore PTFE filter before use. After sonication, aliquots of all samples were further diluted in DMF at ratio of 1:20 per mass. Quality of the dilute dispersions was assessed by measuring hydrodynamic radius via dynamic light scattering (DLS). DLS was conducted using a BI-200SM system (Brookhaven Instruments co.), by collecting the scattered signal from a linearly polarized 532 nm laser at 90°, collection time was 2 min and solutions were kept at 25 °C. Two aliquots were taken from each sample and their diluted counterparts were measured at least 5 times in the DLS instrument, for a total of over 10 measurements per sample. Selected samples were prepared new up to three times to corroborate findings. Hydrodynamic diameter (Equation 6) was used because it correlates to the length and diameter of the rod-like particle in solution, according to the translation diffusion coefficient measured by DLS.

$$D_{eff} = \frac{L}{\ln\left(\frac{L}{d}\right)}$$ Equation 6

F.3.2 Preparation of spinning dispersion and fiber spinning

SWNTs were mixed with Solvent 3 to incipient wetness level (1 drop of solvent per 1.4 mg of SWNTs) and sonicated for 24 h while in DMF at a concentration of 7 mg SWNTs per dl of DMF. Sonicated SWNT dispersion was added to a PAN/DMF solution and excess solvent was removed via distillation, until reaching a solid content concentration of 9.4 g/dl. Dry-jet wet-spinning was conducted on a single filament system designed by Hills Inc, with a spinneret diameter of 200 μm. Spinning dispersion and spinneret were kept to 64 and 70 °C, respectively, and dispersion was extruded to an air gap of 3-5 cm and into a methanol coagulation bath kept at ca. -40 °C. Stretch ratio during spinning was 3× and fibers were stored overnight in methanol at -40 °C prior two stage drawing. 1st stage drawing was conducted at room temperature by stretching the fiber 1.5 times its original length. 2nd stage drawing was done by passing the fiber through a glycerol bath at ~ 170 °C and stretching the fiber 4.5 times its original length. Total draw ratio, calculated as the product of the stretch ratio at each step, was 20.3×.

Spinning dispersion rheology, nanocomposite fibers' structure, and tensile properties, and filler orientation and deformation during axial straining of the macroscopic fibers were measured following the same methods described in Chapter 3.

F.4 Results

F.4.1 Co-solvent effect on SWNT dispersion

Sonicated SWNT dispersions were not stable in pure DMF, neither when any of the pure solvents (1 to 3) in Table F 1 were used instead. However, when SWNTs were slightly wet by solvents 1 to 3 (1 drop of solvent per 1.4 mg of SWNTs) and sonicated in

DMF, the sonicated dispersions were stable. In unstable dispersions, aggregates started forming once sonication was stopped and the measured hydrodynamic radius was > 500 nm. On the other hand, SWNTs did not aggregate when the solvents 1 to 3 were used in conjunction with DMF and the measured hydrodynamic diameter was always lower than 220 nm and as low as 180 nm, as summarized in Figure F 1. For comparison, the smallest hydrodynamic diameter achieved upon PMMA wrapping of SWNTs in Chapter 3 was 169 nm with PMMA of 996,000 g/mol molecular weight (see Figure 3-2 and Figure F 1).

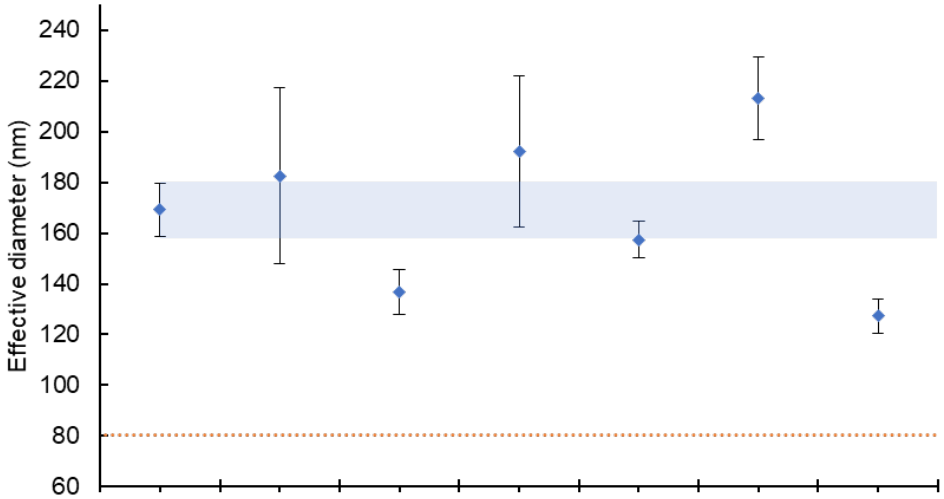

Wetting Solvent	DMF	Solvent 1 (BA/DP)		Solvent 2 (BA)		Solvent 3 (DP/BP or eutectic liquid)	
PMMA present	Yes	No	Yes	No	Yes	No	Yes
Eff. Diameter (nm)	169 ± 10	182 ± 35	137 ± 9	192 ± 30	157 ± 7	213 ± 16	127 ± 7

Figure F 1. Hydrodynamic diameter of SWNT dispersions in DMF after 24 sonication by using different dispersion strategies. SWNT were mixed with different solvents (solvents 1 to 3) to incipient wetness and sonicated in DMF with and without PMMA.
Solvent 1 is a mix of benzaldehyde and diphenylamine (BA/DP), Solvent 2 is benzaldehyde (BA) and Solvent 3 is a eutectic liquid formed by diphenylamine and benzophenone (DP/BP). Dotted line shows the estimated hydrodynamic diameter for an individual SWNT of 1 nm diameter and 500 nm length.

Increased SWNT individualization and dispersion stability upon addition of the co-solvent are explained by co-solvent/filler and co-solvent/solvent interactions. Diphenylamine (DP), benzophenone (BP) and benzaldehyde (BA) can interact with

pristine SWNTs via π-π interactions (see Figure F 2a). On the other hand, the same co-solvent molecules can interact with DMF via polar interactions. We propose that simultaneous interaction of the co-solvent molecules with SWNTs and DMF favors dispersion stability (see Figure F 2b). Interestingly, when SWNTs wet with co-solvent were sonicated in mixtures of DMF and the co-solvent (95/5 and 70/30 vol/vol) the dispersion was not stable, indicating that dispersion quality is also favored by the low interaction between SWNTs and DMF.

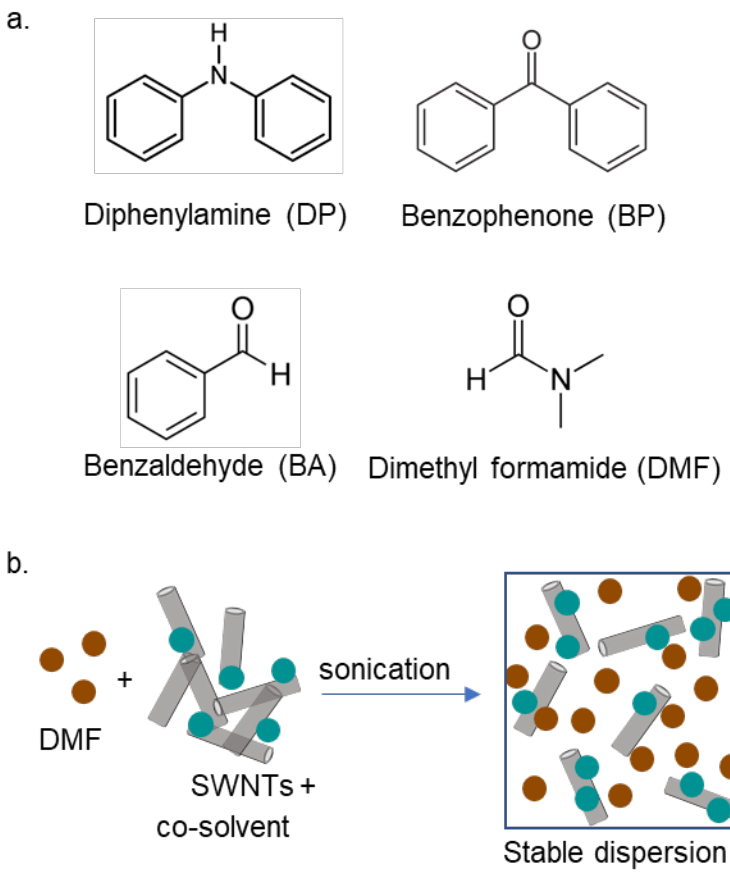

Figure F 2. Chemical structure of solvents used for dispersion of SWNTs (a) and schematic of stabilized SWNT dispersion in DMF via co-solvent addition (b).

SWNTs were also sonicated in DMF and co-solvent while using PMMA to evaluate the hydrodynamic diameter after PMMA wrapping. Combining PMMA wrapping and co-solvent assisted dispersion reduced further the hydrodynamic diameter of the SWNTs in

DMF, as summarized in Figure F 1. The system with the lowest hydrodynamic diameter (127 nm) was that in which PMMA wrapping was done while also using co-solvent 3, i.e. the eutectic liquid obtained from diphenylamine and benzophenone.

F.4.2 PAN fibers with SWNTs dispersed via PMMA and co-solvent

PAN fibers with 1 wt% SWNTs were produced using SWNTs dispersed via PMMA (996,000 g/mol) wrapping in DMF and co-solvent (solvent 3). This nanocomposite fiber had similar tensile properties than those of the pure PAN fiber (see Table F 2) and than those reported in Chapter 4 for a PAN fiber with 1 wt% SWNTs dispersed via PMMA (350,000 g/mol) wrapping in pure DMF (see Table 4-2 or Table F 2).

Table F 2. Structural parameters and mechanical properties of pure PAN fiber and two composite fibers with 1 wt% SWNTs while varying dispersion method of the SWNTs.

	Pure PAN	1 wt% - Chapter 4	1 wt% - This Appendix
SWNT dispersion strategy	NA	350,000 g/mol PMMA	996,000 g/mol PMMA + co-solvent (DMF and solvent 3)
Total draw ratio (TDR)	24×	22.5×	20.3×
Fiber diameter (μm)	11.5 ± 0.2	12.9 ± 0.3	12.1 ± 0.3
X_c (%)	53	54	58
L_{PAN} (nm)	9	11.0	10.5
Ratio $d_{\sim 17°}/d_{\sim 30°}$	1.72	1.71	1.73
f_{PAN}[a]	0.89	0.79	0.80
f_{SWNT}[b]	NA	0.90	0.91
Tensile Strength (MPa)	896 ± 28	802 ± 28	817 ± 25
Tensile Modulus (GPa)	19.2 ± 0.4	20.1 ± 0.4	19.5 ± 0.4
Elongation at break (%)	7.4 ± 0.2	8.5 ± 0.2	8.1 ± 0.2

[a] 2nd order Hermann's orientation factor calculated from azimuthal scans of 17° peak.[b] 2nd order orientation factor of SWNTs calculated from Raman signal by following the G band intensity upon rotation of the fiber with respect to the incident polarized beam.

Mechanical properties did not change despite the fact that SWNT dispersion was improved when using larger molecular weight PMMA and the co-solvent approach (see

Figure F 1). This can be explained by the negative effect that increasing PMMA molecular weight has in the SWNT-PAN interactions, as fully described in Chapter 4. Co-solvent assisted SWNT dispersion could still be used to achieve uniform filler dispersion in nanocomposite polymers and increase filler reinforcement efficiency, but further experimentation is required to validate this hypothesis.

REFERENCES

(1) Latimer, L. H. Process of Manufacturing Carbons. 252,386, 1882.

(2) Snitzer, E.; Osterberg, H. Observed Dielectric Waveguide Modes in the Visible Spectrum. *Journal of the Optical Society of America* **1961**, *51* (5), 499. https://doi.org/10.1364/josa.51.000499.

(3) Park, S.-J. *Carbon Fibers*, 1st ed.; Springer Netherlands, 2015. https://doi.org/10.1007/978-94-017-9478-7.

(4) Bowland, C. C.; Nguyen, N. A.; Naskar, A. K. Roll-to-Roll Processing of Silicon Carbide Nanoparticle-Deposited Carbon Fiber for Multifunctional Composites. *ACS Applied Materials and Interfaces* **2018**, *10* (31), 26576–26585. https://doi.org/10.1021/acsami.8b03401.

(5) Newcomb, B. A. Processing, Structure, and Properties of Carbon Fibers. *Composites Part A* **2016**, *91*, 262–282. https://doi.org/10.1016/j.compositesa.2016.10.018.

(6) Cheng, D.; Li, Y.; Zhang, J.; Tian, M.; Wang, B.; He, Z.; Dai, L.; Wang, L. Recent Advances in Electrospun Carbon Fiber Electrode for Vanidium Redox Flow Battery: Properties, Structures, and Perspectives. *Carbon* **2020**, *in press*. https://doi.org/doi.org/10.1016/j.carbon.2020.08.058.

(7) Johannisson, W.; Zenkert, D.; Lindbergh, G. Model of a Structural Battery and Its Potential for System Level Mass Savings. *Multifunctional Materials* **2019**, *2* (3), 035002. https://doi.org/10.1088/2399-7532/ab3bdd.

(8) Park, J. Functional Fibers, Composites and Textiles Utilizing Photothermal and Joule Heating. *Polymers* **2020**, *12* (1). https://doi.org/10.3390/polym12010189.

(9) Oliva-Avilés, A. I.; Avilés, F.; Seidel, G. D.; Sosa, V. On the Contribution of Carbon Nanotube Deformation to Piezoresistivity of Carbon Nanotube/Polymer Composites. *Composites Part B: Engineering* **2013**, *47*, 200–206. https://doi.org/10.1016/j.compositesb.2012.09.091.

(10) Jiang, H.; Lee, E. C. Highly Selective, Reusable Electrochemical Impedimetric DNA Sensors Based on Carbon Nanotube/Polymer Composite Electrode without Surface Modification. *Biosensors and Bioelectronics* **2018**, *118* (July), 16–22. https://doi.org/10.1016/j.bios.2018.07.037.

(11) Chien, A.-T.; Cho, S.; Joshi, Y.; Kumar, S. Electrical Conductivity and Joule Heating of Polyacrylonitrile/Carbon Nanotube Composite Fibers. *Polymer* **2014**, *55* (26), 6896–6905. https://doi.org/10.1016/j.polymer.2014.10.064.

(12) Kumar, D.; Moharana, A.; Kumar, A. Current Trends in Spinel Based Modified Polymer Composite Materials for Electromagnetic Shielding. *Materials Today Chemistry* **2020**, *17*, 100346. https://doi.org/10.1016/j.mtchem.2020.100346.

(13) Nanot, S.; Thompson, N. A.; Kim, J.-H.; Wang, X.; Rice, W. D.; Hároz, E. H.; Ganesan, Y.; Pint, C. L.; Kono, J. Single-Walled Carbon Nanotubes. In *Springer Handbook of Nanomaterials*; Vajtai, R., Ed.; Springer Berlin Heidelberg: Berlin, Heidelberg, 2013; pp 105–146. https://doi.org/10.1007/978-3-642-20595-8_4.

(14) Kubley, A.; Chauhan, D.; Kanakaraj, S. N.; Shanov, V.; Xu, C.; Chen, R.; Ng, V.; Bell, G.; Verma, P.; Hou, X.; Chitranshi, M.; Pujari, A.; Schulz, M. J. *Smart Textiles and Wearable Technology Innovation with Carbon Nanotube Technology*, 2nd ed.; Elsevier Inc., 2019. https://doi.org/10.1016/B978-0-12-812667-7.00012-4.

(15) Loos, M. Production of CNTs and Risks to Health. In *Carbon Nanotube Reinforced Composites*; William Andrew, 2015; pp 103–123. https://doi.org/10.1016/B978-1-4557-3195-4.00004-7.

(16) Taylor, L. W.; Dewey, O. S.; Headrick, R. J.; Komatsu, N.; Peraca, N. M.; Wehmeyer, G.; Kono, J.; Pasquali, M. Improved Properties, Increased Production, and the Path to Broad Adoption of Carbon Nanotube Fibers. *Carbon* **2020**. https://doi.org/10.1016/j.carbon.2020.07.058.

(17) Mikhalchan, A.; Vilatela, J. J. A Perspective on High-Performance CNT Fibres for Structural Composites. *Carbon* **2019**, *150*, 191–215. https://doi.org/10.1016/j.carbon.2019.04.113.

(18) Jung, Y.; Kim, T.; Park, C. R. Effect of Polymer Infiltration on Structure and Properties of Carbon Nanotube Yarns. *Carbon* **2015**, *88*, 60–69. https://doi.org/10.1016/j.carbon.2015.02.065.

(19) Zhang, F.; Liu, Y. *Interphase Structures and Properties of Carbon Nanotube-Reinforced Polymer Nanocomposite Fibers*; Elsevier Ltd., 2020. https://doi.org/10.1016/b978-0-08-102722-6.00005-5.

(20) Liu, Y.; Kumar, S. Polymer/Carbon Nanotube Nano Composite Fibers − A Review. *Applied Materials & Interfaces* **2014**, *6*, 6069–6087. https://doi.org/dx.doi.org/10.1021/am405136s.

(21) Adegbola, T. A.; Agboola, O.; Fayomi, O. S. I. Review of Polyacrylonitrile Blends and Application in Manufacturing Technology: Recycling and Environmental Impact. *Results in Engineering* **2020**, *7* (June), 100144. https://doi.org/10.1016/j.rineng.2020.100144.

(22) Miao, M. Yarn Spun from Carbon Nanotube Forests: Production, Structure, Properties and Applications. *Particuology* **2013**, *11* (4), 378–393. https://doi.org/10.1016/j.partic.2012.06.017.

(23) Song, J.; Kim, S.; Yoon, S.; Cho, D.; Jeong, Y. Enhanced Spinnability of Carbon Nanotube Fibers by Surfactant Addition. *Fibers and Polymers* **2014**, *15* (4), 762–766. https://doi.org/10.1007/s12221-014-0762-2.

(24) Janas, D.; Koziol, K. K. Carbon Nanotube Fibers and Films: Synthesis, Applications and Perspectives of the Direct-Spinning Method. *Nanoscale* **2016**, *8* (47), 19475–19490. https://doi.org/10.1039/c6nr07549e.

(25) Jung, Y.; Cho, Y. S.; Lee, J. W.; Oh, J. Y.; Park, C. R. How Can We Make Carbon Nanotube Yarn Stronger? *Composites Science and Technology* **2018**, *166*, 95–108. https://doi.org/10.1016/j.compscitech.2018.02.010.

(26) Park, O. K.; Choi, H.; Jeong, H.; Jung, Y.; Yu, J.; Lee, J. K.; Hwang, J. Y.; Kim, S. M.; Jeong, Y.; Park, C. R.; Endo, M.; Ku, B. C. High-Modulus and Strength Carbon Nanotube Fibers Using Molecular Cross-Linking. *Carbon* **2017**, *118*, 413–421. https://doi.org/10.1016/j.carbon.2017.03.079.

(27) Behabtu, N.; Young, C. C.; Tsentalovich, D. E.; Kleinerman, O.; Wang, X.; Ma, A. W. K.; Bengio, E. A.; Ter Waarbeek, R. F.; De Jong, J. J.; Hoogerwerf, R. E.; Fairchild, S. B.; Ferguson, J. B.; Maruyama, B.; Kono, J.; Talmon, Y.; Cohen, Y.; Otto, M. J.; Pasquali, M. Strong, Light, Multifunctional Fibers of Carbon Nanotubes with Ultrahigh Conductivity. *Science* **2013**, *339* (6116), 182–186. https://doi.org/10.1126/science.1228061.

(28) Bai, Y.; Zhang, R.; Ye, X.; Zhu, Z.; Xie, H.; Shen, B.; Cai, D.; Liu, B.; Zhang, C.; Jia, Z.; Zhang, S.; Li, X.; Wei, F. Carbon Nanotube Bundles with Tensile Strength over 80 GPa. *Nature Nanotechnology* **2018**, *13*, 589–598. https://doi.org/10.1038/s41565-018-0141-z.

(29) Chung, D. D. L. L. Processing-Structure-Property Relationships of Continuous Carbon Fiber Polymer-Matrix Composites. *Materials Science & Engineering R* **2017**, *113*, 1–29. https://doi.org/10.1016/j.mser.2017.01.002.

(30) Jolowsky, C.; Sweat, R.; Park, J. G.; Hao, A.; Liang, R. Microstructure Evolution and Self-Assembling of CNT Networks during Mechanical Stretching and Mechanical Properties of Highly Aligned CNT Composites. *Composites Science and Technology* **2018**, *166* (April), 125–130. https://doi.org/10.1016/j.compscitech.2018.04.003.

(31) Wang, X.; Yong, Z. Z.; Li, Q. W.; Bradford, P. D.; Liu, W.; Tucker, D. S.; Cai, W.; Yuan, F. G.; Zhu, Y. T. Ultrastrong, Stiff and Multifunctional Carbon Nanotube Composites. *Materials Research Letters* **2013**, *1* (1), 19–25. https://doi.org/10.1080/21663831.2012.686586.

(32) Mallick, P. K. *Fibre-Reinforced Composites Materials, Manufacturing and Design*; CRC Press, 2007; Vol. 20. https://doi.org/10.1016/0010-4361(89)90651-4.

(33) Newcomb, B. A.; Giannuzzi, L. A.; Lyons, K. M.; Gulgunje, P. V.; Gupta, K.; Liu, Y.; Kamath, M.; McDonald, K.; Moon, J.; Feng, B.; Peterson, G. P.; Chae, H. G.; Kumar, S. High Resolution Transmission Electron Microscopy Study on Polyacrylonitrile/Carbon Nanotube Based Carbon Fibers and the Effect of Structure Development on the Thermal and Electrical Conductivities. *Carbon* **2015**, *93*, 502–514. https://doi.org/10.1016/j.carbon.2015.05.037.

(34) Arias-Monje, P. J.; Davijani, A. A. B.; Lu, M.; Ramachandran, J.; Kirmani, M. H.; Kumar, S. Engineering the Interphase of Single Wall Carbon Nanotubes/Polyacrylonitrile Nanocomposite Fibers with Poly (Methyl Methacrylate) and Its Effect on Filler Dispersion, Filler−Matrix Interactions, and Tensile Properties. *ACS Applied Nano Materials* **2020**, *3* (5), 4178–4186. https://doi.org/10.1021/acsanm.0c00364.

(35) Callister, W. D. *Materials Science and Engineering. An Introduction*, 7th ed.; John Wiley & Sons, Inc, 2007.

(36) Thess, A.; Lee, R.; Nikolaev, P.; Dai, H.; Petit, P.; Xu, C.; Lee, Y. H.; Kim, S. G.; Rinzler, A. G.; Daniel, T.; Scuseria, G. E.; Tománek, D.; Fischer, J. E.; Smalley, R. E.; Thess, A.; Lee, R.; Nikolaev, P.; Dai, H.; Petit, P.; Robert, J.; Xu, C.; Lee, Y. H.; Kim, S. G.; Rinzler, A. G.; Colbert, D. T.; Scuseria, G. E.; Tomanek, D.; Fischer, J. E.; Smalley, R. E. Crystalline Ropes of Metallic Carbon Nanotubes. *Science* **1996**, *273* (5274), 483–487. https://doi.org/10.1126/science.273.5274.483.

(37) Ma, P. C.; Siddiqui, N. A.; Marom, G.; Kim, J. K. Dispersion and Functionalization of Carbon Nanotubes for Polymer-Based Nanocomposites: A Review. *Composites Part A: Applied Science and Manufacturing* **2010**, *41* (10), 1345–1367. https://doi.org/10.1016/j.compositesa.2010.07.003.

(38) Kashiwagi, T.; Fagan, J.; Douglas, J. F.; Yamamoto, K.; Heckert, A. N.; Leigh, S. D.; Obrzut, J.; Du, F.; Lin-gibson, S.; Mu, M.; Winey, K. I.; Haggenmueller, R. Relationship between Dispersion Metric and Properties of PMMA/SWNT Nanocomposites. *Polymer* **2007**, *48* (16), 4855–4866. https://doi.org/10.1016/j.polymer.2007.06.015.

(39) Liu, T.; Kumar, S. Effect of Orientation on the Modulus of SWNT Films and Fibers. *Nano Letters* **2003**, *3* (5), 1–4. https://doi.org/10.1021/nl034071i.

(40) Salvetat, J.; Briggs, G. A. D.; Bonard, J.; Bacsa, R. R.; Kulik, A. J.; Stöckli, T.; Burnham, N. A.; Forró, L. Elastic and Shear Moduli of Single-Walled Carbon Nanotube Ropes. *Physical Review Letters* **1999**, No. c, 2–5. https://doi.org/10.1103/PhysRevLett.82.944.

(41) Huang, Y. Y.; Terentjev, E. M. Dispersion and Rheology of Carbon Nanotubes in Polymers. *International Journal of Material Forming* **2008**, *1* (2), 63–74. https://doi.org/10.1007/s12289-008-0376-6.

(42) Yin, X.; Li, S.; He, G.; Feng, Y.; Wen, J. Preparation and Characterization of CNTs/UHMWPE Nanocomposites via a Novel Mixer under Synergy of Ultrasonic Wave and Extensional Deformation. *Ultrasonics Sonochemistry* **2018**, *43* (December 2017), 15–22. https://doi.org/10.1016/j.ultsonch.2017.12.039.

(43) Moore, V. C.; Strano, M. S.; Haroz, E. H.; Hauge, R. H.; Smalley, R. E.; Schmidt, J.; Talmon, Y. Individually Suspended Single-Walled Carbon Nanotubes in Various Surfactants. *Nano Letters* **2003**, *3* (10), 1379–1382. https://doi.org/10.1021/nl034524j.

(44) Fujigaya, T.; Nakashima, N. Non-Covalent Polymer Wrapping of Carbon Nanotubes and the Role of Wrapped Polymers as Functional Dispersants. *Science and Technology of Advanced Materials* **2015**, *16* (2), 24802. https://doi.org/10.1088/1468-6996/16/2/024802.

(45) Baskaran, D.; Mays, J. W.; Bratcher, M. S. Noncovalent and Nonspecific Molecular Interactions of Polymers with Multiwalled Carbon Nanotubes. *Chemistry of Materials* **2005**, *17* (13), 3389–3397. https://doi.org/10.1021/cm047866e.

(46) Pramanik, C.; Gissinger, J. R.; Kumar, S.; Heinz, H. Carbon Nanotube Dispersion in Solvents and Polymer Solutions: Mechanism, Assembly, and Preferences. *ACS Nano* **2017**, *11*, 12805–12816. https://doi.org/10.1021/acsnano.7b07684.

(47) Davijani, A. A. B.; Kumar, S. Ordered Wrapping of Poly (Methyl Methacrylate) on Single Wall Carbon Nanotubes. *Polymer* **2015**, *70*, 278–281. https://doi.org/10.1016/j.polymer.2015.06.018.

(48) Davijani, A. A. B.; Chang, H.; Liu, C.; Luo, J.; Kumar, S. Stress Transfer in Nanocomposites Enabled by Poly(Methyl Methacrylate) Wrapping of Carbon Nanotubes. *Polymer* **2017**, *130*, 191–198. https://doi.org/10.1016/j.polymer.2017.10.002.

(49) Tallury, S. S.; Pasquinelli, M. A. Molecular Dynamics Simulations of Flexible Polymer Chains Wrapping Single-Walled Carbon Nanotubes. *Journal of Physical Chemistry B* **2010**, *114* (12), 4122–4129. https://doi.org/10.1021/jp908001d.

(50) Rouhi, S.; Alizadeh, Y.; Ansari, R. On the Interfacial Characteristics of Polyethylene/Single-Walled Carbon Nanotubes Using Molecular Dynamics Simulations. *Applied Surface Science* **2014**, *292*, 958–970. https://doi.org/10.1016/j.apsusc.2013.12.087.

(51) Lee, R. S.; Chen, W. H.; Lin, J. H. Polymer-Grafted Multi-Walled Carbon Nanotubes through Surface-Initiated Ring-Opening Polymerization and Click Reaction. *Polymer* **2011**, *52* (10), 2180–2188. https://doi.org/10.1016/j.polymer.2011.03.020.

(52) Mercuri, F.; Sgamellotti, A. Theoretical Investigations on the Functionalization of Carbon Nanotubes. *Inorganica Chimica Acta* **2007**, *360* (3), 785–793. https://doi.org/10.1016/j.ica.2006.07.066.

(53) Worsley, K. A.; Kalinina, I.; Bekyarova, E.; Haddon, R. C. Functionalization and Dissolution of Nitric Acid Treated Single-Walled Carbon Nanotubes. *Journal of the American Chemical Society* **2009**, *131* (50), 18153–18158. https://doi.org/10.1021/ja906267g.

(54) Ska, V.; Kaiser, A. B.; Hrnc, K.; Roth, S. Effect of Chemical Treatment on Electrical Conductivity , Infrared Absorption , and Raman Spectra of Single-Walled Carbon Nanotubes. **2005**, 7174–7181. https://doi.org/10.1021/jp044741o.

(55) Laurent, C.; Flahaut, E.; Peigney, A. The Weight and Density of Carbon Nanotubes versus the Number of Walls and Diameter. *Carbon* **2010**, *48* (10), 2994–2996. https://doi.org/10.1016/j.carbon.2010.04.010.

(56) Pramanik, C.; Nepal, D.; Nathanson, M.; Gissinger, J. R.; Garley, A.; Berry, R. J.; Davijani, A.; Kumar, S.; Heinz, H. Molecular Engineering of Interphases in Polymer/Carbon Nanotube Composites to Reach the Limits of Mechanical Performance. *Composites Science and Technology* **2018**, *166* (April), 86–94. https://doi.org/10.1016/j.compscitech.2018.04.013.

(57) Kim, J.-K.; Mai, Y.-W. *Engineered Interfaces in Fiber Reinforced Composites*, 1st Ed.; Elsevier, 1998.

(58) Baughman, R. H.; Zakhidov, A. A.; De Heer, W. A. Carbon Nanotubes - The Route toward Applications. *Science* **2002**, *297* (5582), 787–792. https://doi.org/10.1126/science.1060928.

(59) Visser, J. On Hamaker Constants: A Comparison between Hamaker Constants and Lifshitz - van Der Waals Constants. *Advances in Colloid and Interface Science* **1972**, *3*, 331–363. https://doi.org/10.1016/0001-8686(72)85001-2.

(60) Detriche, S.; Zorzini, G.; Colomer, J.-F.; Fonseca, A.; Nagy, J. B. Application of the Hansen Solubility Parameters Theory to Carbon Nanotubes. *Journal of Nanoscience and Nanotechnology* **2008**, *8* (11), 6082–6092. https://doi.org/10.1166/jnn.2008.SW16.

(61) Minfang, M.; Winey, K. I. Improved Load Transfer in Nanotube/Polymer Composites with Increased Polymer Molecular Weight. *Journal of Physical Chemistry C* **2007**, *111* (48), 17923–17927. https://doi.org/10.1021/jp0715530.

(62) Rahmat, M.; Hubert, P. Carbon Nanotube-Polymer Interactions in Nanocomposites: A Review. *Composites Science and Technology* **2011**, *72* (1), 72–84. https://doi.org/10.1016/j.compscitech.2011.10.002.

(63) Davijani, A. A. B. Effect of Poly(Methyl Methacrylate) Wrapping on the Structure and Properties of CNT Films, and Polymer/CNT Films and Fibers, Georgia Institute of Technology. Ph.D. Thesis, 2016.

(64) Li, Y.; Yu, Y.; Liu, Y.; Lu, C. Interphase Development in Polyacrylonitrile/SWNT Nanocomposite and Its Effect on Cyclization and Carbonization for Tuning Carbon Structures. *ACS Applied Nano Materials* **2018**, *1* (7), 3105–3113. https://doi.org/10.1021/acsanm.8b00125.

(65) Chae, H. G.; Minus, M. L.; Kumar, S. Oriented and Exfoliated Single Wall Carbon Nanotubes in Polyacrylonitrile. *Polymer* **2006**, *47*, 3494–3504. https://doi.org/10.1016/j.polymer.2006.03.050.

(66) Zhang, H.; Quan, L.; Shi, F.; Li, C.; Liu, H.; Xu, L. Rheological Behavior of Amino-Functionalized Multi-Walled Carbon Nanotube/Polyacrylonitrile Concentrated Solutions and Crystal Structure of Composite Fibers. *Polymers* **2018**, *10* (2). https://doi.org/10.3390/polym10020186.

(67) Newcomb, B. A.; Gi, H.; Gulgunje, P. V.; Gupta, K.; Liu, Y.; Tsentalovich, D. E.; Pasquali, M.; Kumar, S. Stress Transfer in Polyacrylonitrile/Carbon Nanotube Composite Fibers. *Polymer* **2014**, *55* (11), 2734–2743. https://doi.org/10.1016/j.polymer.2014.04.008.

(68) Newcomb, B. A.; Gulgunje, P. V.; Gupta, K.; Kamath, M. G.; Liu, Y.; Giannuzzi, L. A.; Chae, H. G.; Kumar, S. Processing, Structure, and Properties of Gel Spun PAN and PAN/CNT Fibers and Gel Spun PAN Based Carbon Fibers. *Polymer Engineering & Science* **2015**, *55* (11), 2603–2614. https://doi.org/10.1002/pen.24153.

(69) Chae, H. G.; Sreekumar, T. V; Uchida, T.; Kumar, S. A Comparison of Reinforcement Efficiency of Various Types of Carbon Nanotubes in Polyacrylonitrile Fiber. *Polymer* **2005**, *46*, 10925–10935. https://doi.org/10.1016/j.polymer.2005.08.092.

(70) Jain, R.; Minus, M. L.; Chae, H. G.; Kumar, S. Processing, Structure, and Properties of PAN/MWNT Composite Fibers. *Macromolecular Materials and Engineering* **2010**, *295* (8), 742–749. https://doi.org/10.1002/mame.201000083.

(71) Sreekumar, T. V.; Liu, T.; Min, B. G.; Guo, H.; Kumar, S.; Hauge, R. H.; Smalley, R. E. Polyacrylonitrile Single-Walled Carbon Nanotube Composite Fibers. *Advanced Materials* **2004**, *16* (1), 58–61. https://doi.org/10.1002/adma.200305456.

(72) Li, X.; Ji, X.; Qin, A.; He, C. The Plasticized Spinning and Cyclization Behaviors of Functionalized Carbon Nanotube/Polyacrylonitrile Fibers. *RSC Advances* **2015**, *5* (64), 52226–52234. https://doi.org/10.1039/c5ra05696a.

(73) Mirbaha, H.; Nourpanah, P.; Scardi, P.; Mirco, D.; Greco, G.; Valentini, L.; Bon, S. B.; Arbab, S.; Pugno, N. The Impact of Shear and Elongational Forces on Structural Formation of Polyacrylonitrile/Carbon Nanotubes Composite Fibers during Wet Spinning Process. *Materials* **2019**, *12*, 2797. https://doi.org/10.3390/ma12172797.

(74) Wang, B.; Wang, H.; Hong, B.; Zhang, Y. Fibers from Multi-Walled Carbon Nanotube/Polyacrylonitrile Composites. *Polymer Journal* **2005**, *37* (5), 376–379. https://doi.org/10.1295/polymj.37.376.

(75) Park, O. K.; Chae, H. S.; Park, G. Y.; You, N. H.; Lee, S.; Bang, Y. H.; Hui, D.; Ku, B. C.; Lee, J. H. Effects of Functional Group of Carbon Nanotubes on Mechanical Properties of Carbon Fibers. *Composites Part B: Engineering* **2015**, *76*, 159–166. https://doi.org/10.1016/j.compositesb.2015.02.021.

(76) Elagib, T. H. H.; Hassan, E. A. M.; Liu, B.; Han, K.; Yu, M. Evaluation of Composite PAN Fibers Incorporated with Carbon Nanotubes and Titania and Their Performance during the Microwave-Induced Pre-Oxidation. *Carbon Letters* **2020**, *30* (3), 235–245. https://doi.org/10.1007/s42823-019-00092-2.

(77) Karim, S. A.; Mohamed, A.; Abdel-Mottaleb, M. M.; Osman, T. A.; Khattab, A. Mechanical Properties and the Characterization of Polyacrylonitrile/Carbon Nanotube Composite Nanofiber. *Arabian Journal for Science and Engineering* **2018**, *43* (9), 4697–4702. https://doi.org/10.1007/s13369-018-3065-x.

(78) Qiao, B.; Ding, X.; Hou, X.; Wu, S. Study on the Electrospun CNTs/Polyacrylonitrile-Based Nanofiber Composites. *Journal of Nanomaterials* **2011**, *2011*. https://doi.org/10.1155/2011/839462.

(79) Hou, H.; Ge, J. J.; Zeng, J.; Li, Q.; Reneker, D. H.; Greiner, A.; Cheng, S. Z. D. D.; Marburg, P. V; September, R. V; Re, V.; Recei, M.; December, V. Electrospun Polyacrylonitrile Nanofibers Containing a High Concentration of Well-Aligned Multiwall Carbon Nanotubes. *Chemistry of Materials* **2005**, *17* (5), 967–973. https://doi.org/10.1021/cm0484955.

(80) Ge, J. J.; Hou, H.; Li, Q.; Graham, M. J.; Greiner, A.; Reneker, D. H.; Harris, F. W.; Cheng, S. Z. D. Assembly of Well-Aligned Multiwalled Carbon Nanotubes in Confined Polyacrylonitrile Environments: Electrospun Composite Nanofiber Sheets. *Journal of the American Chemical Society* **2004**, *126* (48), 15754–15761. https://doi.org/10.1021/ja048648p.

(81) Kumar, S.; Gupta, V. B. Manufactured Fibres for High Performance, Industrial and Non-Conventional Applications. In *Manufactured Fibre Technology*; p 1997. https://doi.org/10.1007/978-94-011-5854-1_18.

(82) Lu, M.; Liao, J.; Gulgunje, P. V; Chang, H.; Arias-Monje, P. J.; Ramachandran, J.; Breedveld, V.; Kumar, S. Rheological Behavior and Fiber Spinning of Polyacrylonitrile (PAN)/Carbon Nanotube (CNT) Dispersions at High CNT Loading. *in review* **2020**.

(83) Chatterjee, T.; Krishnamoorti, R. Rheology of Polymer Carbon Nanotubes Composites. *Soft Matter* **2013**, *9* (40), 9515–9529. https://doi.org/10.1039/c3sm51444g.

(84) Gupta, V. B. Solution-Spinning Processes. In *Manufactured Fibre Technology*; 1997; pp 124–138. https://doi.org/10.1007/978-94-011-5854-1_6.

(85) Chien, A.; Newcomb, B. A.; Sabo, D.; Robbins, J.; Zhang, Z. J.; Kumar, S. High-Strength Superparamagnetic Composite Fibers. *Polymer* **2014**, *55* (16), 4116–4124. https://doi.org/10.1016/j.polymer.2014.06.028.

(86) Cao, Z.; Li, W.; Suo, X.; Liu, Y.; Lu, C. Structures and Cyclization Behaviors of Gel-Spun Cellulose/Polyacrylonitrile Composite Fibers. *Polymer Testing* **2020**, *81* (July 2019), 106276. https://doi.org/10.1016/j.polymertesting.2019.106276.

(87) Chang, H.; Luo, J.; Liu, H. C.; Zhang, S.; Park, J. G.; Liang, Z.; Kumar, S. Stabilization Study of Polyacrylonitrile/Cellulose Nanocrystals Composite Fibers. *ACS Applied Polymer Materials* **2019**, *1* (5), 1015–1021. https://doi.org/10.1021/acsapm.9b00057.

(88) Chang, H.; Luo, J.; Liu, H. C.; Bakhtiary Davijani, A. A.; Wang, P. H.; Lolov, G. S.; Dwyer, R. M.; Kumar, S. Ductile Polyacrylonitrile Fibers with High Cellulose Nanocrystals Loading. *Polymer* **2017**, *122*, 332–339. https://doi.org/10.1016/j.polymer.2017.06.072.

(89) Liu, H. C.; Luo, J.; Chang, H.; Bakhtiary Davijani, A. A.; Wang, P. H.; Kumar, S. Polyacrylonitrile Sheath and Polyacrylonitrile/Lignin Core Bi-Component Carbon Fiber. *Carbon* **2019**, *149*, 165–172. https://doi.org/10.1016/j.carbon.2019.04.004.

(90) Chang, H.; Lu, M.; Luo, J.; Park, J. G.; Liang, R.; Park, C.; Kumar, S. Polyacrylonitrile/Boron Nitride Nanotubes Composite Precursor and Carbon Fibers. *Carbon* **2019**, *147*, 419–426. https://doi.org/10.1016/j.carbon.2019.03.026.

(91) Chien, A. T.; Liu, H. C.; Newcomb, B. A.; Xiang, C.; Tour, J. M.; Kumar, S. Polyacrylonitrile Fibers Containing Graphene Oxide Nanoribbons. *ACS Applied Materials and Interfaces* **2015**, *7* (9), 5281–5288. https://doi.org/10.1021/am508594p.

(92) Zhang, D.; Karki, A. B.; Rutman, D.; Young, D. P.; Wang, A.; Cocke, D.; Ho, T. H.; Guo, Z. Electrospun Polyacrylonitrile Nanocomposite Fibers Reinforced with Fe3O4 Nanoparticles: Fabrication and Property Analysis. *Polymer* **2009**, *50* (17), 4189–4198. https://doi.org/10.1016/j.polymer.2009.06.062.

(93) Zhu, J.; Wei, S.; Rutman, D.; Haldolaarachchige, N.; Young, D. P.; Guo, Z. Magnetic Polyacrylonitrile-Fe@FeO Nanocomposite Fibers - Electrospinning, Stabilization and Carbonization. *Polymer* **2011**, *52* (13), 2947–2955. https://doi.org/10.1016/j.polymer.2011.04.034.

(94) Kaneko, T.; Watanuki, Y.; Toyama, T.; Kojima, Y.; Nishimiya, N. Characterization and Hydrogen Sorption Behaviors of FeNiCr-Carbon Composites Derived from Fe, Ni and Cr-Containing Polyacrylonitrile Fibers Prepared by Electrospinning Method. *International Journal of Hydrogen Energy* **2017**, *42* (15), 10014–10022. https://doi.org/10.1016/j.ijhydene.2017.03.079.

(95) Gao, Z.; Zhu, J.; Rajabpour, S.; Joshi, K.; Kowalik, M.; Croom, B.; Schwab, Y.; Zhang, L.; Bumgardner, C.; Brown, K. R.; Burden, D.; Klett, J. W.; van Duin, A. C. T. T.; Zhigilei, L. V.; Li, X. Graphene Reinforced Carbon Fibers. *Science Advances* **2020**, *6* (17), eaaz4191. https://doi.org/10.1126/sciadv.aaz4191.

(96) Salim, N. V.; Jin, X.; Razal, J. M. Polyacrylonitrile/Liquid Crystalline Graphene Oxide Composite Fibers – Towards High Performance Carbon Fiber Precursors. *Composites Science and Technology* **2019**, *182* (December 2018), 107781. https://doi.org/10.1016/j.compscitech.2019.107781.

(97) Ahn, D.; Choi, H. J.; Kim, H. dong; Yeo, S. Y. Properties of Conductive Polyacrylonitrile Fibers Prepared by Using Benzoxazine Modified Carbon Black.

Polymers **2020**, *12* (1). https://doi.org/10.3390/polym12010179.

(98) Szparaga, G.; Król, P.; Brzezińska, M.; Rabiej, S.; Boguń, M. Nanocomposite Precursor Polyacrylonitrile Fibers for Medical Applications. *Advances in Polymer Technology* **2016**, *35* (2), 1–8. https://doi.org/10.1002/adv.21542.

(99) Peng, H.; Wang, D.; Zhang, L.; Li, M.; Liu, M.; Wang, C.; Fu, S. Amorphous Cobalt Borate Nanosheets Grown on MoS2 Nanosheet for Simultaneously Improving the Flame Retardancy and Mechanical Properties of Polyacrylonitrile Composite Fiber. *Composites Part B: Engineering* **2020**, *201* (August), 108298. https://doi.org/10.1016/j.compositesb.2020.108298.

(100) Khodabakhshi, S.; Fulvio, P. F.; Andreoli, E. Carbon Black Reborn: Structure and Chemistry for Renewable Energy Harnessing. *Carbon* **2020**, *162*, 604–649. https://doi.org/10.1016/j.carbon.2020.02.058.

(101) Dittrich, B.; Wartig, K. A.; Hofmann, D.; Mülhaupt, R.; Schartel, B. Flame Retardancy through Carbon Nanomaterials: Carbon Black, Multiwall Nanotubes, Expanded Graphite, Multi-Layer Graphene and Graphene in Polypropylene. *Polymer Degradation and Stability* **2013**, *98* (8), 1495–1505. https://doi.org/10.1016/j.polymdegradstab.2013.04.009.

(102) Carbon Black - Global Market Trajectory & Analytics https://www.researchandmarkets.com/reports/338646/carbon_black_global_market_trajectory_and (accessed Sep 7, 2020).

(103) Xu, J.; Yu, J.; Xu, J.; Sun, C.; He, W.; Huang, J.; Li, G. High-Value Utilization of Waste Tires: A Review with Focus on Modified Carbon Black from Pyrolysis. *Science of the Total Environment* **2020**, *742*, 140235. https://doi.org/10.1016/j.scitotenv.2020.140235.

(104) Rodat, S.; Abanades, S.; Grivei, E.; Patrianakos, G.; Zygogianni, A.; Konstandopoulos, A. G.; Flamant, G. Characterisation of Carbon Blacks Produced by Solar Thermal Dissociation of Methane. *Carbon* **2011**, *49* (9), 3084–3091. https://doi.org/10.1016/j.carbon.2011.03.030.

(105) Garley, A.; Arias-Monje, P. J.; Hoff, S. E.; Sharp, M.; Kumar, S.; Heinz, H. Interaction of Poly(Methyl Acrylate) with Carbon Nanotubes as a Function of CNT Diameter, Chirality and Temperature. *in review* **2020**.

(106) Ozawa, H.; Fujigaya, T.; Niidome, Y.; Hotta, N.; Fujiki, M.; Nakashima, N. Rational Concept to Recognize/Extract Single-Walled Carbon Nanotubes with a Specific Chirality. *Journal of the American Chemical Society* **2011**, *133* (8), 2651–2657. https://doi.org/10.1021/ja109399f.

(107) Berton, N.; Lemasson, F.; Poschlad, A.; Meded, V.; Tristram, F.; Wenzel, W.; Hennrich, F.; Kappes, M. M.; Mayor, M. Selective Dispersion of Large-Diameter Semiconducting Single-Walled Carbon Nanotubes with Pyridine-Containing Copolymers. *Small* **2014**, *10* (2), 360–367. https://doi.org/10.1002/smll.201301295.

(108) Arnold, M. S.; Blackburn, J. L.; Crochet, J. J.; Doorn, S. K.; Duque, J. G.; Mohite, A.; Telg, H. Recent Developments in the Photophysics of Single-Wall Carbon Nanotubes for Active and Passive Material Elements in Thin Film Photovoltaics. *Physical chemistry chemical physics* **2013**, *15*, 14896–14918. https://doi.org/10.1039/C3CP52752B.

(109) Kar, T.; Bettinger, H. F.; Scheiner, S.; Roy, A. K. Noncovalent π-π Stacking and CH-π Interactions of Aromatics on the Surface of Single-Wall Carbon Nanotubes: An MP2 Study. *Journal of Physical Chemistry C* **2008**, *112* (50), 20070–20075. https://doi.org/10.1021/jp807809u.

(110) Meng, J.; Zhang, Y.; Cranford, S. W.; Minus, M. L. Nanotube Dispersion and Polymer Conformational Confinement in a Nanocomposite Fiber: A Joint Computational Experimental Study. *Journal of Physical Chemistry B* **2014**, *118* (31), 9476–9485. https://doi.org/10.1021/jp504726w.

(111) Tallury, S. S.; Pasquinelli, M. A. Molecular Dynamics Simulations of Polymers with Stiff Backbones Interacting with Single-Walled Carbon Nanotubes. *Journal of Physical Chemistry B* **2010**, *114* (29), 9349–9355. https://doi.org/10.1021/jp101191j.

(112) Gao, J.; Loi, M. A.; De Carvalho, E. J. F.; Dos Santos, M. C. Selective Wrapping and Supramolecular Structures of Polyfluorene-Carbon Nanotube Hybrids. *ACS Nano* **2011**, *5* (5), 3993–3999. https://doi.org/10.1021/nn200564n.

(113) O'Connell, M. J.; Boul, P.; Ericson, L. M.; Huffman, C.; Wang, Y.; Haroz, E.; Kuper, C.; Tour, J.; Ausman, K. D.; Smalley, R. E. Reversible Water-Solubilization of Single-Walled Carbon Nanotubes by Polymer Wrapping. *Chemical Physics Letters* **2001**, *342* (3–4), 265–271. https://doi.org/10.1016/S0009-2614(01)00490-0.

(114) Yang, H.; Bezugly, V.; Kunstmann, J.; Filoramo, A.; Cuniberti, G. Diameter-Selective Dispersion of Carbon Nanotubes via Polymers: A Competition between Adsorption and Bundling. *ACS Nano* **2015**, *9* (9), 9012–9019. https://doi.org/10.1021/acsnano.5b03051.

(115) PubChem https://pubchem.ncbi.nlm.nih.gov/ (accessed Apr 16, 2020).

(116) Wypych, G. *Handbook of Solvents*; ChemTec, 2001.

(117) Arias-Monje, P. J. P. J.; Lu, M.; Ramachandran, J.; Kirmani, M. H.; Kumar, S. Processing, Structure and Properties of Polyacrylonitrile Fibers with 15 Weight Percent Single Wall Carbon Nanotubes. *Polymer* **2020**, *211*, in press. https://doi.org/10.1016/j.polymer.2020.123065.

(118) Zhang, Y.; Fan, H.; Wang, Y.; Zuo, B.; Zhang, W.; Wang, S.; Wang, X. Influence of the Linkage Type between the Polymer Backbone and Side Groups on the Surface Segregation of Methyl Groups during Film Formation. *Soft Matter* **2015**, *11* (47), 9168–9178. https://doi.org/10.1039/c5sm01504a.

(119) Chen, Y.; Xu, Y.; Perry, K.; Sokolov, A. P.; More, K.; Pang, Y. Achieving Diameter-Selective Separation of Single-Walled Carbon Nanotubes by Using Polymer Conformation-Confined Helical Cavity. *ACS Macro Letters* **2012**, *1* (6), 701–705. https://doi.org/10.1021/mz3001308.

(120) Tange, M.; Okazaki, T.; Iijima, S. Selective Extraction of Large-Diameter Single-Wall Carbon Nanotubes with Specific Chiral Indices by Poly(9,9-Dioctylfluorene-Alt-Benzothiadiazole). *Journal of the American Chemical Society* **2011**, *133* (31), 11908–11911. https://doi.org/10.1021/ja204698d.

(121) Gao, J.; Kwak, M.; Wildeman, J.; Herrmann, A.; Loi, M. A. Effectiveness of Sorting Single-Walled Carbon Nanotubes by Diameter Using Polyfluorene Derivatives.

Carbon **2011**, *49* (1), 333–338. https://doi.org/10.1016/j.carbon.2010.09.036.

(122) Nish, A.; Hwang, J. Y.; Doig, J.; Nicholas, R. J. Highly Selective Dispersion of Single-Walled Carbon Nanotubes Using Aromatic Polymers. *Nature Nanotechnology* **2007**, *2* (10), 640–646. https://doi.org/10.1038/nnano.2007.290.

(123) Neimark, A. V. Thermodynamic Equilibrium and Stability of Liquid Films and Droplets on Fibers. *Journal of Adhesion Science and Technology* **1999**, *13* (10), 1137–1154. https://doi.org/10.1163/156856199X00839.

(124) Detriche, S.; Nagy, J. B.; Mekhalif, Z.; Delhalle, J. Surface State of Carbon Nanotubes and Hansen Solubility Parameters. *Journal of Nanoscience and Nanotechnology* **2009**, *9* (10), 6015–6025. https://doi.org/10.1166/jnn.2009.1568.

(125) Shea, M. J.; Mehlenbacher, R. D.; Zanni, M. T.; Arnold, M. S. Experimental Measurement of the Binding Configuration and Coverage of Chirality-Sorting Polyfluorenes on Carbon Nanotubes. *Journal of Physical Chemistry Letters* **2014**, *5* (21), 3742–3749. https://doi.org/10.1021/jz5017813.

(126) Gerstel, P.; Klumpp, S.; Hennrich, F.; Poschlad, A.; Meded, V.; Blasco, E.; Wenzel, W.; Kappes, M. M.; Barner-Kowollik, C. Highly Selective Dispersion of Single-Walled Carbon Nanotubes via Polymer Wrapping: A Combinatorial Study via Modular Conjugation. *ACS Macro Letters* **2014**, *3* (1), 10–15. https://doi.org/10.1021/mz400472q.

(127) Zhao, J.; Jia, Y.; Wei, N.; Rabczuk, T. Binding Energy and Mechanical Stability of Two Parallel and Crossing Carbon Nanotubes. *Proceedings of the Royal Society A: Mathematical, Physical and Engineering Sciences* **2015**, *471* (2180). https://doi.org/10.1098/rspa.2015.0229.

(128) Hwang, J. Y.; Nish, A.; Doig, J.; Douven, S.; Chen, C. W.; Chen, L. C.; Nicholas, R. J. Polymer Structure and Solvent Effects on the Selective Dispersion of Single-Walled Carbon Nanotubes. *Journal of the American Chemical Society* **2008**, *130* (11), 3543–3553. https://doi.org/10.1021/ja0777640.

(129) Duan, W. H.; Wang, Q.; Collins, F. Dispersion of Carbon Nanotubes with SDS Surfactants: A Study from a Binding Energy Perspective. *Chemical Science* **2011**, *2* (7), 1407–1413. https://doi.org/10.1039/c0sc00616e.

(130) Allegra, G.; Ganazzoli, F.; Bontempelli, S. Good- and Bad-Solvent Effect on the Rotational Statistics of a Long Chain Molecule. *Computational and Theoretical Polymer Science* **1998**, *8* (1–2), 209–218. https://doi.org/10.1016/S1089-3156(98)00038-5.

(131) Hsu, H. P.; Paul, W.; Binder, K. Standard Definitions of Persistence Length Do Not Describe the Local “Intrinsic” Stiffness of Real Polymer Chains. *Macromolecules* **2010**, *43* (6), 3094–3102. https://doi.org/10.1021/ma902715e.

(132) Roerdink, E.; Challa, G. Influence of Tacticity of Poly(Methyl Methacrylate) on the Compatibility with Poly(Vinylidene Fluoride). *Polymer* **1978**, *19* (2), 173–178. https://doi.org/10.1016/0032-3861(78)90034-4.

(133) Chang, L.; Woo, E. M. Tacticity Effects on Glass Transition and Phase Behavior in Binary Blends of Poly(Methyl Methacrylate)s of Three Different Configurations. *Polymer Chemistry* **2010**, *1* (2), 198–202. https://doi.org/10.1039/b9py00237e.

(134) Min, K. E.; Paul, D. R. Effect of Tacticity on Permeation Properties of Poly(Methyl Methacrylate). *Journal of Polymer Science Part B: Polymer Physics* **1988**, *26* (5), 1021–1033. https://doi.org/10.1002/polb.1988.090260507.

(135) Liu, T.; Xiao, Z.; Wang, B. The Exfoliation of SWCNT Bundles Examined by Simultaneous Raman Scattering and Photoluminescence Spectroscopy. *Carbon* **2009**, *47* (15), 3529–3537. https://doi.org/10.1016/j.carbon.2009.08.023.

(136) Heller, D. A.; Barone, P. W.; Swanson, J. P.; Mayrhofer, R. M.; Strano, M. S. Using Raman Spectroscopy to Elucidate the Aggregation State of Single-Walled Carbon Nanotubes. *Journal of Physical Chemistry B* **2004**, *108* (22), 6905–6909. https://doi.org/10.1021/jp037690o.

(137) Dresselhaus, M. S.; Dresselhaus, G.; Saito, R.; Jorio, A. Raman Spectroscopy of Carbon Nanotubes. *Physics Reports* **2005**, *409* (2), 47–99. https://doi.org/10.1016/j.physrep.2004.10.006.

(138) Ehli, C.; Oelsner, C.; Guldi, D. M.; Mateo-Alonso, A.; Prato, M.; Schmidt, C.; Backes, C.; Hauke, F.; Hirsch, A. Manipulating Single-Wall Carbon Nanotubes by Chemical Doping and Charge Transfer with Perylene Dyes. *Nature Chemistry* **2009**, *1* (3), 243–249. https://doi.org/10.1038/nchem.214.

(139) Chen, J.; Yan, L.; Song, W.; Xu, D. Interfacial Characteristics of Carbon Nanotube-Polymer Composites: A Review. *Composites Part A: Applied Science and Manufacturing* **2018**, *114* (August), 149–169. https://doi.org/10.1016/j.compositesa.2018.08.021.

(140) Yamane, A.; Sawai, D.; Kameda, T.; Kanamoto, T.; Ito, M.; Porter, R. S. Development of High Ductility and Tensile Properties upon Two-Stage Draw of Ultrahigh Molecular Weight Poly(Acrylonitrile). *Macromolecules* **1997**, *30* (14), 4170–4178. https://doi.org/10.1021/ma9614095.

(141) Choi, Y. H. Polyacrylonitrile/Carbon Nanotube Composite Fibers: Effect of Various Processing Parameters on Fiber Structure and Properties, Georgia Institute of Technology, 2010.

(142) Liu, T.; Kumar, S. Quantitative Characterization of SWNT Orientation by Polarized Raman Spectroscopy. *Chemical Physi* **2003**, *378*, 257–262. https://doi.org/10.1016/S0009-2614(03)01287-9.

(143) Namasivayam, M.; Andersson, M. R.; Shapter, J. Role of Molecularweight in Polymer Wrapping and Dispersion of MWNT in a PVDF Matrix. *Polymers* **2019**, *11* (1), 1–12. https://doi.org/10.3390/polym11010162.

(144) Liu, J.; Zhang, L. Computational Simulation in Elastomer Nanocomposites. In *Progress in Rubber Nanocomposites*; Elsevier Ltd, 2017; pp 523–555. https://doi.org/10.1016/B978-0-08-100409-8.00015-2.

(145) Deng, L.; Eichhorn, S. J.; Kao, C. C.; Young, R. J. The Effective Young's Modulus of Carbon Nanotubes in Composites. *ACS Applied Materials and Interfaces* **2011**, *3* (2), 433–440. https://doi.org/10.1021/am1010145.

(146) Cooper, C. A.; Young, R. J.; Halsall, M. Investigation into the Deformation of Carbon Nanotubes and Their Composites through the Use of Raman Spectroscopy. *Composites Part A: Applied Science and Manufacturing* **2001**, *32* (3–4), 401–411.

https://doi.org/10.1016/S1359-835X(00)00107-X.

(147) Robinson, I. M.; Zakikhani, M.; Day, R. J.; Young, R. J.; Galiotis, C. Strain Dependence of the Raman Frequencies for Different Types of Carbon Fibres. *Journal of Materials Science Letters* **1987**, *6* (10), 1212–1214. https://doi.org/10.1007/BF01729187.

(148) Haggenmueller, R.; Zhou, W.; Fischer, J. E.; Winey, K. I. Production and Characterization of Polymer Nanocomposites with Highly Aligned Single-Walled Carbon Nanotubes. *Journal of Nanoscience and Nanotechnology* **2016**, *3* (1/2), 105–110. https://doi.org/10.1166/jnn.2003.173.

(149) Haggenmueller, R.; Gommans, H. H.; Rinzler, A. G.; Fischer, J. E.; Winey, K. I. Aligned Single-Wall Carbon Nanotubes in Composites by Melt Processing Methods. *Chemical Physics Letters* **2000**, *330* (3–4), 219–225. https://doi.org/10.1016/S0009-2614(00)01013-7.

(150) Weng, B.; Xu, F.; Lozano, K. Mass Production of Carbon Nanotube-Reinforced Polyacrylonitrile Fine Composite Fibers. *Journal of Applied Polymer Science* **2014**, *40302*, 1–9. https://doi.org/10.1002/app.40302.

(151) Jestin, S.; Poulin, P. Wet Spinning of CNT-Based Fibers. In *Nanotube Superfiber Materials: Changing Engineering Design*; Elsevier, 2013; pp 167–209. https://doi.org/10.1016/B978-1-4557-7863-8.00006-2.

(152) Heikkilä, P.; Harlin, A. Electrospinning of Polyacrylonitrile (PAN) Solution: Effect of Conductive Additive and Filler on the Process. *Express Polymer Letters* **2009**, *3* (7), 437–445. https://doi.org/10.3144/expresspolymlett.2009.53.

(153) Kaur, N.; Kumar, V.; Dhakate, S. R. Synthesis and Characterization of Multiwalled CNT–PAN Based Composite Carbon Nanofibers via Electrospinning. *SpringerPlus* **2016**, *5* (1). https://doi.org/10.1186/s40064-016-2051-6.

(154) Weisenberger, M. C.; Grulke, E. A.; Jacques, D.; Rantell, T.; Andrews, R. Enhanced Mechanical Properties of Polyacrylonitrile/Multiwall Carbon Nanotube Composite Fibers. *Journal of Nanoscience and Nanotechnology* **2003**, *3* (6), 535–539. https://doi.org/10.1166/jnn.2003.239.

(155) Mirbaha, H.; Scardi, P.; D'Incau, M.; Arbab, S.; Nourpanah, P.; Pugno, N. M. Supramolecular Structure and Mechanical Properties of Wet-Spun Polyacrylonitrile/Carbon Nanotube Composite Fibers Influenced by Stretching Forces. *Frontiers in Materials* **2020**, *7* (July), 1–13. https://doi.org/10.3389/fmats.2020.00226.

(156) Bashir, Z. Co-crystallization of Solvents with Polymers: The X-ray Diffraction Behavior of Solvent-containing and Solvent-free Polyacrylonitrile. *Journal of Polymer Science Part B: Polymer Physics* **1994**, *32* (6), 1115–1128. https://doi.org/10.1002/polb.1994.090320616.

(157) Luo, J.; Chang, H.; Bakhtiary Davijani, A. A.; Liu, H. C.; Wang, P. H.; Moon, R. J.; Kumar, S. Influence of High Loading of Cellulose Nanocrystals in Polyacrylonitrile Composite Films. *Cellulose* **2017**, *24* (4), 1745–1758. https://doi.org/10.1007/s10570-017-1219-8.

(158) Guo, H.; Minus, M. L.; Jagannathan, S.; Kumar, S. Polyacrylonitrile/Carbon

Nanotube Composite Films. *ACS Applied Materials and Interfaces* **2010**, *2* (5), 1331–1342. https://doi.org/10.1021/am100155x.

(159) Sawai, D.; Kanamoto, T.; Yamazaki, H.; Hisatani, K. Dynamic Mechanical Relaxations in Poly(Acrylonitrile) with Different Stereoregularities. *Macromolecules* **2004**, *37* (8), 2839–2846. https://doi.org/10.1021/ma0352330.

(160) Zhang, Y.; Song, K.; Meng, J.; Minus, M. L. Tailoring Polyacrylonitrile Interfacial Morphological Structure by Crystallization in the Presence of Single-Wall Carbon Nanotubes. *ACS Applied Materials and Interfaces* **2013**, *5*, 807–814. https://doi.org/10.1021/am302382m.

(161) Guo, H. Structure, Processing, and Properties of Polyacrylonitrile/Carbon Nanotubes Composite Films, 2007. https://doi.org/hdl.handle.net/1853/22555.

(162) Eom, Y.; Park, Y.; Mee, Y.; Chul, B. Effects of Conformational Change of Polyacrylonitrile on the Aging Behavior of the Solutions in N,N-Dimethyl Formamide. *Polymer* **2017**, *108*, 193–205. https://doi.org/http://dx.doi.org/10.1016/j.polymer.2016.11.060.

(163) Pötschke, P.; Fornes, T. D.; Paul, D. R. Rheological Behavior of Multiwalled Carbon Nanotube/Polycarbonate Composites. *Polymer* **2002**, *43* (11), 3247–3255. https://doi.org/10.1016/S0032-3861(02)00151-9.

(164) Yang, Z.; Peng, H.; Wang, W.; Liu, T. Dry-Jet Wet-Spun PAN/MWCNT Composite Fibers with Homogeneous Structure and Circular Cross-Section. *Journal of Applied Polymer Science* **2010**, *116* (5), 2658–2667. https://doi.org/10.1002/app.

(165) Sawai, D.; Yamane, A.; Takahashi, H.; Kanamoto, T.; Ito, M.; Porter, R. R. Development of High Ductility and Tensile Properties by a Two-Stage Draw of Poly (Acrylonitrile): Effect of Molecular Weight. *Journal of Polymer Science Part B: Polymer Physics* **1998**, *36* (4), 629–640. https://doi.org/10.1002/(SICI)1099-0488(199803)36:4<629::AID-POLB9>3.0.CO;2-J.

(166) Guo, H.; Rasheed, A.; Minus, M. L.; Kumar, S. Polyacrylonitrile/Vapor Grown Carbon Nanofiber Composite Films. *Journal of Materials Science* **2008**, *43*, 4363–4369. https://doi.org/10.1007/s10853-008-2556-7.

(167) Chazot, C. A. C.; Hart, A. J. Understanding and Control of Interactions between Carbon Nanotubes and Polymers for Manufacturing of High-Performance Composite Materials. *Composites Science and Technology* **2019**, *183* (June), 107795. https://doi.org/10.1016/j.compscitech.2019.107795.

(168) Cronin, S. B.; Swan, A. K.; Ünlü, M. S.; Goldberg, B. B.; Dresselhaus, M. S.; Tinkham, M. Resonant Raman Spectroscopy of Individual Metallic and Semiconducting Single-Wall Carbon Nanotubes under Uniaxial Strain. *Physical Review B* **2005**, *72* (3), 1–8. https://doi.org/10.1103/PhysRevB.72.035425.

(169) Tsagaropoulos, G.; Eisenberg, A. Dynamic Mechanical Study of the Factors Affecting the Two Glass Transition Behavior of Filled Polymers. Similarities and Differences with Random Ionomers. *Macromolecules* **1995**, *28* (18), 6067–6077. https://doi.org/10.1021/ma00122a011.

(170) Robertson, C. G.; Rackaitis, M. Further Consideration of Viscoelastic Two Glass Transition Behavior of Nanoparticle-Filled Polymers. *Macromolecules* **2011**, *44* (5),

1177–1181. https://doi.org/10.1021/ma102631h.

(171) Savage, G. *Carbon-Carbon Composites*; Springer: Dordrecht, 1993. https://doi.org/10.1007/978-94-011-1586-5.

(172) Zhang, S.; Hao, A.; Nguyen, N.; Oluwalowo, A.; Liu, Z.; Dessureault, Y.; Park, J. G.; Liang, R. Carbon Nanotube/Carbon Composite Fiber with Improved Strength and Electrical Conductivity via Interface Engineering. *Carbon* **2019**, *144*, 628–638. https://doi.org/10.1016/J.CARBON.2018.12.091.

(173) Jin, Y.; Zhang, Y.; Zhang, Q.; Zhang, R.; Li, P.; Qian, W.; Wei, F. Multi-Walled Carbon Nanotube-Based Carbon/Carbon Composites with Three-Dimensional Network Structures. *Nanoscale* **2013**, *5* (13), 6181–6186. https://doi.org/10.1039/c3nr01069d.

(174) Zhou, Z.; Wang, X.; Faraji, S.; Bradford, P. D.; Li, Q.; Zhu, Y. Mechanical and Electrical Properties of Aligned Carbon Nanotube/Carbon Matrix Composites. *Carbon* **2014**, *75*, 307–313. https://doi.org/10.1016/j.carbon.2014.04.008.

(175) Chae, H. G.; Minus, M. L.; Rasheed, A.; Kumar, S. Stabilization and Carbonization of Gel Spun Polyacrylonitrile/Single Wall Carbon Nanotube Composite Fibers. *Polymer* **2007**, *48* (13), 3781–3789. https://doi.org/10.1016/j.polymer.2007.04.072.

(176) Liu, Y.; Chae, H. G.; Kumar, S. Gel-Spun Carbon Nanotubes/Polyacrylonitrile Composite Fibers . Part III : Effect of Stabilization Conditions on Carbon Fiber Properties. *Carbon* **2011**, *49*, 4487–4496. https://doi.org/10.1016/j.carbon.2011.06.045.

(177) Chae, H. G.; Choi, Y. H.; Minus, M. L.; Kumar, S. Carbon Nanotube Reinforced Small Diameter Polyacrylonitrile Based Carbon Fiber. *Composites Science and Technology* **2009**, *69* (3–4), 406–413. https://doi.org/10.1016/j.compscitech.2008.11.008.

(178) Tajaddod, N.; Li, H.; Minus, M. L. Low-Temperature Graphitic Formation Promoted by Confined Interphase Structures in Polyacrylonitrile/Carbon Nanotube Materials. *Polymer* **2018**, *137*, 346–357. https://doi.org/10.1016/j.polymer.2018.01.007.

(179) Liu, Y.; Chae, H. G.; Kumar, S. Gel-Spun Carbon Nanotubes/Polyacrylonitrile Composite Fibers. Part I: Effect of Carbon Nanotubes on Stabilization. *Carbon* **2011**, *49*, 4466–4476. https://doi.org/10.1016/j.carbon.2011.06.043.

(180) Park, O. K.; Lee, S.; Joh, H. I.; Kim, J. K.; Kang, P. H.; Lee, J. H.; Ku, B. C. Effect of Functional Groups of Carbon Nanotubes on the Cyclization Mechanism of Polyacrylonitrile (PAN). *Polymer* **2012**, *53* (11), 2168–2174. https://doi.org/10.1016/j.polymer.2012.03.031.

(181) Li, Z. Q.; Lu, C. J.; Xia, Z. P.; Zhou, Y.; Luo, Z. X-Ray Diffraction Patterns of Graphite and Turbostratic Carbon. *Carbon* **2007**, *45* (8), 1686–1695. https://doi.org/10.1016/j.carbon.2007.03.038.

(182) Endo, M. Structure of Mesophase Pitch-Based Carbon Fibres. **1988**, *23*, 598–605. https://doi.org/10.1016/0010-4361(88)90140-1.

(183) Huang, Y.; Young, R. J. Effect of Fibre Microstructure upon the Modulus of PAN- and Pitch-Based Carbon Fibres. *Carbon* **1995**, *33* (2), 97–107. https://doi.org/10.1016/0008-6223(94)00109-D.

(184) Meinl, J.; Schönfeld, K.; Kirsten, M.; Kittler, K.; Michaelis, A.; Cherif, C. Optimization of the Temperature Program to Scale up the Stabilization of Polyacrylonitrile Fibers. *Composites Part A: Applied Science and Manufacturing* **2017**, *96*, 37–45. https://doi.org/10.1016/j.compositesa.2017.02.010.

(185) Gulgunje, P. V.; Newcomb, B. A.; Gupta, K.; Chae, H. G.; Tsotsis, T. K.; Kumar, S. Low-Density and High-Modulus Carbon Fibers from Polyacrylonitrile with Honeycomb Structure. *Carbon* **2015**, *95*, 710–714. https://doi.org/10.1016/j.carbon.2015.08.097.

(186) Nunna, S.; Naebe, M.; Hameed, N.; Creighton, C.; Naghashian, S.; Jennings, M. J.; Atkiss, S.; Setty, M.; Fox, B. L. Investigation of Progress of Reactions and Evolution of Radial Heterogeneity in the Initial Stage of Thermal Stabilization of PAN Precursor Fibres. *Polymer Degradation and Stability* **2016**, *125*, 105–114. https://doi.org/10.1016/j.polymdegradstab.2016.01.008.

(187) Hou, Y.; Sun, T.; Wang, H.; wu, D. Effect of Heating Rate on the Chemical Reaction during Stabilization of Polyacrylonitrile Fibers. *Textile Research Journal* **2008**, *78* (9), 806–811. https://doi.org/10.1177/0040517507090500.

(188) Fitzer, E.; Frohs, W.; Heine, M. Optimization of Stabilization and Carbonization Treatment of PAN Fibres and Structural Characterization of the Resulting Carbon Fibres. *Carbon* **1986**, *24* (4), 387–395. https://doi.org/10.1016/0008-6223(86)90257-5.

(189) Liu, Y.; Chae, H. G.; Kumar, S. Gel-Spun Carbon Nanotubes/Polyacrylonitrile Composite Fibers. Part II: Stabilization Reaction Kinetics and Effect of Gas Environment. *Carbon* **2011**, *49*, 4477–4486. https://doi.org/10.1016/j.carbon.2011.06.042.

(190) Lu, M.; Arias-monje, P. J.; Ramachandran, J. Accelerating Stabilization Reaction of Polyacrylonitrile (PAN) Fibers with Carbon Nanotubes (CNT). *in preparation* 5–6.

(191) Yargı, Ö.; Ugur, S.; Pekcan, Ö. Temperature Dependence of Oxygen Diffusion Into Polymer/Carbon Nanotube Composite Films. *Polymer Engineering & Science* **2012**, *52*, 172–179. https://doi.org/10.1002/pen.22061.

(192) Xue, Y.; Liu, J.; Lian, F.; Liang, J. Effect of the Oxygen-Induced Modification of Polyacrylonitrile Fibers during Thermal-Oxidative Stabilization on the Radial Microcrystalline Structure of the Resulting Carbon Fibers. *Polymer Degradation and Stability* **2013**, *98* (11), 2259–2267. https://doi.org/10.1016/j.polymdegradstab.2013.08.016.

(193) Ramachandran, J.; Lu, M.; Arias-Monje, P. J.; Hamza, M.; Shirolkar, N.; Kumar, S.; Kimarni, M. H.; Shirolkar, N.; Kumar, S. Towards Designing Strong Porous Carbon Fibers through Gel Spinning of Polymer Blends. *Carbon*. https://doi.org/10.1016/j.carbon.2020.10.029.

(194) Abeykoon, N. C.; Bonso, J. S.; Ferraris, J. P. Supercapacitor Performance of Carbon Nanofiber Electrodes Derived from Immiscible PAN/PMMA Polymer Blends. *RSC Advances* **2015**, *5* (26), 19865–19873. https://doi.org/10.1039/c4ra16594b.

(195) Jo, E.; Yeo, J. G.; Kim, D. K.; Oh, J. S.; Hong, C. K. Preparation of Well-Controlled Porous Carbon Nanofiber Materials by Varying the Compatibility of Polymer Blends.

Polymer International **2014**, *63* (8), 1471–1477. https://doi.org/10.1002/pi.4645.

(196) Bahl, O. P.; Manocha, L. M. Shrinkage Behaviour of Polyacrylonitrile during Thermal Treatment. *Die Angewandte Makromolekulare Chemie* **1975**, *48* (1), 145–159. https://doi.org/10.1002/apmc.1975.050480109.

(197) Markets&Markets. Carbon Fiber Market by Raw Material, Fiber Type, Product Type, Modulus, Application, End-use Industry & Region. Report code AD 1611 https://www.marketsandmarkets.com/Market-Reports/carbon-fiber-396.html (accessed Oct 10, 2020).

(198) Baker, D. A.; Rials, T. G. Recent Advances in Low-Cost Carbon Fiber Manufacture from Lignin. *Journal of Applied Polymer Science* **2013**, *130* (2), 713–728. https://doi.org/10.1002/app.39273.

(199) Nunna, S.; Blanchard, P.; Buckmaster, D.; Davis, S.; Naebe, M. Development of a Cost Model for the Production of Carbon Fibres. *Heliyon* **2019**, *5* (10), e02698. https://doi.org/10.1016/j.heliyon.2019.e02698.

(200) Ellringmann, T.; Wilms, C.; Warnecke, M.; Seide, G.; Gries, T. Carbon Fiber Production Costing: A Modular Approach. *Textile Research Journal* **2016**, *86* (2), 178–190. https://doi.org/10.1177/0040517514532161.

(201) Zhang, W.; Wang, M.; Zhang, W.; Liu, W.; Yang, C.; Shen, R.; Wu, G. Significantly Reduced Pre-Oxidation Period of PAN Fibers by Continuous Electron Beam Irradiation: Optimization by Monitoring Radical Variation. *Polymer Degradation and Stability* **2018**, *158* (2018), 72–82. https://doi.org/10.1016/j.polymdegradstab.2018.10.027.

(202) White, T. L.; Pauluaskas, F. L.; Bigelow, T. S. System to Continuously Produce Carbon Fiber via Microwave Assisted Plasma Processing. 7,824,495 B1, 2010.

(203) Lu, M.; Xu, J.; Arias-monje, P. J.; Gulgunje, P. V; Gupta, K.; Shirolkar, N.; Maffe, A. P.; DiLoreto, E.; Ramachandran, J.; Sahoo, Y.; Agarwal, S.; Meredith, C.; Kumar, S. Continuous Stabilization of Polyacrylonitrile (PAN) - Carbon Nanotube (CNT) Fibers by Joule Heating. *in review*.

(204) Wang, P.-H.; Ghoshal, S.; Gulgunje, P.; Verghese, N.; Kumar, S. Polypropylene Nanocomposites with Polymer Coated Multiwall Carbon Nanotubes. *Polymer* **2016**, *100*, 244–258. https://doi.org/10.1016/j.polymer.2016.07.070.

(205) Salovey, R.; Lakdawala, K. Rheology of Polymers Containing Carbon Black. *Annual Technical Conference - Society of Plastics Engineers* **1987**, *27* (14), 934–937.

(206) Arrigo, R.; Malucelli, G. Rheological Behavior of Polymer/Carbon Nanotube Composites: An Overview. *Materials* **2020**, *13* (12), 1–27. https://doi.org/10.3390/ma13122771.

(207) Nobile, M. R.; Naddeo, C.; Raimondo, M.; Guadagno, L. Effect of Functionalized Carbon Nanofillers on the Rheological Behavior of Structural Epoxy Resins. *AIP Conference Proceedings* **2019**, *2196* (December). https://doi.org/10.1063/1.5140300.

(208) Jain, S.; Goossens, J. G. P.; Peters, G. W. M.; Van Duin, M.; Lemstra, P. J. Strong Decrease in Viscosity of Nanoparticle-Filled Polymer Melts through Selective Adsorption. *Soft Matter* **2008**, *4* (9), 1848–1854. https://doi.org/10.1039/b802905a.

(209) Mackay, M. E.; Dao, T. T.; Tuteja, A.; Ho, D. L.; Van Horn, B.; Kim, H. C.; Hawker, C. J. Nanoscale Effects Leading to Non-Einstein-like Decrease in Viscosity. *Nature Materials* **2003**, *2* (11), 762–766. https://doi.org/10.1038/nmat999.

(210) Eom, Y.; Kim, B. C. Effects of Chain Conformation on the Viscoelastic Properties of Polyacrylonitrile Gels under Large Amplitude Oscillatory Shear. *European Polymer Journal* **2016**, *85*, 341–353. https://doi.org/10.1016/j.eurpolymj.2016.10.037.

(211) Scher, H.; Zallen, R. Critical Density in Percolation Processes. *The Journal of Chemical Physics* **1970**, *53* (9), 3759–3761. https://doi.org/10.1063/1.1674565.

(212) Liang, J. Z.; Yang, Q. Q. Effects of Carbon Black Content and Size on Conductive Properties of Filled High-Density Polyethylene Composites. *Advances in Polymer Technology* **2018**, *37* (6), 2238–2245. https://doi.org/10.1002/adv.21882.

(213) Feng, J.; Chan, C. M. Double Positive Temperature Coefficient Effects of Carbon Black-Filled Polymer Blends Containing Two Semicrystalline Polymers. *Polymer* **2000**, *41* (12), 4559–4565. https://doi.org/10.1016/S0032-3861(99)00690-4.

(214) Mingxuan Lu, Prabhakar V. Gulgunje, Pedro J. Arias-Monje, Jeffery Luo, J. R. and S. K. Enhanced Electrical Conductivity of Polyacrylonitrile (PAN) Fiber at Low Carbon Nanotube (CNT) Loading Utilizing Core-Sheath Structure. **2019**.

(215) Mirabedini, A.; Foroughi, J.; Wallace, G. G. Developments in Conducting Polymer Fibres: From Established Spinning Methods toward Advanced Applications. *RSC Advances* **2016**, *6* (50), 44687–44716. https://doi.org/10.1039/c6ra05626a.

(216) Foroughi, J.; Spinks, G. M.; Wallace, G. G. Conductive Polymer Fibers. In *Handbook of Smart Textiles*; Tao, X., Ed.; Springer Science+Business Media, 2015; pp 31–62. https://doi.org/10.1007/978-981-4451-45-1.

(217) Gupta, A.; Harrison, I. R. New Aspects in the Oxidative Stabilization of PAN-Based Carbon Fibers. *Carbon* **1996**, *34* (11), 1427–1445. https://doi.org/10.1016/S0008-6223(96)00094-2.

(218) Alway-Cooper, R. M.; Anderson, D. P.; Ogale, A. A. Carbon Black Modification of Mesophase Pitch-Based Carbon Fibers. *Carbon* **2013**, *59*, 40–48. https://doi.org/10.1016/j.carbon.2013.02.048.

(219) Hansen, C. M. *Hansen Solubility Parameters: A User´s Handbook*; CRC Press: Cambridge, 2000.

(220) Lindvig, T.; Michelsen, M. L.; Kontogeorgis, G. M. A Flory-Huggins Model Based on the Hansen Solubility Parameters. *Fluid Phase Equilibria* **2002**, *203* (1–2), 247–260. https://doi.org/10.1016/S0378-3812(02)00184-X.

(221) Copyright Statement : The Use of Solubility Parameters to Select Membrane Materials for Pervaporation of Organic Mixtures A Thesis Submitted in Partial Fulfilment of The, 1994, Vol. 1994.

(222) Li, H.; Liu, J.; Papadakis, R. Direct Measurement of the Surface Energy of Single-Walled Carbon Nanotubes through Atomic Force Microscopy. *Journal of Applied Physics* **2019**, *126* (6). https://doi.org/10.1063/1.5108935.

(223) Roh, S. C.; Choi, E. Y.; Choi, Y. S.; Kim, C. K. Characterization of the Surface

Energies of Functionalized Multi-Walled Carbon Nanotubes and Their Interfacial Adhesion Energies with Various Polymers. *Polymer* **2014**, *55* (6), 1527–1536. https://doi.org/10.1016/j.polymer.2014.02.015.

(224) Surface Energy Data for Poly(methyl acrylate) http://www.accudynetest.com/polymer_surface_data/polymethyl_acrylate.pdf (accessed Apr 16, 2020).

(225) Shen, J.; He, Y.; Wu, J.; Gao, C.; Keyshar, K.; Zhang, X.; Yang, Y.; Ye, M.; Vajtai, R.; Lou, J.; Ajayan, P. M. Liquid Phase Exfoliation of Two-Dimensional Materials by Directly Probing and Matching Surface Tension Components. *Nano Letters* **2015**, *15* (8), 5449–5454. https://doi.org/10.1021/acs.nanolett.5b01842.

(226) Technical Note TN306e, Application Report, Kruss Scientific www.kruss-scientific.com/fileadmin/user_upload/website/literature/kruss-tn306-en.pdf.

(227) van Oss, C. J. *Interfacial Forces in Aqueous Media*; CRC Press, 1994.

(228) Surface tension values of some common test liquids for surface energy analysis http://www.surface-tension.de/ (accessed Apr 16, 2020).

(229) Wu, S. Interfacial And Surface Tensions of Polymers. *Journal of Macromolecular Science, Part C* **1974**, *10* (1), 1–73. https://doi.org/10.1080/15321797408080004.

(230) Hobbs, S. Y.; Dekkers, M. E. J.; Watkins, V. H. Effect of Interfacial Forces on Polymer Blend Morphologies. *Polymer* **1988**, *29* (9), 1598–1602. https://doi.org/10.1016/0032-3861(88)90269-8.

(231) Ravati, S.; Favis, B. D. Morphological States for a Ternary Polymer Blend Demonstrating Complete Wetting. *Polymer* **2010**, *51* (20), 4547–4561. https://doi.org/10.1016/j.polymer.2010.07.014.

(232) Li, Y.; Niu, J.; Shen, Z.; Feng, C. Size Effect of Single-Walled Carbon Nanotube on Adsorption of Perfluorooctanesulfonate. *Chemosphere* **2013**, *91* (6), 784–790. https://doi.org/10.1016/j.chemosphere.2013.01.093.

(233) Dahal, U. R.; Dormidontova, E. E. Spontaneous Insertion, Helix Formation, and Hydration of Polyethylene Oxide in Carbon Nanotubes. *Physical Review Letters* **2016**, *117* (2), 1–6. https://doi.org/10.1103/PhysRevLett.117.027801.

(234) Barber, A. H.; Cohen, S. R.; Wagner, H. D. External and Internal Wetting of Carbon Nanotubes with Organic Liquids. *Physical Review B - Condensed Matter and Materials Physics* **2005**, *71* (11), 2–6. https://doi.org/10.1103/PhysRevB.71.115443.

(235) Piggott, M. R. Debonding and Friction at Fibre-Polymer Interfaces. I: Criteria for Failure and Sliding. *Composites Science and Technology* **1987**, *30* (4), 295–306. https://doi.org/10.1016/0266-3538(87)90017-0.

(236) Hine, P. J.; Ward, I. M. Measuring the Elastic Properties of High-Modulus Fibres. *Journal of Materials Science* **1996**, *31* (2), 371–379. https://doi.org/10.1007/BF01139154.

(237) He, W. S.; Shih, Y. F.; Lin, J. J.; Dai, S. A. Effects of Poly(Oxyethylene)-Block Structure in Polyetheramines on the Modified Carbon Nanotube/Poly(Lactic Acid) Composites. *Composites Part A: Applied Science and Manufacturing* **2015**, *78*, 18–

26. https://doi.org/10.1016/j.compositesa.2015.07.018.

(238) Yoon, J. T.; Lee, S. C.; Jeong, Y. G. Effects of Grafted Chain Length on Mechanical and Electrical Properties of Nanocomposites Containing Polylactide-Grafted Carbon Nanotubes. *Composites Science and Technology* **2010**, *70* (5), 776–782. https://doi.org/10.1016/j.compscitech.2010.01.011.

(239) Liao, W. H.; Yang, S. Y.; Wang, J. Y.; Tien, H. W.; Hsiao, S. T.; Wang, Y. S.; Li, S. M.; Ma, C. C. M.; Wu, Y. F. Effect of Molecular Chain Length on the Mechanical and Thermal Properties of Amine-Functionalized Graphene Oxide/Polyimide Composite Films Prepared by in Situ Polymerization. *ACS Applied Materials and Interfaces* **2013**, *5* (3), 869–877. https://doi.org/10.1021/am302494c.

(240) Connor, M.; Bidaux, J. E.; Månson, J. A. E. A Criterion for Optimum Adhesion Applied to Fibre Reinforced Composites. *Journal of Materials Science* **1997**, *32* (19), 5059–5067. https://doi.org/10.1023/A:1018657131178.

(241) Pukánszky, B.; Tüdős, F. Miscibility and Mechanical Properties of Polymer Blends. *Makromolekylare Chemie. Macromolecular Symposia* **1990**, *38*, 221–231.

(242) Zhang, L.; Wang, J.; Fuentes, C. A.; Zhang, D.; Van Vuure, A. W.; Seo, J. W.; Seveno, D. Wettability of Carbon Nanotube Fibers. *Carbon* **2017**, *122*, 128–140. https://doi.org/10.1016/j.carbon.2017.06.027.

(243) Ozcan, C.; Hasirci, N. Evaluation of Surface Free Energy for PMMA Films. *Journal of Applied Polymer Science* **2008**, *108*, 438–446. https://doi.org/10.1002/app.

(244) Cabral Adão, M. H. V.; Vieira Saramago, B. J.; Catarino Fernandes, A. Estimation of the Surface Properties of Styrene-Acrylonitrile Random Copolymers from Contact Angle Measurements. *Journal of colloid and interface science* **1999**, *217* (1), 94–106. https://doi.org/10.1006/jcis.1999.6279.

(245) SPscientific. High Boiling Point Solvents https://www.spscientific.com/uploadedFiles/Product_Applications/Genevac/How to Evaporate High Boiling Point Solvents.pdf (accessed Jan 6, 2020).

(246) Popov, V. N.; Van Doren, V. E.; Balkanski, M. Elastic Properties of Crystals of Single-Walled Carbon Nanotubes. *Solid State Communications* **2000**, *114* (7), 395–399. https://doi.org/10.1016/S0038-1098(00)00070-3.

(247) Cai, L.; Bahr, J. L.; Yao, Y.; Tour, J. M. Ozonation of Single-Walled Carbon Nanotubes and Their Assemblies on Rigid Self-Assembled Monolayers. *Chemistry of Materials* **2002**, *14* (10), 4235–4241. https://doi.org/10.1021/cm020273o.

(248) Yokoi, T.; Iwamatsu, S. I.; Komai, S. I.; Hattori, T.; Murata, S. Chemical Modification of Carbon Nanotubes with Organic Hydrazines. *Carbon* **2005**, *43* (14), 2869–2874. https://doi.org/10.1016/j.carbon.2005.06.022.

(249) Davis, V. A.; Parra-vasquez, A. N. G.; Green, M. J.; Rai, P. K.; Behabtu, N.; Prieto, V.; Booker, R. D.; Schmidt, J.; Kesselman, E.; Zhou, W.; Fan, H.; Adams, W. W.; Hauge, R. H.; Fischer, J. E.; Cohen, Y.; Talmon, Y.; Smalley, R. E.; Pasquali, M. True Solutions of Single-Walled Carbon Nanotubes for Assembly into Macroscopic Materials. *Nature Nanotechnology* **2009**, *4* (12), 830–834. https://doi.org/10.1038/nnano.2009.302.

(250) Bin Kim, C.; Jeong, K.-B.; Joo Yang, B.; Song, J.-W.; Ku, B.-C.; Lee, S.; Lee, S.-K.;

Park, C. Facile Supramolecular Processing of Carbon Nanotubes and Polymers Enabling Electromechanical Sensors. *Angewwandte Chemie* **2017**, *129*, 16398–16403. https://doi.org/10.1002/ange.201708111.

(251) Liu, J.; Liu, T.; Kumar, S. Effect of Solvent Solubility Parameter on SWNT Dispersion in PMMA. *Polymer* **2005**, *46* (10), 3419–3424. https://doi.org/10.1016/j.polymer.2005.02.086.

(252) Chang, H.; Luo, J.; Bakhtiary Davijani, A. A.; Chien, A. T.; Wang, P. H.; Liu, H. C.; Kumar, S. Individually Dispersed Wood-Based Cellulose Nanocrystals. *ACS Applied Materials and Interfaces* **2016**, *8* (9), 5768–5771. https://doi.org/10.1021/acsami.6b00094.

VITA

Pedro J. Arias-Monje was born in San Vicente del Caguán, Caquetá, a small municipality at the south of Colombia known among nationals because of its role in the country's internal conflict. After completing his secondary education in his hometown, he pursued a bachelor's and then a master's degree (class of 2013 and 2016, respectively) in Chemical Engineering at Universidad Nacional de Colombia, in Bogotá. His undergraduate's and master's research focused on the synthesis and use of titania nanotube arrays in photoelectrocatalytic applications, including water splitting and waste-water treatment, and the synthesis of other carbon nanomaterials as nitrogen-doped reduced-graphene oxide and carbon nanofibers. Interested in the use of nanomaterials in catalysis and the processing, structure and properties of nanomaterials and nanocomposites, he was granted a Fulbright-Colciencias scholarship to pursue a Ph.D. at Georgia Institute of Technology in the United States of America. He has served as mentor, master thesis co-advisor and primary instructor of courses at the senior undergrad level, and has also coauthored over a dozen peer reviewed research articles. At Georgia Tech, he was recognized as Graduate Student Instructor of the Year at the Institute level in 2019 and begun advocacy towards equity in education.